Antimicrobial coatings for soft materials

Emilia Kulaga

Thèse présentée pour obtenir le grade de

Docteur de l'Université de Haute Alsace

Discipline : Chimie-Matériaux

Par

Emilia Kułaga

Antimicrobial Coatings for Soft Materials

Soutenance publique le 31 Janvier 2014

Membre du Jury

Directeur de Thèse	Dr. Karine Anselme
Co-*directeur de Thèse*	Dr. Lydie Ploux
Co-*directeur de Thèse*	Dr. Vincent Roucoules
Rapporteur	Prof. Emmanuel Pauthe
Rapporteur	Dr. Dominique Debarnot
Examinateur	Prof. Bernard Martel
Examinateur	Dr. Fouzia Boulmedais

Abstracts

English

Despite strict operative procedures to minimize microbial contaminations, bacterial infection of implants significantly raises postoperative complications of surgical procedures. One of the promising approaches is to adjust and control antimicrobial properties of the implant surface.

New types of antibacterial coatings prepared via plasma polymer functionalization step have been developed. These coatings contain and release in a control way a bioactive agent. Controlled release was achieved by the fabrication of plasma polymer multilayer systems, which consist of two layers of Maleic Anhydride Plasma Polymer deposited on the surface of Polypropylene made surgical mesh. In between plasma polymer layers, silver nanoparticles are trapped as an antibacterial agent reservoir.

Owing to differences between mechanical properties of the plasma-polymer thin films and the elastic bulk substrates, tensile strengths generate cracks within the plasma polymer, which might be used as diffusive channels for bioactive substances, here silver ions. The cracks can be controlled mechanically in a reversible way (**Figure 0-1**).

The tailoring of the spontaneous release of bioactive agent is achieved by the modification of the second plasma polymer deposition conditions. In addition, during mechanical stimulation of the designed material, control over silver ion release is achieved through an elongation-dependent releasing process allowed by the reversible control of the cracks. In the field of textiles and other soft

biomaterials, this strategy is promising due to the mechanical stresses that naturally occur at the implant location.

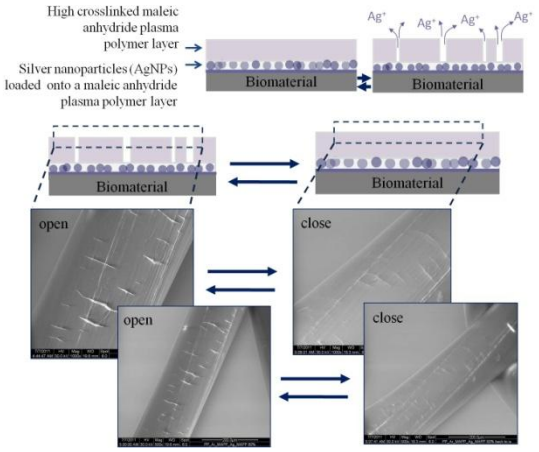

Figure 0-1: Plasma multilayer system consisting in two plasma polymer layers and a silver nanoparticles reservoir.

In regard of possible application of the developed system as a future biomaterial, the impact of different types of commonly used sterilization procedures on the properties of developed material was studied. The effects of autoclaving and electron beam sterilization methods on the surface chemistry, the dispersion of embedded silver nanoparticles in the plasma polymer and the cracks formation of the developed material was verified. Results showed the compatibility of the developed system with electron beam sterilization method.

The antibacterial properties of the new material have been evaluated. The effect of developed system on planktonic bacteria, bacterial adhesion and biofilm formation on stretched and unstretched system was studied. The membrane integrity of the adhered bacteria and bacteria in biofilms was followed during the study as an indicator of the physiologic state of bacteria. Results suggested that the sensitivity of bacteria to low concentrations of released silver ions resulted

in the formation of different types of structures of the biofilms on the studied materials.

The results give a strong base on the future of intelligent, silver containing materials that control the release at the site of infection. Our results show that low doses of silver may be sufficient to control infection by acting on the structure of bacterial biofilms.

Français

Les infections bactériennes lorsqu'elles se développent à partir d'implants sont très difficiles à traiter, l'issue courante étant un retrait pur et simple de l'implant incriminé. Dans ce cadre, les revêtements des biomatériaux ont un rôle important à jouer pour, d'une part, prévenir l'adhésion bactérienne et d'autre part, éliminer les bactéries présentes. Ces revêtements antibactériens doivent par ailleurs permettre une intégration tissulaire des biomatériaux aux cellules rencontrées sur le site de l'implantation.

Dans ce travail une nouvelle famille de revêtements antibactériens a été développée. Ils contiennent et libèrent de manière contrôlée un agent bioactif. Ils sont constitués de multicouches de polymère plasma d'anhydride maléique déposées à la surface de fibres de polypropylène tressées et constituant le matériau à implanter. Entre chaque dépôt de polymère plasma (agissant comme couche barrière), des nanoparticules d'argent sont piégées formant ainsi des réservoirs d'agent antibactérien. En raison des différences de propriétés mécaniques entre les films minces plasma et le substrat massique élastique (i.e. tissu de fibre de polypropylène), la résistance à la traction génère des fissures dans les couches polymère plasma, qui sont utilisées comme

canaux de diffusion pour les substances bioactives (dans notre cas les ions argent). Avant étirement, la libération spontanée des ions argent par simple diffusion aux travers des couches barrières peut être contrôlée en jouant sur le taux de réticulation des couches plasma. Au cours de l'étirement, le contrôle réversible de l'ouverture des fissures permet une libération maîtrisée des ions argent (**Figure 0-1bis**).

Dans le domaine des textiles et d'autres biomatériaux souples, cette stratégie est prometteuse en raison des contraintes mécaniques qui se produisent naturellement sur le site de l'implantation.

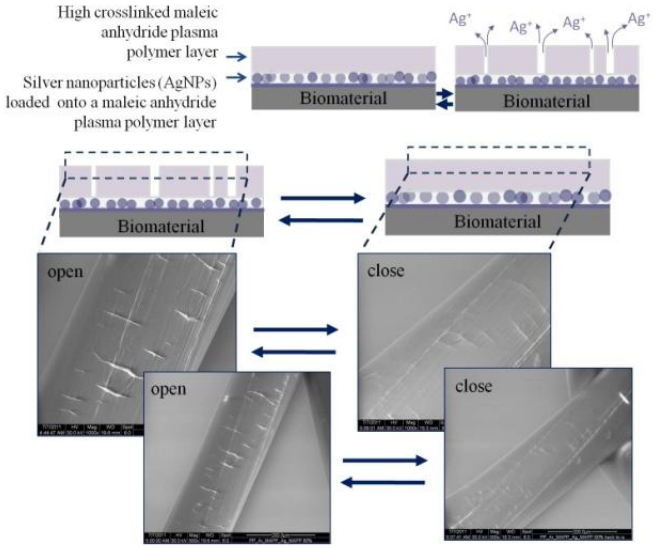

Figure 0-1bis: Système multicouche plasma constitué de deux couches de polymère plasma autour d'un réservoir de nanoparticules d'argent.

L'impact de différents types de procédures de stérilisation couramment utilisés (autoclave et irradiation par faisceau d'électrons) sur les propriétés du matériau développé a également été étudié. En particulier, l'incidence sur la chimie de surface, la dispersion des nanoparticules d'argent et la formation de fissures sous étirement a été regardée. La méthode de stérilisation par faisceau d'électrons permet de conserver les propriétés finales recherchées.

Enfin, les propriétés antibactériennes du nouveau matériau ont été étudiées. L'effet du relargage des ions argent sur des bactéries *Escherichia coli* planctoniques, l'adhésion bactérienne et la formation de biofilm sur le système étiré et non-étiré a été évalué. L'intégrité membranaire des bactéries adhérées et des bactéries dans les biofilms a été suivie au cours de l'étude comme indicateur de l'état physiologique des bactéries. Les résultats ont suggéré que la sensibilité des bactéries aux concentrations faibles d'ions d'argent libérés aboutit à la formation de différents types de structures de biofilms sur les matériaux étudiés.

L'ensemble des résultats obtenus donne une base solide pour le développement de matériaux intelligents capables de contrôler la libération du principe actif sur le site de l'infection. Nos résultats montrent qu'une faible dose d'argent peut suffire à contrôler l'infection en agissant sur la structure des biofilms formés.

Acknowledgement

First of all I want to thank my supervisors Dr. Karine Anselme, Dr. Lydie Ploux and Dr. Vincent Roucoules for giving me the opportunity to perform my PhD under their supervision. I admire their patience and trust they gave me to work on my project. I am grateful for their help, discussions and cordiality during the course of my work.

Also I thank the committee Prof. Emmanuel Pauthe, Dr. Dominique Debarnot, Prof. Bernard Martel and Dr. Fouzia Boulmedais for having agreed to consider report and examine this work.

I am very grateful to collaborators we have been working with during this thesis. I want to thank Dr. Lavinia Balan for fruitful collaboration, all the discussions and help in data interpretation. Florent Kuntz and Ludovic Frechard from Aerial provided their expertise and assistance in the electron beam sterilization process.

Also very valuable to me were the efforts of many people who contributed to my work. I thank Dr. A. Ponche and Philippe Fioux for help in XPS data interpretation. Stephan Knopf and Loïc Vidal for long hours they spent with my samples in front of SEM and TEM microscopes and for many interesting talks during these hours; Gautier Shrodj for help in mechanical tests. Patrick Lamielle manufactured stretching devices and many other things that I needed during my work. I also thank Patrick for many interesting talks during coffee breaks and for convincing me to try paragliding. I am very grateful to Tatiana Bourgade and Jules Valentin for help in cytotoxicity assessment experiments. I also thank Philippe Kunemann and Dr. Karine Mougin for introducing me to new instruments and techniques.

My thanks also go to my colleagues who have helped me in my research, experiments and who were there for scientific discussions. This includes Judith

Böhmler, Nicolas Cottenye, Patricia Davidson, Doris Campos, Felix Sima, Janina Möller, Helena Marques, Mia Mateescu, Florent Badique, Debora Tavares, Paulo Autran, Jalal Bacharouche, Yaroslav Odarchenko and Lilian Paiva.

More special thanks for Nelly Hobeika for all the discussions we had, for spending a lot of her free time with me and for being good friend.

Besides all my friends from Mulhouse and other places I thank my family and Nicolas Ducruet, who provided support and mental backup whenever it was needed.

Funding for this project from Region Alsace is also gratefully acknowledged.

Table of Contents

General Introduction

Bioactive materials: toward new mechanoresponsive polymeric materials

Implantation of biomaterials during surgery is a common and often life-saving procedure. However the use of implants is also one of the most important risk factor of biofilm-associated nosocomial infections and may expose the recipient to a lifelong risk and health problems. Some of these infections are extremely resistant to antibiotics and host defenses. Therefore, the most useful and standard therapy usually consists of removing implant which causes tissue damage, further increases the susceptibility to infections, activates host defenses and stimulates the generation of inflammatory mediators [1]. So, new solutions have to be found as alternative methods of control, such as infection-resistant materials.

Bioengineering field of implant materials is undergoing rapid new developments and one of the possible strategies to prevent infections is incorporation of bioactive agents (i.e. drugs) at the surface of implant coatings. The efficiency and durability of such bioactive coatings are strongly related to the control of the rate of drug release. For this purpose, researchers are focusing on the development of adaptive surfaces, known as stimuli-responsive materials, and able to release bioactive agent in a controlled way. Today, triggered release is possible through artificial stimuli [2] such as light-irradiation [3, 4], magnetic [5, 6], ultrasonic [7], thermal [8-10], electric [11] and, as well, natural stimuli like pH changes [12], redox gradients [13] and enzymatic stimuli [14]. Surprisingly, only

few study report developments of adaptive surfaces which respond to mechanical stimuli [15-18]. The benefit of developing such mechanoresponsive surfaces is that mechanical constraints naturally exists in the human body e.g., in the muscles, joints, arteries.

Mechanical stimuli responsive material was used for the first time in the work of Arm *et al*. [17], in which the authors controlled the release of proteins from biodegradable polymer implant. Another example has been described in the work of Mertz *et al.* [19], which was based on deposition of exponentially and linearly growing polyelectrolyte multilayers. The system, consisting in nanometer-sized multilayer barriers, was deposited on or between multilayer compartments and was designed to respond to mechanical stimuli and to act as nanovalves. The diffusion of drugs through the barrier from one compartment to another was switched on/off by tuning the mechanical stretching and thereby opening or closing nanopores in the barrier. Recent work of the same group [20] has reported a study on nanoassemblies, which consisted of a first polyelectrolyte multilayer stratum loaded with enzymes and capped with a second polyelectrolyte multilayer acting as a mechanically sensitive nanobarrier. The biocatalytic activity of the film is reversibly switched on/off by mechanical stretching, which exposes enzymes through the capping barrier, similarly to mechanisms involved in proteins like fibronectin during mechanotransduction.

Finally, study of Bacharouche *et al.* [21] reported the first example of synthetic surfaces allowing specific interactions with proteins or cells promoted by mechanical action in a fully reversible manner. Silicone sheets were first treated with plasma and then functionalized by grafting sequentially under stretching poly(ethyleneglycol) (PEG) chains and biotin or arginine-glycine-aspartic acid (RGD) peptides. At rest position, these ligands were not accessible for their receptors. Under stretching, the surface became specifically interactive to streptavidin, biotin-antibodies or adherent for cells and the interactions were

fully reversible by stretching/unstretching both for proteins and cells, revealing a reversible exposure process of the ligands.

In this work, our objective was to develop a new antibacterial mechanoresponsive coating for textile material. As mentioned before, the need of implants with controlled antibacterial properties is increasing due to the risk of infections which follows the implantation of biomaterials. Here, the main idea is to use the mechanical stimuli already present in the implantation site to reversibly switch on/off the release of the antimicrobial agent.

For this purpose, polypropylene mesh material is used as the substrate and the antibacterial coating consists in a multilayer plasma polymer system and a silver nanoparticles reservoir (**Figure 0-1**). Silver nanoparticles as silver ions source are used as the antibacterial agent. System is designed to release only silver in an ionic form, since studies have shown that silver nanoparticles may induce cytotoxicity when in contact with human cells [22]. Tailoring of the release of silver ions is achieved by mechanical stimulation of the designed material and these results are presented in terms of elongation-dependent release measurements. Results show that taking advantages of different mechanical properties between the different layers, cracks are induced under elongation in the plasma polymer overlayer. The diffusion of silver ions through the plasma overlayer is switched on/off by tuning the mechanical stretching and thereby opening and closing cracks. Antibacterial properties and efficiency of open/close crack system of the material are verified. Bacterial colonization and biofilm formation on the developed systems are studied.

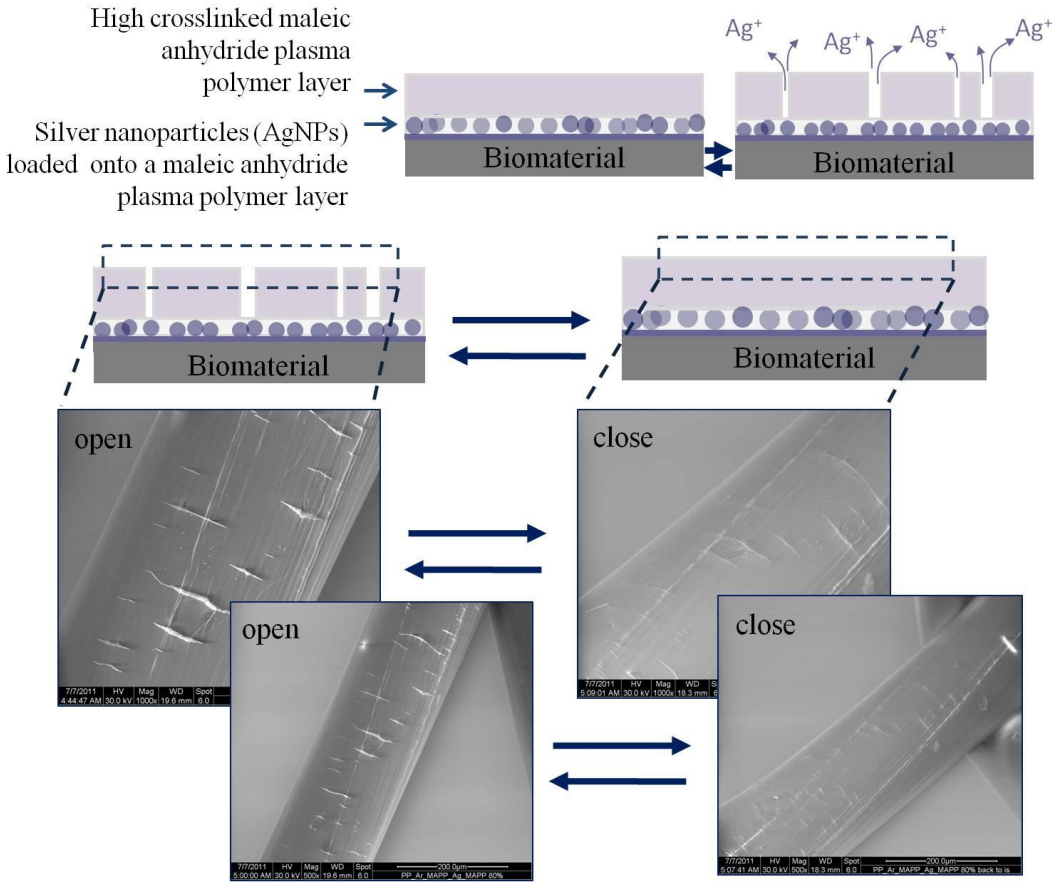

Figure 0-1: Plasma multilayer system consisted of two plasma polymer layers and silver nanoparticles reservoir.

This thesis consists of four chapters:

The first chapter is a literature review on the relevant concepts of this work: biofilm growth and development (**Figure 0-2**), implant-related infections, preventive applications used nowadays and research strategies. Focus is put on antibacterial polymers and antibacterial surfaces. Nanosilver as a product for biomedical use is also described. Plasma polymerization is introduced, as method for deposition of thin layer.

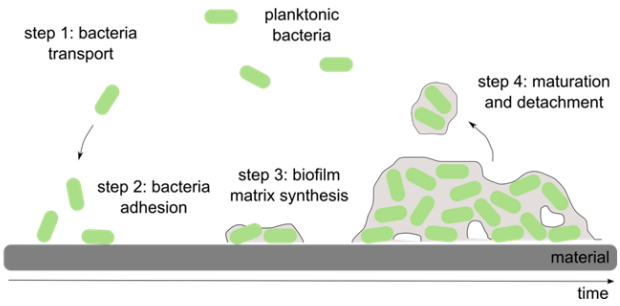

Figure 0-2: Biofilm formation process. Illustration from Ploux *et al.* [23].

The second chapter describes the polypropylene mesh used and the different steps for elaborating the antimicrobial multilayer plasma system. It consists of a first plasma polymer layer, which is enriched in silver nanoparticles and covered with a second plasma polymer overlayer (**Figure 0-1**). Effect of different crosslink densities in the overlayer on the release properties is studied. Then, the release of the active agent in a controlled way through the presence of mechanically reversible fragmentations in the top-layer is discussed. For example, the possibility to reversibly switch on/off the release of Ag^+ ions is shown in **Figure 0-3**.

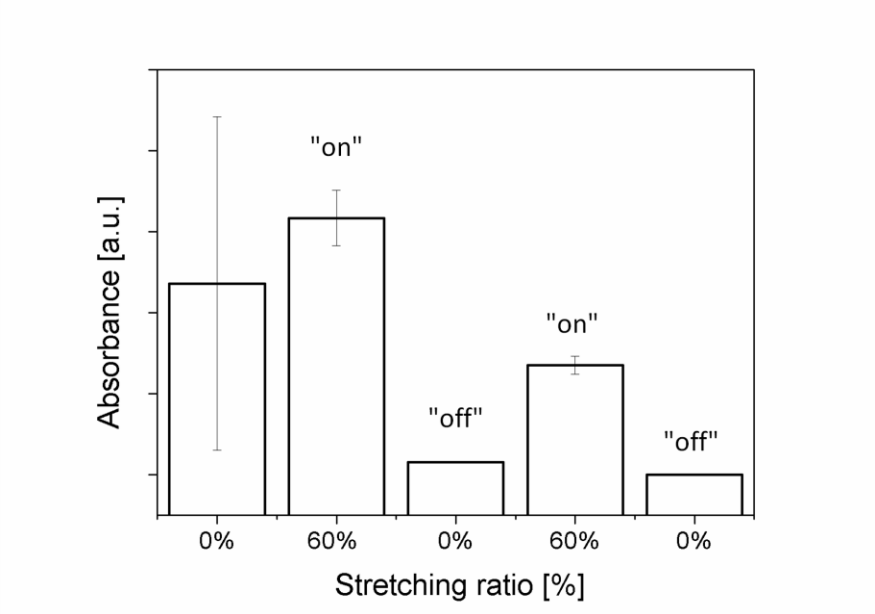

Figure 0-3: Release of Ag species followed by UV-Vis spectroscopy sample during elongation (60%) /retraction (0%) cycles (100% of elongation means twice the initial length).

The third chapter describes the influence of sterilization procedures on plasma-deposited thin films. This topic is very rarely discussed in literature. Due to a growing interest of using maleic anhydride plasma polymer-based coatings for biomedical application, there is a need to investigate the impact of different types of sterilization on the properties of such surfaces. In this chapter, we examine the effects of autoclaving and electron beam sterilization on surface chemistry and the impact on the cracks formation.

Finally, the fourth chapter focus is put on antibacterial properties of the material. We discuss the impact of the material properties on planktonic bacteria and show that, taking advantage of open/close cracks systems, it is possible to modulate the colonization of the implant by bacteria (**Figure 0-4**). We discuss the changes in biofilm structure triggered by small doses of silver. At the end, a general conclusion is given with some ideas for future works.

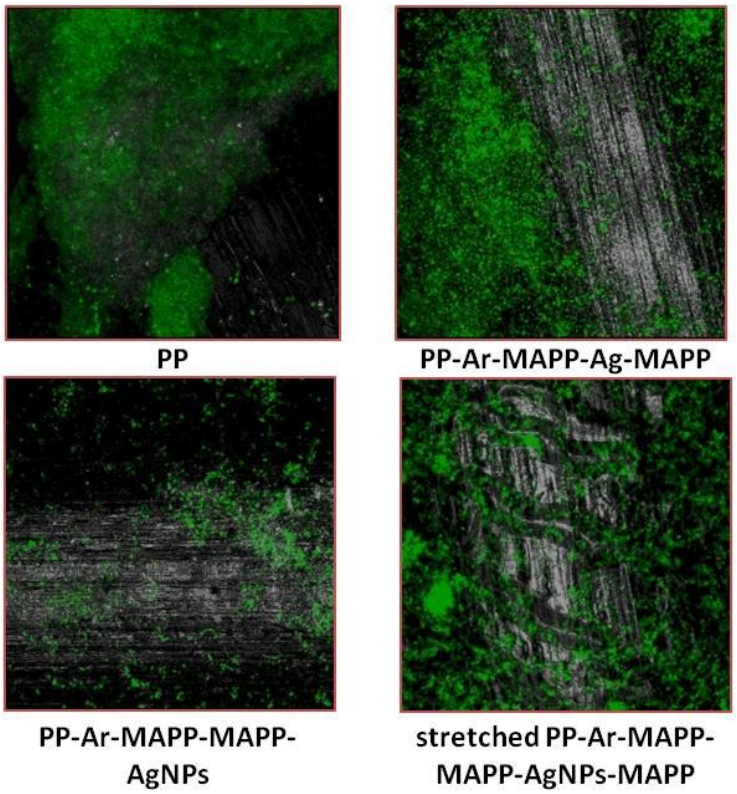

Figure 0-4: Biofilm formation study of *E. coli* SCC1 bacteria, conducted on the neat polypropylene and plasma/silver nanoparticles-modified surfaces. Typical images illustrating differences in biofilm quantity after 168 hours of incubation in static conditions.

CHAPTER I

1 Bibliographic synthesis

1.1 Biofilm and associated infections

1.1.1 Biofilm

Biofilms are very complex ecosystems consisting of microorganisms attached to the surface and enclosed in polysaccharide matrix, generally defined as “microbial cells immobilized in a matrix of extracellular polymers acting as an independent functioning ecosystem, homeostatically regulated” [24]. Aside from microbial components and depending on the surface composition and its environment, non-cellular materials like minerals, crystals, corrosion particles, clay particles, blood components may also be found in the polymer matrix. For example, in natural environments, biofilms are very complex due to the high variety of species in an ecosystem [25]. On the other hand, on medical devices, they may be simpler and be composed of a single species, for example coccoid or rod-shape organisms [25].

Biofilms play a role in a variety of industrial and medical environments. They have beneficial contribution in the wastewater treatment plants, denitrification of the drinking water, hazardous xenobiotic detoxification, heavy metal removal from the contaminated waters [26, 27]. They protect the plants against soil borne diseases, improve crop productivity by regulating nutrient and water flow across the roots [28] and stimulate plant growth under salt stress [29]. They can improve the physico-chemical characteristics of the soils [28]. In aquatic

industrial environments, biofilms cause corrosion, reduce heat transfer, liberate noxious gases, and can serve as a reservoir for pathogens [30]. Biofilms also naturally occur in the human body such as dental plaque [31] or in intestine [32]. Unbeneficial existence of biofilms include for example periodontal diseases associated with caries and infections of urogenital systems [33].

Because biofilm formation and device-related infections are an issue of growing importance in our daily life, the understanding of biofilm growth mechanisms and factors that influence this process are essential.

1.1.2 How does biofilm grow?

Formation of biofilm and its maturation is a multistage process and is dependent on a number of variables. The environment conditions such as temperature, humidity, pH of medium, atmospheric conditions, nutrition conditions have a strong influence on the biofilm development [34]. The type of microorganism and the nature of surface on which the attachment starts plays also a crucial role [35].

Classical biofilm formation is described in [23]. It starts with surface conditioning by the medium (protein, ions etc.). This process can strongly modify surface properties and therefore influence biofilm formation. Further, the transport of bacteria from the medium to the surface occurs (**Figure 1-1, step 1**) and is followed by the bacterial adhesion (**Figure 1-1, step 2**).

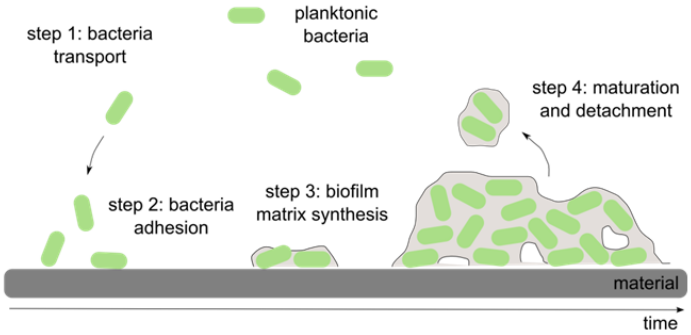

Figure 1-1: Biofilm formation process. Illustration from *Ploux et al.* [23].

Factors that influence planktonic process are the gravitational (sedimentation), hydrodynamic (fluid flow, cell mobility), thermodynamic forces (Brownian motion), Van der Waals forces, electrical double layer forces and also steric hindrance, temperature. Brownian motion plays a major role in the diffusive transport closer to the surface of material. When bacterium is close enough to the surface, with a distance depending on the compositions of cell surface, substrate and environmental medium, direct interactions take place between cell surface and the substrate through attractive and repulsive forces (Van der Waals and double layer interactions). When cell attaches to the substrate, the distance is less than 1.5 nm. Then, the strength of the attachment is governed by short range interactions (hydrogen bonding, Van der Waals forces, electrostatic, ionic and dipole interactions [36]), which provokes the resistance to detachment [37, 38]. Bacterial adhesion is then qualified as irreversible. Irreversible adhesion can be strengthened when bacteria express adhesion proteins like curli or fimbriae to enhance the possibility of adhesion on the surfaces.

The reversible part of bacterial adhesion can be described as a physico-chemical process [39-41] using the Derjaguin-Landau-Verwey-Overbeek

(DLVO) theory [42]. In this approach the bacterial cells are considered as colloids and only physicochemical parameters as surface tension, surface charge are considered to explain adhesion. It is now well accepted in the literature that this vision is too simple to completely describe the process and studies have shown the influence of other important parameters such as surface wetness [43], local pH variation [44], and osmolarity variation [45].

The third part of biofilm development (**Figure 1-1**, **step 3**) starts when bacteria develop intercellular connections and polymeric matrix [46-48]. The growth of biofilm continues and colonies are spreading until biofilm structures become complex and contain several layers of microorganisms [49]. Microorganisms are producing extracellular polymer substances (EPS) [46], which contain nutrients, surfactants, proteins, nucleic acids, lipids and polysaccharides (colonic acid, alginate, dextran, chitosan) [50]. Microbial cells are enclosed in this complex matrix. EPS influence the adhesion of microbial biofilm to the surface and play for bacteria a role as a protective matrix from the environment [51]. At this step of development, coagregation can also occur. This is a process of cell to cell adherence [52] which can be highly specific and governs the development of multi species biofilms in many different environments (e.g. dental plaque [53] urogenital systems [54]).

The last step of biofilm development is the detachment of biofilm parts and the release of free bacteria (**Figure 1-1, step 4**). This process can be enhanced by survival mechanisms caused for example in response to stresses like a lack of nutrition [55]. It promotes the genetic diversity of bacteria in biofilms due to cell communication by gene transfer [56]. It has also important implications on medical aspects and public health due to increased resistance against antibiotics or antimicrobial agents and the host immune system attacks of biofilm-associated infections [46].

Finally, biofilms can reach a thickness of several tens of micrometers. For example the thickness of the biofilm recovered from indwelling bladders catheters was varied between 3 and 490 µm [57]. They have high stability and can have high species diversity. Bacteria in mature biofilm show unique physiological characteristics that are significantly different from planktonic cultured phenotypes [58]. Microbial gene expression is altered in biofilm. For example Sauer *et al*. [58] used gene analysis together with protein identification to observe changes in biofilm physiology of biofilm-grown populations. They observed that the average difference in detectable protein regulation between each of the five stages of development was 35% (approximately 525 proteins). Additionally, when planktonic cells were compared with maturation stage of biofilm cells, more than 800 proteins were shown to have a sixfold or greater change in expression level. Brozel *et al*. [59] have shown global gene expression changes in attached *Pseudomonas aeruginosa* cells and found more than 11 proteins whose levels were altered during various stages of attachment. Microbial cells in biofilm are also able to communicate by gene transfer [56] and by secretion of diffusible signaling molecules through a biochemical system which is known as Quorum Sensing [60, 61]. As a result, biofilms offer bacteria an increased resistance against antimicrobial agents (antibiotics, detergents), host immune system attacks and unfavorable environmental conditions.

1.1.3 Methods of characterization of biofilm

As mentioned before, biofilms are complex systems, which are highly hydrated and consist of many microorganisms. A classical method to characterize biofilm is the visualization under electron microscopy. In this case biofilm often needs a dehydratation step with various graded solvents [62]. This process distorts the real thickness of biofilm and creates artefacts in the structure determination

[62]. Another possibility is the use of specific stains. For example, after labeling of matrix [63], the nature of polysaccharides in biofilms and their association with the cells can be investigated using high magnification transmission electron microscopy (TEM) [62]. But here again, it is needed to dry samples which also cause modifications in biofilms characteristics.

The aforementioned disadvantages have been overcome with the development of Confocal Laser Scanning Microscopy (CLSM) and Epifluorescence Microscopy. After staining procedure, the examination of biofilm can be determined in the native, liquid environments, with the possibility of investigation of both its structure and its dimensions [62, 64]. The possibility of inserting genes expressing fluorescent proteins, like green fluorescent protein (GFP), in the genome of bacteria have also been developed. In this approach, bacteria produce fluorescent molecules either constantly or initiated by antibiotics for instance [65-67], allowing the observations of living bacteria. This approach allows following the biofilm development together with metabolic state of bacterial cells.

In general, images obtained by CLSM, can be treated and analyzed by a large number of specific or unspecific softwares (CellC [68], ImageJ [69] for example). For treatment of three-dimensional biofilm image stacks obtained by CLSM microscopy novel computer programs such as Comstat [70], Comstat2 [70, 71] or bioImage_L [72] have been specifically developed. Their use allows to describe the structural organization of microbial communities by the quantification of mean biofilm thickness and substratum coverage for example. Comstat and Comstat2 also provide parameters like roughness and surface to biovolume ratio [70-72].

Aside from the aforementioned methods of biofilm visualization, it is possible to measure the total biomass (i.e. the quantity of microbial cells in the biofilm) accumulation by optical measurements after adequate staining with crystal

violet. Total amount of proteins or staining intensity of bacteria is assessed by measurements of the absorbance at 490 nm or examination by bright light optical microscopy directly on surfaces [73, 74] or after detaching bacteria from the surface by sonication, vortexing or with a brush or a swab [62]. In the second case, cells are then plated and counted [62, 75, 76]. However, with this method the modification of the biofilm characteristics are possible. In this approach, it is also possible to weight the detached bacteria and thus determine the biomass with, however, a weak sensitivity of measurements. These techniques are usually used for characterization and quantification of biofilms formed on infected implants [62]. The disadvantages of this method are the modification of biofilm characteristics and the absence of information about localization of bacteria on the implant. However, localization of bacteria on the implant surface can be crucial in case of studies on complex surfaces, for example polymeric meshes, due to the existence of preferable areas of bacterial adhesion on implant surface [77]. Additionally, information about architecture of the biofilms cannot be retrieved using these methods of biofilm investigation.

1.1.4 Biofilms- related infections on biomaterials

1.1.4.1 Introduction to biomaterials

Use of biomaterials dates as far as ancient civilizations: Artificial noses, ears or teeth were found in Egyptian's mummies [78]. Through the centuries advancement, using artificial materials to replace or restore body functions of degenerated tissues or to assist in healing is progressing. Surgical techniques and sterilization methods now allow the use of biomaterials in many biomedical applications [79]. Biomaterials in form of sutures, bone implant, vascular graft, heart valves, lenses or dental implants are used nowadays [79]. In spite of the

prefix bio- which is usually related to life or living objects, the use of prefix bio- in biomaterial implies that the material derives from life or is beneficial for life [80]. The consensus in definition of biomaterial was firstly achieved on Consensus Conference on Definitions in Biomaterials Science, in 1987, by the European Society for Biomaterials [80]. Biomaterial was then defined as 'a *non viable material used in a medical device, intended to interact with biological systems*'. However, further debates on this subject took place few years later. The expression "*non viable*" was removed from the definition [81]. Finally, in 1999, the definition of biomaterial was established as "*a material intended to interface with biological systems to evaluate, treat, augment or replace any tissue, organ or function of the body*" [81]. Under further developments of new types of substances and medical technologies, in 2009, Williams [81] suggested to redefine the biomaterial definition as "*a substance that has been engineered to take a form which, alone or as part of a complex system, is used to direct, by control of interactions with components of living systems, the course of any therapeutic or diagnostic procedure, in human or veterinary medicine*".

Biomaterials are chosen based on their properties, to match them with the surrounding tissues. The choice of biomaterial based on its ability to match with the host tissue is essential to produce the desired tissue remodeling. Considering the structural or mechanical compatibility with tissues, metals are often chosen for hard tissue applications and polymers for soft tissue applications. Commonly used low modulus materials are polymers, mainly polypropylene (PP), polyethylene (PE), polyurethane (PUE), poly(methyl methacrylate) (PMMA), polyethylene(terephthalate) (PET), poly(tetrafluoroethylene) (PTFE), hydrogels and some biodegradable polymers such as polyglycolide acid (PGA), polylactic acid (PLA). Their advantages are the large variety of chemical compositions, properties and forms such as solids, gels, films, fibers and the easiness of polymer fabrication into complex shape

and structures (see **Figure 1-2**). Disadvantages of polymers as biomaterials are their low resistance against sterilization processes (ethylene oxide, gamma irradiation, electron beam irradiation) and insufficient mechanical properties to use them as orthopedic implants. These disadvantages are overcome by using metallic implants such as stainless steel, titanium or titanium alloys, tantalum, or gold [79, 82]. These materials have high mechanical strength, resistance and they are very stiff. However, mismatch of stiffness between bone and metallic implant is often causing implant loosening. Other disadvantages of metals as biomaterials are insufficient biocompatibility and tendency to corrode, or provoke allergic tissue reactions due to release of metal ions [79, 82]. These disadvantages can be overcome by the use of bioceramic materials such as diamond like carbon, alumina, zirconia, hydroxyapatites and bioglasses. These materials are biocompatible and resistant to corrosion. Some properties of bioceramic materials, which are similar to human bones in terms of mineral composition, make this material especially adequate for bone implants. In addition, bioceramics are resistant to various methods of sterilizations. Another type of biomaterials is composite materials. They consist of mixture of above mentioned monolithic materials, for example metal-polymer composites or hydroxyapatite-polymer composite for bone tissue replacement. Controlling the volume fractions and local arrangements of the reinforcement phase, it is possible to design materials with appropriate structures and to tailor the properties to suit the requirements of mechanical properties for the material. It is concluded by Ramakrishna *et al*. [79] that composite materials offer greater potential of structural biocompatibility than the homogenous monolithic materials.

In case of biomaterials for abdominal wall reconstruction, pelvic floor reconstruction and stress urinary incontinence treatment, the use of polymeric meshes is accepted. Biomaterials in this case should be resistant, have good tissue tolerance, be easily manipulated, flexible, and elastic in more than one

dimension. They should correspond to tissue dynamics as closely as possible and should resist degradation over time [83]. However, the resistance to the infection should be improved in case of polymeric meshes biomaterials. Therefore, composite materials associating polymer and antibacterial agent which would prevent infection on the site, should be a good perspective.

In conclusion, physical, chemical and mechanical properties have all to be considered for determining the most appropriate biomaterial for a specific application. However, additional factors must also be taken into account, e.g. bio-integration, biocompatibility and capacity to resist to biomaterial-related infections. For this reason, to develop a composite material made of polymer which provides desired mechanical characteristics corresponding to surrounded tissue dynamics and an antibacterial agent e.g. silver nanoparticles would be a promising strategy for mesh implants.

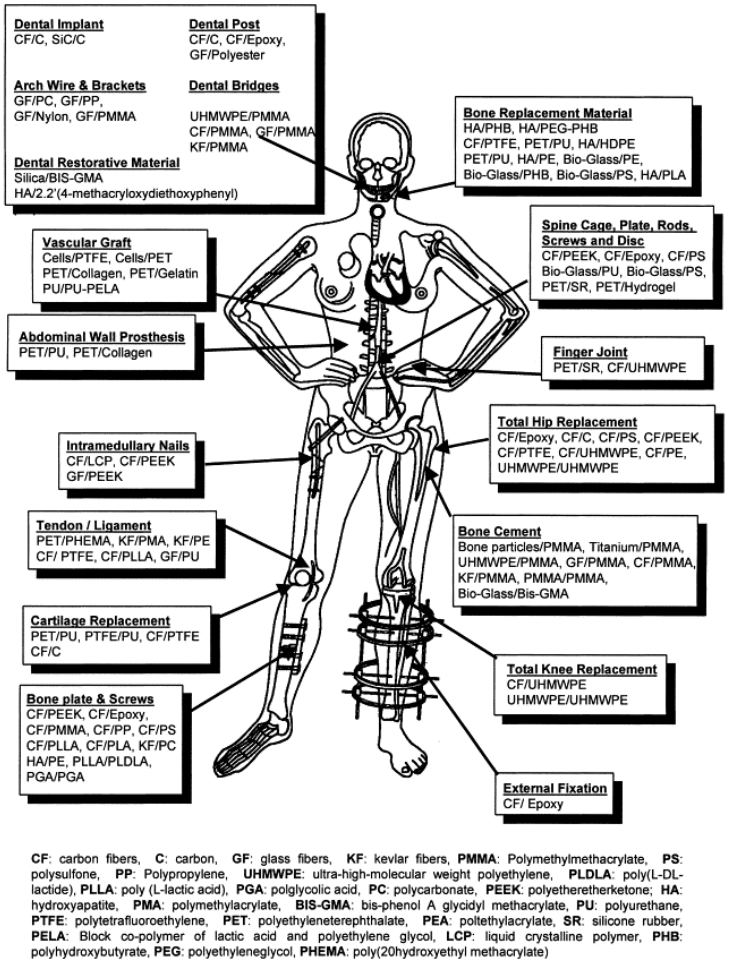

Figure 1-2: Various applications of polymer biomaterials as implants. Illustration from Ramakrishna *et al.* [79].

1.1.4.2 Biomaterial-related infections

Infections are the most common and serious cause of postoperative complications in patients surgically-treated with implants. Infections associated with surgical implants are generally difficult to cure and have a larger adverse impact on quality of life [84-86]. Common sites of primary infection are the mouth (through bleeding gums), catheter entries (such as the subvenous catheter), and implanted medical devices (such as an artificial hip joint) (**Figure**

1-3) [87]. Infections of urinary and vascular catheters then account for the majority of device-related infections. Once bacteria enter the circulatory system, they can reach all parts of the body and cause secondary infections. Their most common sites include brain, kidneys, intervertebral spaces, and bones around implanted medical devices.

Microorganisms which cause contaminations and infections after surgical procedures can be residents of already existing infections in the patient body (appendicitis, deep organ abscesses). They also often originate from the patient's skin [88] or can come from the hospital environment. In these last cases, adhesion of bacteria to biomaterial surfaces is usually initiated at the place where biomaterial touches the skin [89] or other hospital strains [90]. The origin of infection is then related to inadequate cleaning of the patient before the operation, inadequate care of decontamination of operated area or inadequate care of operated tissue after surgery. Common skin pathogens like staphylococci (*Staphylococcus epidermidis and Staphylococcus aureus)* are frequently detected microorganisms in device-related infections [89, 91]. Other environmental pathogens detected on infected implants are *E.coli, Pseudosomonas, Klebsiella, Enterobacter, Bacteroides, Candida albicans* [92].

In this context, biofilms formed in later stages of infection protect bacterial cells against defensive mechanisms of the host organism, hamper phagocytosis, cause disturbances in chemotaxis and reduce antibiotic and antibody penetration. Furthermore, when multi-species biofilm are formed on biomaterials, [46] interspecies transfer of antimicrobial resistance traits, symbiotic interactions and sequential colonization patterns can enhance the virulence of the infection [93].

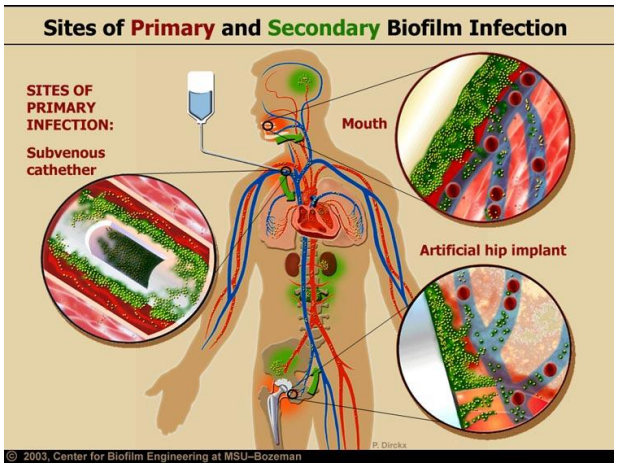

Figure 1-3: Three examples of the many possible points of entry for bacteria are shown here, along with common areas of secondary infection (highlighted in green). Adapted from Center of Biofilm Engineering, with permission from the authors.

Aside from the consequences related to infections, the presence of biofilm can lead to implant biodegradation. This is potentially the case with polymeric biomaterials, which can lose their functionality due to this process [94]. Factors that influence the rate of degradation are pH, environment, oxygen, salts, redox potential and temperature. The exoenzymes from microorganisms may accelerate material degradation by breaking down complex polymers yielding smaller molecules or short chains e.g., oligomers, dimers and monomers, that are the molecules small enough to pass the semi-permeable outer bacterial membranes and be utilized as a carbon and energy sources [95].

The cost of treating device-related infections is generally high and together with long term antibiotic treatment, prolonged operation times, size of the operated area and surgical techniques applied, put at risk patient health. For these reasons, there is a growing interest in the field of biomaterial-related research to provide new coatings and/or materials able to prevent bacterial adhesion and biofilm formation [96, 97].

1.2 Inhibition of biofilm formation and prevention of related infections

1.2.1 Prevention of biofilm formation

Prevention of biofilm formation is necessary because it is almost impossible to remove biofilm without removing the implant from patient. However, the technique that is able to fully prevent or control the formation of unwanted biofilm without causing side effects is not known so far. Another problem is the accurate diagnosis. Infection can be suspected based on clinical observations like swelling, warmth, erythema, tenderness or microbiological data (positive culture blood culture in a patient with prosthetic heart valve, imaging findings such as echocardiogram). Also advanced imaging studies (e.g., computed tomography, magnetic resonance imaging or nuclear scans) can be helpful in diagnosis of inflammatory post-surgical changes [98]. Hence, the implant-related infections can be distinguished and confirmed only upon surgical exploration. Because this approach compromises the health of patient, different preventive strategies are used. They are listed below.

1.2.1.1 Cleaning

To prevent biofilm formation a thorough cleaning is need using water, oxidizers, enzymatic products or detergents, which weakens the physical stability of the biofilm, making it easier to remove by brushing, flashing or other physical treatment [99-101]. An effective cleaning procedure break up or dissolve EPS matrix of biofilm, allowing the disinfectants to gain access to bacterial cells [102]. Efficient cleaning process can remove up to 90% of microorganisms from

the surface, but it is not efficient enough to kill them [99]. Additionally, it may not be appropriate for medical devices e.g. porous materials since disinfectant can be absorbed and the residuals can irritate the tissues after implantation [101]. Therefore, other methods are necessary (e.g., sterilization) to inhibit bacterial development on biomaterials.

1.2.1.2 Sterilization

Sterilization is a process that destroys or eliminates all forms of microbial life and is carried out in health-care facilities by physical or chemical methods [101]. Sterilization of biomaterials is needed due to exposure of these materials to microorganisms during the production step. The current methods include dry heating, autoclaving, irradiation (Gamma ray or Electron beam) and gaseous chemicals (**Figure 1-4**). The dry heat and autoclaving in high temperature (120-180°C) and high pressure (100 kPa) sterilization methods are efficient, but the exposure of material to these conditions, especially polymeric material, may induce changes in material properties e.g., mechanical, chemical and structural changes [103-105]. In case of hydrophilic polymers, using heat and steam as methods of sterilization render the implant mechanically weaker [106] or less biocompatible [107].

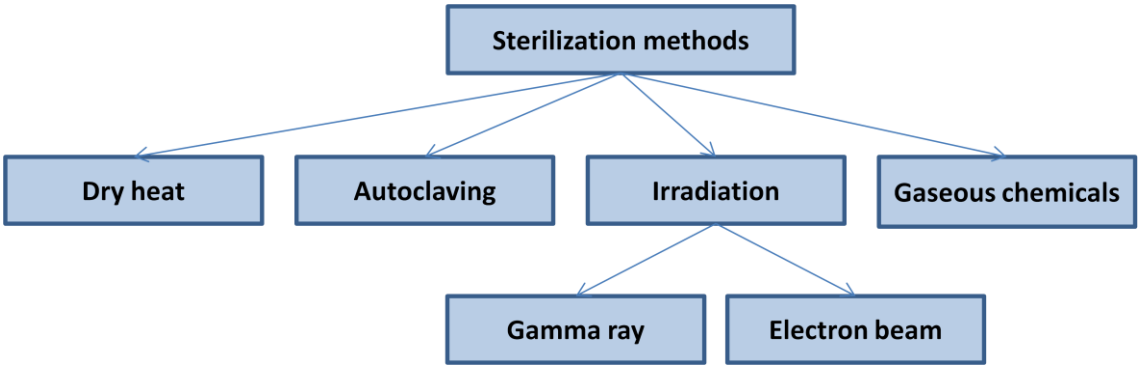

Figure 1-4 Sterilization methods used for biomedical polymers [94].

The use of ethylene oxide gas as a sterilization method is widely applied in the medical device industry and in hospitals especially for polymer materials. Ethylene oxide gas is used as a sterilizing agent due to its capability of efficiently killing all the species and forms of micro-organisms in a short time. Ethylene Oxide is bactericidal, virucidal, and sporicidal [108]. The advantage of this method of sterilization is its compatibility with majority of plastic materials. The process depends on few parameters which include relative humidity, ethylene oxide concentration, temperature, pressure changes and time of exposure. It may include as well preconditioning, post cycle aeration and humidification. Limiting factors of this type of sterilization are toxic residuals which can be detected in for example polyurethane (PU 75D, PU 80A) and polyamide materials [109]. Other sterilizing agents include hydrogen/peroxide/plasma, glutaraldehyde, steam formaldehyde, paracetic acid, chlorine dioxide and ozone [101].

In the case of irradiation, gamma ray and electron beam are the two mainly-used techniques. These methods have been used for a number of medical products such as tissue for transplantation, pharmaceuticals and medical devices [101]. These sterilization techniques are based on the penetrating ability, and short processing time to deliver required doses. It is one of the most cost effective solutions for sterilizing medical devices. Sterilization with Cobalt-66 irradiation is ideal for medical products such as surgical sutures and drapes, metallic bone implants, knee and hip prostheses, and syringes [110]. A variety of polymeric materials (polyethylene, polyesters, polystyrene, polysulfones and polycarbonate) can be sterilized by this method [110]. Comparing to gamma rays, electron beams have a considerable less penetrating ability [110]. The factor, which has to be considered using irradiation, is the dose. The most commonly validated dose used to sterilize medical devices is 25 kGy [110]. High energy dose e.g. 500 kGy in case of polyester polymers can initiate degradation, dimerization of a polymer [111, 112]. Irradiation can cause

changes in structure of material, oxidation, delamination and cracking in material [111, 113, 114]. Other modifications can take place such as cross-linking [115], branching and degradation of additives often used in medical polymers [116]. These processes may cause decrease in stability, promote the release of volatile fractions and cause toxicity [116, 117].

As previously mentioned, electron beam irradiation induces crosslinking in polymers. This can be used to improve the properties of a final product by improving tensile and impact strength and chemical resistance through irradiation. In case of plasma polymers, by choosing the level of e-beam exposure, irradiation can advantageously influence the mechanical properties of plasma polymers.

These approaches which are physical and chemical treatments applied directly on material surfaces decrease the possibility of contamination. Other ways to reduce the possibility of biofilm formation and avoid the degradation of material are antibiotic treatments applied to patient.

1.2.1.3 Antimicrobial therapies

Antimicrobial approaches are used to prevent implant-associated infections by decreasing bacterial adherence to the implant surface and/or reducing the concentration of bacteria in the immediate vicinity of the implant. These approaches are applied after placement of surgical implant [118]. Systemic antibiotic prophylaxis provides protection from organisms which disseminate through bloodstream from a different site that the site of surgery [119]. However, biofilms are often resistant to antibiotic treatment due to low antibiotic penetration into biofilm matrix because of sorption to or reaction with the components of biofilm matrix [51, 120]. Additional protection from implant associated infections is local application of antimicrobial agents (antibiotics or antiseptics). It provides higher drug concentration at the crucial implantation site

[118]. Antimicrobial agents on the skin (skin antisepsis), irrigation of the surgical wound [121] or dipping of surgical implant before implantation in antimicrobial solution are strategies applied for that purpose [118, 122]. These strategies have been shown to be efficient in practical cases. For example, dipping the implant in the antimicrobial solution reduces bacterial adherence to the implant surface and/or minimizes the concentration of bacteria in the immediate vicinity of the implant [123]. However, analysis of the existing clinical practices indicates that, although some antimicrobial strategies constitute the standard of care for preventing infections associated with surgical implants, such strategies are applied based on clinical experience, often in “nonstandardized fashion and without clear evidence of clinical efficacy” [124]. Furthermore, the consequence of antibiotic and other antimicrobial therapies, systematically and in high doses, is the reason of dramatic increase of bacterial resistance [125]. Therefore, these treatments should be limited.

In conclusion there is a need of a new approach based on local delivery (at the implant location) of antibacterial agent. For example, antibacterial agent delivered in a control way from the implant surface to the environment is a promising approach. Control release would also allow to prolong the lifetime of an implant with antibacterial properties.

1.2.2 Research strategies of development of new antimicrobial polymer materials

Polymeric materials offer great possibilities in the materials design and properties. Antibacterial (i.e., preventive and bactericidal) properties can be obtained through various strategies. From the exploitation of intrinsic properties of a material or a coating surface, the most common strategies for the incorporation of biocidal agent in the material possibly leading to the release of

the agent, are presented below. In the first part of this section, the influences of topography, chemistry and mechanical properties of the surface on bacterial adhesion and bacterial colonization are described as potential ways to provide bacterial colonization preventive properties to the material. In the second part, antibacterial strategies based either on the release of bioactive agent or on the contact-active principle are shown (**Figure 1-5**).

Contact active polymers exhibit biocidal action through contact with bacteria [126, 127] (**Figure 1-7 a**). For inert polymers, surface modifications such as chemical grafting [128, 129], layer-by-layer deposition [130, 131] or plasma polymerization [132] can render polymer surface able to exhibit contact active antibacterial properties (**Figure 1-7 b**) for example by preventing bacterial attachment [133].

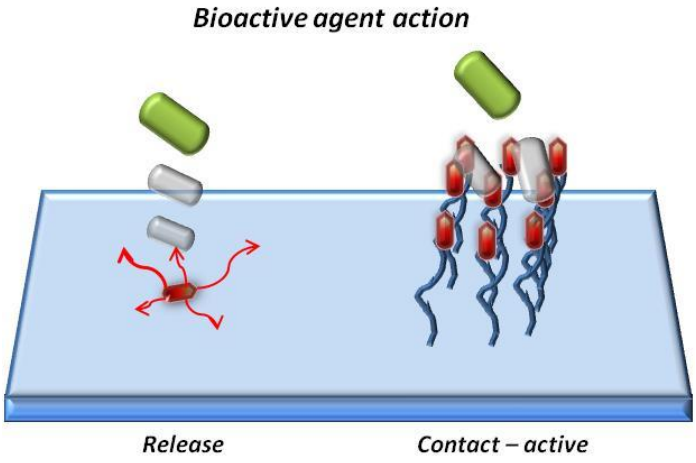

Figure 1-5: Principles for antibacterial properties of polymers through, releasing or contact-active principle.

1.2.2.1 Influence of the surface properties on bacterial adhesion

The material surface properties are crucial factors that influence the process of biofilm formation. They are therefore relevant candidates for controlling the bacterial adhesion preventive properties of a material. Surface topography and surface chemistry are considered the parameters the best known for their action on bacterial adhesion. Other rarely mentioned parameters are mechanical properties, which can as well have a strong impact on bacterial adhesion.

1.2.2.1.1 Surface topography

In spite of numerous studies in the literature, the exact mechanisms of the impact of topographical features on bacterial adhesion and biofilm formation are still poorly understood. Reviews on this subject have been published [23, 134]. Usually it is considered that the size and orientation of topographical features, can influence the arrangement and the resulting behavior of cells on the surfaces and may affect biofilm development [135]. However, several studies suggested that the influence of surface roughness is much less important than chemistry of the surface [136-138]. Additionally, it should be noted that the importance of the surface topography in bacterial behavior on the surface, especially bacterial localization according to topographical features, is often overvalued, due to observations realized in non-aqueous condition of culture [134, 135].

Bacterial responses to topographical features of surface are species and strain depended [134]. However, some general trends have been highlighted. Bacterial responses to surface topography with surface features higher that bacterial cell size are supposed to be similar to smooth surfaces, except that transport of bacteria to the surface can be modified due to the topographical features. Furthermore, preferential bacterial adhesion at the bottom of surface

crevices has been demonstrated for concave features with sizes similar or higher than bacterial size [139]. However, considering feature size, shape, distance between features has not been taken under consideration. Several works have also demonstrated that greatest bacterial cell retention occurred on material roughness R_a value close to bacterial size (e.g., 0.9 µm of Ra for 1 µm diameter) [140-142], suggesting that bacteria preferentially adhere on or are retained in features with similar sizes. This result is illustrated in **Figure 1-6**. When the characteristic dimensions of confined spaces approach those of bacterial cells, their interactions with surface change. This would be due to the contact area between cell and substratum, which is greater, enhancing therefore binding energy and the propensity for the microorganisms to be retained on the surface [140]. Then, tuning the periodicity of structures within relevant cellular scale, lead to distinctive differences in bacterial assembly [135], but roughness and surface topographical features do not always result in bacterial localization or alignment on the surface, especially when topographical features are at the nanometric scale [134, 143]. Nevertheless, it has been proposed, and recently showed, that macromolecular structures of the bacterial cell wall, such as flagella or pili, may allow bacteria to sense and/or attach to topographical features of nanometric size [144].

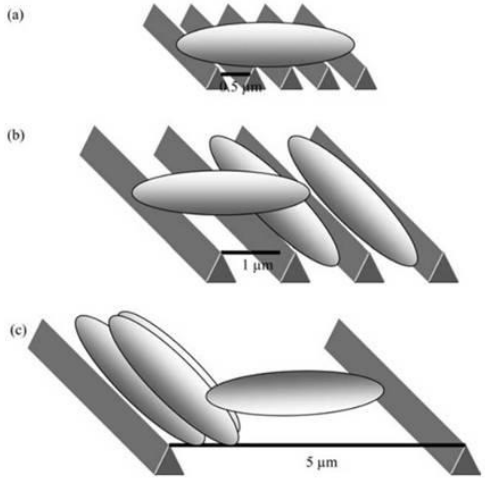

Figure 1-6 The shape of surface features is important in determining the number of cells retained at any directionality. A) surface grooves close together; b) surface grooves of microbial size; c) wider than cell size surface features. Illustration adapted from ref. [140]

Experimentally, influence of nanotopography has been demonstrated. For example the statistical difference in initial deposition rate of bacteria was observed on surfaces modified at a nanoscale level (unworn and overworn contact lenses), where the surface roughness R_a was equal to 4 nm and 10 nm respectively [145]. Correlation between surface nanoroughness and bacterial adhesion was shown by Bakker *et al.* [146] using linear regression analysis. Their results showed positive relation between mean surface nanoroughness (which ranges from 2.3 nm up to 12.9 nm) and the deposition of micron-sized bacteria. Results of Mitik-Dineva [147] have shown an influence of small topographical changes of etched glass surfaces on bacterial adhesion. Contrarily to so far mentioned studies, decrease of surface roughness R_a of 1 nm after etching, resulted in increase in the number of attached bacteria. Surface nanotopographical features influence on bacterial adhesion and cell orientation was also studied by Ploux *et al*. [148]. In this study, surface consisting of 160 nm period modulation and 50 nm deep grooves were

prepared by plasma polymerization and UV-Irradiation. Authors observed statistically significant higher number of adherent bacteria on patterned surface. However in case of bacterial cell orientation, these surface grooves had no influence. Authors suggested that this can be explained by small depth and the sharpness of the grooves, which could prevented energetically favorable cell-surface binding [148].

1.2.2.1.2 Surface chemistry

Chemistry of the material surface have been already shown to have influence on the bacterial adhesion. In particular, parameters such as surface hydrophobicity and charge are influencing bacterial adhesion.

In the study of Tegoulia *et al.* [149], bacterial adhesion of *S. aureus* was studied on self-assembled monolayers (SAMs). These surfaces had methyl, hydroxyl carboxylic acid and tri(ethylene oxide) terminated groups. Authors observed that bacteria adhered the most to carboxylic acid and methyl terminated surfaces. The lowest adhesion of bacteria was observed in case of tri(ethylene oxide) surfaces. Authors suggested that stable interfacial water layer on the material surface, may play a role in this case, preventing from direct contact between bacteria and surface. Park *et al*. [150] studied bacterial adhesion using *S. epidermidis* and *E. coli*, on polyurethane (PU) surface which was modified with poly(ethylene glycol) (PEG) (mol. wt. 1000, PEG1k) with terminated hydroxyl, amino and sulfonate groups, poly(ethylene glycol) (mol. wt. 3350, PEG3.4k) and PEG3.4k-Heparin, respectively. Inhibition of bacterial adhesion was observed for surfaces modified with PEG1k-SO3, PEG3.4k and PEG3.4k-heparin. These results were correlated with the increase of hydrophilic character of the surface. Decrease of bacterial adhesion related to increase of hydrophilic character of the surfaces was also observed in another study [151]. Authors modified surfaces of poly(methyl methacrylate) (PMMA), polystyrene (PS) and silicone

materials with a glycoprotein (structure consisting of a thread-like peptide backbone with densely packed carbohydrate side chains). Bacterial response was studied using *Staphylococcus aureus* and *S. epidermidis.* In this case also, bacterial adhesion was greatly reduced on coated hydrophilic substrates. However, impacts specifically associated to hydrophilic and charge characteristics of the surface are difficult to decouple. For example, Kiremitci-Gumustedereliogl ou [152] have used polymeric biomaterial surfaces such as poly(hydroxyethylmethacrylate) and its copolymers with a series of acrylic monomers—acrylic acid and dimethylaminoethyl methacrylate—polyetherurethane and polypropylene (PP), to study bacterial adhesion. Surfaces had different wettabilities, charges and charge densities. Bacteria used in their study was non-pathogenic and pathogenic strains of *Escherichia coli*. Results showed that uropathogenic strains were greatly adhering to hydrophobic PP surfaces, but most likely not adhering to hydrophilic polymers. However, nonpathogenic *E. coli* strain was showing opposite behavior towards the same surfaces.

In general, studies on influence of charge on bacterial behavior are showing that, positively charged surfaces promote bacterial adhesion and influence biofilm formation due to attractive electrostatic interactions between negatively charged bacteria and positively charged surface. Negatively charged surfaces seems to repel the bacteria probably due to repulsive electrostatic interactions [153-155]. Moreover, this is strongly depending on bacteria strain [156, 157].

Ploux *et al*. [148] have studied bacterial response to surfaces prepared via plasma polymerization and UV-irradiation. Authors showed that surface wettability has not played a role in the bacterial response to the different surfaces. However, they have noticed, that, due to negatively charged UV-treated surfaces, which are rich in $–C(=O)-O^-$ groups, bacterial adhesion was hindered for a part on these surfaces, probably due to electrostatic repulsions between bacteria surface and surface of substrate. In the study of Baikun *et al*.

[158], surface charge of material had less direct influence on bacterial adhesion. However, adhesion of eight strains of bacteria was significantly correlated with total adhesion free energy between bacteria and surface. Studies of Gottenbos *et al.* [153] have studied adhesion of *Staphylococcus aureus*, *Staphylococcus epidermidis*, *Escherichia coli*, *Pseudomonas aeruginosa* on positively charged poly(methacrylate) surface and negatively charged poly(methyl methacrylate) surface. Their results showed that, all bacteria adhered most rapidly to the positively charged surface. However, there was no surface growth of the Gram-negative strains on positively charged surface. On the negatively charged surfaces, bacteria were adhering in a slower manner, but surface growth of the adhering bacteria was exponential for both Gram-positive and Gram-negative strains. These results demonstrate that the influence of surface charge is complex.

Surface chemistry has also been shown to influence biofilm formation. Ploux *et al.* [159] focused on differences in biofilm morphology and long-term variations in growth dynamics of biofilm. By using NH_2 and CH_3 terminated self assembled monolayers (SAM) on silicon wafers, the authors have shown low impact of surface chemistry on quantity of adhered bacteria but a strong impact on biofilm morphology, i.e., spatial distribution of bacteria and kinetics of biofilm formation. Bacteria on CH_3 -terminated surfaces were organized in clusters while bacteria on NH_2 terminated surfaces formed tree-like biofilm morphology. Furthermore, the biofilm detachment was also dependent on the substrate, suggesting that the surface wettability influences the signal controlling the detachment of biofilm parts.

1.2.2.1.3 Surface mechanical properties

As previously mentioned the third crucial parameter that influences bacterial adhesion is mechanical properties of the surface. Few studies have shown the

evidence of the possibility of controlling bacterial adhesion by tailoring the material mechanical properties [160, 161]. Bakker *et al*. [160] were focused on determining the importance of surface tension and elastic modulus on bacterial adhesion. Authors have worked with marine bacterial strains *Halomonas pacifica, Psychrobacter and Marinobacter hydrocarbonoclasticus* and polyurethane coatings deposited on glass. Coatings had different surface tensions values, achieved by changing the amount of fluorine, whereas using more or less branched polymers, different elastic moduli values were obtained. Study was performed under different mass transport conditions, in a parallel plate and stagnation point flow chamber. Results showed that bacterial adhesion in the parallel plate flow chamber was not influenced by the elastic modulus of the coatings. However, influence of surface tension exists predominantly for deposition in the parallel plate flow chamber. Authors concluded that low surface tension bacteria should adhere preferentially to low surface tension surfaces. In case of stagnation point flow chamber, bacteria were adhering in higher numbers to hard surfaces, than to coatings of lower elastic modulus values. High energy collisions in the stagnation point flow chamber were assumed to cause a rebound effect which was due to the dissipation of elastic energy during or after collision. This was the reason for decrease in deposition rates.

Influence of mechanical properties of material surfaces on controlling the adhesion of *Staphylococcus epidermidis* bacteria and its colony growth was studied by Lichter *et al*. [161]. Authors used polyelectrolyte multilayer (PEM) thin films made of poly(allylamine) hydrochloride (PAH) and poly(acrylic acid) (PAA). The chemical functionality and mechanical properties of the films were adjusted by variations of the layer-by-layer assembly conditions (choice of polyanion/polycation) or by changes of pH. Especially the elastic modulus or stiffness values for these polymeric films can be adjusted by manipulation of pH values, independently of physicochemical characteristics. Authors have found

that with increasing elastic modulus values (between 1 MPa and 100 MPa) for the polyelectrolyte multilayered film, the adhesion of *S. epidermidis* and *E. coli* bacteria were increasing. It was shown that *S. epidermidis* exhibits mechanoselective adhesion and authors have proved that this correlation was independent from other surface properties such as posited physicochemical regulators of bacterial adhesion, surface roughness, surface interaction energy and surface charge density. Additionally, it was found that this correlation is not limited to a single type or shape of bacteria. Authors have concluded that mechanical properties of the surface are parameters, which allow to modulate bacterial colonization on the surfaces.

Recently, our group demonstrated for the first time that the surface mechanical properties is an approach to control not only bacterial adhesion but even proliferation of already adhering bacteria [162]. Authors attributed the anti-adhesive effect of surface to visco-elastic properties of oligonucleotide coated surfaces. These surfaces possessed high shear modulus (6.10^5 Pa) and low viscosity (0,0038 kg/m^2). Bacterial number was reduced by a factor 20-fold compared to control.

Influence of surface stiffness on bacterial adhesion was also very recently shown by Saha *et al.* [163]. Authors have prepared polyelectrolyte films from poly(l-lysine) (PLL) and a hyaluronan derivative modified with photoreactive vinylbenzyl groups (HAVB). Further nanomechanical properties of these films were modified by UV light illumination. Bacterial behavior of Gram positive *Lactococcus lactis* and Gram negative *E. coli* was studied on non-cross-linked and cross-linked films. Results showed that *E. coli* exhibited a more rapid growth on non-cross-linked softer films compared to the stiffer ones. However *L. lactis* was shown to grow slowly on both films, independently of their rigidity.

1.2.2.2 Different strategies to achieve antibacterial materials

Releasing of bioactive agent strategy can be expressed by the bulk or only by the surface (**Figure 1-7**). Bioactive agent release strategy can come from polymers that consist of bioactive repeating units (interconnected bioactive monomers), that exhibit bactericidal action through release of antibacterial agent (**Figure 1-7 c**) e.g., antibiotic molecules (Penicilin V, cephradine) which is attached during synthesis to the polymer chain via hydrolytically labile ester bonds [164]. Another strategy is to release antibacterial agent, which is embedded in the polymer matrix (e.g., silver [165], Cu [166], ZnO particles [167], chloroxidine or active chlorine [168]). As previously mentioned, the bioactive agent release principle can be applied also for material coating (**Figure 1-7 d**). The incorporation of bioactive agent, which can be e.g., organic antibiotics [169, 170], nitric oxide [171] or silver [172, 173] can be achieved by different techniques of deposition such as dip coating, spin coating, Langmuir-Blodgett, Layer by Layer and plasma polymerization.

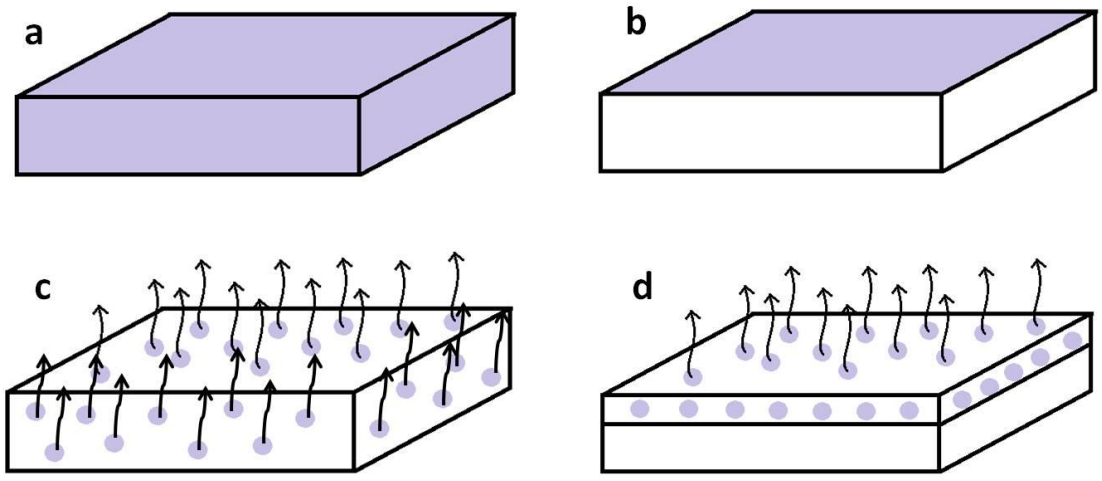

Figure 1-7: Antimicrobial polymeric materials. (a) antibacterial strategy expressed by bulk material, (b) biocidal macromolecule attached to the polymeric material surface, (c) antibacterial agent released from polymer matrix (d) antibacterial agent released from coating.

An antibacterial coating-polymer system should have following features [174, 175]: easily and inexpensively synthesized, stable in long-term usage and storage at the temperature of its intended application, not soluble in water for a water disinfection application, does not decompose to and/or emit toxic products, should not be toxic or irritating to those who are handling it, active against broad spectrum of pathogenic microorganisms upon brief contact.

The first commonly used strategy is to attach antimicrobial polymers to the surface. This can be done using mainly chemical grafting [128, 129], layer by layer deposition [130, 131] or plasma polymerization [132].

It has been reported that various polycations possess antibacterial properties in solution, presumably by interacting with and disrupting bacterial cell membranes. For example, Poly(4-vinyl-*N*-alkylpyridinium bromide) (polycation) was covalently attached to glass slides to create a surface that kills bacteria on contact [126]. Amino glass slides were acylated with acryloyl chloride, copolymerized with 4-vinylpyridine, and *N*-alkylated with alkyl bromides from propyl to hexadecyl. The final surfaces, depending on the alkyl group, were able to kill up to 94 ± 4% of *Staphylococcus aureus* cells sprayed on them [126]. It was shown that if the immobilized polycationic chains are sufficiently long and flexible to be able to penetrate the bacterial cell walls, their antibacterial properties are preserved and expressed even in a dry state. This gives the possibility to use such molecules to coat the surfaces, rendering the surface antibacterial.

Another example of “nonrelease" approach to making materials bactericidal by covalently attaching certain hydrophobic polycations to their surfaces was shown in the work of Lin *et al.* [176]. Alkylated polyethylenimine (PEIs) chains attached to flat surfaces, by rupture of bacterial cell membranes, made these surfaces bactericidal toward Gram-positive and Gram-negative pathogenic bacteria.

Antimicrobial polymer (tertiary amine 2-(dimethylamino)ethyl methacrylate) which was grown directly on the surfaces of glass and paper using atom transfer radical polymerization (ATRP) was synthesized by Lee *et al*. [177]. Following the polymerization, the tertiary amino groups were quaternized using an alkyl halide to produce a large concentration of quaternary ammonium groups on the polymer-modified surfaces. Incubation of *Escherichia coli* or *Bacillus subtilis* on these surfaces have reveled the antimicrobial properties of the surfaces. Using the same surface repeatedly did not show decreased antibacterial activity of modified glass surfaces. In this case, quaternary amines are the biocides which are believed to cause cell death by disrupting cell membranes and allowing release of the intracellular content [177].

In study of Jampala *et al.* [178] quaternary ammonium (QA) groups revealed antibacterial properties on stainless steel and filter paper surfaces. These surface functionalities were achieved via nonequilibrium, low-pressure plasma-enhanced process. These films of ethylenediamine (ED) generated by plasma are rich in secondary and tertiary amines. These functional structures were covalently attached to the stainless steel surface by treating stainless steel with O_2 and hexamethyldisiloxane plasma, prior to ED plasma treatment. QA structures were formed by reaction of the plasma-deposited amines with hexyl bromide and subsequently with methyl iodide. In another study, the plasma polymerization of propionaldehyde was used to generate surfaces with aldehyde groups onto which amine-terminated starburst dendrimers were covalently immobilized by reductive amination [179]. Amine groups were then quarternised. In vitro tests revealed reduction of bacterial attachment by 50% in this case. This general approach allows grafting of other amine macromolecules on plasma aldehyde or carboxylic surfaces.

Thierry *et al.* [180] have used an allyl glycidyl ether plasma polymer layer with surface epoxy groups for covalent binding of antibacterial peptides such as lysozyme. After blocking of epoxy surface groups with ethanolamine, no

nonspecific adsorption of lysozyme took place, indicating that allyl glycidyl ether plasma polymers could be used for biodiagnostic and biotechnology applications. These surfaces deposited on stainless steel in the study of Vreuls *et al.* [181] showed biocidal activity against Gram+ and Gram− bacteria. From 3 to 6 $\log_{10}$ reductions of both Gram+ and Gram− bacterial strains adhesion were obtained to the coated surfaces compared to uncoated stainless steel substrates and depending on the particular antibacterial peptide immobilized. Additionally, the antibacterial surfaces were resistant to several cleaning conditions. This is an important concern due to leaching, de-lamination, rearrangement and ageing of the coating, which can lead to insufficient long term biofilm resistance of the surface [181].

Using plasma polymer pre-treatment, polyethylene surface was modified by Conte *et al.* [182]. Further, lysozyme in its active form was immobilized on the surface of polymer. Lysozyme in its active form damages bacterial cell wall. Antimicrobial activity of modified polyethylene surface was verified by observations of death rate of *Micrococcus lysodeikticus* cells which were in contact with the substrate. Results demonstrated the antibacterial activity of this new system, which was coming from the activity of the immobilized enzyme. Antimicrobial activity was related to the concentration of immobilized lysozyme.

1.2.2.2.1 Release of bioactive agent strategy

Some biocides can be polymerized to provide antibacterial materials. Then, the material consists of bioactive repeating units, i.e. polymers are just interconnected biocides. In other cases, biocide is tethered via hydrolytically labile bond to main polymer chain. Releasing of monomer which is biocide in the first case or biocide molecule previously tethered to main polymer chain in the second case, provides antibacterial effect based on releasing properties. The purpose of these structures is to prolong and/or control the antibacterial

effect of the material. For instance, polymerization of antibiotics was performed as a way to prolong activity and reduce the toxicity [164]. The work of Nathan *et al.* showed that antibiotics Penicillin V and Cephradine exhibited full antimicrobial activity if the biocides were tethered via hydrolytically labile bond. Their activity was retained under release [164]. Another strategy, copolymerization of methacrylate modified Norfloxacin and PEG-methacrylates lead to bioactivity of the final product [183]. Following the same idea, direct modification of Vancomycin with PEG-methacrylate and subsequent polymerization allowed to preserve antibacterial activity of the final product [184]. However, the antibacterial action was in this case coming from partial solubility of the copolymer in water [184]. Further, penicillin molecule attached to polyacrylate nanoparticles, showed higher antibacterial activity than free antibiotics in solution [185]. Interesting results were achieved by mimicking the natural polymers-polyphenols. Synthesis resulted with activity pattern based on phenol release in order to achieve killing of microbial cells [186].

Releasing of active agent can be also achieved by fabrication of materials loaded with biocide. Biocide in this case is not chemically bounded to polymer chain. These systems are often achieved by polymer matrices loaded with biocides like silver, Cu, ZnO particles, active chlorine. For biomedical application concepts of self-assembled structures from amphiphilic have also been developed in the field of drug delivery. These macromolecules are soluble in dilute aqueous media and their ability to assemble into micelles and vesicles are used to carry drugs and genes [187, 188]. A class of antimicrobial polymers was developed by Worley *et al.* using N-halamine groups attached to polymer backbone [168]. The design of these molecules allowed the long-term storage of active chlorine which kills microbial cells by oxidizing the phospholipids of the cell membrane [189].

1.2.2.2.1.1 Release of antimicrobial agent from coatings

In many cases, there is no possibility to embed the antibacterial agent such as antibiotic molecule into the bulk due to technical limitations e.g. thermal resistance of these molecules. For this reason, coatings, particularly polymeric coatings, are the optimal solution when deposited after the medical device is manufactured. The strategy is based on the use of coated surfaces able to release bioactive agent.

Promising approach is to use controlled release, where antibacterial agent is embedded in polymer coating and released in a control way. Various antibacterial compounds have been studied and loaded into polymer bulk or composite film such as organic antibiotics [169, 170], nitric oxide [171] and silver [172, 173]. Different techniques of deposition can be used: dip coating [190], spin coating [191], Langmuir-Blodgett [192], Layer by Layer [193] and plasma polymerization [194]. This gives the opportunity to functionalize and tailor the surfaces of implants by applying various polymers onto it and achieving antibacterial properties. For example, local delivery of antibiotics has been applied for a long time in materials like cements, for orthopedic and orthodontic implants [195]. Upon hardening, in situ release of antibiotics has been shown to prevent adhesion and growth of significant numbers of bacteria. Plasma-based approaches include also materials with grafted antibiotics. Aumsuwan *et al.* [196, 197] used a microwave plasma of maleic anhydride to graft commonly used antibiotics such as penicillin and ampicillin. It was firstly achieved by a hydrolysis process, which formed carboxylic acid groups on the surface followed by the immobilization of the antibiotic molecule through a polyethylene glycol spacer. The length of the spacer was not long enough to penetrate the entire bacterial cell. However it was providing mobility to antibiotic molecules, leading to inhibition of bacterial wall synthesis. Moreover, a release of antibiotic molecules from these surfaces was shown. 10% in case of

ampicillin and 32% in case of penicillin have been released after 24 h of immersion in Phosphate buffered saline (PBS) solution. The loss of ampicillin and penicillin from the surface did not alter the effectiveness of the surfaces against gram-positive and gram-negative bacteria. Nablo *et. al*. [171, 198, 199] have synthesized antibacterial coatings based on release of nitric oxide (NO). It was shown that NO destroy colonies of plated bacteria [200]. Mechanism this of antibacterial action is coming from oxidative and nitrosative stress generated by reactive intermediates of NO (e.g., peroxynitrite and dinitrogen trioxide) that may result in damage to DNA, proteins, and/or cells [201]. Coating showed excellent material stability and antibacterial efficiency. However, the use of NO in the implant coating is questionable. It has been found that NO is an important mediator in numerous mammalian biological processes, including neural transmission, septic shock, and apoptosis [202, 203]. This reveals high risk of cytotoxicity of this product as a potential antibacterial agent released from implant surface [204]. Numerous examples of coatings with silver (nanoparticles or silver salts) are found in literature [173, 194, 205, 206]. Antibacterial action of these coatings is often based on releasing properties of silver ions. These examples will be discussed in further sections.

1.2.2.3 The choice of antibacterial agent

1.2.2.3.1 Antibiotics and antiseptics

Antibiotics have been used against bacterial infection since their discovery by Fleming in 1928 [207]. The treatments using antibiotics are also used against medical device related infections [98, 208]. To accomplish a sustained level of antibiotic at the site of infection and to overcome the protection that biofilms provide for bacteria, controlled local release has been proposed [195, 209]. Strategy based on delivery of gentamycin from biodegradable surface coatings

made of poly D,L-Lactide (PDLLA) [210] or mixtures of antibiotics like rifampicin and fusidic acid in PLLA matrix have been used [211]. The effectiveness of this approach was shown in a rabbit tibia infection model, resulting in effective killing of *Staphylococcus aureus* infection. In another study, approach using chlorohexadine diacetate release from coating made of Polyvinylopyrrolidone (PVP) was shown to be efficient against infection only upon fast release [212]. Darouiche *et al*. [213] have used coating with minocycline and rifampin to prevent colonization of a grit-blasted titanium implant. In vivo results showed that these devices significantly protected medical device from colonization and infection of *Staphylococcus aureus*. Another approach using coatings containing combinations of antibiotics and antiseptics like minocycline and rifampin or chlorohexidin and silver-sulfadiazine have been applied to the internal and external surface of catheters [214, 215]. Results showed reduction of catheter colonization and catheter related blood-stream infections. Disadvantage of using antibiotics or antiseptics loaded medical devices is that release is finite. For long term release, the concentration of the antimicrobial agent will eventually drop, below minimal inhibitory concentration [216]. This is general characteristics of coatings where there is certain reservoir of an antibacterial agent. It is disadvantageous when release cannot be fully controlled. However once the release is controlled and antibacterial agent released in suitable doses, the lifetime of this kind of coatings can be prolonged together with antibacterial properties. However, the major disadvantage of using antibiotics as a infection preventive strategy is that more and more multi-drug resistant bacterial strains are developing [217, 218].

1.2.2.3.2 Antibacterial polymers

Antibacterial macromolecular systems are known since more than three decades [219] when firstly biologically active polymers of 2-methacryloxytroponones were described [220]. These polymers and

copolymers, containing quaternary ammonium/phosphonium salts (polyelectrolytes, polymethacrylate containing side biguanide groups and polyvinylbenzyl ammonium chloride) or N-halamine groups in different areas of the polymer structure [221] have been reviewed considering their process of synthesis [222], chemical diversity of antimicrobial systems [174], and different approaches of preparation [174] (synthesis of novel monomers, attaching bioactive substrates such as quaternary ammonium or phosphonium groups, attaching cyclic N-halamine compounds to synthetic monomers or polymers, or modification of naturally occurring macromolecules). Their antimicrobial activity have been considered as well [174]. In particular, mechanisms of action and applications have been reviewed recently [223]. Tew *et al*. [224] were focused on antimicrobial polymers that that can mimic the biological activity of the antimicrobial natural host-defense peptides. Biological activity of these systems is considered to be influenced by the amphiphilicity of the polymer or oligomer as a whole, rather than the activity of an antimicrobial moiety either embedded or covalently attached. Majority of antimicrobial polymers are designed as cationic hydrophilic–hydrophobic macromolecular systems [223]. Target for those system to reveal antibacterial action is cytoplasmic membrane which regulates the transfer of solutes and metabolites between cytoplasm of bacterial cell and external environment [225]. Bacterial membrane has selective permeability properties which gives the opportunity to damage the structural organization and integrity of this membrane. Polymers are designed to have a hydrophilic polar functional block bearing cationic charge and a hydrocarbon non-polar hydrophobic block or are formed with random copolymers formed by a hydrophobic monomer and a hydrophilic comonomer with a functional group [174, 186, 222, 226]. These structures then, have high binding affinity for bacterial cells [226]. For example, in case of N-halamines, polymers with N-halamine functional groups have been developed to stabilize the antimicrobial properties of free halogens such as chlorine or bromine. In N-halamines, one or more halogen atoms are covalently bonded to the nitrogen atoms of the

compounds providing stability and slow release of free active halogen species into the environment. The main biocidal impact of the N-halamines is coming from a specific action of oxidative halogen rather than polymer action itself. Cl^+ or Br^+ halogen targeted at a biological receptor such as thiol groups or amino groups in proteins upon direct contact with a cell, leads to cell inhibition or cell inactivation [223].

The advantages of using antimicrobial polymers e.g. for coatings include reduction of residual toxicity comparing to low molecular weight antimicrobial agents, increase of their selectivity, and prolongation of the lifetime of the antimicrobial coating. Antimicrobial polymers can render the surface of biomaterial resistant to microbial colonization, and can provide better protection for materials exposed to the atmosphere after sterilization procedure and before implantation. The polymers which action is based on contact active principle could be advantageous in case of permanent implants, providing them protection from infection. However, disadvantages of antimicrobial polymers often include expensive process of synthesis, decomposition or partial solubility in some cases, loss of activity upon use or toxicity to mammalian cells. Degradation due to elevated temperatures could also be a limiting factor to processing of these materials into desired forms. For these reasons, better control of the infection at the implantation site would be achieved with a polymeric coating embedding an antibacterial agent active against a broad spectrum of bacterial species e.g. silver nanoparticles.

1.2.2.3.3 Silver as a product for antibacterial purposes

Since ancient times, silver is known to be a good antimicrobial, antifungal and antiviral agent. In recent years, the use of silver as a biocide in solution, suspension, and especially in nanoparticles form has increased. Silver has been widely used in many bactericidal applications as well as in medical field to

treat burns and variety of infections [227]. Metallic silver is inert in the presence of human tissues but ionizes in the presence of moisture, body fluids, and secretions to release the biologically active Ag^+ [228]. The release of Ag^+ depends on the size of metallic nanoparticles [229]. For example release is accelerated by particle size reduction [230]. In consequence, size-dependent interaction and properties of nanoparticles insight researchers to explore potential benefits from implementing disinfecting filters, drug delivery systems and coating materials with nanosilver [194, 231].

1.2.2.3.3.1 Mechanism of silver ion antibacterial action

The silver in the form of Ag^+ have been shown to be effective against a large number of bacteria and fungi, which absorb and concentrate silver ions from dilute solutions (1ppm). Using solution with a concentration of Ag^+ of 60 ppm should be sufficient to control the majority of bacterial and fungal pathogens [228]. However the level of concentration needed to control the bacterial growth is most probably depending on the type of bacteria and experimental conditions (e.g., type of medium). The mechanisms of this efficiency are only partially understood so far. One possible mechanism is based on the fact that silver ions have the capability to exchange with the ions in the environment (e.g. Ca^+, Zn^+) and attach to bacterial cells [232]. Ag ions bind protein residues [233] on cell membranes of sensitive bacteria and are adsorbed intracellulary by pinocytosis [228]. The consequence of the ions binding to cell membrane is the damage of it, the disturbance of bacterial electron transport and of the production of cell's energy by impeding the ATP production. Ag^+ species also interact with the oligonucleotide bases in DNA and affect DNA ability to replicate [227]. Oxidative stress can also play a role in the mechanisms of DNA damage [234]. Another potential way of antimicrobial properties of silver ion can come from inhibition of respiratory enzymes through reactive oxygen species (ROS) formation [235, 236]. Also, Ag^+ indirectly leads to Fe^{2+} leakage by stimulating the production of

superoxide, disturbing internal iron homeostasis and by directly or indirectly disrupting intracellular Fe-S clusters [237]. It was found also that attachment of silver ions (or nanoparticles) to the cell wall caused accumulation of envelope protein precursors which resulted in immediate dissipation of the proton motive force [238]. Mechanisms of action are based also on interaction between Ag^+ and phosphorous- and sulfur-containing compounds found in variety of proteins [239]. Ag^+ disrupts disulfide bond formation *in vivo,* which affect protein shape, functionality and stability [237].

1.2.2.3.3.2 Toxicity of silver ions for human cells

The use of silver in composite materials, polymers, metal coatings and scaffolds affects bacteria and disturbs their biological functions but the question arises about the toxicity of silver ions for the human cells. Due to the similarities in the structural elements of human and bacterial cells, important is to know the way of interference of silver ions and human tissue. A disruption of cell and tissue functions coming from silver ions were reported by Schrand *et al.* [240] including the induction of ROS, degradation of mitochondrial membrane integrity, disruption of actin cytoskeleton and reduction of proliferation after stimulation with nerve growth factor when exposing neuroblastoma cells to silver nanoparticles. In case of high release rate of silver, the cytotoxic effect appears. It was reported that in case of the use of biomedical products for wound treatment (silver wound dressing), some patients showed hepatotoxicity and argyria-like symptoms, and the silver levels in plasma and urine were elevated as well as liver enzymes [241]. Hardes *et al*. [242] used silver-coated orthopedic implants in humans, which proved their effectiveness on reducing infections. Results showed no side-effects of this medical device towards human. The silver-levels in the blood did not exceed 56.4 parts per billion (ppb) and were considered as non-toxic. Additionally authors excluded significant changes in liver and kidney functions. Materials with well-controlled release of

silver ions seem therefore to be reasonable as a next step toward infection preventive medical devices.

1.2.2.3.3.3 Role of silver nanoparticles in the antibacterial properties

Usually, it is assumed that the silver nanoparticles (AgNPs) antibacterial action is mainly based on the ability of silver ion to release from NPs. However, it was also shown that AgNPs can have their own antimicrobial effect without the release of ion forms [228, 243] by penetration of the cell membrane [234]. Nanoparticles may attach to the cell membrane that contains electron donor groups like sulfur, oxygen, and nitrogen. Electrostatic interaction may take place between negatively charged electron donor groups and positively charged AgNPs, which brings structural and functional changes in the microbial cell membrane, disturbing the permeability by modifying the cell potential and inhibiting cell respiration [244]. In addition, AgNPs may bind to thiol groups of bacteria proteins, disturbing the activity of cell and causing death [234, 245]. Some studies also show that silver nanoparticles express antiviral action as well [246, 247]. It has been shown that silver nanoparticles exert an action against HIV-1 at concentrations nontoxic for human cells. The action involves virion binding, inhibition of replication and inactivation [247].

1.2.2.3.3.4 Silver nanoparticles incorporated in materials as a research strategies for antibacterial materials

With rapid development of nanotechnology, applications where silver is used as an engineered nanomaterial are increasing. Different forms of silver in different kind of materials are incorporated to exploit the antimicrobial properties of silver. Nanosilver was incorporated in various materials such as engineering polymers like nylon 6,6 [248], polyurethanes [249-251], poly(methyl methacrylate [252, 253] and as well in carbohydrates and biopolymers [254-258]. Silver

incorporated in other types of materials like silver-impregnated zeolite powders and activated carbon materials [259, 260], dendrimer–silver complexes and composites [261-263] were also synthesized. Today, the possibility to impregnate or coat alginates, polyurethane, silicones and textile fibers with ionisable silver compounds provides clinicians with efficacious means of prevention from infections in wound care and device-related infections. The particles or other forms of silver can be incorporated into the bulk of the material by mixing (composite) or by a surface modification procedure (coating).

Factors, which influence the efficiency of silver incorporated materials, are:

- Rate of release which is usually fast. This may limit the time of protection,
- Silver needs to be oxidized in order to exhibit high efficiency against bacteria in case of silver nanoparticles-loaded coatings.

Recent literature reports have explored antibacterial properties of silver-containing materials. Examples based on relevancy for the use in biomedical purposes are presented below [172, 243, 264-272].

1.2.2.3.3.4.1 Silver in inorganic systems (bioceramics)

Silver nanoparticles antimicrobial properties in bulk materials have been explored in the field of bone tissue regeneration, mainly with bioceramics. By using silver nanoparticles with the size in range 1-2 nm, the authors have increased the antimicrobial effect by two-to-three orders of magnitude comparing to antimicrobial activity of a silver-containing surface [264]. This approach was based on decorating bigger 20-50 nm carrier particles consisting of a phosphate-based, biodegradable ceramic, with silver nanoparticles. When growing, microorganisms were dissolving the carrier particles and the release of silver was triggered. Electrospun, fibrous and porous poly(lactide-co-glyclolide) (PLGA) was used as a matrix for composite consisting in silver (0.5 wt%) on

amorphous tricalcium phosphate nanoparticles. Authors performed antibacterial tests which showed a prolonged effect of the scaffolds with silver uniformly dispersed on the tricalcium phosphate, comparing to current clinically used methods, based on soaking the scaffolds with a tetracycline solution prior to implantation [265].

Hydroxyapatite (HA) coatings with incorporated silver species have also shown decreased probability of infection and decrease of the biofilm growth [266, 267]. The results showed that, HA coatings expressing antimicrobial properties and releasing Ag ions killed methicillin-resistant *Staphylococcus aureus in vivo*.

Multilayer approach has been also investigated for the development of silver embedded films adherent on SiOx surface. Ag nanoparticle-embedded synthetic catecholamine polymer films showed enhanced antibacterial effects compared to the films without Ag and the bare SiOx surface [273]. Eksik *et al.* [268] have developed a series of triglyceride oil based polymer-silver nanocomposites using electron transfer reaction and free radical polymerization processes. These nanocomposite materials exhibited an antibacterial effect against gram-positive, gram-negative, and spore forming bacteria. Furno *et al*. [274] have used supercritical carbon dioxide to impregnate silicone with nanoparticles of metallic silver. It was found that efficiency of those systems on bacteria killing depended on the silver ion release rates from the coating.

1.2.2.3.3.4.2 Silver in organic polymer systems

Polymeric hydrogels have been used for the incorporation of antibacterial agents, including silver, with good results [270, 271, 275, 276]. The advantage of these systems is their physicochemical properties and good mechanical properties, also suitable for coatings. These systems have ability to absorb water due to hydrophilic functional groups attached to polymer backbone. Moreover, hydrogels are resistant to dissolution due to cross-links between chains. Hydrogels can serve as matrix, which allows the diffusion of some

molecules. An example is shown by Vachon *et al.* [270] who proposed a novel dressing material based on a sulfonated triblock polymer. This polymer possesses an ion-exchange capability that allows binding and controlled release of a variety of therapeutic agents. The polymer was coated onto a polyester fabric and then modified by ion exchange to prepare sodium, silver, or doxycycline salts. Results showed that polymer hydrogel which had an ion-exchange capability allowed to control the release of silver and other therapeutic agents. Jones *et al.* [172] have determined the antimicrobial activity of a silver-containing Hydrofiber® dressing (AQUACEL® Ag) on aerobic and anaerobic microorganisms, using the zone-of-inhibition method. The results showed that the material makes silver available at the dressing–agar interface at a concentration that is effective against a broad range of aerobic, anaerobic, and antibiotic-resistant microorganisms. Varaprasad *et al*. [271] have also synthesized hydrogel matrices by polymerizing acrylamide in the presence of poly(vinyl sulfonic acid sodium salt) and a trifunctional crosslinker (2,4,6-triallyloxy 1,3,5-triazine, TA) using redox initiating system (ammonium persulphate/ Tetramethylethylenediamine (TMEDA)). Silver nanoparticles were generated throughout the hydrogel networks using *in situ* method by incorporating the silver ions and doing a subsequent reduction with sodium borohydride. Results showed an interesting arrangement of silver nanoparticles in the hydrogel matrices such as a shining sun shape (ball) (~ 5 nm) with apparent smaller grown nanoparticles (~ 1 nm). The developed hydrogels showed also antibacterial properties, which was evaluated by the zone-of-inhibition method. In another work, hydrogel networks with cross-linked polymers like poly(acryl amide), carboxymethyl cellulose, starch and gum acacia were used as matrix. Silver nanoparticles were loaded *in situ* using silver nitrate solution followed by reduction with borohydride [277].

Another antibacterial Ag/polymer nanocomposite was developed by Zaporojtchenko *et al.* [272]. Uniform dispersion of nanoparticles in polymer

matrix was obtained using co-sputtering of metal and poly(tetrafluoroethylene) approach. The bactericidal activity due to silver release from the surface was tested against *S. aureus* and *S. epidermidis* bacteria. The efficiency of the coatings against different bacteria species was demonstrated at extremely small metal consumption: Ag: ~0.1 g m^{-2}. Composite films containing silver nanoparticles and organic molecules were also synthesized by researchers using layer-by-layer (LbL) deposition method [278-283]. Interactions used to fabricate such films include ligand - silver ion – ligand bridges [278] and covalent bonding. Often the deposition is based on alternating adsorption of oppositely charged polyelectrolytes [278, 284]. These multilayer films are used as reservoirs for silver. Dai *et al*. [278] have used Polyethylene-imine (PEI) stabilized Ag colloids in solution to synthesize antibacterial films by performing alternative adsorption of polyacrylic acid and PEI stabilized colloids using LbL technique. The reduction of silver ions was performed by addition of $NaBH_4$ solution. Prepared LbL films which contained silver nanoparticles or silver ions have shown to inhibit bacterial growth. Similarly Li *et al.* [280] have used LbL method for synthesis of poly(acrylic acid) - Ag^0/poly(allyl-amine hydrochloride) films. These films as well have shown antibacterial activity related to the release of silver ions from the film. Silver-loaded hollow microcapsules made of hydrogen bonded poly(acrylic acid)/polyacrylamide multilayer thin films using LbL method was developed by Lee *et al.* [281]. By the number of loading cycles researchers were able to control the size and amount of loaded silver in the films. The concept of developing drug delivery system composed of liposome-$AgNO_3$ aggregates – embedded in polyelectrolyte multilayer films using LbL method was proposed by Malcher *et al*. [283]. These films were build using poly(L-lysine)/hyaluronic acid polyelectrolytes. Coating showed strong antibacterial properties revealed under thermal stimuli, however spontaneous release of silver ions and/or erosion of $AgNO_3$-liposome aggregates have led to loss of the functionality of the coating.

Polyelectrolyte multilayers films prepared by LbL technique have emerged as a simple, multistep approach to functionalize surfaces for biomedical applications however some disadvantage can be named such as need of several step in the material development; not sufficient stability of the films caused by processes as interdiffusion, echange of polyelectrolytes in the LbL assemblies, diffusion of external molecules within the films [285]; use of chemical solvents (tetrahydrofuran, toluene [283]) which potentially leave the residues on the medical device and can be toxic to human cells. Some of these disadvantages can be overcome by the use of another approach to develop Ag/polymer coatings such as plasma polymerization [194, 286-288].

Plasma polymer acts as a matrix for the out-diffusion of the silver ions. As we have seen before, nanoparticles and ions have been incorporated in release matrices, by many ways, but the major advantage of plasma polymers for this purpose is the good adhesion to the substrate and the possibility to deposit polymer coating with very low thickness. Mechanical properties of substrate material are not significantly affected in this case. Additionally, plasma polymer can be used to control the diffusion rate via plasma polymer overlayer. The part describing plasma polymer incorporated with silver nanoparticles will be detailed in section 2.2.

1.3 Plasma Polymerization

1.3.1 What is plasma?

“There are more things between anode and cathode that dreamt of in our philosophy”.

H. Raether (1909-1986)

Plasma is considered as fourth state of matter and it is the most abundant state in the universe. Plasma is present in nature in the sun, stars, in the tails of comets and as flashes of lightning. With the application of sufficient heat, solid materials transform into liquid state and, then, with further application of heat it transfer into gas. Once the electrons receive sufficient energy to separate from the atoms or molecules of gas and become electrically conductive, the gas undergoes a phase transition to a partially or completely ionized gas (**Figure 1-8**).

Plasmas are composed of positively and negatively charged ions, electrons, radicals, neutral atoms and also atoms and molecules in excited state, which exhibit collective behavior. Plasmas can be divided into two main categories: hot plasma (near equilibrium plasma) and cold plasma (non-equilibrium plasma). Hot plasmas are in thermodynamical equilibrium and are strongly ionized with high density of energy. The temperatures of ions and electrons are equal. Cold plasmas are in thermodynamical disequilibrium, with low level of ionization (magnitude of 10^{-4}), with a density of energy lower than hot plasmas. Cold plasmas are characterized by three temperatures (T_c – electron temperature, T_i- ionic temperature and T_n- neutral temperature).

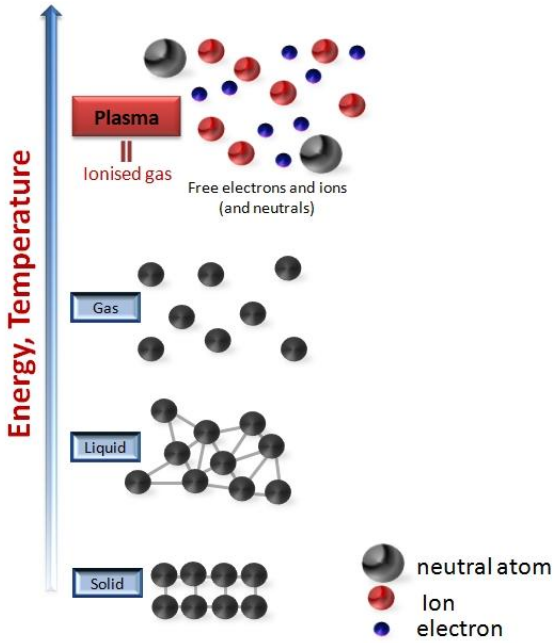

Figure 1-8: Different states of matter.

In this work, we have used low temperature plasma (cold plasma) to treat the substrate materials at low temperatures, which limits the problem related to degradation of material.

1.3.1.1 Low temperature plasmas

Plasma can be obtained using different forms of energy (thermal, electric current, electromagnetic radiations, light from laser). Properties of plasma such as electron density or temperature can change depending on the type of energy supplied and the amount of energy transferred to the plasma. Low temperature plasmas are characterized by non-equilibrium between electron temperature and gas temperature. Hence, the main parameters, which define the characteristics of plasmas are its temperatures, types and densities of radicals

and its level of ionization. Plasma is produced by passing an electric current through the gas. Different power sources such as direct current, alternating current or frequencies (low frequency, radio frequency, microwave etc) are used for generating of discharges such as atmospheric and low pressure glow discharge, corona, magnetron and dielectric barrier discharge (DBD) [289].

In an alternating current (ac) glow discharge, the mechanism depends on the frequency of excitation. At low frequencies, the system can be looked upon a direct current (DC) glow discharge with alternating polarity. By increasing the frequency of the applied voltage, positive ions become immobile, because they can no longer follow the periodic changes in the field polarity, and only respond to time-averaged fields. At frequencies above 500 kHz, the half cycle is so short that all electrons and ions stay within the interelectrode volume. This reduces the loss of charged particles from the system. Regeneration of electrons and ions occurs within the plasma body, through collisions of electrons with gas molecules. In radiofrequency plasma (13.56 MHz) therefore, no contact between the electrodes and the plasma is required. The plasma can be initiated and sustained by external electrodes, at much lower voltage that is required for maintaining a direct current glow discharge [290, 291]

1.3.1.1.1 Plasma polymerization

The term « plasma polymer » usually describes a polymer film obtained by the activation of an organic precursor (often a gas) with electric impulses. The polymer film obtained often presents a molecular structure different from the ones obtained by other conventional techniques. As shown on **Figure 1-9**, a plasma polymer presents a heterogeneous chemical structure due to the high rate of the activated monomer recombination during the film formation, leading to a highly cross-linked and amorphous film, while conventional polymers are composed of a single unit of monomer repeated regularly. The structure of

plasma film can be tailored by the experimental conditions during the process: using strong dissociating conditions for the monomer results in a film being highly cross-linked, while smoother conditions often lead to a structure close to films obtained by conventional methods (degree of retention).

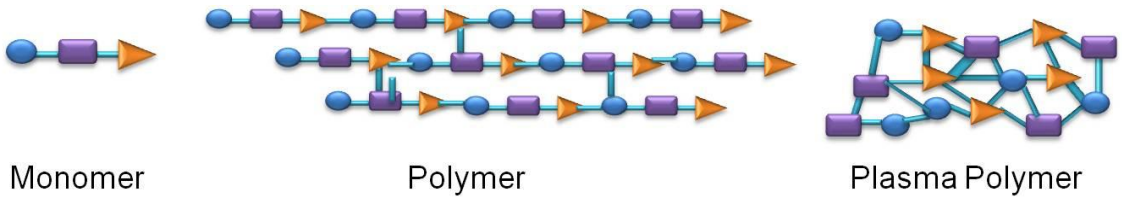

Figure 1-9 Schematic representation of monomer, conventional polymer and plasma polymer.

A variety of precursors can be used for the formation of plasma polymer thin film deposits. This method of polymerization presents the advantage of demanding lower quantities of precursors and limitating the number of side reactions that can happen in other media (solvent termination in liquid medium for instance). The plasma technology is used to deposit films on various substrates (polymers, metals and ceramics) of various geometries without degrading it. The resulting good adhesion between the plasma film and the underneath material allows the use of the plasma technology in a broad spectrum of applications, from protecting layer to adhesion primers. The main drawback comes from the cost of used gases during the process and the fact that formation mechanisms are not to date perfectly understood.

1.3.1.1.1.1 The formation mechanisms

In a given plasma, the electrons distribution of energy is often described by the Druyvesteyn approximation (**Figure 1-10 a**) [292]. Most of electrons show an energy comprised between 1-6 eV, enough to dissociate almost all chemical bonds existing in organic materials, creating free radicals responsible of the polymerization mechanism. Only a small fraction of the electrons possesses

energy higher than 8 eV allowing the ionization of organic molecules. With a particular set of experimental conditions (pressure, type of gaz, power) it is possible to ionize all organic molecules and dissociate all bonds of organic molecules.

a)

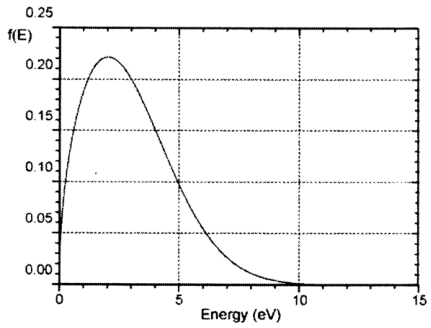

b)

Bond energies and enthalpies of formation of free radicals

Bond energies		Enthalpies of formation of free radicals		
Species	Energy (eV)	Species	Energy (kJ/mol)	Energy (eV)
Diatomic molecules				
C–H	3.3	·CH·	596.3	6.1
C–N	7.8	CH_2:	430.1	4.4
C–Cl	4.0	CH_3·	146.0	1.5
C–F	5.7	HC=C·	566.1	5.8
C=O	11.2	$HC=CH_2$·	300.0	3.1
C–C	6.3	NH:	350.0	3.6
Polyatomic molecules				
C=C	7.6	NH_2·	185.4	1.9
C ≡ C	10.0	:Si:	456.6	4.7
CH_3-H	4.5	·SiCl·	195.0	2.0
C_2H_5-H	4.3	$SiCl_2$:	−163.0	−1.7
CH_2CH-H	4.8	$SiCl_3$·	−318.0	−3.3
CHC-H	5.7	C_6H_5·	328.9	3.4
		C_6F_5·	−547.7	−5.0

Figure 1-10 (a) Electron density distribution in function of their energy [292]. **(b)** Table with values of often studied bonding energies.

The overall mechanism of plasma film formation is shown on **Figure 1-11** .

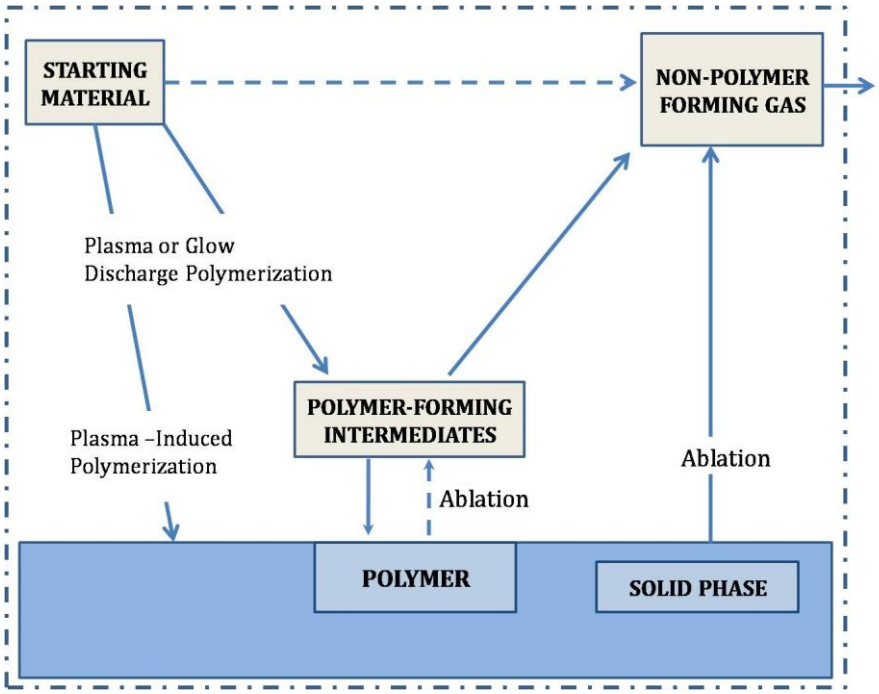

Figure 1-11 Schematic diagram of glow discharge polymerization , reproduced from [293].

After activation of the precursor by the plasma phase, the growth of polymer film can happen both in the plasma phase and onto the substrate surface. The rate of polymerization in the plasma phase and onto the substrate surface is highly dependent on the process conditions. For example, plasma polymerization at atmospheric pressure tends to favorite the growth in the plasma phase due to higher collision rate between species.

1.3.1.1.1.2 Growth kinetics

At low pressure the precursor activation leads to the creation of a single or bi free radical(s) in the structure of the precursors by mechanisms such as dehydrogenation, ring opening or bond dissociation and these radicals randomly react with the surrounding species. This polymerization mechanism is illustrated by the 3 step models proposed by H. Yasuda [294, 295]

First step: Activation of the precursor (creation of free radicals) by collisions between the precursor molecules and the active species (electrons, ions, radicals) in the plasma phase.

$$M_i \longrightarrow M_i^*$$
$$M_k \longrightarrow M_k^*$$

Second step: The polymerization starts by chemical reactions between the activated and non-activated molecules of precursor, in the plasma phase or onto the substrate surface.

$$M^*+M \longrightarrow M\text{-}M^*$$
$$M^*i+M \longrightarrow M_{i+1}^*$$

Third step: Polymerization stops with the recombination of two activated molecules (two molecules of activated precursor and/or a molecule of activated precursor and an activated specie from plasma phase (electrons, ions, radicals))

$$M_i^* + M_k \longrightarrow M_i\text{-}M_k$$

Even after the termination and the obtainment of a stable polymer film, the latter can still be re-activated by the surrounding plasma phase, as represented by cycle n° I and II shown on **Figure 1-12** (cycle I: reactivation by mono radical / cycle II: activation by bi-radicals).

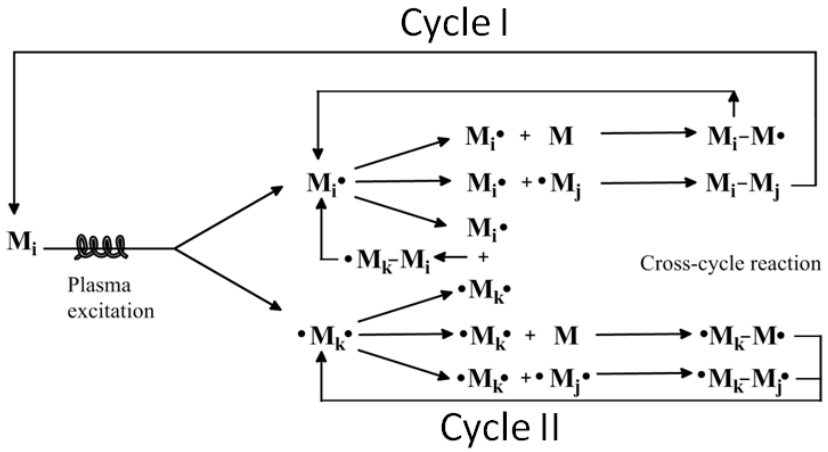

Figure 1-12: General mechanism of plasma step growth.

Other mechanisms have been proposed considering the different processes of dissociation of precursors and the subsequent recombination mechanism [295]. The review of J. Friedrich [132] in 2011 sums up all growth mechanisms of plasma polymers. Tibbitt [296] and Stille [297] models propose mechanisms, where precursor molecules are not totally dissociated. For instance, in the case of ethylene polymerization, the formation of macrocycle molecules was observed through recombination of free radicals, induced by dehydrogenation. Additionally, several studies show the role of ions during the growth of plasma polymer [298, 299].

1.3.1.1.1.3 Influence of the plasma parameters

a. Nature of the gaz

Several studies showed the influence of the gas nature on the plasma's discharge. For instance, to obtain a homogeneous and luminescent discharge at low pressure and atmospheric pressure, the use of a neutral gas (Helium or Argon) is advised. The use of N_2 or O_2 permits to obtain a reactive plasma [300]. The most studied case is the SiO_2 deposit film, where

the addition of an oxidizing gas such as O_2 or N_2O leads to the formation of amorphous silica [301]. The use of N_2 or NH_3 allows the grafting of amino-based functions on the surface of a material. The use of polymerizable gazes (CF_4, $C2H_2$, CH_4) brings new chemical functions onto the surface of a material [302, 303].

b. Power of the discharge

The influence of the discharge's power has been widely studied [304, 305]. The power used has a high influence on the kinetics of forming reactive species in the plasma, especially on the density of electrons, the radiation and the ionic bombardment. The plasma power influences both the growth rate of the polymer film and its chemical structure [306].

To control the power of the plasma's discharge, the control of electric parameters and the precursor's flux is necessary. To allow standardization in the comparison between plasma depositions, H. Yasuda introduced the W/FM parameter [307] (W is the power of the discharge, F the precursor's stream and M the molecular weight of the precursor). The W/FM parameter corresponds to an energy brought to a unit of precursor mass. The **Figure 1-13** shows the deposition kinetics as a function of the W/FM parameter.

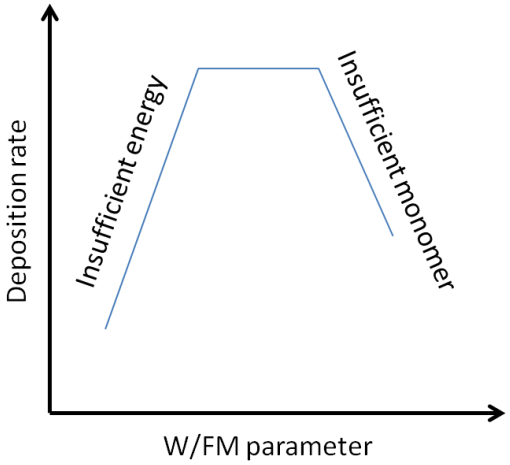

Figure 1-13 Polymer deposition kinetics as a function of W/FM parameter, (W is the power of the discharge, F the precursor's stream and M the molecular weight of the precursor), according to the theory of H. Yasuda [307].

The curve can be decomposed into 3 areas. The first (on the left) corresponds to a growth regime where the energy is insufficient. In this area, the precursor dissociation is a process limited by the quantity of matter brought in the plasma reactor. When increasing the W/FM parameter, the kinetics of film formation increases linearly until reaching a plateau. The last area (on the right) corresponds to a growth regime where the energy is in excess, the growth of the film is limited by the high dissociation occurring and the ablation process. The stable area, is a region where, speed of deposit is maximized, due to optimized conditions of monomer flow and power of discharge.

Additionally to the study of the film growth, several studies related the influence of the W/FM parameter on the structure of plasma film polymer. These studied were done at low pressure with different molecules such as carboxylates [308, 309] natrium based [310], fluoro [311] or siloxanes [312]. In the first regime, the deficiency in energy allows to keep intact the

reactivity of the monomers. In certain cases, the formation of oligomer structure close to conventional polymer has been observed [313]. In the last regime, the high dissociation of the monomer leads to an increase of the functionality and the obtention of a highly cross-linked polymers. To prevent this high dissociation, the use of plasma in pulsed mode allows the preservation of monomer functionality [294, 314].

c. The pulsed mode

This mode is principally described by its Duty Cycle (DC) time, as shown on Equation 1

$$DC = \frac{t_{on}}{t_{off}+t_{on}} \quad , \qquad \textbf{Equation 1}$$

t_{on} - time where precursor's monomer is excited by the plasma phase

t_{off} - time where precursor's monomer is not excited by the plasma phase

The use of low DC times allows to diminish the effective power (P_{eq}) of the plasma to limit the precursor's dissociation. During the t_{on} period, the precursor's monomer is excited by the plasma phase. The radicals formed in the precursor's monomer will then recombine during the t_{off} period. Several studies showed that the use of pulsed mode allows a smoother polymerization where the retention rate of chemical functions is higher [315, 316].

The actual power received by the substrate during the pulse duration (P_{eq}) is a result of DC and the input power value (P_{peak})

$$P_{eq} = P_{peak} \times DC$$ **Equation 2**

Better functional retention can be achieved using low DC values and high values of input power. During the whole cycle, the equivalent power received by substrate is lower than input power. Use of pulsed plasma over continuous plasma has advantages like increased operational stability, reduction of trapped radicals in the film, lower deposition surface temperatures and decreased high-energy ion bombardment and UV flux to the surface [317].

Control over the chemistry of plasma deposited film can be achieved with better efficiency by use of radio frequency plasma and variation of plasma-on and plasma-off times, instead of continuous wave plasma. With relatively long plasma-off time, the domination of radical-monomer type processes leads to the structures which reassemble standard polymer-like structures [317-320]. Varying plasma-on time and plasma off-time it is possible to obtain plasma polymer film through free radical polymerization (a chain polymerization in which the kinetic-chain carriers are radicals [321]). For monomers, which have in structure double or triple bonds, the growth mechanisms take place during the off-time, retaining the original chemical structure of the monomer with the preservation of desired functionalities. Pulsed plasma improves the chance to achieve more regular structures using classic monomers with great tendency of chemical polymerization [322-326].

Possible modifications of surface properties such as electrochemical charge or amount of oxidation as well as attachment or modification of surface-bound chemical groups can be achieved by plasma processes. Properties like hardness, resistance to chemical corrosion or physical abrasion, wettability, water absorption capacity and as well affinity to specific molecules can be tailored by choosing specifically and precisely the plasmas [327].

d. Other parameters

The general characteristics of the plasma reactor, such as volume, shape, oscillation frequency of the electric field, temperature, influence also the film growth [328]. The position of the substrate in regards to the gas injection allows the recuperation of condensed species in the plasma phase or in “post-discharge” [329]. In the latter case, the substrate is placed in the gas stream to collect ionized species of the plasma without modifying the substrate surface. Form in which precursor is introduced to the reactor, also influence the plasma polymer film. For example, the use of precursors in the state of vapor or aerosols allows obtaining dense films. Borra [330] and Badyal [331] groups developed ultrasonic injections systems of precursors to insert the precursor in nano-drops. Their results showed that the resulting fragmentation of the precursor was then lower. Pressure is also playing an important role in the process of plasma polymer film growth. In this case, according to Debye’s equation, the rise of the pressure in the reactor increases the density of plasma’s particles, decreasing the average free paths of the electrons, leading ultimately in the rise of collisions. Thereby, kinetic energy of plasma species is also decreasing, which does not favor generation of inelastic collisions, which are responsible for generating new plasma species. Above mentioned parameters have influence on physico-chemical properties and architecture of plasma polymer films.

1.4 Conclusions

In this frame, the goal of the present work is to develop an antibacterial coating, especially design for soft biomaterial such as polypropylene mesh, which will exhibit antibacterial properties, allowing the control over bioactive agent releasing properties. The final material should exhibit anti-biofilm formation properties to prevent the common problems of mesh-related infections after surgical operations.

The following chapter will be focused on describing the elaboration of mechanically-sensitive materials made of plasma polymer multilayers and bioactive agents. These systems are developed on modified polypropylene-made mesh substrate using solvent-free steps based on plasma polymerization. Tailored release of an active agent is achieved by mechanical stimulation of the designed material. Silver, stored as AgNPs in the plasma polymer multilayer system and released in the material surroundings in its bioactive ionic form process, is described. One of the main features of this system is that, taking advantage of different mechanical properties between the different layers, a system of cracks in the plasma polymer overlayer allows control of the diffusion of silver ions. The antibacterial properties are evaluated and described in the following part. The stability of the properties of the film under the stress of elongation is also shown.

The emphasis of this research is the use of control release of silver ions from mechanoresponsive plasma polymeric coating deposited on the biomaterial as a tool for non-antibiotic and anti-biofilm strategies for implant related infections.

CHAPTER II

Introduction

Use of a mesh-biomaterial in abdominal wall reconstruction, pelvic floor reconstruction and stress urinary incontinence is a common procedure to decrease morbidity, decrease the rate of recurrences and improve the outcome of patient [83, 332-335].

Introduction of a polypropylene (PP) mesh during surgical procedure to increase the strength of abdominal wall was an important breakthrough in 1962. PP is non-toxic, cannot be absorbed, and can be cut and modeled without deforming. It displays good mechanical characteristics such as durability and flexibility [336] and can be sterilized. Positive effects of the use of such mesh has stimulated the research for the optimal mesh. Meshes are available in a variety of geometrical designs, pore size and morphology of monofilament fiber [83, 336, 337]. Surgical meshes available on the market can be made of absorbable synthetic, non-absorbable synthetic or organic material. Absorbable meshes contain glycolic acid (GA) and poly(lactic acid) (PLA) in various ratios. In the case of non-absorbable meshes, the most common is expanded polytetrafluoroethylene (ePTFE), PTFE, PP. Organic meshes have human or porcine origin. Meshes are available as monofilament or multifilament yarns and a knitted or woven structure. Ideal mesh has following characteristics: it should be flexible; it should have elasticity in more than one dimension, allowing it to stretch in more than one direction and then return to its original shape. In this way, mesh should match the tissue dynamics as closely as possible [83]. In regard to these requirements, existing polymeric mesh materials fulfill the above mentioned criteria. However the infection preventive feature of a mesh is not achieved yet.

Meshes show different characteristics concerning tissue ingrowths, rate of recurrence and rate of infection according to their morphological, chemical, and physical-chemical properties [332, 337].

Therefore, there is a need of development of a mesh which specifically prevents the infection on the implantation site.

In this regard, surface modification of existing PP mesh material can be promising way to render the surface of polymeric mesh implants as antibacterial. For this purpose, in this work, plasma polymerization is used as a fast, solventless method to change surface properties of PP mesh by deposition of plasma polymer nano-thick layer. Silver nanoparticles as a reservoir of antibacterial agent, which can be released to the environment, are enclosed in this plasma polymer and protected from spontaneous release by deposition of second plasma polymer layer. Due to particular characteristic of a second plasma polymer layer, control of the release properties of silver ions from the coating is possible under mechanical stimulation.

In this chapter, detailed description of elaboration process and characterization of a multilayer plasma polymer systems, which consist of two layers of maleic anhydride plasma polymer deposited on the surface of polypropylene-made surgical mesh is given. AgNPs as an antibacterial agent reservoir were trapped between the two plasma polymer layers. Owing to differences between the mechanical properties of the plasma polymer thin films and the elastic bulk substrate, tensile stresses generate cracks within the plasma polymer overlayer, which might be used as diffusive channels for Ag^+ species. The aperture of the cracks is shown to be mechanically controlled in a reversible way, allowing the control over releasing properties. Moreover, first investigations of the antibacterial properties of the materials are presented.

This chapter consists of a scientific paper that has been recently published in a peer-reviewed journal.

2 Mechanically responsive antibacterial plasma polymer coatings for textile biomaterials

Emilia Kulaga, Lydie Ploux, Lavinia Balan, Gautier Schrodj

and Vincent Roucoules

INSTITUT DE SCIENCE DES MATERIAUX DE MULHOUSE

IS2M - C.N.R.S. - UMR 7361 - UHA

15, RUE JEAN STARCKY

68057 MULHOUSE Cedex

FRANCE

Kulaga, E., Ploux, L., Balan, L., Schrodj, G. and Roucoules, V. (2013), Mechanically Responsive Antibacterial Plasma Polymer Coatings for Textile Biomaterials. Plasma Processes Polym. doi: 10.1002/ppap.201300091

2.1 Abstract

We have developed a new type of mechanically responsive material on the basis of a plasma-modified soft biomaterial substrate (polypropylene surgical mesh). A first plasma deposited layer, enriched in a bioactive agent (silver nanoparticles), has been covered by a second plasma polymer layer that acts as a barrier to spontaneous release. The release of the active agent in a controlled manner was achieved by the presence of mechanically-reversible fragmentations in the top-layer of deposited plasma polymer, induced by mechanical stimuli. Characterization of the material was performed by Scanning Electron Microscopy, Transmission Electron Microscopy, Attenuated Total Reflexion–Fourier Tranform Infra-Red, Xray Photoelectron and Ultra Violet-Visible Spectroscopies. The antibacterial properties of the material have been verified.

2.2 Introduction

Hospital infections are a major cause of morbidity and mortality [338]. Today, more than 1 million people all over the world suffer from nosocomial infectious complications [338]. Most frequently, these infections are associated with surgical wounds, the urinary tract or respiratory tract and directly involve invasive medical devices such as catheters or implants [339-341]. Medical devices thus act as passive surfaces prone to bacterial adhesion and biofilm formation [23, 342]. Nowadays, preventive strategies are used to fight bacterial colonization of such devices, in addition to oral treatments with antibiotics. They directly involve the biomaterial, which is modified to specifically exhibit anti-adhesive or antibacterial chemical surface properties [343-347]. In hospital environments, more and more devices with biopassive (in this case, the surface chemistry prevents bacterial adhesion without any antibacterial effect) or bioactive (here, the surface chemistry has a biological i.e., antibacterial effect) surfaces are exploited [348-350]. Nevertheless, they are mainly dedicated to external use and are rarely employed for implants. For internal use, drug delivery systems are preferred, aimed at fighting both planktonic and attached bacterial populations, and at controlling the dose of antibacterial agent delivered to the patient, the lifespan of the implant and the lifespan of its antibacterial effect [351, 352]. Until now, however, these objectives have remained a challenge for most surgical situations. Solutions need to be specifically developed for each of them according to their specific constraints.

Typically, polymer meshes used as implants for abdominal and gynecological repairs are favorable to bacterial infections due to the uneven topography of meshes and, in the specific case of gynecological repairs, the large quantity of bacteria present at the implantation location. Antibacterial smart coatings dedicated to such soft and deformable materials are therefore needed. Nevertheless, aside from the difficulty in controlling drug delivery dose and kinetics, coatings on soft and deformable materials are highly sensitive to

damage that may be induced by movements of the patient, affecting the lifespan of the biomaterial.

In addition, bacterial resistance to antibiotics continues to increase, while antibiotics are the only (and thus essential) treatment to fight infections [353-356]. This implies the necessity of reducing the use of antibiotics in systems dedicated to local and long-term drug delivery. Therefore, the use of alternative antibacterial agents is now highly desired in the medical field. In this framework, silver species that have long been known to have antimicrobial activity are used in more and more biomedical sectors [165, 279, 357, 358]. No toxicity to human cells has been highlighted for silver ions (Ag^+) up to micromolar concentrations [359, 360]. Besides aiming to avoid potential toxicity due to the specific nanoparticle form, AgNPs can be the source of Ag+ delivery, without release in the patient body. As with other inorganic nanoparticles, AgNPs exhibit inherent and unique characteristics such as large specific surface areas, controlled surface composition and reactivity, which endow them with remarkable physical, chemical and biological properties [361-363]. They can constitute efficient reservoirs for delivery of Ag^+ through their oxidation in contact with body fluids. Furthermore, despite undisputable bacterial resistance to heavy metals [364-366] resistance to silver remains low compared to antibiotics [367, 368]. The risk of significantly reducing silver's antibacterial efficiency through increasing its use as an antibacterial agent in medical devices is still low, due to the rare exploitation of silver for human health.

In this context, recent efforts have been made to develop Ag-containing coatings and plasma polymerization appears as a good candidate offering great flexibility. One of the main advantages is that plasma coatings can be deposited onto practically any type of material and device [328, 369-375]. Several examples are reported in the literature based on the use of plasma polymerization deposition and co-sputtering of a silver target under low pressure plasma conditions. Boldyryeva *et al.* [376] and Hlidek *et al.* [377] investigated the potential of using DC glow discharge deposition and an

unbalanced magnetron operating in a Ar/n-hexane or nitrogen/hydrocarbon working gas mixture to form Ag/C:H or Ag/C:H:N composite films. The authors demonstrated the possibility of controlling the size of the silver particles by changing the power during the deposition step, but no information on the release of Ag^+ was given. Later, Zanna *et al.* [378] reported the synthesis of nanocomposite thin films composed of silver particles enclosed in an organosilicon matrix. The film deposition was carried out by combining radiofrequency glow discharge fed with argon (Ar) and hexamethyldisiloxane with simultaneous silver sputtering. The authors focused their work on the stability of such coatings. Aging was studied under saline conditions and different mechanisms were suggested depending on the initial concentration of silver particles in the film. In particular, for films with high silver content, the coating thickness decreased with immersion time, due to significant silver release and matrix erosion assigned to a percolation-like effect. However, a strongly-bonded polymer layer remained even after long periods of immersion. Recently, Beier *et al.* improved the resistance of Ag-rich-organosilicon plasma films to abrasion by working at atmospheric pressure and directly spraying a silver nitrate solution within the plasma [379].

In other works, more effort has been focused on controlling the amount of AgNPs loaded in the film as well as controlling the rate of release of Ag^+ in order to avoid cytotoxic overdoses. Körner *et al.* [288] showed that plasma polymer coatings with embedded AgNPs can be deposited in a low pressure radio frequencies plasma reactor using an asymmetrical setup with an Ag electrode. The plasma polymer was deposited from a reactive gas/monomer mixture of CO_2/C2H_4 yielding a functional hydrocarbon matrix. Argon was simultaneously used to sputter Ag atoms from the Ag electrode, forming nanoparticles within the growing polymer matrix. By adjusting the process parameters, the coating could be tailored (e.g., Ag content, Ag particle's morphology and distribution) to different requirements for specific applications and act as efficient reservoirs for Ag^+. In addition, Vasilev *et al.* [287] used

amine plasma polymer films loaded with AgNPs. The quantity of nanoparticles loaded was controlled by the time of loading with $AgNO_3$ and by the thickness of the plasma polymer layer. The authors also demonstrated control over the release of Ag^+ by depositing a thin (< 20 nm) plasma polymer overlayer.

Very interestingly, the works reported by Körner *et al.* and Vasilev *et al.* clearly demonstrated that the amount of AgNPs and the rate of release of Ag^+ can be tuned by playing with the properties of the plasma polymer. However, these adjustments are only possible during fabrication of the biomaterials. Once the Ag-containing coating is implanted, the release process cannot be adjusted anymore. It can also be strongly affected by arbitrary variations occurring in the surrounding medium. In other words, the biomaterial is bioactive but the rate of the release process still passive. The challenge of creating materials with full control of the release process after implantation thus remains totally open.

Recently, we proposed a new concept for a drug delivery system dedicated to soft materials, providing control of duration and doses of delivery [194]. Based on Ag^+ release driven by mechanical stimuli, the concept was proved for PDMS model materials. In the present work we propose a new generation of bioactive biomaterials that are able to adjust their release of bioactive agent under mechanical stimuli thanks to the same concept. This was achieved by the fabrication of multilayer plasma polymer systems, which consisted of two layers of maleic anhydride plasma polymer deposited on the surface of polypropylene-made surgical mesh. AgNPs were trapped between the two plasma polymer layers and acted as an antibacterial agent reservoir. Owing to differences between the mechanical properties of the plasma polymer thin films and the elastic bulk substrate, tensile stresses generate cracks within the plasma polymer overlayer, which might be used as diffusive channels for Ag^+ species. The originality of the system is that the aperture of the cracks can be mechanically controlled in a reversible way.

This new system makes it possible to tailor doses of the antibacterial agent released over time and thus to prolong the lifetime of the antibacterial properties of the material. In the case of surgical polypropylene meshes and more generally in the field of textiles for implants and other soft biomaterials, this strategy is promising. Cracks will be created in a controlled way before implantation, and crack opening and subsequent Ag^+ release will be induced by mechanical stresses naturally occurring at the location of the implant.

2.3 Experimental

2.3.1 Materials

Undyed, knitted, pure polypropylene (PP) mesh was provided by Cousin Biotech (Biomesh®P1). Briquettes of maleic anhydride (99.5% purity), silver nitrate solution (0.1 M) and $NaBH_4$ (98% purity) were obtained from Sigma-Aldrich and used as received.

2.3.2 Plasma reactor

Plasma treatments were carried out in an electrodeless cylindrical glass reactor (6 cm diameter, 680 cm^3 volume, base pressure of 5 x 10^{-4} mbar and leak rate better than 1.0 x 10^{-10} $kg.s^{-1}$) enclosed in a Faraday cage (see **Figure 2-16 in supporting information**). The chamber was fitted with a gas inlet, a Pirani pressure gauge, a two-stage rotary pump (Edwards) connected to a liquid nitrogen cold trap and an externally wound copper coil (4 mm diameter, 5 turns). All joints were grease-free. An L-C matching network (Dressler, VM 1500 W-ICP) was used to match the output impedance of a 13.56 MHz radio-frequency (R.F.) power supply (Dressler, Cesar 133) to the partially ionized gas loaded by minimizing the standing wave ratio of the transmitted power. During electrical pulsing, pulse shape was monitored with an oscilloscope. The average power <P> delivered to the system was calculated using the following expression: $<P> = P_p [t_{on} / (t_{on} + t_{off})]$, where P_p is the average continuous wave power output and $t_{on} / (t_{on} + t_{off})$ is defined as the duty cycle.

2.3.3 Antibacterial coating

PP substrates (2 x 4 cm²) were placed in the center of the plasma reactor chamber followed by evacuation back down to the initial pressure (~ 5 x 10^{-4} mbar). It is worth noticed here that the PP mesh was at floating potential. They were first activated by argon plasma during 1 min at 60 W (*PP/Ar*). Subsequently, maleic anhydride vapor was introduced into the reaction chamber (pressure of 0.2 mbar) with a flow rate of approximately 1.6 x 10^{-9} $kg.s^{-1}$. At this stage, the plasma was ignited and run for 30 min. The deposition conditions corresponded to: power output = 20 W, duty cycle = 2% and frequency = 816 Hz and deposition rate = ~0.3 ± 0.2 $nm.min^{-1}$. Upon completion of deposition, the R.F. generator was switched off and the flow of monomer was maintained in the system for a further 2 min period prior to venting up to atmospheric pressure. Prior to use, plasma polymer modified substrates were immersed in deionised water to promote the hydrolysis of maleic anhydride groups into dicarboxylic acid groups (*PP/Ar/MAPP*). Then, silver was loaded directly on the *PP/Ar/MAPP* surface by immersion of the coated substrate into a 1.0 mM silver nitrate solution for 30 min. Silver cations diffused into the reservoir and formed electrostatic pairs with carboxylate groups. Ag^+ ions bound to carboxylate were reduced to zero-valent Ag nanoparticles using an aqueous solution of $NaBH_4$ (2.0 mM). Then, the *PP/Ar/MAPP/Ag* material was placed in the chamber of the plasma reactor and the system was pumped down to base pressure. Maleic anhydride vapor was introduced into the reaction chamber at a constant pressure of 0.2 mbar. The plasma was ignited and run for 10 min according to the following conditions: power output = 20 W, duty cycle = 50% and frequency = 816 Hz The deposition rate was ~12.5 ± 0.5 $nm.min^{-1}$. Upon completion of deposition, the R.F. generator was switched off and the flow of monomer was maintained in the system for a further 2 min period prior to venting up to atmospheric pressure. The integrity of the plasma polymer layers was checked after immersion in a phosphate buffered saline (PBS) solution or

in the bacterial culture medium by scanning electron microscopy. Then, the final bioactive coating (*PP/MAPP/Ag/MAPP*) was sterilized either with an electron beam (Aerial, Illkirch, France) or dry heating (1 h, 100 °C). Modifications in the bioactive coating properties potentially induced by changing the procedure of sterilization have been studied and will be the subject of a future paper. Importantly, the results presented in the next section, which demonstrate that the release of Ag^+ and its control could be perfectly controlled by playing with mechanical stresses, was confirmed for both procedures of sterilization

2.3.4 Elongation of the bioactive materials

Elongation of the coated meshes was performed on a homemade stretching device (see **Figure 2-17 in supporting information**) with a speed of 24 µm/s. Samples were subjected to stretching/unstretching cycles where the elongation rates were set to 20%, 40% or 80% of the initial sample length (100% of elongation means twice the initial length).

2.3.5 Electron Microscopy

Scanning electron microscopy (SEM) images were acquired using an FEI environmental microscope (Quanta 400 model) working at 30 keV. Samples were observed using high vacuum mode.

Transmission electron microscopy (TEM) images were obtained using a Philips CM20 instrument with a Lab6 cathode, at an acceleration voltage of 200 kV. Cross-sections of samples were obtained using a microtome (LKB model 8800).

2.3.6 Infrared Analysis

Attenuated total reflection Fourier transform infrared (ATR-FTIR) spectra were recorded with a Brucker IFS 66 FTIR spectrometer equipped with an ATR accessory from Specac. The spectrometer was equipped with a nitrogen cooled MCT detector. Spectra were the result of the sum of 256 scans and were recorded in the range of 4000–650 cm^{-1} with a spectral resolution of 4 cm^{-1}. A single reflection Ge crystal (refractive index ~ 4.0) with a 65 ° beam incidence was used. The spectrum of a freshly cleaned Ge crystal was used as a background.

2.3.7 UV-Visible analysis

UV-Visible absorption measurements were carried out with a Perkin-Elmer Lambda 750 rapid-scan spectrometer equipped with two Hamamatsu R 955 photomultipliers. The light sources were deuterium (DL) and tungsten-halogen (THL) lamps (12V) working in the range of 190–3300 nm. Spectra were the result of the sum of 100 scans. Microsoft Windows based Perkin-Elmer UV Winlab software was used for data acquisition and analysis. Spectra were recorded between 250 and 800 nm. Two types of measurements were done using a UV-Visible spectrophotometer: *i)* UV-Visible absorbance of samples coated with the plasma polymer multilayer system and *ii) UV/Vis absorban*ce of released Ag^+ and AgNPs. For the first type of measurement, the *PP/Ar/MAPP/Ag/MAPP* sample was placed in the holder of the instrument and the measurement was performed. For the second type, the release of Ag^+ and AgNPs from the plasma polymer multilayer system into distilled water was followed during stretching of the material. In this case, the limit of detection was ~3 ppm $AgNO_3$ (see **Figure 2-18 in supporting information**). For testing the effect of elongation on the release of silver, the sample was stretched under ambient atmosphere and immediately immersed in 9 ml of distilled water. After

24 h, the water was removed, divided into three parts (3 ml each), placed into polystyrene cuvettes and analyzed in the range of 250–800 nm to detect potentially released AgNPs. A 0.5 mL aliquot of a freshly prepared $NaBH_4$ solution with a concentration of 2.0 x 10^{-3} M was then added to reduce silver from the ionic form to zero valent AgNPs. After 5 min, these samples were analyzed and the surface plasmon absorbance peak around 400 nm was observed. The corresponding peak area was measured. Then, the stretching ratio was changed and the sample was immersed in distilled water for another 24 h period. The UV/Vis absorbance of the new solution was measured by repeating the aforementioned procedure.

2.3.8 XPS analysis.

XPS spectra of PP and PP-functionalized surfaces were recorded with a VG SCIENTA SES-200 spectrometer equipped with a concentric hemispherical analyzer. The incident radiation was generated by a monochromatic Al K_α X-ray source (1486.6 eV) operating at 420 W (14 kV; 30 mA). Photo-emitted electrons were collected at a take-off angle of 90 ° from the sample with electron detection in the constant analyzer energy mode. Signals for survey spectra were recorded with a pass energy of 500 eV. For high-resolution spectra of C1s, O1s and Ag3d components, the pass energy was set to 100 eV. The analyzed surface area of PP mesh sample was approximately 3 mm^2 and the base pressure in the analysis chamber during experimentation was about 10^{-9} mbar. Charging effects on these isolating samples were compensated for by using a Flood Gun. The spectrometer energy scale was calibrated using the Ag $3d_{5/2}$, Au $4f_{7/2}$ and Cu $2p_{3/2}$ core level peaks, set respectively at binding energies of 368.2, 84.0 and 932.7 eV. Peak fitting was performed with mixed Gaussian-Lorentzian (30%) components with equal full-width-at-half-maximum (FWHM) using CASAXPS software.

2.3.9 Differential Scanning Calorimetry (DSC) measurements

A METTLER TOLEDO DSC 1 was used for thermal analysis and crystallinity determination. The polypropylene sample was heated from -100 °C to 250 °C, cooled to -100 °C and re-heated to 250 °C. The heating and cooling rates were +/- 10 °C/min. Crystallinity was calculated during the heating cycles by comparing experimental peak areas to the theoretical one obtained in the case of 100% crystalline polypropylene (207.1 J/g).

2.3.10 Mechanical tests

An INSTRON 4505 (Zwick upgraded) dynamometer was used to perform tensile tests at room temperature. In all experiments, the initial length between jaws was 40 mm. During conventional tests, the rate was set to 5 mm/min. Each curve corresponds to the average of five experiments. During cyclic tensile tests, the rate was set to 10 mm/min for both loading and unloading steps. The number of cycles was 50 and the elongation was 20% or 60% of the initial length.

2.3.11 Antibacterial assay: On-plate diffusion test

Bacterial culture experiments were conducted with the *Escherichia coli* (*E.coli*) K12 (PHL628) strain [66, 380] This strain expresses curli and produces exo-cellular polymeric substances (EPS). One milliliter of bacteria stock culture (stored at -80 °C) was used to inoculate 10 ml of selective growth medium (M63G [380], pH = 6.8), resulting in a pre-culture that was grown further overnight at 30 °C. This culture was then used to inoculate a second pre-culture (10 vol.-% of the last pre-culture), which was grown for 4 h under the same conditions. One hundred microliters of this fresh bacterial suspension was

spread on Luria-Bertani (LB) agar-supplemented growth medium (15 $g.L^{-1}$) in order to form a thin bacterial film.

The sterilized samples were placed in contact with agar plates previously homogeneously inoculated (with the top side of the samples in contact with the agar). After overnight incubation at 30 °C, bacterial growth around the samples was observed in order to identify the potential presence of zones without bacterial growth (growth-inhibition areas).

2.3.12 Antibacterial assay: Analysis of biofilm development

Experiments were conducted with the PHL628-based *E.coli* SCC1 strain [380]. This strain is auto-fluorescent through a GFP-based genetic insertion. Bacteria taken from frozen stock (-80 °C) were inoculated on an agar plate of LB medium for an overnight culture. One colony of bacteria was inoculated in 10 mL of LB medium and cultivated at 30 °C overnight for a first pre-culture. A second pre-culture was inoculated with the first pre-culture (10 vol-%) in 10 mL of selective M63G medium and cultivated at 30 °C overnight. A third pre-culture was inoculated from the second pre-culture (10 vol-% of the second pre-culture) for 4 h at 30 °C. The final culture used to perform the experiment was inoculated from the 4 h pre-culture (10 vol-%). Its absorbance at 600 nm (Abs_{600}) was adjusted to 0.01 (i.e, 10^6 bacteria/mL). Coated-mesh samples, previously sterilized by e-beam with a dose of 25 kGy, were placed into small Petri dishes (Ø 35 mm) on sterilized-in-oven (180 °C for 1 h) silicon wafers. Stainless steel wire was used to maintain the sample on the dish bottom. Samples were inoculated with 4 mL of the final bacterial culture and incubated for 168 h (i.e., one week) at 30 °C. Samples were then thoroughly and carefully rinsed to eliminate non-adherent or loosely attached bacteria from the substrate surfaces. For this purpose, 2 mL of supernatant (i.e. bacterial suspension for the first rinse and NaCl solution for further rinsing steps) were removed, kept for further bacterial concentration measurement and replaced by 2 mL of fresh NaCl

solution. The rinsing step was performed without direct flushing, with the stream directed toward the walls of a petri dish and with attention to the force and content of the rinsing fluid. The material samples remained immersed in liquid during the rinsing steps, without creating any air-sample interface. The rinsing step was repeated 16 times.

Material samples were kept immersed in the last rinsing solution. They were then observed *in situ* by using an upright Confocal Laser Scanning Microscope (CLSM; Carl Zeiss, LSM700) equipped with a long working distance objective (LD EC Epiplan Neofluar 50x/0.55 DIC M27; working distance of 9.1 mm). Three-dimensional pictures were taken of at least at five different, randomly chosen locations on each sample. Image processing was performed using the ImageJ® V.1.44a software with the LSM toolbox V4.0g plugin [381], allowing separation of fluorescence and reflection images from Zeiss LSM raw data. Images so extracted were then analyzed with the COMSTAT2® software to determine the quantity of biofilm (biomass) [70].

Antibacterial analyses were conducted on *PP/Ar/MAPP/Ag/MAPP* samples with and without stretching at 60% of their initial length as well as on *PP* and *PP/Ar/MAPP/Ag* samples, used as negative and positive controls, respectively. Two samples of each material type were used for each experiment. The experiment was repeated at least 3 times.

2.4 Results and discussion

The antibacterial coatings, consisting of multi-layer plasma polymer systems, were fabricated by following a multi-step procedure schematized in **Figure 0.1**. A first step of Ar plasma treatment applied to the polypropylene mesh (step b) was followed by deposition of a minimally cross-linked plasma polymer thin film with an anhydride-rich structure (step c). Subsequent immersion in water led to the opening of cyclic anhydride groups and the formation of carboxylic acids.

Successive immersion in solutions of silver ions and reductive agent readily triggered the immobilization of silver nanoparticles onto the plasma polymer layer (step d). The last step in the procedure consisted of depositing a highly cross-linked plasma polymer overlayer.

The originality of this work derives from the fact that the aforementioned procedure led to a multi-layered plasma polymer system in which cracks in the overlayer were anticipated under mechanical strains and in a controlled manner, aimed at creating diffusive channels for better control of Ag^+ species release.

2.4.1 Polypropylene mesh substrates *(PP)*

2.4.1.1 Mechanical properties

The polypropylene implant used in this work was biomesh®P1 (parietal reinforcement implant) from Cousin Biotech. Images of this substrate are shown in **Figure 2-1a**. The diameter of each fiber was about 200 µm. The nominal aperture was estimated to 0.60 ± 0.05 mm^2 with 8 threads per centimeter and an open area of 47.7%. Such a mesh design can be elongated almost twice its initial length (100% elongation) before failure. It is obvious that the strength and extensibility of the mesh differed considerably according to the direction of stretching.

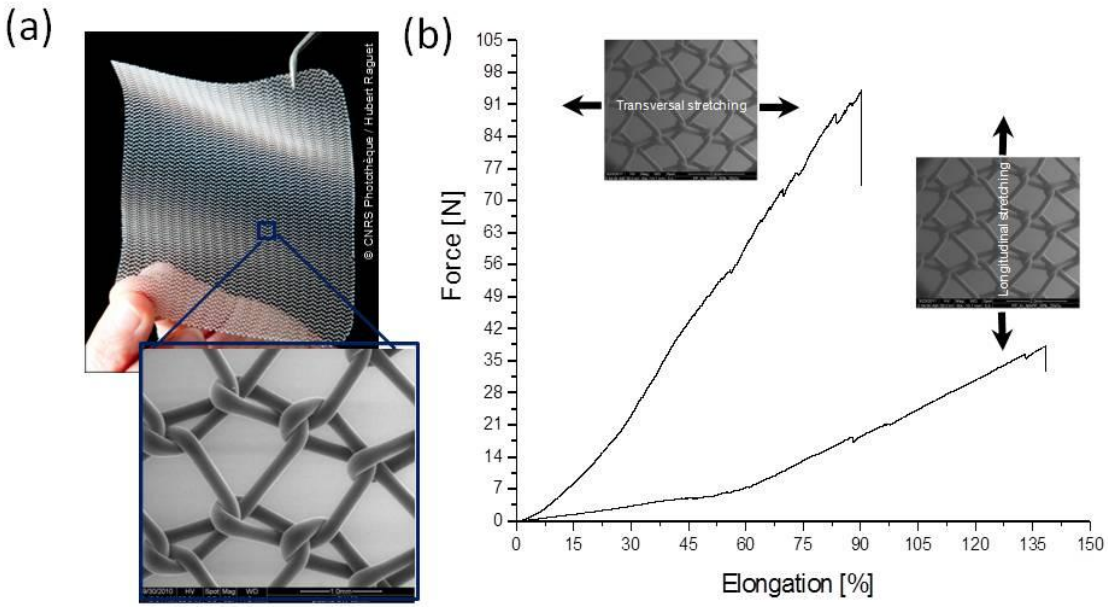

Figure 2-1: a) Photograph (© CNRS Photothèque / Hubert Raguet) and scanning electron microscopy of Biomesh®P1 used in this work (Cousin Biotech) and b) typical load–displacement curves during transverse and longitudinal elongation.

Figure 2-1 (b) shows typical loading curves recorded during uniaxial tensile tests using transversal or longitudinal elongation. In both cases, two different regimes in the load-elongation curves were observed, evolving from a non-linear to a quasi-linear regime. During transverse stretching, the material displayed an initially, relatively high stiffness (defined as F/δ where F is the applied force and δ the displacement produced by F) that gradually increased, changing to a high, linear stiffness above ~30% of the failure strain. When the tensile was applied longitudinally, the same behavior was observed but the stiffness was much less and the transition between the non-linear and quasi-linear regimes occurred at about 70% of maximal elongation. The corresponding failure strain was 3-fold less compared to transverse elongation. The origin of different regimes during stretching is well-explained in the literature [382]. The non-linear regime is mainly driven by the mesh design,

while the quasi-linear regime is determined by the mechanical properties of each individual fiber.

Cyclical loading of mesh samples at strains of 20 ± 5% (equivalent to 0.010 Hz) and 60 ± 5% (equivalent to 0.003 Hz), for 50 sinusoidal loading cycles, produced significant permanent deformation in the mesh design (see **Figure 2-19 in supporting information**). The permanent deformation was strongly dependent on the direction in which the stress was applied. In contrast, it was quasi-independent of the elongation ratio. During transverse stretching, the permanent deformation corresponded to 7.5% of the elongation while it reached 30% in the case of longitudinal stretching.

In the following parts of this work, coated- and uncoated-polypropylene substrates were only elongated in the transverse mode in order to *i)* minimize permanent deformations and *ii)* preferentially induce elongation of each individual fiber.

2.4.1.2 Physicochemical properties.

Spectra a) in **Figure 2-2** shows the X-ray diffraction pattern of the polypropylene substrate, revealing the partially crystalline character of the material [383].

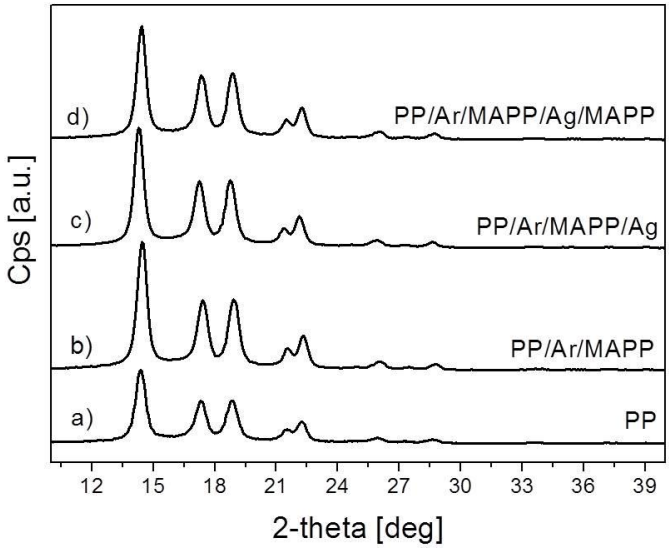

Figure 2-2: X-ray diffraction pattern of a) polypropylene substrate, b) (a) coated with the first plasma polymer layer, c) (b) loaded with silver nanoparticles, d) (c) coated with a second plasma polymer layer.

The degree of crystallinity was estimated to be 47 ± 5% by DSC measurements (see **Figure 2-20 in supporting information**). The XPS elemental composition of the surface is given in **Table 2-1**. The C(1s) envelope was fitted with two peaks at 285.0 eV and 286.5 eV (see **Figure 2.3, spectrum a** and **Table 2-4 in supporting information**). The peak at 285.0 eV was attributed to C-C or C-H bonds, while the peak at 286.5 eV was attributed to C-O bonds. The presence of the latter peak suggests that untreated *PP* contained a low level of oxidized carbon centers on its surface.

	Atomic concentration [%]					
Element	***(a)***	***(b)***	***(c)***	***(d)***	***(e)***	***(f)***
	PP	***(a)* + Ar**	***(b)* + MAPP**	***(c)* + hydrolysis**	***(d)* + Ag NP**	***(e)* + MAPP**
C	91.0	84.0	64.5	66.3	69.8	62.8
O	2.2	11.5	28.0	26.7	9.8	28.5
Au*	*6.8*	*4.5*	*7.5*	*7.0*	*6.2*	*6.2*

Ag	10.9	2.5
Na	3.3	

Table 2-1: Surface atomic composition at each step of material development, a) polypropylene mesh, b) (a) expose to Ar plasma, c) (b) coated with a first maleic anhydride plasma polymer layer, d) (c) hydrolyzed, e) (d) loaded with silver nanoparticles, f) (e) coated with second plasma polymer layer; ** The presence of gold is due to detection of the gold sample holder during analysis because of the mesh design.*

2.4.2 Functional plasma polymer deposition onto polypropylene mesh substrates

An anhydride containing plasma polymer layer was deposited onto the polypropylene substrate and subsequently hydrolyzed to form carboxylic acid groups. An activation step using Ar plasma was used in order to strengthen the interface between the polypropylene surface and the plasma polymer layer. XPS results revealed that exposure to Ar plasma led to an increase in oxygen content accompanied by the appearance of two new peaks at 288.0 eV and 289.4 eV belonging to C=O and O-C=O groups, respectively (see **Figure 2-3 - spectrum b, Table 2-1** and **Table 2-4 in supporting information**). The concentration of C-O groups increased to 4.2% after plasma treatment while the concentration of C-C or C-H groups decreased to 87.3%.

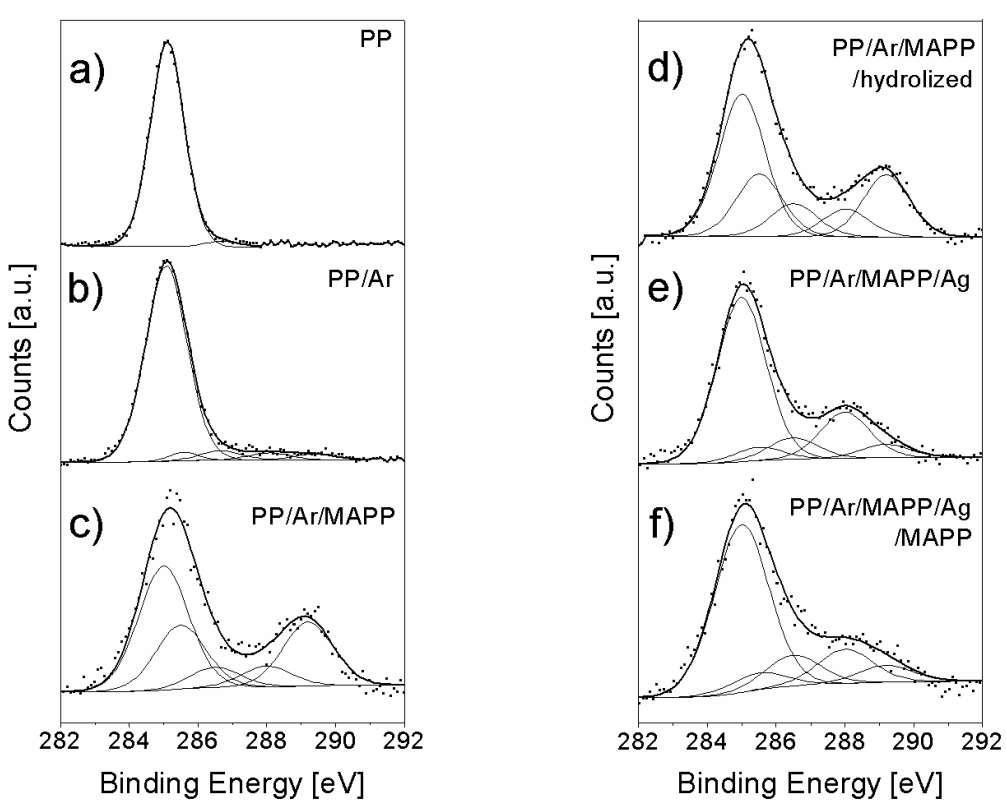

Figure 2-3: High resolution C(1s) XPS spectra of a) polypropylene mesh substrate, b) (a) exposed to Ar plasma, c) (b) coated with a first maleic anhydride plasma polymer layer, d) (c) hydrolyzed, e) (d) loaded with silver nanoparticles, f) (e) coated with a second maleic anhydride plasma polymer layer.

This phenomenon is already well-described in the literature [384]. Bombardment of polypropylene substrates by energetic Ar species mainly results in etching phenomena due to the physical removal of molecules (e.g., fragments of molecules), or the break-up of bonds, chain scission, and degradation processes. This quickly engenders an increase in surface roughness and the formation of radicals at the polypropylene surface. Incorporation of oxygen is thought to occur by the reaction of surface free radicals with atmospheric oxygen, reaction with oxygen-containing species within the plasma (e.g., residual water adsorbed on the reactor walls) and with oxygen from the air at the end of the deposition process, leading to the

formation of COOH groups at the surface. The infrared spectrum (**Figure 2-4 - spectrum b**) confirmed this reaction scheme and showed the appearance of a new broad band centered at 1735 cm^{-1} [A] belonging to COOH vibrations.

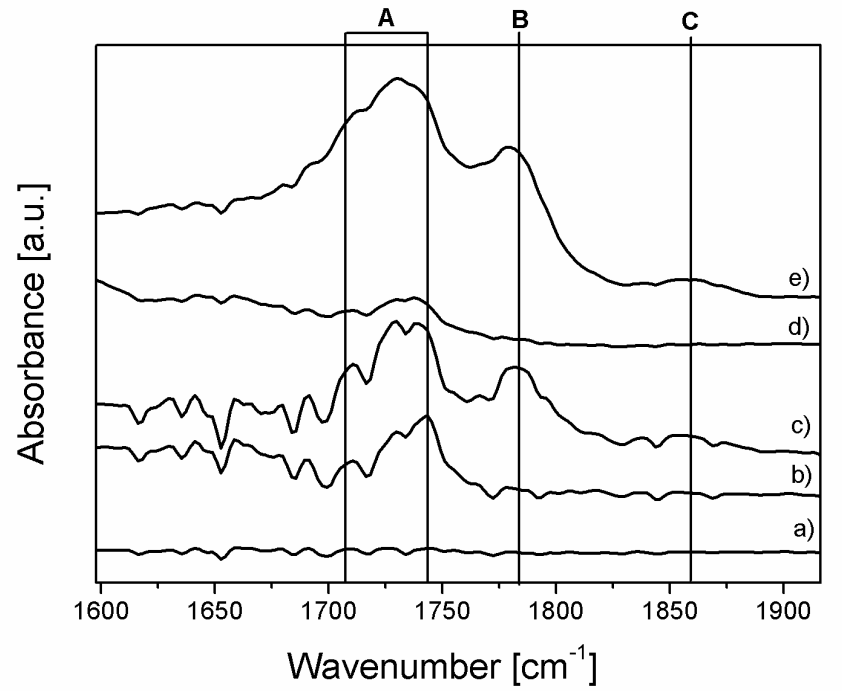

Figure 2-4: Infrared spectra of a) polypropylene mesh substrate, b) (a) exposed to Ar plasma, c) (b) coated with a first maleic anhydride plasma polymer layer and hydrolyzed, d) (c) loaded with silver nanoparticles, e) (d) coated with a second maleic anhydride plasma polymer layer.

A functional coating was deposited onto the Ar-activated polypropylene surfaces using pulsed plasma polymerization of maleic anhydride. While uniform coating was obtained on fibers, the final thickness was strongly dependent on the complex structure of the PP mesh. The thickness was estimated by ellipsometry to be 10 ± 5 nm. A well-adhered coating containing a variety of oxygenated carbon functionalities was achieved. XPS analysis of the plasma polymer layer indicated five new types of carbon in the C(1s) envelope: hydrocarbon (CHx ~ 285.0 eV), carbon singly-bonded to an anhydride group (C-C(O)-O- ~ 285.5 eV), carbon singly-bonded to oxygen (-C-O ~ 286.6 eV), carbon doubly-bonded to oxygen (O-C-O/-C=O ~ 288.0 eV), and acid/anhydride

groups (O=C-O/O=C-O-C=O ~ 289.4 eV) (see **Table 2-4 in supporting information)**. The plasma deposition conditions (t_{off} = 1200 μs, t_{on} = 25 μs, P_p = 20 W, and deposition rate = 3.4 ± 0.5 mn.min^{-1}) gave rise to 22% of all surface carbon atoms belonging to acid or anhydride cyclic repeat units (on the basis of the C(1s) envelope peak fitting).

Hydrolysis of the plasma polymer coatings was introduced as an extraction process of the unreacted monomer fraction (e.g., low molecular weight water soluble fractions). After hydrolysis, infrared spectra indicated broadening of the band at 1735 cm^{-1} ([A]) attributable to the formation of new carboxylic groups, and resulting from the overlap between the free carboxylic band at 1740 cm^{-1}, the intermolecular hydrogen-bonded carboxylic acid band at 1720 cm^{-1} and the intramolecular hydrogen-bonded carboxylic acid band at 1685 cm^{-1} (**Figure 2-4 – spectrum c**). The presence of characteristic asymmetric and symmetric C=O stretching cyclic absorbance bands ([B] and [C]) for anhydride groups in the infrared background indicated that hydrolysis had not occurred throughout the entire thickness of the plasma polymer film.

Sample	Contact Angle [°]	Thickness [nm]
PP	99 +/- 5	
PP_Ar	64 +/- 4	
PP_Ar_MAPP	66 +/- 4	10 +/- 5
PP_Ar_MAPP-Hydr	14 +/- 3	11 +/- 5
PP_Ar_MAPP_Ag	65 +/- 10	92 +/- 2
PP_Ar_MAPP_Ag_MAPP	51 +/- 2	125 +/- 4*

Table 2-2: Contact angle and thickness values measured on a) polypropylene mesh substrate, b) (a) exposed to Ar plasma, c) (b) coated with a first maleic anhydride plasma polymer layer, d) (c) hydrolyzed, e) (d) loaded with silver nanoparticles, f) (e) coated with a second maleic anhydride plasma polymer layer. * *The overlayer thickness was in addition to the thickness for the Ag-loaded first layer.*

Contact angle measurements taken at each stage of this reaction scheme were found to be consistent with the aforementioned description (**Table 2-2**). A change in the water contact angle (99 ° to 64 °) occurred upon argon plasma treatment, indicating increased interactions with water. Maleic anhydride plasma polymer deposition produced a slight increase in the contact angle (up to 66 °, a typical value reported in the literature for such plasma polymers [385]) followed by a decrease after hydrolysis (14 °) indicating here again increased interactions with water due to high surface coverage with carboxylic acid groups. A negligible change in thickness of the plasma polymer layer occurred after hydrolysis (**Table 2-2**).

The aforementioned treatment did not affect the crystalline character of the polypropylene fibers or the mechanical properties of the polypropylene mesh (see **Figure 2-20** and **Figure 2-19 of supporting information** respectively).

2.4.3 Nanoparticle loading within the plasma polymer layer

The pKa values of maleic anhydride plasma polymers films have previously been found to be pKa_1 = 3.5 and pKa_2 = 10.5 [371]. So, according to the experimental conditions (pH ~ 6–7), a portion of the carboxylic acid groups was deprotonated. These carboxylate groups allowed the attachment of silver ions via electrostatic interactions by immersing the coated substrate into a silver nitrate solution. It is interesting to recall here that hydrolysis of a plasma polymer thin film led to extraction of low molecular weight water soluble fractions of the film, thus creating a nanoporous structure which also helps the loading of Ag^+ ions [386]. Silver ions were therefore anticipated to diffuse within the entire thickness of the first plasma polymer layer. Then, Ag^+ ions were reduced to zero-valent AgNPs using aqueous $NaBH_4$ solution as a reducing agent. TEM images indicated that particles were generated (**Figure 2-5a**) with a broad size distribution centered on 38 nm (**Figure 2-5b),** and EDX analysis confirmed the presence of silver particles (**Figure 2-21 in supporting**

information). The thickness of the plasma polymer thin film loaded with nanoparticles was estimated to 92 ± 2 nm (**Table 2-2)**. The increase in thickness compared to the first plasma polymer layer alone can be explained by the formation of silver nanoparticles at the top of the plasma polymer layer. The change may also have been induced by the growth of silver nanoparticles inside the polymer matrix. Thus, tensile stress resulting from particle growth should have been transferred to the polymer matrix leading to expansion of the plasma polymer layer. The work of Vasilev *et al.* [287] clearly shows that this quantity can be tuned by playing with the Ag^+ loading time, time of reduction and thickness of the plasma polymer thin film. Here, the thickness of the plasma polymer layer was set to ~ 10 nm and the Ag^+ loading time to 30 min, keeping in mind that the quantity of silver particles could be easily adjusted if necessary. Concerning the reducing step, we examined the effect of the reducing time on the quantity of embedded silver nanoparticles and found that most of the Ag^+ species had been consumed after 30 min of reduction (see **Figure 2-22 in supporting information**).

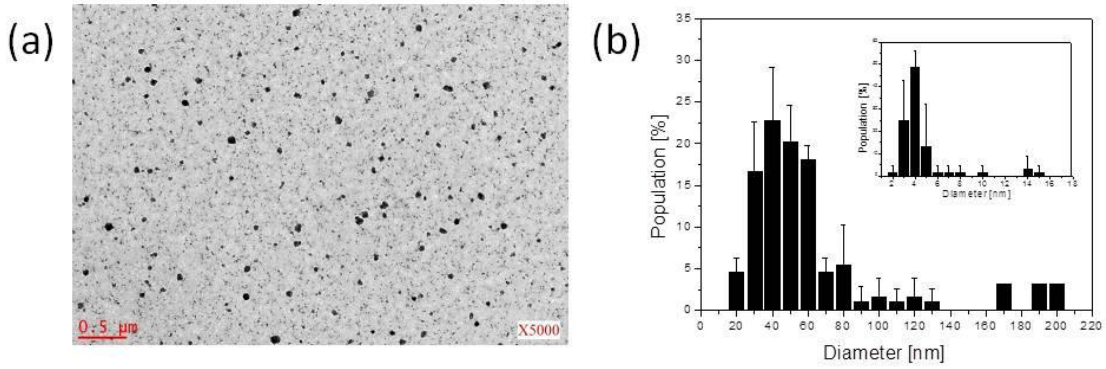

Figure 2-5: a) TEM images of the nanoparticle-loaded plasma polymer thin film and b) size distribution of the silver nanoparticles (inner graph shows results for particle diameters in the range of 2–20 nm).

The aforementioned procedure let to silver-rich plasma polymer layers, inducing a change in color of the sample toward pale yellow (**Figure 2-6a**). UV-Visible absorption spectra of the neat plasma polymer and the silver-loaded plasma polymer layer are shown in **Figure 2-6b**.

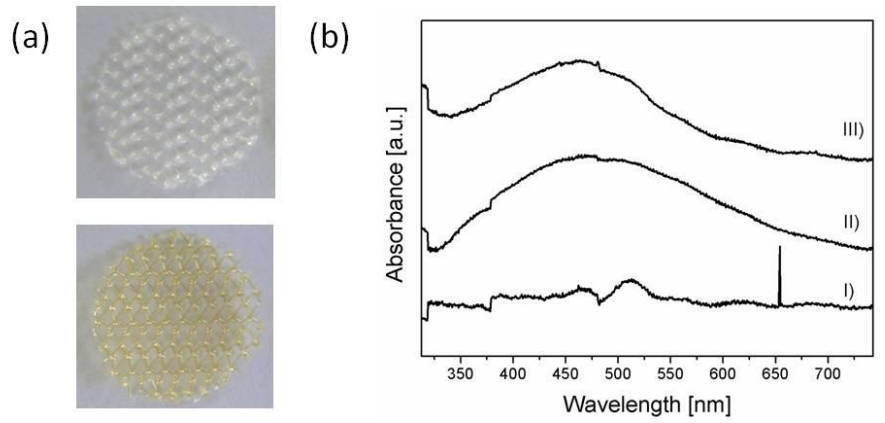

Figure 2-6: **a)** Optical images of untreated PP (top) and PP covered with the plasma polymer multilayer system (bottom). **b)** UV-visible absorbance spectra of I) polypropylene mesh substrate, II) (a) exposed to Ar plasma and then coated with a first maleic anhydride plasma polymer layer.

Compared with the unmodified polypropylene substrate, all Ag-nanoparticle containing systems displayed optical absorption due to the collective surface plasma resonance (SPR) of conductive silver electrons. A new broad peak centered at ~480 nm therefore appeared after reduction (**Figure 2-6b - spectrum II)**. The presence of a metallic form of silver was also confirmed by XPS analysis that allowed the detection of Ag $3d_{3/2}$ and Ag $3d_{5/2}$ photoemission X-ray lines at 367.9 eV and 373.9 eV, respectively (**Figure 2-7 - spectrum a**). The reducing step also induced changes in the XPS C(1s) envelope, revealing an increase in the contribution of C-C/C-H and O-C-O/-C=O groups at the expense of O=C-O-C=O/HO-C=O groups (**figure 2.3 - spectrum e** and **Table 2-4 in supporting information)**.

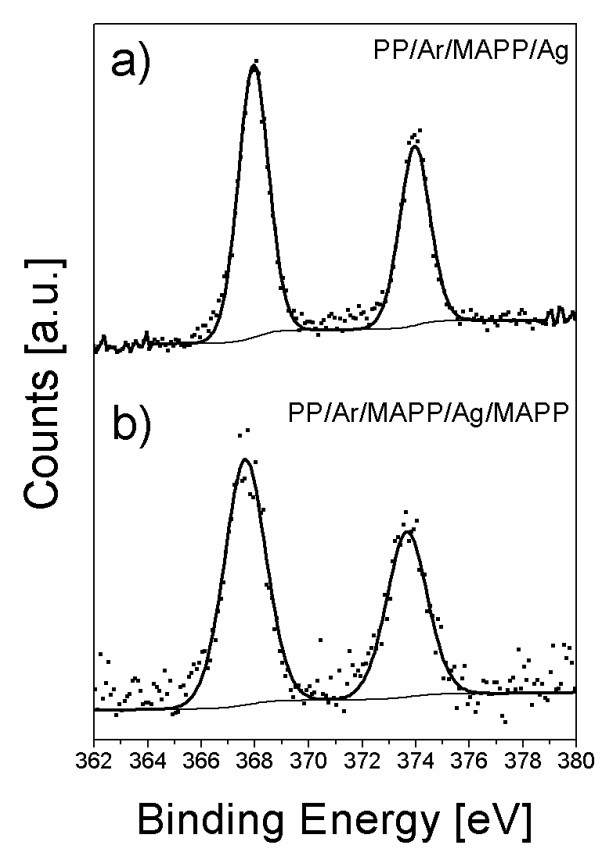

Figure 2-7: High resolution Ag(3d) XPS spectra of a) polypropylene mesh substrate exposed to Ar plasma, coated with a first maleic anhydride plasma polymer layer, hydrolyzed and loaded with silver nanoparticles, b) (a) coated with a second maleic anhydride plasma polymer layer.

2.4.4 Plasma polymer overlayer.

The last step of the elaboration procedure consisted of depositing a highly cross-linked plasma polymer overlayer. This was done by using a high duty cycle (50%) during deposition. Indeed, it is well known that a less selective chemistry occurs during plasma “on” excitation periods, where the predominance of fragmentation of monomer molecules to atoms or fragments leads to more cross-linked and less ‘polymer-like’ structures at relatively short off-times (e.g., high duty cycle) [326, 387]. XPS results confirmed this tendency. The contribution of the binding energy peak at 289.4 eV corresponding to O=C-

O-C=O/HO-C=O groups decreased, relatively, to 6.2 at.%, accompanied by a significant increase of the contribution of the peak at 285.0 eV associated with cross-linked carbon/hydrocarbon (C_xH_y) species (**Figure 2.3 - spectra f** and **Table 2-4 in supporting information**). This was also confirmed by infrared analysis (**Figure 2-4 - spectra e**), with significant enhancement of carboxylic acid bands at the expense of cyclic anhydride stretching and cyclic unconjugated anhydride stretching vibrations. Once again, the final thickness of the second plasma layer was strongly dependent on the complex structure of the PP mesh. The thickness of this cross-linked overlayer was estimated by ellipsometry to be 125 $\pm$ 4 nm (**Table 2-2)**. By XPS analysis, the Ag $3d_{3/2}$ and Ag $3d_{5/2}$ photoemission X-ray lines of silver were also detected at 367.7 eV and 373.8 eV, respectively (**Figure 2-7 – spectrum b**). Plasma polymerization results from the well-known competition between deposition and etching during process [388]. Both the coating and the surface were bombarded by ions from the plasma leading mainly to fragmentation during the deposition. Due to surface mobility, a fraction of the silver species could migrate to the near-surface regions of the plasma polymer layer. TEM images of a cross-section of the plasma polymer system are shown in figure 8 (**Figure 2-8a**). They clearly show silver nanoparticles embedded in the first plasma polymer layer and covered by a second thick plasma polymer layer (**Figure 2-8b**). They also confirm the presence of nanoparticles in the near surface region of the plasma polymer overlayer. Careful survey of **Figure 2-6b** indicates a single absorption band at 480 nm before plasma deposition (**Figure 2-6b - spectrum b**), while this band was shifted to a lower wavelength (~ 460 nm) after plasma deposition (**Figure 2-6b - spectrum c**). It is well known that SPR absorption is sensitive to many factors, including the geometric parameters, microstructure and aggregated structure of the particles as well as the nature of the surrounding matrixes [389]. Physical and/or chemical changes in the interactions between particles and the polymer matrix during plasma deposition may induce changes in the electronic band structure and optical inter-band transitions of the particle

surface, which, as a consequence, affect the optical absorbance of the composite [386].

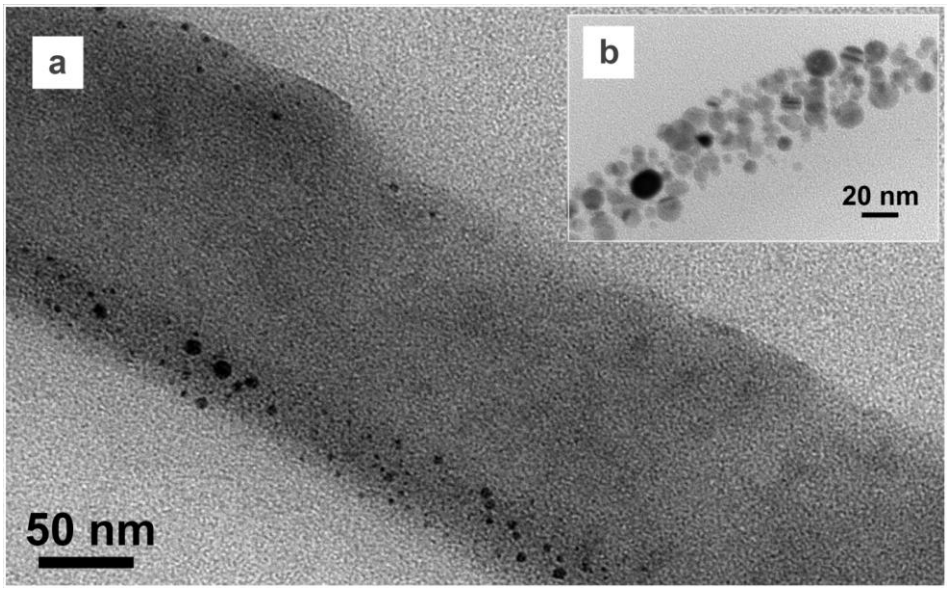

Figure 2-8: TEM images of cross-sections of the plasma polymer multilayer system at two different magnifications.

2.4.5 Control over the rate of release before stretching

In aqueous environments, silver particles are oxidized into silver ions, Ag^+, according to the reaction described in **Figure 2-9**.

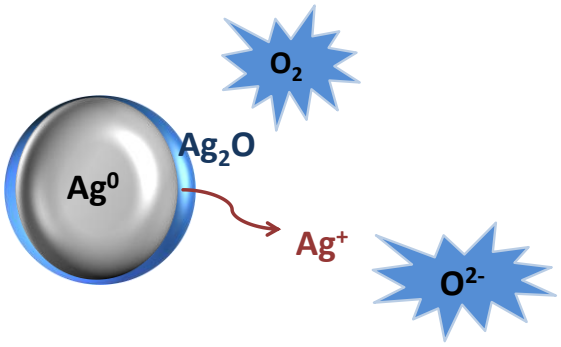

$$4\ Ag^{(0)} + O_2 \longrightarrow 4\ Ag^+ + 2\ O^{2-} \longleftrightarrow Ag_2O$$

Figure 2-9: Schematic illustration of the oxidation process of silver nanoparticles.

By depositing a plasma polymer overlayer, a barrier against diffusion of silver ions was created. In this section, we explored the effect of the crosslink density within the second plasma polymer layer as a parameter influencing the release behavior of silver ions from the coating. Increasing the crosslink density improved the barrier properties of the developed multilayer system and allowed control of the time (t_0) after which ions started to be released to the environment (the lowest concentration of silver detectable with the UV spectrometer used in this study is ~ 3 ppm). The crosslink density of the second plasma polymer layer was modified by changing the conditions of plasma deposition according to **Table 2-3**. The silver release was studied by immersion of samples of the multilayer system in distilled H_2O and subsequent evaluation of the solution concentration of silver by measuring its content in AgNPs before and after reduction with $NaBH_4$ (see **Figure 2-23 in supporting information**).

Sample	Power [W]	Time of deposition [min]	Duty cycle [%]
MAPP	20	10	50
MAPP I	20	5	100
MAPP II	50	1	100

Table 2-3: Conditions of plasma polymerization chosen for testing the barrier properties of the plasma polymer overlayer.

Figure 2-10 shows that the deposition of a second plasma polymer overlayer (MAPP, **Table 2-3**) significantly reduced the rate of Ag^+ release in comparison with the system without a second layer. The time, t_0, needed to detect any release of silver ions in the immersion solution increased to 24 hours. By increasing the crosslink density of the plasma polymer overlayer (MAPP I, **Table 2-3**), the rate of Ag^+ release was further reduced and t_0 increased to 1 week. Further increases in the crosslink density (MAPP II, **Table 2-3**) blocked the release of silver ion up to 16 weeks. The conditions of deposition of the overlayer are thus able to determine the time, t_0, needed to start the release of Ag^+ into the environment. The rate of Ag^+ release decreases when cross-linking of the overlayer increases.

To evaluate the influence of the surrounding liquid medium used during the release assays, similar experiments were undertaken in PBS buffer solution or M63G bacterial culture medium. In each case, $NaBH_4$ was used as a reducing agent and the integrity of the plasma polymer multilayer was checked by SEM analysis after immersion in the solution. Then, release experiments were repeated with increasing densities of crosslinking in the overlayer. Similar tendencies as those obtained in water were observed, independent of the nature of the solution used for the release.

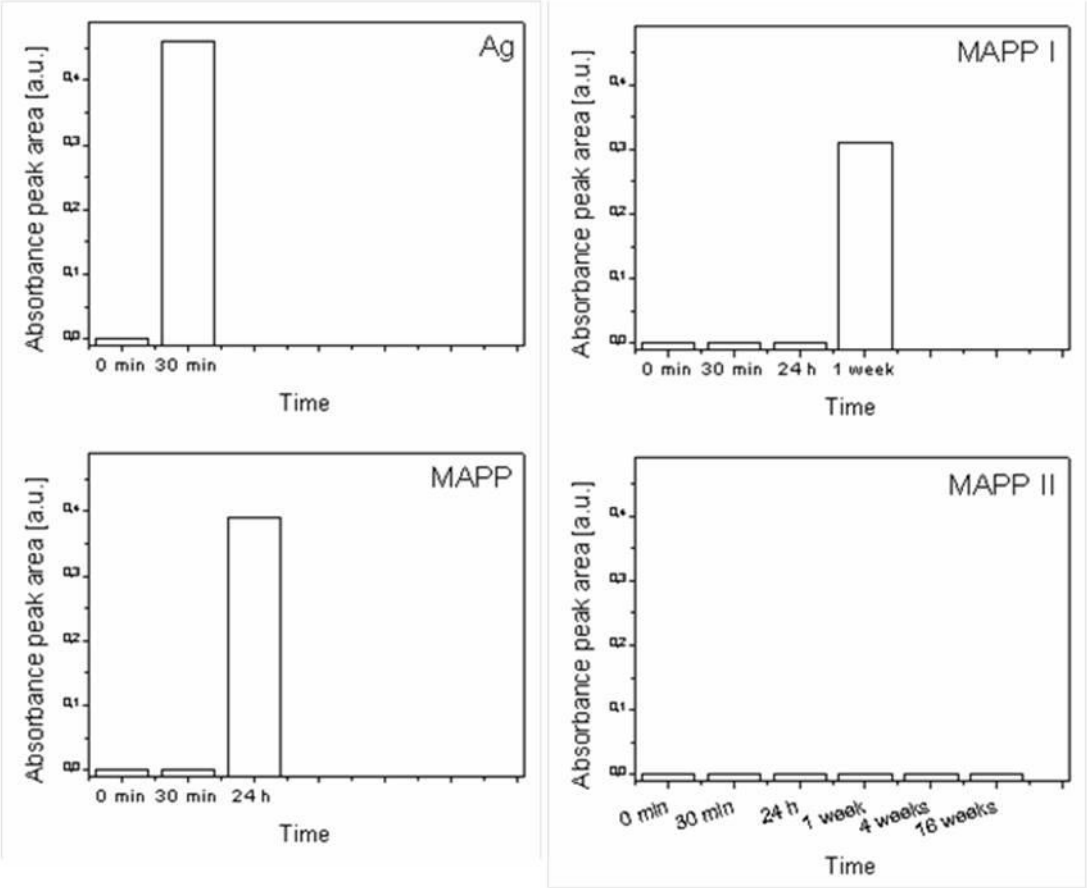

Figure 2-10: Duration of immersion until the presence of released silver was detected. In the case of MAPP II, no signal was detected even after 16 weeks.

The final conditions for deposition of the second plasma polymer layer were selected after UV-Visible measurements during release tests during stretching of the sample. For MAPP I and MAPP II it was not possible to detect any UV-Visible signal, even after 48 hours. In order to obtain experimental results in a reasonable experimental time, the overlayer with the lowest crosslink density (MAPP) was selected for all the following experiments. In this case, a UV-Visible signal was detected within 24 hours.

2.4.6 Control over the rate of release while undergoing stretching.

Figure 2-11 shows SEM images of polypropylene mesh substrate coated with the plasma polymer multilayer system while mechanical strain was applied (e.g., 40%, 60% and 80% of elongation from the initial length, **Figure 2-11 - images a, b and c**, respectively). The rate of elongation was 24 µm/s and the elongation was applied in the direction shown by the white arrows. As already mentioned, cracks in the overlayer were desired to create diffusive channels for Ag^+ species. Under stretching, plasma polymer multilayer coatings revealed remarkable fractures at their surfaces. The lengths of these fractures were perpendicular to the direction of elongation. This behavior was explained by the nature of the composite system that was strained: it was formed by the superposition of stiff layers at the top of a flexible polypropylene fiber. The fragmentation was thus relied on the transfer of the tensile stress of the substrate to the surface plasma polymer layer, as well as on the tensile properties and thickness of this layer [372]. In order to obtain accurate details on the density of the potential channels so created, image and statistical analysis were performed on 0.1 x 0.1 mm² area samples of polypropylene fibers. The density of the cracks and their size were found to be strongly correlated with the elongation state. The density of cracks and the total area of the apertures increased with the stretching ratio (**Figure 2-24a in supporting information**), while the mean value of the apertures did not vary (**Figure 2-24b in supporting information**), indicating a uniform growth in crack size with increasing elongation. Interestingly, most of the apertures in the plasma polymer layer were between 40 µm² and 150 µm², independent of the elongation state (**Figure 2-12**).

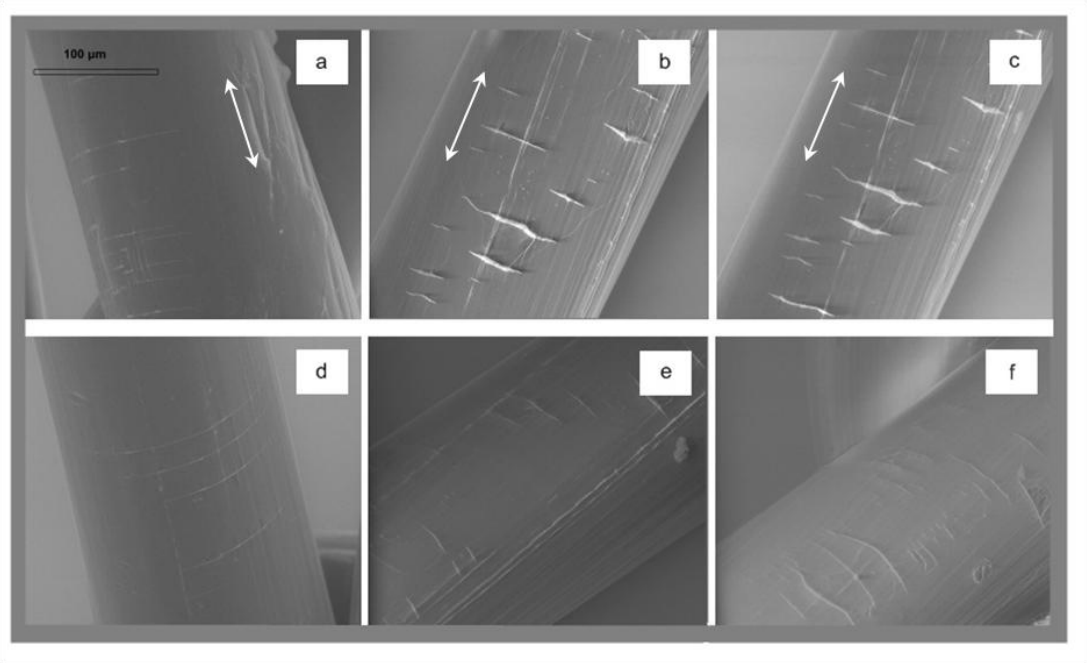

Figure 2-11: SEM images of the plasma polymer multilayer system undergoing stretching/unstretching cycles at (a)-(d) 40% of elongation, (b)-(e) 60% of elongation and (c)-(f) 80% of elongation.100% of elongation means twice the initial length.

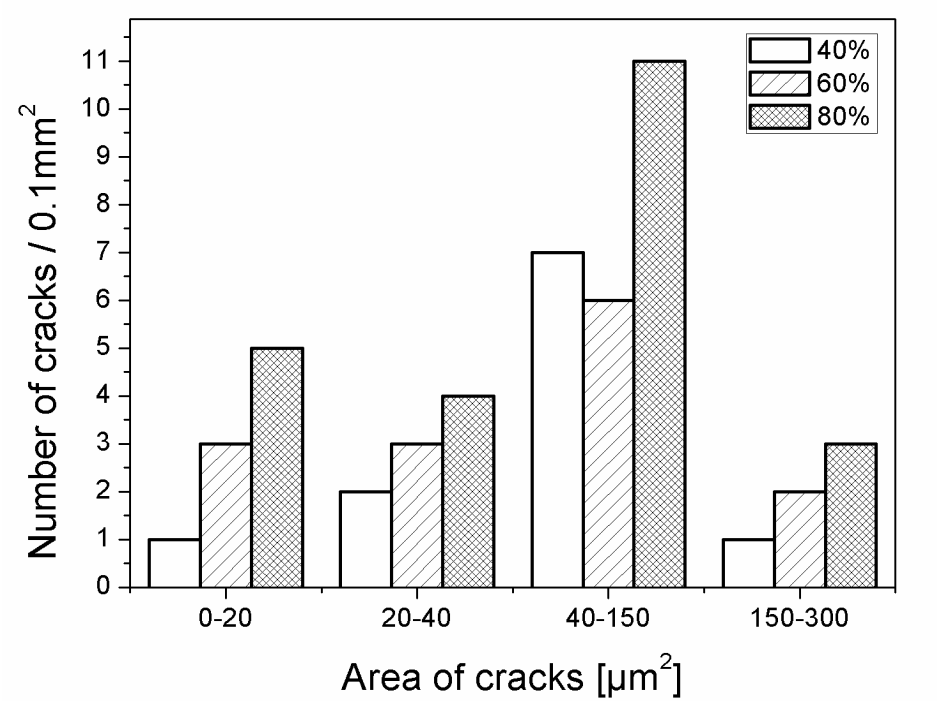

Figure 2-12: Size and number of cracks as a function of the stretching ratio.

A remarkable result was the closure of the cracks (e.g., closure of the diffuse channels) when the material was switched back to its initial length (the rate of retraction was also 24 µm/s) (**Figure 2-11 - images d, e and f**). SEM images clearly show that the mechanism of closure was a collapsing rather than a self-healing process. The cracks were not completely closed, allowing silver ions to continue to diffuse. Therefore, the flux of diffusion of silver ions can be tailored by playing with the mechanical stimulation (here, elongation cycles) and crack opening/closing cycles. The effect of the degree of stretching on the diffusion of silver ions was investigated. The results showed a regular increase in the amount of released silver ions when the degree of stretching was increased up to 80 %. This can be due to a continuous opening of the cracks during stretching.

The release of silver ions was measured under a series of stretching/unstretching cycles applied to the plasma polymer multilayer systems. The evolution of the UV absorbance is shown in **Figure 2-13**.

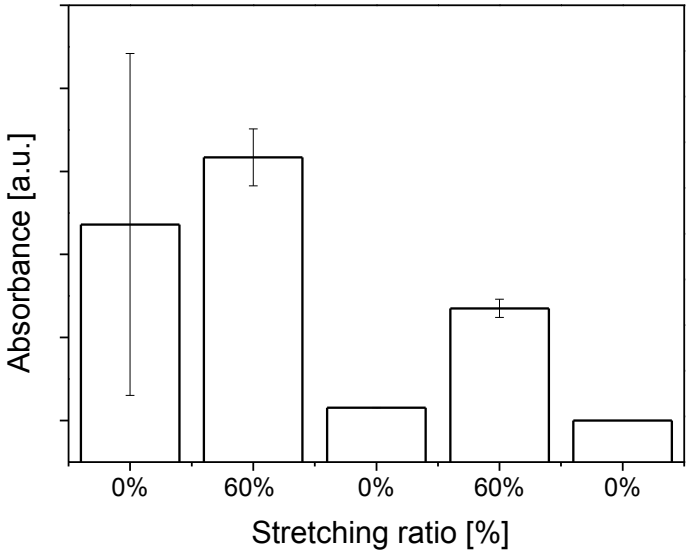

Figure 2-13: Release of Ag species followed by UV-Visible spectroscopy in the case of a PP/Ar/MAPP/Ag/MAPP sample during a series of elongation/retraction cycles. Absorbance values correspond to mesh elongation or retraction maintained during 24 hours.

In the absence of any cracks, a background signal was obtained, originating from the diffusion of silver species through the pores of the native plasma polymer layers or of silver species located at the near surface region of the plasma polymer overlayer. When this substrate was stretched at 60%, a strong increase in UV absorbance was observed due to the aperture of the diffusive channels, allowing an increase in the flux of silver ions from the material to the solution. When the surface was switched back to its initial position, a drop in the intensity of UV absorbance was observed, indicating that the flux of silver ions was reduced. This cycle was repeated three times and appeared fully reversible.

These results clearly show that a multilayer plasma polymer system allowing the release of a bioactive agent (here, silver ions as an antibacterial agent) under stretching was successfully created and that the releasing process was fully reversible.

2.4.7 Antimicrobial activity of the multilayer system

The barrier role of the plasma-polymer overlayer and recovery of its antibacterial action through the elongation-related release were investigated by preliminary microbiological experiments. The diffusion of silver ions through the plasma polymer overlayer, with or without stretching, was evaluated with samples placed on semi-solid nutritive agar that was previously inoculated with a thin film of bacterial suspension. After 24 hours of incubation, a film of bacteria was visible on the agar gel, indicating normal growth of the previously inoculated bacteria. Nevertheless, bacterial growth was inhibited, as expected, in the near surroundings of *PP/Ar/MAPP/Ag* samples, in agreement with silver delivery from the sample (**Figure 2-14- image a**). In contrast, bacterial colonization was not inhibited around the sample covered by a plasma polymer overlayer *(PP/Ar/MAPP/Ag/MAPP)*, and was even observed between fibers of the mesh, in contact with the silver-containing coating (**Figure 2-14- image b**). The efficiency of the barrier effect of the plasma polymer overlayer was thus clearly confirmed. Importantly, the antibacterial effect was recovered under mechanical stimulation (**Figure 2-14 - image c**), which is related to the opening of cracks in the plasma polymer overlayer, providing diffusive channels for the antibacterial agent. This result thus highlighted the relevance of the open/close crack system to control bacterial colonization in the near surroundings of the biomaterial.

The antibacterial efficiency of the open/close crack system on the growth of a biofilm was also evaluated. **Figure 2-15** shows the quantity of biofilm (i.e., biomass) developed after 168 hours of incubation.

Biofilm development on *PP/Ar/MAPP/Ag/MAPP* was similar to on *PP* samples, indicating that Ag^+ species were not present in a sufficient quantity to affect the growth of the bacteria, in agreement with the barrier role of the second plasma polymer overlayer. In contrast, the biofilm quantity was significantly reduced on *PP/Ar/MAPP/Ag* and stretched *PP/Ar/MAPP/Ag/MAPP* samples, due to the greater release of Ag^+. Inhibitions of biofilm development on stretched samples were moderate (around 50% compared to uncoated *PP* samples), but clearly demonstrate that the open/close crack system allows modulation of the bacterial colonization of the biomaterial.

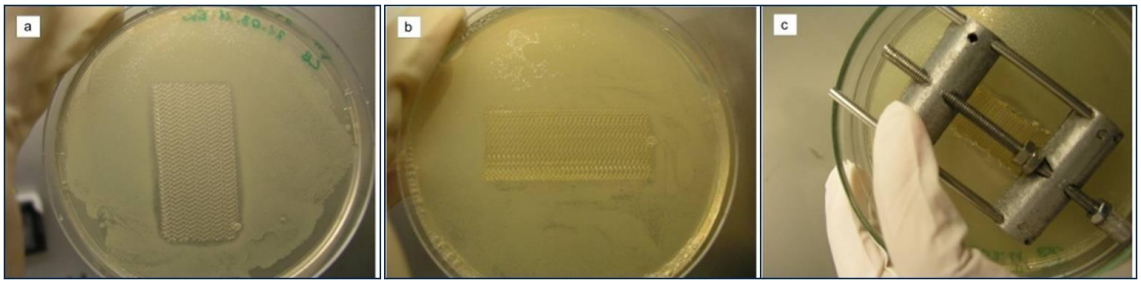

Figure 2-14: Bacterial growth on nutritive agar plates in the surroundings of **a)** a PP/Ar/MAPP/Ag system, **b)** a PP/Ar/MAPP/Ag/MAPP system and **c)** a PP/Ar/MAPP/Ag/MAPP system undergoing stretching.

Further investigations are now under development. Preliminary assays already suggest that, aside from biomass, biofilm structure is also affected by the small amount of silver ions released from the stretched *PP/Ar/MAPP/Ag/MAPP*. Since lack of cohesion is known to enhance biofilm susceptibility to systemic treatments with antibiotics [390], changes in biofilm structure due to treatment with silver ions, even in low quantities, may open the way for a more efficient fight against biofilm development on biomaterials.

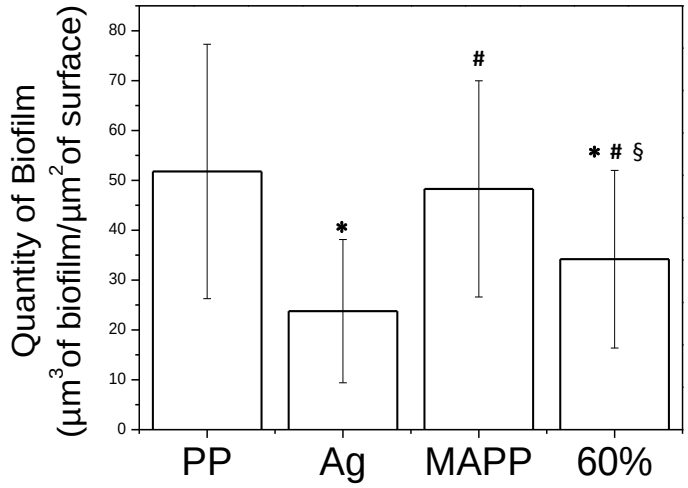

Figure 2-15: Quantity of biofilm (i.e., biomass) on PP/Ar/MAPP/Ag and PP/Ar/MAPP/Ag/MAPP systems with and without stretching compared to uncoated PP systems. *∗ Significant difference compared to PP (p>99.5%); # Significant difference compared to Ag (p>99.5%); § Significant difference compared to MAPP (p>99.5%).*

2.5 Conclusions

Mechanically sensitive materials made of plasma polymer multilayers and bioactive agents can be developed on modified polypropylene substrate using solvent-free steps based on plasma polymerization. Tailored release of an active agent can be achieved by mechanical stimulation of the designed material. This has been demonstrated for silver, stored as AgNPs in the plasma polymer multilayer system and released in the material surroundings in its bioactive ionic form. Taking advantage of different mechanical properties between the different layers, a system of cracks in the plasma polymer overlayer allowed control of the diffusion of silver ions. Its antibacterial properties have been confirmed. The stability of the properties of the film under the stress of elongation has been also proven (no delamination).

This work shows that, taking advantage of open/closed crack systems, it is possible to control the flux of an antibacterial agent and to modulate bacterial colonization of the biomaterial. This original approach offers a great opportunity to readdress the persistent challenge of obtaining effective and long-lasting antibacterial coatings.

2.6 Acknowledgements

The authors gratefully acknowledge the financial support from Region Alsace in France. The authors would like to thank Cousin Biotech for providing polypropylene mesh substrates. Florent Kuntz and Ludovic Frechard from Aerial are kindly acknowledged for their expertise and assistance in the electron beam sterilization process.

2.7 Keywords

Maleic anhydride; plasma polymerization; antibacterial coating; silver particles; controlled release; responsive materials.

2.8 Supporting information

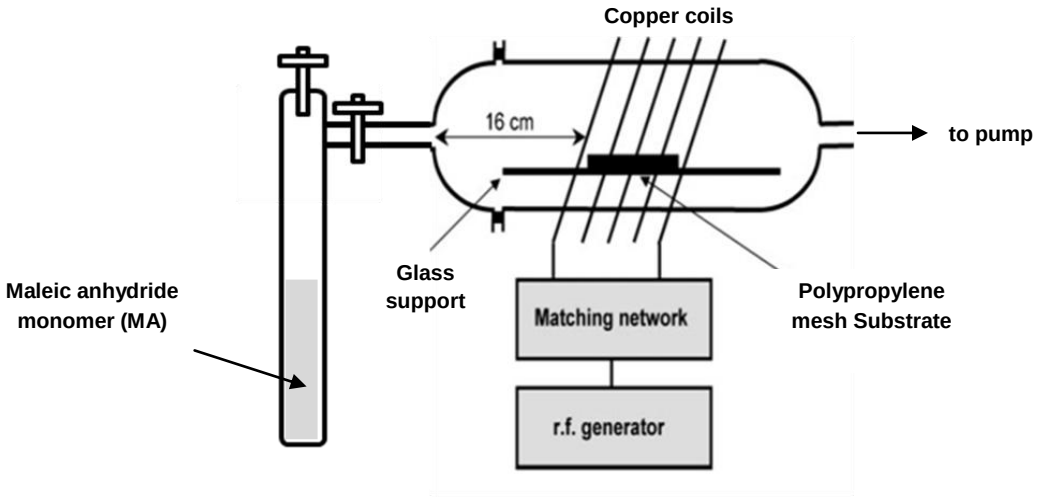

Figure 2-16: Schematic plasma reactor set-up with inlet of monomer and substrate positioning (not scaled).

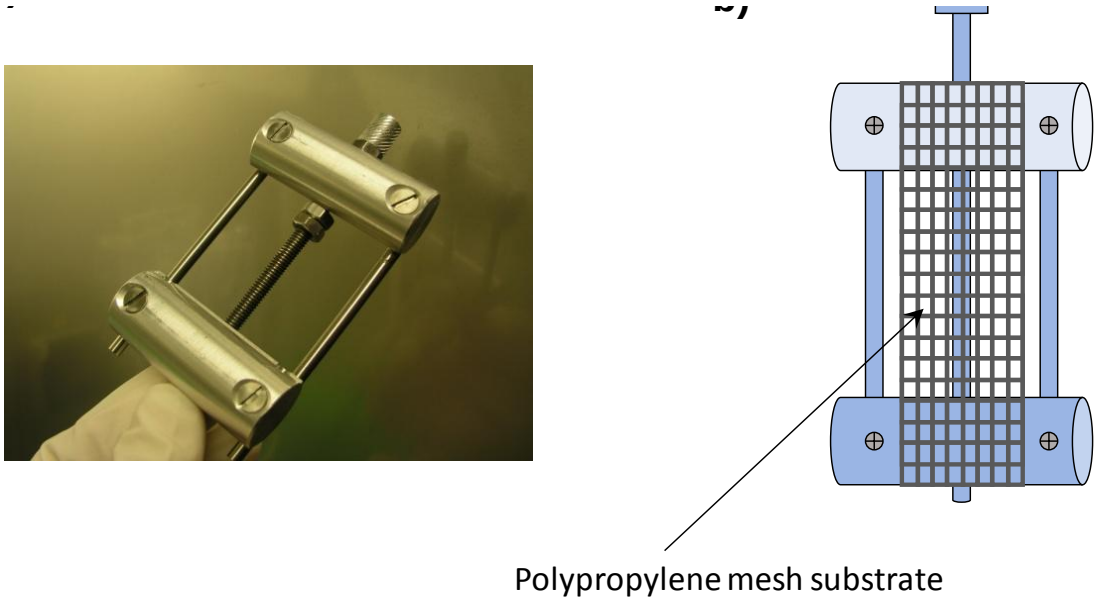

Figure 2-17: a) Photograph (IS2M) and b) schematic illustration of the homemade stretching device.

a)

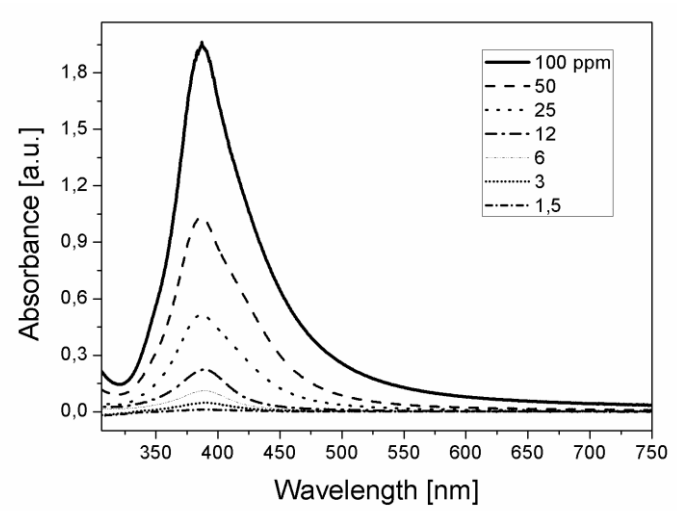

b)

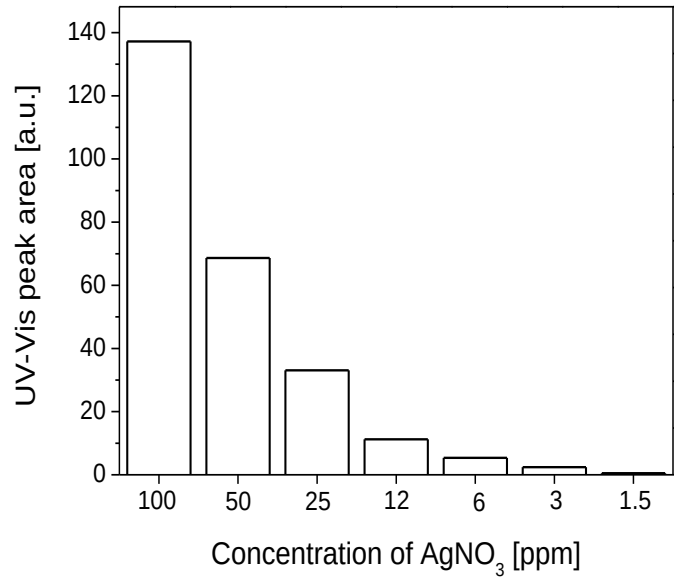

Figure 2-18: Area of UV-Visible spectrum signal after NaBH4 reduction of different solutions of $AgNO_3$.

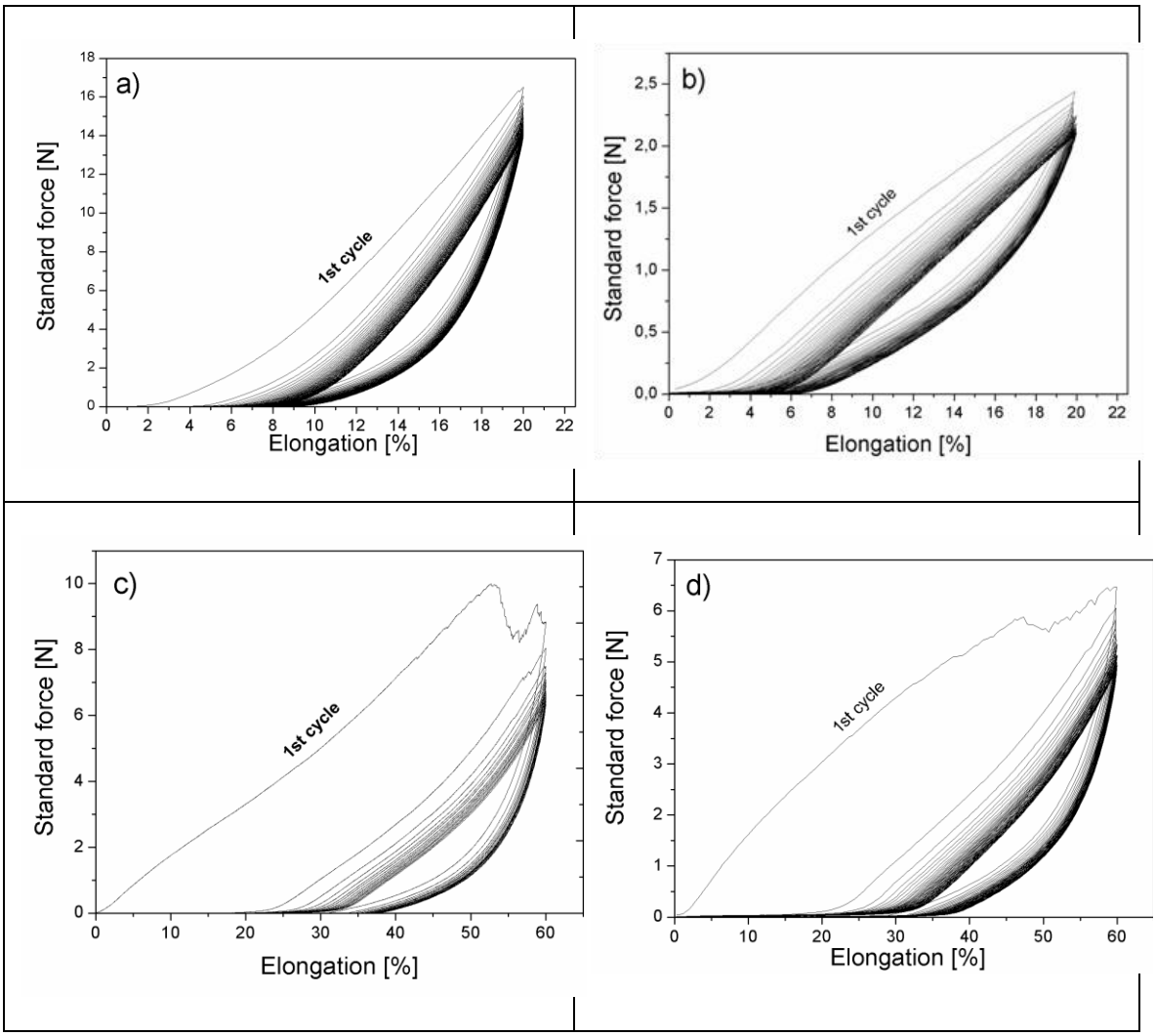

Figure 2-19: Typical loading-displacement curves of polypropylene meshes according to the direction of elongation and the stretching ratio (100% of elongation means twice the initial length). a) Transverse and 20% of elongation, b) transverse and 60% of elongation

	Assignment	***PP***		***(a)*** ***PP* + Ar**		***(b)*** ***(a)* + MAPP**		***(c)*** ***(b)* + hydrolysis**		***(d)*** ***(c)* + Ag NP**		***(e)*** ***(d)* + MAPP**	
		eV	at.%	eV	at.%	eV	at.%	eV	at.%	eV	at.%	eV	at.%
C(1s)	C-C	285.0	97.1	285.0	87.4	285.0	42.4	285.0	43.5	285.0	63.7	285.0	63.1
	C*-C(O)=O			285.5	2.6	285.5	21.8	285.5	19.0	285.5	5.1	285.5	6.2
	C-O	286.6	2.9	286.6	4.2	286.5	6.9	286.5	10.1	286.5	8.3	286.5	11.5
	O-C-O/-C=O			288.0	3.2	288.0	7.1	288.0	8.4	288.0	17.8	288.0	12.9
	O=C-O-C=O/HO-C=O			289.4	2.6	289.2	21.8	289.2	19.0	289.2	5.1	289.2	6.2
O(1s)	C-O / O-C-O/-C=O	532.8	100.0	532.8	100.0	532.7	92.7	532.6	92.8	531.7	74.5	532.5	90.3
	O=C-O-C=O/ HO-C=O					534.6	7.3	534.5	7.2	533.5	25.5	533.8	9.7
Ag(3d)	Ag 3d 5/2									367.9	60.3	367.8	60.3
	Ag 3d 3/2									373.9	39.7	373.8	39.7

Table 2-4: Surface atomic composition at each step of material development, **a)** polypropylene mesh, **b)** (a) Ar plasma treated, **c)** (b) coated with a first maleic anhydride plasma polymer layer, **d)** (c) hydrolyzed, **e)** (d) loaded with silver nanoparticles, **f)** (e) coated with a second plasma polymer layer

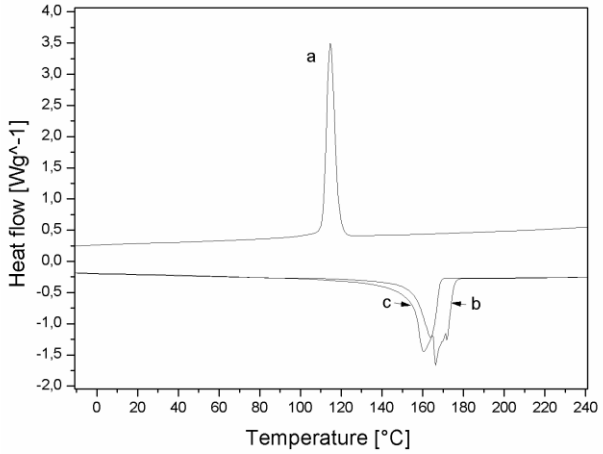

Figure 2-20: DSC analysis of polypropylene mesh: a – melting peak , b – crystallization peak (first heating), c - crystallization peak (second heating). The degree of crystallinity was estimated to be 47 ± 5%. For this purpose, the samples of polypropylene were analyzed over the temperature range from -100 °C to 250 °C. A heating rate of 10 °C/min was used. The thermal history of the sample was erased by thermal treatments consisting of cooling the sample from 250 °C to -100 °C at 10 °C/min. The integrated area under the melting curve was calculated to obtain the enthalpy, which was further divided by the thermodynamic heating of fusion of 100 % crystalline polypropylene (207 J/g according to Vander Wal A, Mulder JJ and Gaymans RJ. Facture of polypropylene: 2. The effect of crystallinity. Polymer. 1998, 39, 5477).

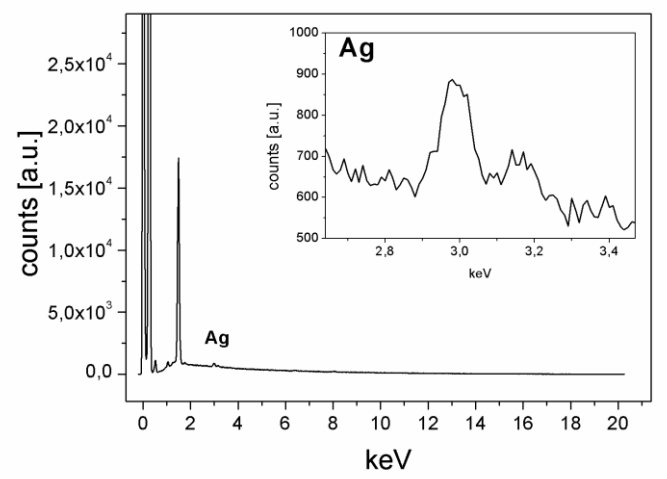

Figure 2-21: EDX analysis of the first plasma polymer layer after loading with silver particles (PP/Ar/MAPP/Ag).

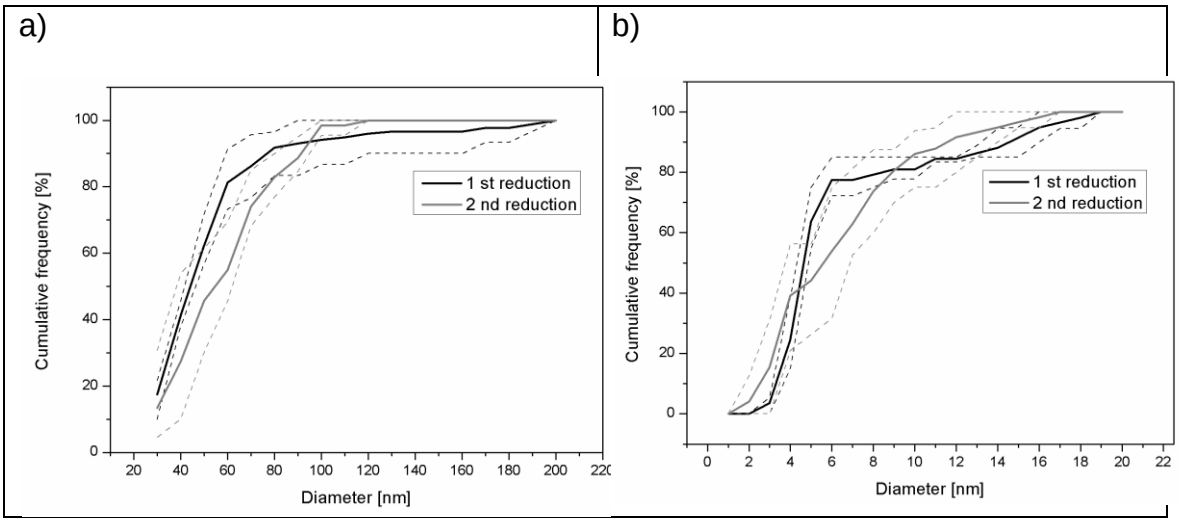

Figure 2-22: Statistical distribution of particle sizes (range: a) 20–200 nm; b) 1–20 nm) after loading with silver particles (PP/Ar/MAPP/Ag) and either a single immersion (black line) or two successive immersions (grey line) in NaBH4 solution.

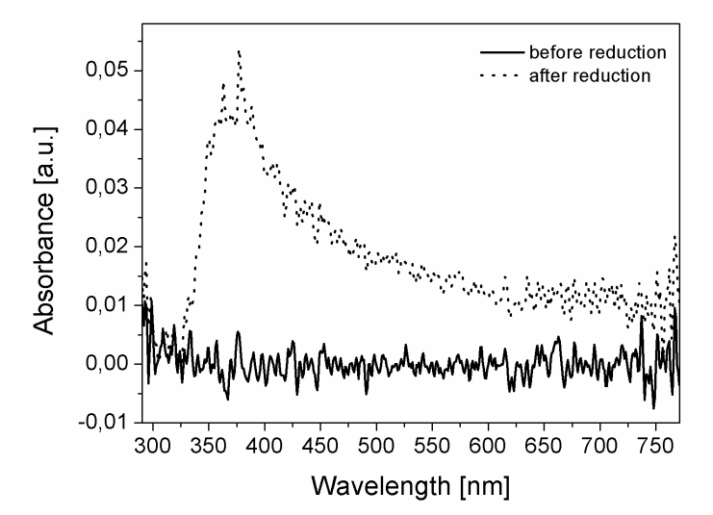

Figure 2-23: UV-Visible spectra of the release solution after immersion of the plasma polymer multilayer system in water, recorded before and after reduction with NaBH4 solution.

a)

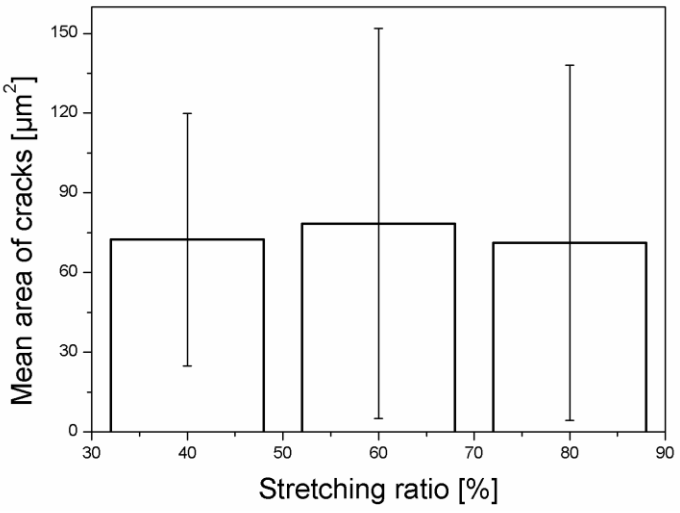

b)

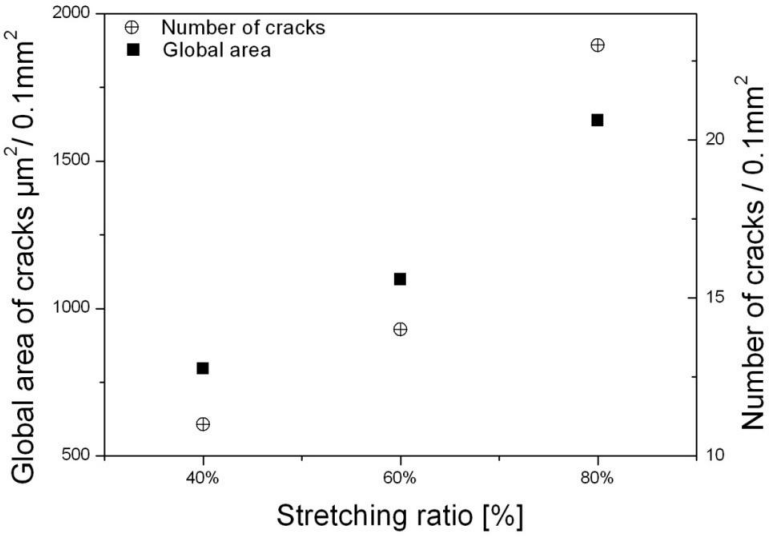

Figure 2-24: a) Mean area of cracks and **b)** global area of cracks as a function of the stretching ratio.

CHAPTER III

3 Effect of ageing and sterilization on plasma multilayer system

3.1 Introduction

In the previous chapter, we have seen the details of the multistep procedure to elaborate a new generation of bioactive coating, dedicated to soft implant and able to adjust the release of bioactive agent under mechanical stimuli (see section 2). A plasma multilayer coating was deposited on the surface of polypropylene made surgical mesh. Silver nanoparticles were trapped between two plasma polymer layers and acted as an antibacterial reservoir. Owing to the differences between mechanical properties of the plasma polymer thin films and the polypropylene fiber, tensile strength generates cracks within the plasma polymer overlayer which might be used as diffusive channels for Ag^+ species.

Since the biomaterial device has to be sterile before the implantation in the body, the sterilization step is considered as the last step of the surface modification during elaboration. But ageing is also an important step to be considered as it can dramatically affect the properties of the plasma polymer coating in combination with the sterilization step.

Concerning ageing, it is well known that plasma deposited films undergo certain chemical reactions when they are exposed to atmosphere. For example, freshly deposited plasma polymers typically contain radicals, which rapidly react with in-diffusing oxygen during exposure to air. This ageing process is well known as auto-oxidation [391]. It consist in two steps [391]. The primary ageing step is that molecular oxygen reacts with C-radical sites. This results in the formation of

peroxy radicals (C-O-O•). Secondary reaction step is the decay of these peroxy radicals and formation of different oxygen functionalities like C=O and COO.

Besides, there are many different sterilization methods available; each with different mode of action can contribute to modification of surface properties. Predicting what would be the outcome after a sterilization process on a specific material like coated substrates is very complicated, if not impossible. The best way to determine how a specific sterilization process affects the surface properties is a comprehensive test of the coating properties before and after sterilization, and as well the tests during the ageing period. In general manner, it is known that the use of heat (steam), radiation (β/ electrons or γ) or chemicals (mostly ethylene oxide) can affect the mechanical and optical properties of polymer [392, 393]. Radiation, in particular the effect of γ-rays, has shown to induce chain scission leading to mechanical and thermal degradation effects [394]. Steam sterilization, carried out in a temperature range of 120-130°C, does not affect molecular structure of polymer, however it leads to post-crystallization and physical aging effects [395]. Chemical sterilizing agents like ethylene oxide have a limited effect on polymer [392, 393]. However, an evidence of toxic potential of medical grade plastics sterilized using ethylene was showed [396]. Ethylene oxide diffusion in complex substrates is also an issue which has to be considered for sterilization and aeration conditions [397]. Results of modern alternative sterilization processes such as electron irradiation, UV irradiation and the application of ozone is limited. All of these three methods are capable of forming radicals in polymers, which might result in similar degradation effects as the γ –radiation [392].

Few authors have study more specifically the influence of sterilization step on plasma polymer coatings. Haddow *et al*. [398] demonstrated that plasma polymer modified surfaces containing carboxylic acid groups can function successfully after a standard ethylene oxide sterilization procedure. Study of Calderon *et al*. [399] performed on plasma-polymerized allylamine films have shown good stability during autoclaving process. The influence of autoclaving,

γ-irradiation, ethylene oxide exposure and Ar/H_2 low pressure plasma treatment have been also investigated on the surface chemistry of thin films of plasma polymerized diethylene glycol dimethyl ether [400]. This study revealed that all types of sterilization methods influenced the surface chemistry.

So, depending on material properties the method used for a particular device has to be carefully selected.

The present chapter focuses on the stability of the plasma polymer multilayer coating on polypropylene mesh when undergoing ageing and standard sterilization procedures. More precisely, we examine the effects of i) ageing and ii) autoclaving and electron beam sterilization on surface properties of our system made of plasma polymerized layers of maleic anhydride. This study has important impact due to the recent growing interests of plasma modified surfaces used for a biomedical applications [133, 179, 194, 374, 401-404].

3.2 Materials and methods

3.2.1 Plasma multilayer systems

Details of the elaboration steps and characterization of the plasma multilayer system are fully described in section 2.

Briefly, PP substrates were placed in the center of the plasma reactor chamber followed by evacuation back down to the initial pressure (~ 5×10^{-4} mbar). They were first activated by argon plasma during 1 min at 60 W (*PP/Ar*). Subsequently, maleic anhydride vapor was introduced into the reaction chamber (pressure of 0.2 mbar) with a flow rate of approximately 1.6×10^{-9} $kg.s^{-1}$. At this stage, the plasma was ignited and run for 30 min. The deposition conditions corresponded to: power output = 20 W, duty cycle = 2% and frequency = 816 Hz. Upon completion of deposition, the R.F. generator was

switched off and the flow of monomer was maintained in the system for a further 2 min period prior to venting up to atmospheric pressure. Prior to use, plasma polymer modified substrates were immersed in deionised water to promote the hydrolysis of maleic anhydride groups into dicarboxylic acid groups (*PP/Ar/MAPP*). Then, silver was loaded directly on the *PP/Ar/MAPP* surface by immersion of the coated substrate into a 1.0 mM silver nitrate solution for 30 min. Silver cations diffused into the reservoir and formed electrostatic pairs with carboxylate groups. Ag^+ ions bound to carboxylate were reduced to zero-valent Ag nanoparticles using an aqueous solution of $NaBH_4$ (2.0 mM). Then, the *PP/Ar/MAPP/Ag* material was placed in the chamber of the plasma reactor and the system was pumped down to base pressure. Maleic anhydride vapor was introduced into the reaction chamber at a constant pressure of 0.2 mbar. The plasma was ignited and run for 10 min according to the following conditions: power output = 20 W, duty cycle = 50% and frequency = 816 Hz. Upon completion of deposition, the R.F. generator was switched off and the flow of monomer was maintained in the system for a further 2 min period prior to venting up to atmospheric pressure. Samples were then stored until use in ambient environment.

3.2.2 Ageing

3.2.2.1 Before elongation

After completion of deposition of the second plasma polymer layer, coated substrates were stored in polystyrene box in room temperature and ambient atmosphere. Time of ageing before elongation was 1h, 10 days and 20 days for respective samples.

3.2.2.2 Before sterilization

After completion of deposition of the second plasma polymer layer, coated substrates were stored in polystyrene box in room temperature and ambient atmosphere for 3 days.

3.2.2.3 After sterilization

After sterilization, samples were kept in polystyrene sealed box in a room temperature and ambient atmosphere. Analysis of samples was conducted *i)* the same day after sterilization, *ii)* after 3 days of ageing.

3.2.3 Techniques of sterilization

3.2.3.1 Autoclave

Samples were put into glass Petri dishes and autoclaved (Varioklav 400, H + P Labortechnik, Germany) for 15 min at 121ºC and high pressure (100 kPa). Samples were cooled to room temperature and kept in Petri dish prior to analysis.

3.2.3.2 Electron beam irradiation

Electron beam radiation was performed by the Center of Irradiation Aérial (CRITT Aérial, Illkirch). The radiation station contains a *Van de Graaf* electrostatic generator with a tension ranging from 0.5 to 2.5 MV, a current intensity ranging from 0.01 to 200 µA and a maximum power around 500 W. This apparatus is known for its excellent tension's stability (fluctuation around 0.5 % of the nominal tension) and intensity's stability (fluctuation around 1% of the nominal intensity)

To perform sterilization, substrates were packed in the polystyrene box and set for sterilization with doses of 25 kGy. The samples were left sealed until being used for XPS, SEM, TEM investigations and antibacterial assays.

3.2.4 Surface characterization

3.2.4.1 Scanning Electron Microscopy

SEM observations were performed using a FEI environmental microscope (Quantana 400 model) working at 30 keV. Samples were stretched on a homemade stretching device with a speed of 24 µm/s and the elongation was set to 20%, 40% or 80% of the initial sample size respectively (see details in section 2.3.4).

3.2.4.2 X-ray Photoelectron Spectroscopy

XPS spectra of PP-functionalized surfaces were recorded with a VG SCIENTA SES-200 spectrometer equipped with a concentric hemispherical analyzer. The incident radiation was generated by a monochromatic Al K_α X-ray source (1486.6 eV) operating at 420 W (14 kV; 30 mA). Photo-emitted electrons were collected at a take-off angle of 90° from the sample with electron detection in the constant analyzer energy mode. Signals for survey spectra were recorded with pass energy of 500 eV. For high-resolution spectra of C1s, O1s and Ag3d components, the pass energy was set to 100 eV. The analyzed surface area of PP mesh sample was approximately 3 mm^2 and the base pressure in the analysis chamber during experimentation was about 10^{-9} mbar. Charging effects on these isolating samples were compensated for by using a Flood Gun. The spectrometer energy scale was calibrated using the Ag $3d_{5/2}$, Au $4f_{7/2}$ and Cu $2p_{3/2}$ core level peaks, set respectively at binding energies of 368.2, 84.0 and 932.7 eV. Peak fitting was performed with mixed Gaussian-Lorentzian

(30%) components with equal full-width-at-half-maximum (FWHM) using CASAXPS software

3.2.4.3 Transmission Electron Microscopy

TEM observations were performed using Philips CM20 instrument with Lab6 cathode at an acceleration voltage 200 kV. For the investigations of influence of sterilization methods on silver nanoparticles immobilized in the multilayer system (see section 3.3.2.3), plasma polymer multilayer system was deposited on copper grids, instead of polypropylene surface, to facilitate the study.

3.2.5 Antibacterial assay

Experiments were conducted with the PHL628-based *E.coli* SCC1 strain [380]. Bacteria taken from frozen stock (-80 °C) were inoculated on an agar plate of Luria–Bertani (LB, LB purchased from Sigma-Aldrich) medium for an overnight culture. One colony of bacteria was inoculated in 10 mL of LB medium and cultivated at 30 °C overnight for a first pre-culture. A second pre-culture was inoculated with the first pre-culture (10 vol-%) in 10 mL of selective M63G medium and cultivated at 30 °C overnight. A third pre-culture was inoculated from the second pre-culture (10 vol-% of the second pre-culture) for 4 h at 30 °C. The final culture used to perform the experiment was inoculated from the 4h pre-culture (10 vol-%). Its absorbance at 600 nm (Abs_{600}) was adjusted to 0.01 (i.e, 10^6 bacteria/mL). Coated-mesh samples, previously sterilized by autoclave or e-beam (25 kGy), were placed into small Petri dishes (Ø 35 mm) on sterilized-in-oven (180 °C for 1 h) silicon wafers. Stainless steel wire was used to maintain the sample on the dish bottom. Samples were inoculated with 4 mL of the final bacterial culture and incubated for 4 h at 30 °C. Samples were then thoroughly and carefully rinsed to eliminate non-adherent or loosely attached bacteria from the substrate surfaces. For this purpose, 2 mL of supernatant (i.e.

bacterial suspension for the first rinse and NaCl solution for further rinsing steps) were removed, kept for further bacterial concentration measurement and replaced by 2 mL of fresh NaCl solution. The rinsing step was performed without direct flushing, with the stream directed toward the walls of a Petri dish. Samples remained immersed in liquid during the rinsing steps, without creating any air-sample interface. The rinsing step was repeated 6 times. The effect of the samples on bacterial growth in the planktonic state was tested by measuring the absorbance of each supernatant at 600 nm (A_{600}). Results are expressed in terms of Inhibition rate compared to bacterial colonization on PP reference sample.

3.3 Results and discussion

3.3.1 Effect of ageing

Experiment was designed to show the effect of ageing on plasma polymer multilayer system deposited on polypropylene mesh. Physical and topographical changes of the surface of plasma polymer multilayer system deposited on the mesh were investigated by means of SEM microscopy observations. Changes in the surface chemical composition were investigated by means of XPS spectroscopy measurements.

3.3.1.1 Scanning Electron Microscopy observations

3.3.1.1.1 Before elongation

No difference was observed before elongation for freshly prepared (1h), 10 days and 20 days after ageing for PP/Ar/MAPP/Ag/MAPP samples. More details can be found in section 3.3.2.

3.3.1.1.2 Under elongation

Figure 3-1 shows SEM images of PP/Ar/MAPP/Ag/MAPP while mechanical strain was applied (e.g., 40%, 60% and 80% of elongation comparing to the initial length of the sample). Observation experiments were performed 1 hour after preparation of the samples. The rate of elongation was 24 µm/s.

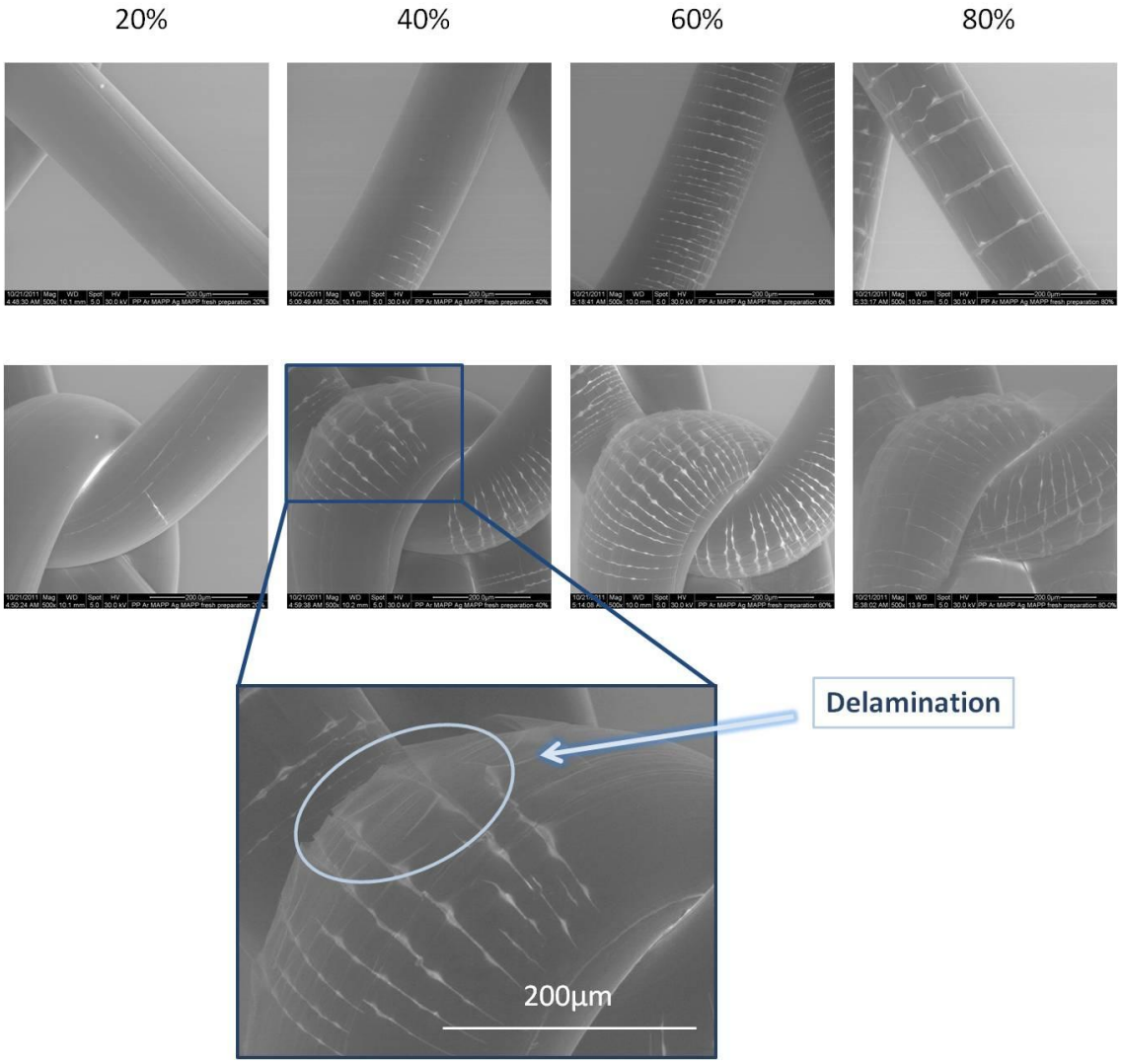

Figure 3-1: Plasma polymer multilayer system deposited on polypropylene mesh substrate. Stretching and observation experiment was performed one hour after preparation of the sample.

As previously mentioned in section 2.4.6, under stretching, PP/Ar/MAPP/Ag/MAPP revealed remarkable fractures at their surfaces. This behavior was explained by the nature of the composite system that was strained: it was formed by the superposition of stiff layers at the top of a flexible polypropylene fiber. The fragmentation was thus relied on the transfer of the tensile stress of the substrate to the surface plasma polymer layer, as well as on the tensile properties and thickness of this layer [372].

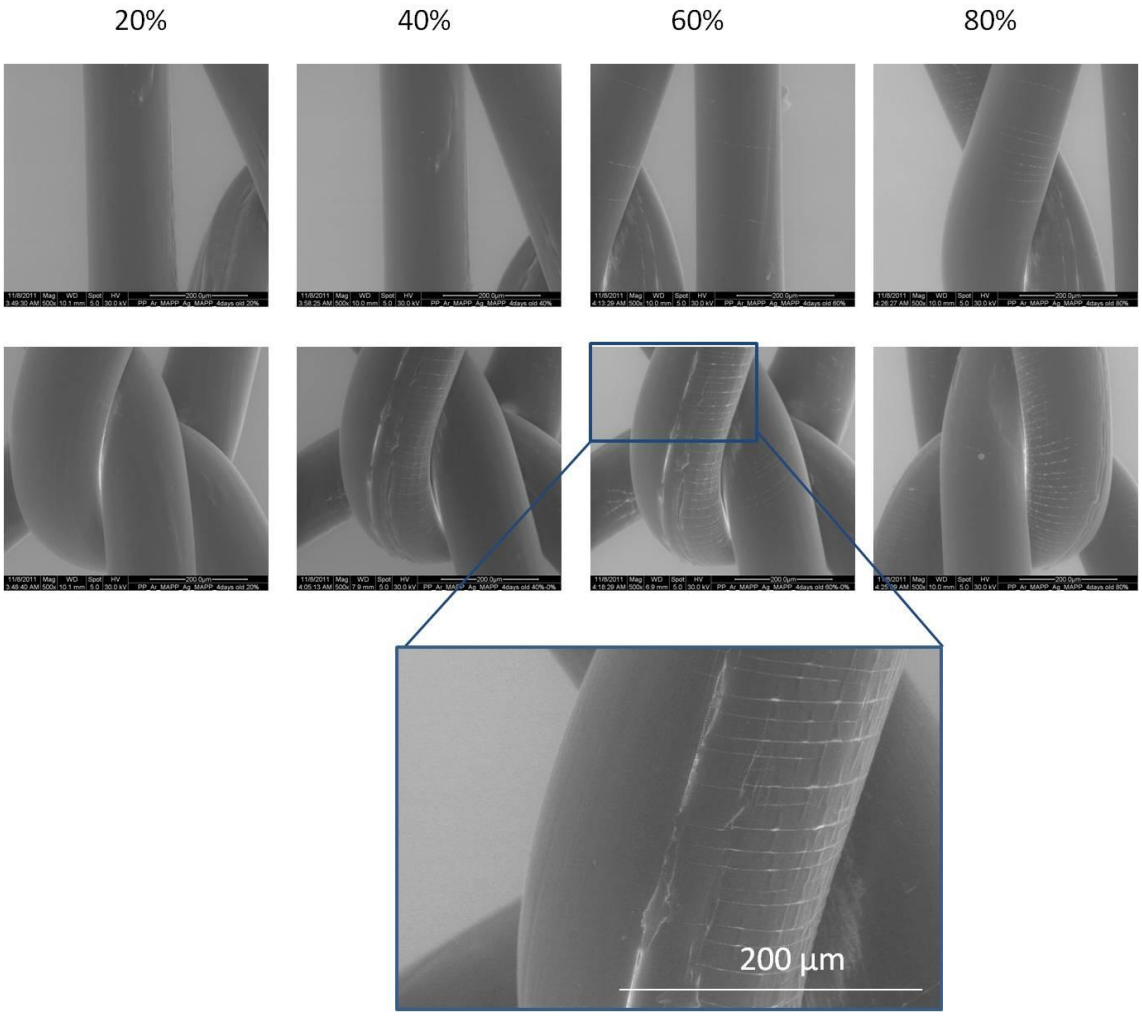

Figure 3-2: Plasma polymer multilayer system deposited on polypropylene mesh substrate. Stretching and observation experiment was performed 10 days after preparation of the sample.

Figure 3-2 shows, that plasma polymer and/or interface between deposited layer and polypropylene material undergo changes during ageing process which can be seen by different fracturation processes of the surface during stretching. When experiment is conducted on freshly prepared sample (1 h of ageing) the apparition of cracks takes place immediately at ~20 % of elongation (**Figure 3-1** 20%). For similar stretching ratio and for samples aged during 10 days (see **Figure 3-2** 20%) or 20 days (see **Figure 3-3** 20%), cracks are not likely to appear neither on the fiber nor on the weave. When the stretching ratio was increasing, cracks are well seen along the fiber but more likely to appear first at the weave where tensile stresses are higher (**Figure 3-1** 40%). After 10 days (**Figure 3-2** 40%) or 20 days (see **Figure 3-3** 40%) of ageing, cracks are only visible close to weave.

The adhesion between plasma polymer multilayer system and polypropylene substrate and/or between second and first plasma polymer deposited layer seems also to change during ageing process. This can be already seen at 60% or 80% of elongation (**Figure 3-1**), where partial delamination of the layer close to cracks occurs (**Figure 3-1**). After ageing process (both 10 and 20 days) this is no longer the case. Cracks are formed regularly with similar sizes of aperture and no delamination occurs.

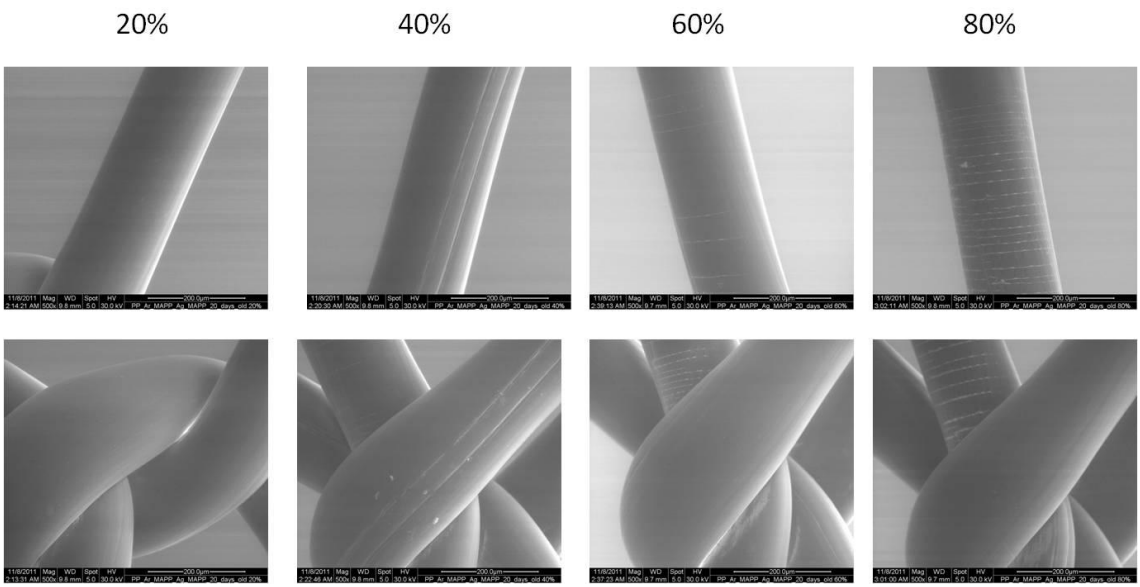

Figure 3-3: Plasma polymer multilayer system deposited on polypropylene mesh substrate. Stretching and observation experiment was performed 20 days after preparation of the sample.

In conclusion, after ageing, plasma polymer matrix becomes softer and the intensity of internal tensions in plasma polymer interfacial tensions are lower. This is most likely due to the influence of humidity. Because of high concentration of oxygen, plasma polymer coating can act as a sponge adsorbing water molecules from the environment via hydrolysis bounding. This increase in water concentration inside the plasma polymer matrix plays the role of plasticizer, tuning polymer more flexible and less crackable. Tension at the interface between polypropylene and plasma polymer is lower, since delamination does not occur after ageing process.

3.3.1.2 XPS

Surface atomic concentration measured by means of XPS spectroscopy on PP/Ar/MAPP/Ag/MAPP before and after ageing (in this case ageing time is 7 days) revealed increase in O/C ratio after ageing. Besides the decrease of 1% in oxygen atomic concentration in case of aged sample, detection of 1.3% of

sodium element was observed which come from $NaBH_4$ solution which is used during synthesis of silver nanoparticles. Presence of sodium element may indicate process of migration of substrate species during ageing time due to surface mobility (see **Table 3-1**).

Atomic concentration [%]		
Element	*(a)* PP/Ar/MAPP/Ag/MAPP Fresh	*(b)* PP/Ar/MAPP/Ag/MAPP/ Aged
Au 4f	13,43	19,88
C 1s	64,16	56,87
O1s	20,81	19,84
Ag 3d5/2		
Na 1s		1,28
Cu 2p 3/2	1,61	2,13

Table 3-1: Surface atomic composition of **(a)** plasma polymer multilayer system freshly prepared **(b)** plasma polymer multilayer system after aging. * *Gold and copper elements are from sample holder, possible to detect due to mesh pores.*

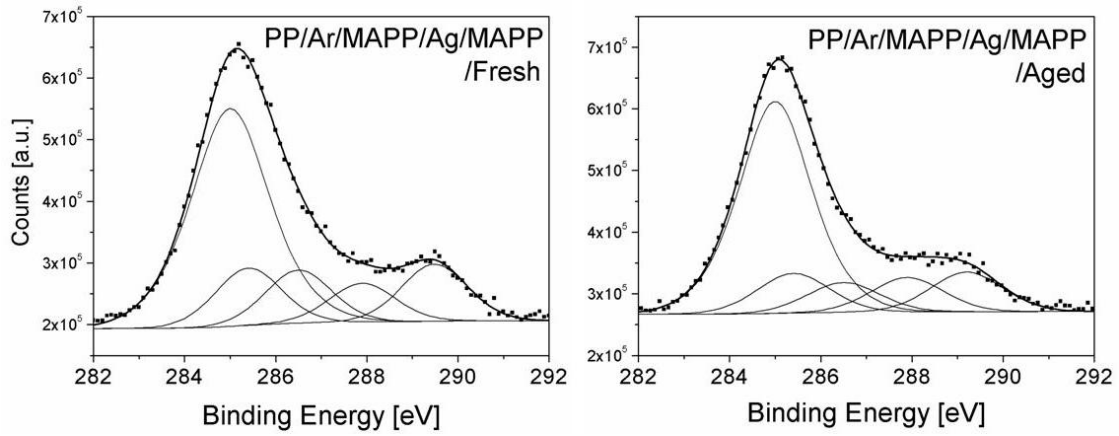

Figure 3-4: High resolution spectra of C(1s) recorded for plasma polymer multilayer system after preparation and after ageing for 7 days.

High resolution XPS analysis of carbon C(1s) envelope of both freshly prepared and aged PP/Ar/MAPP/Ag/MAPP revealed five types of carbon functionalities: hydrocarbon (CHx ~ 285.0 eV), carbon singly-bonded to an anhydride group (C-C(O)-O- ~ 285.4 eV), carbon singly-bonded to oxygen (-C-O ~ 286.5 eV), carbon doubly-bonded to oxygen (O-C-O/-C=O ~ 287.9 eV), and acid/anhydride groups (O=C-O/O=C-O-C=O ~ 289,5 eV) (see **Figure 3-4** and **Table 3-2)**.

Assignment		PP/Ar/MAPP/Ag/MAPP			
		Fresh		Aged	
		eV	at.-%	eV	at.-%
C(1s)	C-C	285	56,48	285	60,61
	C*-COO	285,4	12,06	285,4	10,87
	C-O	286,5	11,21	286,5	8,21
	O-C-O/-C=O	287,9	8,19	287,9	9,44
	O=C-O-C=O/HO-C=O	289,5	12,06	289,2	10,87
O(1s)	O=C-O-C=O	532,1	81,61	532,56	61,2
	O=C-O-C=O/HO-C=O	533,35	18,39	533,81	38,80

Table 3-2: Results of C(1s), O(1s) peak decomposition of high resolution spectra recorded for freshly prepared and aged for 7 days plasma polymer multilayer system deposited of PP mesh substrate.

After ageing, a decrease of carbon atoms belonging to O=C-O/O=C-O-C=O groups from 12.06% to 10.87% (see **Table 3-2**) and a decrease of C-O functionality from 11.21% to 8.21% (see **Table 3-2**) was accompanied by an increase in C-C/C-H functionalities associated with cross-linked carbon/hydrocarbon (C_xH_y) species (on the basis of the C(1s) envelope peak fitting). An increase in O-C-O/-C=O groups is also observed. These changes include hydrolysis of anhydride groups and migration of short chains of plasma polymer to the extreme surface.

3.3.2 Effect of sterilization

3.3.2.1 Scanning Electron Microscopy observations

3.3.2.1.1 Before sterilization

Studies using SEM microscopy observation allow to visually compare the surface morphology of PP before and after autoclave and E-beam sterilization procedures. **Figure 3-5** (A and B) shows fragment of fiber of virgin PP mesh. Paralleled lengthways grooves (fibrillar strands) are visible due to polymer processing (extrusion) [405, 406]. On the **Figure 3-6** (A and B) PP/Ar/MAPP/Ag/MAPP is shown. No significant changes of the surface were visible after deposition of plasma polymer multilayer system, only small circular irregularities can be detected.

3.3.2.1.2 After autoclave sterilization

After autoclave sterilization of PP (**Figure 3-5** (C and D)), number of small dark color bubbles and several areas with pieces of torn biomaterial are found. Also an undirected tears like deformations on the surface are visible (**Figure 3-5** (D)). Defects of the surface observed on PP and PP modified surfaces after autoclave sterilization (see **Figure 3-5** (C and D) and **Figure 3-6** (C and D) suggest degradation of the material caused by hot steam. Similar results were obtained for polypropylene mesh alone subjected to autoclave treatment [407] and to polypropylene mesh subjected to resterilization using autoclave repeated treatments [408]. It is known that polypropylene material can be heated up to 140°C for short periods of time. The melting point of polypropylene is 160°C which is about 40 degrees higher than autoclaving temperature. However the humid environment caused by steam and 121°C temperature seems to be

enough to induce physical changes in the surface of polypropylene and plasma modified polypropylene meshes.

Result of autoclave sterilization treatment on PP/Ar/MAPP/Ag/MAPP is shown on **Figure 3-6** (C and D). Surface of the substrate which was sterilized at 121°C in the steam autoclave showed some changes comparing to plasma modified multilayer system deposited on PP mesh without sterilization (**Figure 3-6**). Beside paralleled lengthways grooves and small circular irregularities visible on the fiber, a number of undirected tears and small bubbles are also noticeable. On the **Figure 3-6** D, dark spots are observed, which are very similar to ones found on PP surface after autoclave sterilization.

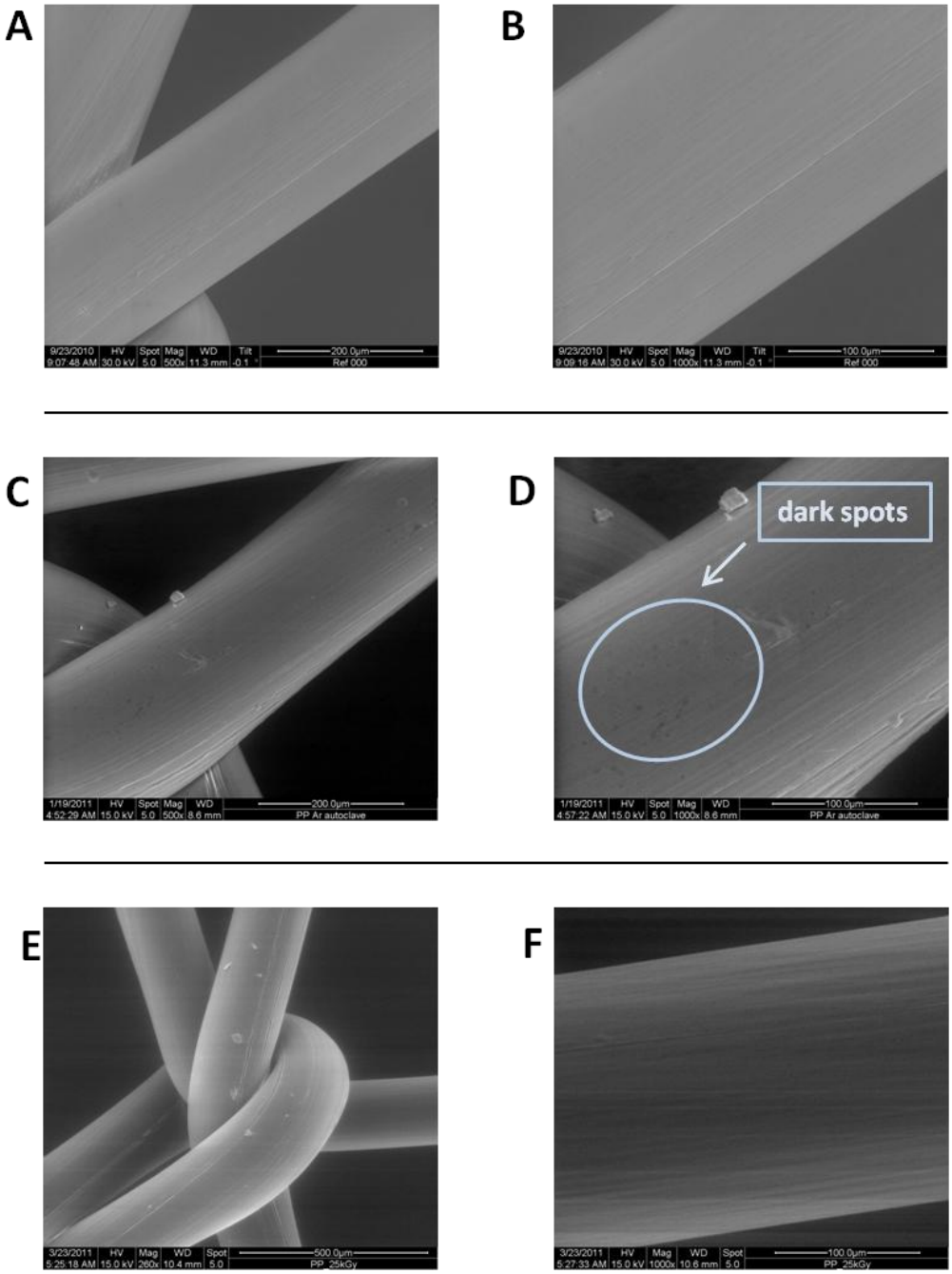

Figure 3-5: SEM micrograph of polypropylene mesh (A and B), Polypropylene mesh after autoclave sterilization (C and D) and Polypropylene mesh after electron beam irradiation (E and F). Microphotographs A, C and E are taken under 500 x magnification and microphotographs B,D and F are taken under 1000 x magnification.

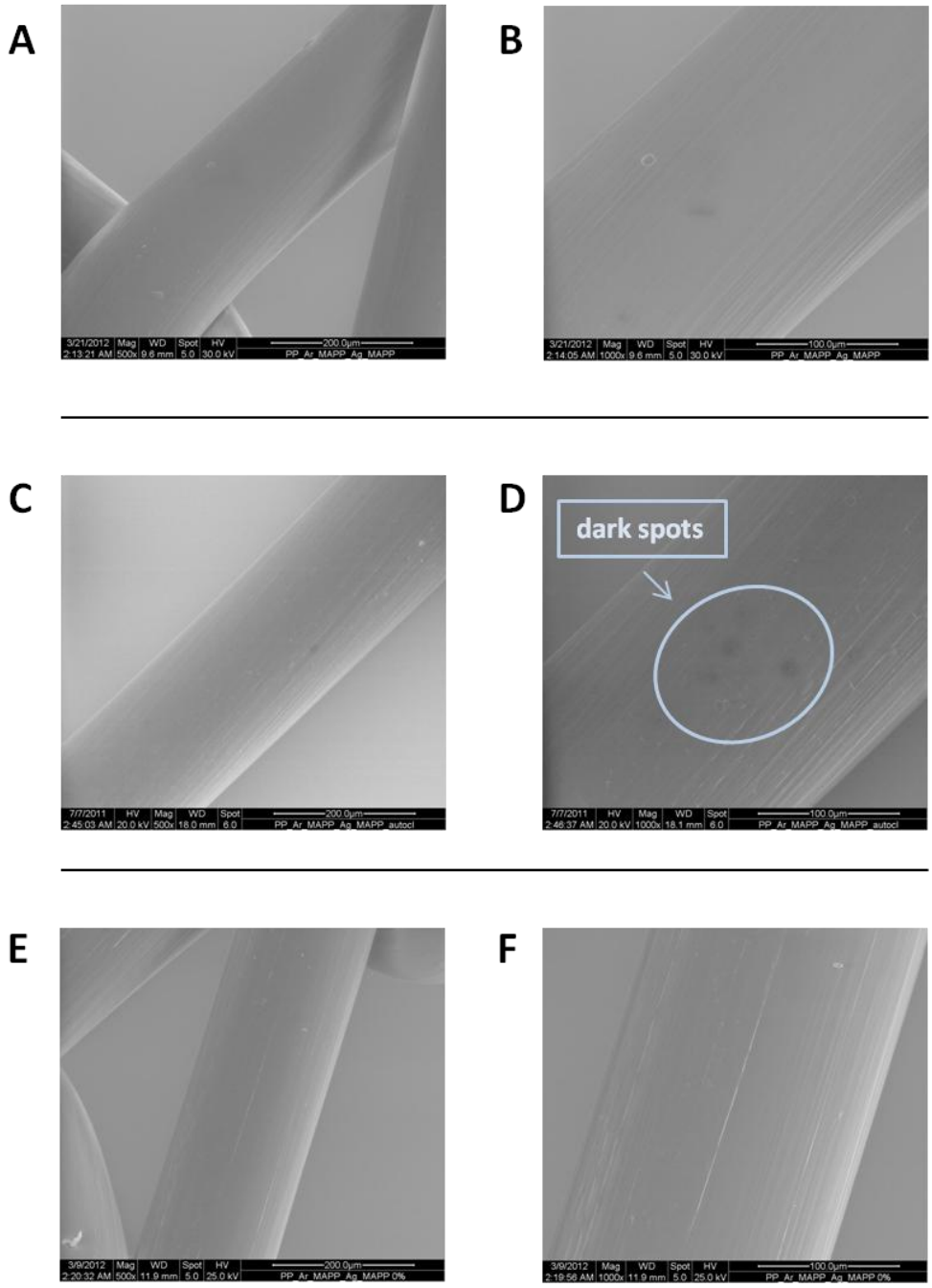

Figure 3-6: SEM micrograph of plasma polymer multilayer system deposited on Polypropylene mesh (A and B), plasma polymer multilayer system after autoclave sterilization (C and D) and plasma polymer multilayer system after electron beam irradiation (E and F). Microphotographs A, C and E are taken under 500 x magnification and microphotographs B,D and F are taken under 1000 x magnification.

3.3.2.1.3 After electron beam sterilization

On the **Figure 3-5** (E and F) polypropylene after electron beam sterilization at 25 kGy dose is shown. This sterilization treatment had no significant influence on the surface of PP. Several defects which are seen on the **Figure 3-5** (E) can come from the elaboration processing of native PP.

SEM micrographs of plasma polymer multilayer system sterilized by electron beam irradiation with the 25 kGy dose showed no changes in the physical and topographical shape of the meshes. Paralleled lengthways grooves and very few small circular irregularities can be observed on the fiber (**Figure 3-6** E, F). Results showed no differences or signs of thread-like or dark spot-like degradations after using this method of sterilization.

To conclude, Scanning Electron Microscopy observations suggest that preferable method of sterilization for multilayer system is electron beam irradiation with the dose of 25 kGy. Autoclave treatment influence surface structure unfavorably.

3.3.2.2 XPS analysis

Surface atomic concentration of plasma polymer multilayer system and plasma polymer multilayer system after sterilization by means of autoclave and electron beam irradiation is presented in **Table 3-3**.

Atomic concentration [%]			
Element	*(a)* PP/Ar/MAPP/Ag/MAPP	*(b)* PP/Ar/MAPP/Ag/MAPP /autoclave	*(c)* PP/Ar/MAPP/Ag/MAPP /25kGy
Au 4f	6.2	7.35	12.6
C 1s	62.8	62.88	60.17
O1s	28.5	28.02	21.81
Ag 3d5/2	2.5	0.61	0.4
Na 1s		1.15	2.84
Cu			2.18
O/C	0.45	0.44	0.36

Table 3-3: Surface atomic composition of **(a)** plasma polymer multilayer system. **(b)** plasma polymer multilayer system after autoclaving and **(c)** plasma polymer multilayer system after electron beam irradiation. * *Gold and copper elements are from sample holder, possible to detect due to mesh pores.*

No significant change was observed in O/C elemental concentration ratio for PP/Ar/MAPP/Ag/MAPP before and after autoclave sterilization (0.45 and 0.44 respectively). However, decrease in O/C elemental concentration ratio from 0.45 before electron beam sterilization to 0.36 after electron beam sterilization was observed (see **Table 3-3**). Atomic concentration of silver has decreased from 2.5 % before sterilization (**Table 2-1**) to 0.6 % in case of autoclave sterilization and 0.4 % after electron beam sterilization (**Table 3-3**). No other significant changes were observed after autoclave sterilization.

	Assignment	*(a)* PP/Ar/MAPP/Ag/MAPP		*(b)* PP/Ar/MAPP/Ag/MAPP /autoclave		(c) PP/Ar/MAPP/Ag/MAPP /25kGy	
		eV	at.%	eV	at.%	eV	at.%
C(1s)	C-C	285	63,13	285	66,32	285	58,05
	C*-C(O)=O	285,5	6,25	285,5	5,22	285,4	10,66
	C-O	286,5	11,49	286,5	10,99	286,5	11,25
	O-C-O/-C=O	288	12,88	288	12,26	288	9,39
	O=C-O-C=O/HO-C=O	289,2	6,24	289,2	5,22	289,19	10,66
O(1s)	C-O / O-C-O/-C=O	532.5	90.3	532,6	82,34	532,9	51,18
	O=C-O-C=O/ HO-C=O	533.8	9.7	531	17,66	533,85	48,82
Ag(3d)	Ag 3d 5/2	367.8	60.3	367,78	60,27	368,49	47,47
	Ag 3d 3/2	373.8	39.7	373,8	39,73	374,57	52,53

Table 3-4: Results of C(1s), O(1s) and Ag(3d) peak decomposition of high resolution spectra recorded for **a)** plasma polymer multilayer system, **b)** plasma polymer multilayer system after autoclave sterilization, **c)** plasma polymer multilayer system after electron beam irradiation with the dose of 25 kGy.

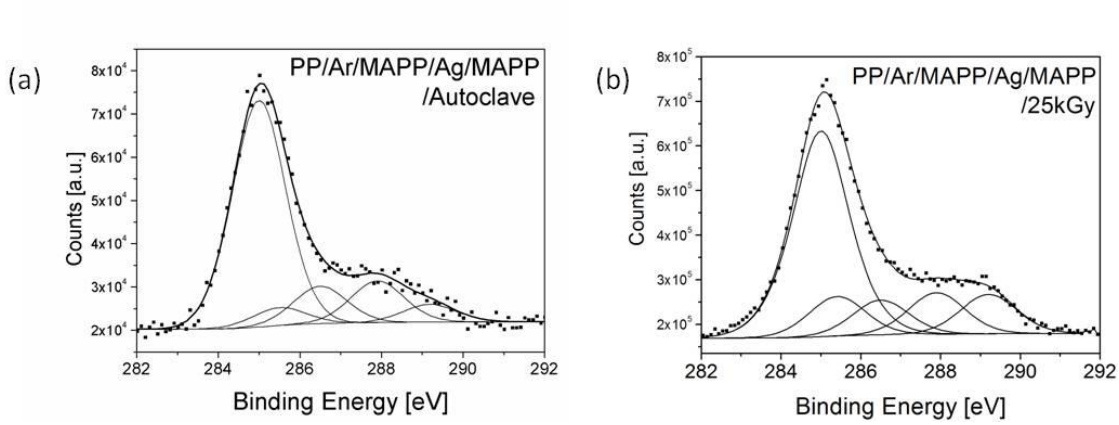

Figure 3-7: High resolution spectra of C(1s) recorded for plasma polymer multilayer system after **a)** autoclave sterilization, **b)** electron beam irradiation with the dose of 25 kGy.

XPS analysis of PP/Ar/MAPP/Ag/MAPP subjected to sterilization by means of autoclave (**Figure 3-7 a**) and electron beam irradiation (**Figure 3-7 b**) revealed five types of carbon in the C(1s) envelope: hydrocarbon (CHx ~ 285.0 eV), carbon singly-bonded to an anhydride group (C-C(O)-O- ~ 285.5 eV), carbon singly-bonded to oxygen (-C-O ~ 286.5 eV), carbon doubly-bonded to oxygen (O-C-O/-C=O ~ 288.0 eV), and acid/anhydride groups (O=C-O/O=C-O-C=O ~ 289.2 eV) (see **Figure 3-7** and **Table 3-4)**. Decrease of carbon atoms belonging to O-C-O/-C=O group from 12.9% (see **Table 3-4)** to 9.39% (see **Table 3-4**) was recorded after electron irradiation sterilization (on the basis of the C(1s) envelope peak fitting) while no change is observed after autoclave sterilization. The contribution of O=C-O-C=O/COOH, groups have increased after electron beam sterilization at the expense of C-C/C-H, (associated with cross-linked carbon/hydrocarbon (C_xH_y) species) and O-C-O/-C=O groups.

XPS analysis allowed also the detection of Ag $3d_{3/2}$ and Ag $3d_{5/2}$ photoemission X-ray lines at 367.7 eV and 373.8 eV, respectively (**Table 3-4**). As previously explained, plasma polymerization results from the well-known competition between deposition and etching during process [388]. Both the coating and the surface were bombarded by ions from the plasma leading mainly to

fragmentation during the deposition. Due also to surface mobility, a fraction of the silver species could migrate to the near-surface regions of the plasma polymer layer. Decrease of Ag concentration in the near surface region was observed after autoclave sterilization. This can be explained by dissolution of silver nanoparticles due to swelling of plasma polymer and washing off nanoparticles during autoclave process. However, in case of electron beam bombardment the decrease in silver concentration might be explained by modifications of plasma polymer such as initiation of further crosslinking that quenches any remaining radicals or chain scission due to electron displacement and generation of free radicals [409, 410]. These free radicals react with oxygen from atmosphere and form acid groups (increase of O=C-O-C=O/COOH groups, **Table 3-4**). At the same time migration of short carbon chains from the bulk of plasma polymer to the surfaces takes place.

To conclude, effect of autoclave sterilization did not affect the main chemical character of coating. However, chemistry of surface was influenced by electron beam irradiation method.

3.3.2.3 TEM analysis

3.3.2.3.1 Before sterilization

Particles size and particles distribution in the plasma polymer matrix before sterilization are described and commented in details in section 2.4.3. The differences in particles distribution can be seen on **Figure 3-8** A and **Figure 3-9** A.

3.3.2.3.2 After autoclave sterilization

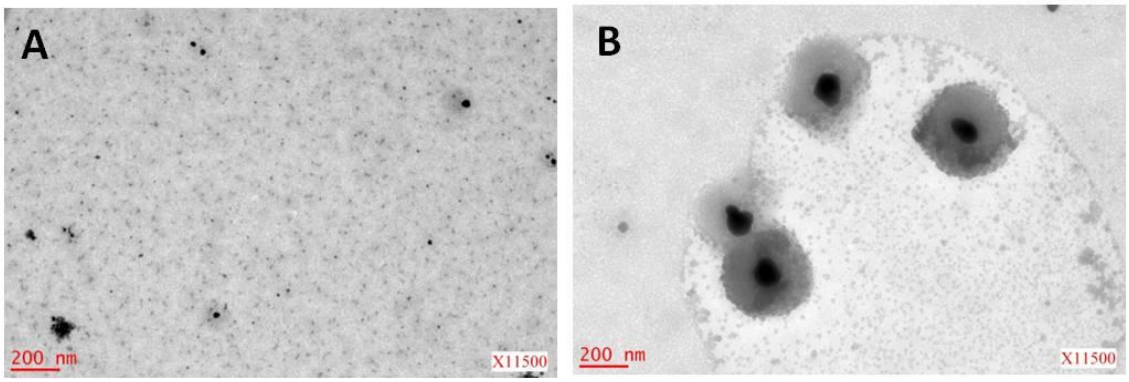

Figure 3-8: TEM micrograph of plasma multilayer system **A)** before sterilization with autoclave, **B)** after sterilization with autoclave.

Because it is well known that thermal treatment has an impact on silver nanoparticles nucleation [411, 412], synthesis [413], shape and size [413, 414] influence of autoclave sterilization on silver nanoparticles embedded in the multilayer system was verified by means of Transmission Electron Microscopy.

TEM microphotographs of PP/Ar/MAPP/Ag/MAPP before and after autoclave sterilization are shown in **Figure 3-8**. Before sterilization, silver nanoparticles seen as dark spots are uniformly distributed (see also section 2.4.3). Since the temperature is one of the key parameters that can allow to control the particle growth, the particles shape and size distribution during the synthesis, the autoclave treatment (121°C) should influence the silver nanoparticles embedded in the multilayer plasma polymer system [415]. This is due to the fact that during the synthesis stabilizer was not used [415]. **Figure 3-8** represents PP/Ar/MAPP/Ag/MAPP after autoclave treatment. Humid environment and high temperature during sterilization have affected the size and distribution of silver nanoparticles in the multilayer system. Visually compared microphotographs prove that autoclave sterilization used for thin polymeric film systems with embedded nanoparticles should be carefully considered due to changes that it

induces. Furthermore these modifications can change the release of silver ions kinetics, antibacterial properties and toxicity of the final material [22, 416, 417].

3.3.2.3.3 After electron beam sterilization

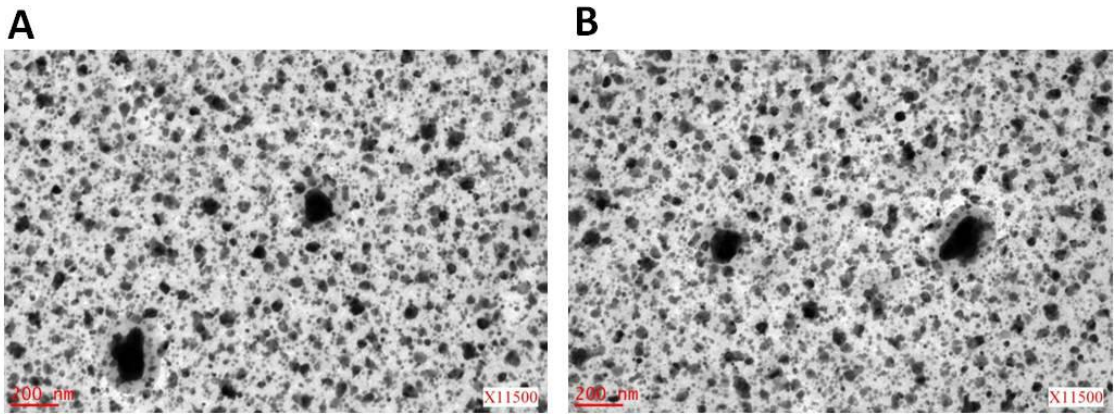

Figure 3-9: TEM micrograph of plasma multilayer system **A)** before sterilization with electron beam using 25kGy dose, **B)** after sterilization with electron beam using 25 kGy.

The effect of electron beam method of sterilization was also verified. **Figure 3-9** (A) shows a microphotograph of PP/Ar/MAPP/Ag/MAPP before the electron beam irradiation sterilization. After electron beam sterilization no aggregation or any other modification of silver nanoparticles was observed using TEM microscopy.

3.3.2.4 Antibacterial assay

As we have seen in the previous sections, autoclave sterilization method has a major impact on the surface properties of plasma polymer multilayer system. It causes physical degradation of plasma polymer film and aggregation and changes in distribution of silver nanoparticles. Electron beam sterilization however, has an impact only on the chemistry of the PP/Ar/MAPP/Ag/MAPP surface. Further we have verified how these changes influence the bacterial

response to the multilayer plasma polymer system. For this reason, effect of the plasma polymer multilayer system samples sterilized by autoclave and electron beam (with the dose of 25 kGy), on bacterial growth in the planktonic state after 4 h of incubation was tested. Results are expressed in terms of inhibition rate compared to bacterial colonization on PP reference sample.

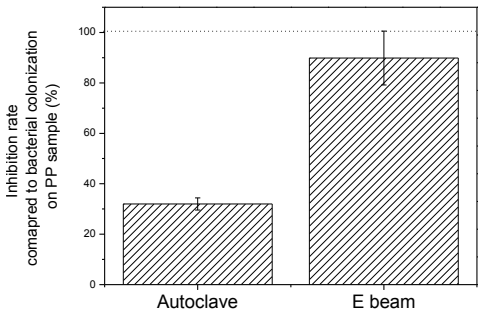

Figure 3-10: Inhibition rate of planktonic bacteria compared to bacterial colonization on PP sample after 4h of bacterial culture.

Figure 3-10 shows that bacteria proliferate easier on the sample which undergo autoclave sterilization comparing to sample that undergo electron beam sterilization. Comparing to bacterial proliferation on PP sample, the inhibition rate of bacterial proliferation on plasma multilayer system in case of autoclave sterilization is 32%. In case of electron beam sterilization inhibition rate value reaches 89%. This can be caused by dissolution of silver nanoparticles in the plasma polymer layer during autoclave treatment resulting in the lower concentration of silver ion release during antibacterial tests which can result in higher bacterial survival and proliferation.

In conclusion, these results indicate that in case of plasma polymer thin films with embedded silver nanoparticles, choice of method of sterilization is crucial and can influence further bacteria-material interaction tests and antibacterial properties of the material. Autoclave sterilization influences silver nanoparticles

directly and thus causes a change in the antibacterial properties of the final material.

3.3.3 Combining effect of ageing and sterilization

Preliminary results from tests of combined effects of ageing and sterilization on plasma polymer multilayer system deposited on polypropylene mesh were obtained. Tests were performed in the same manner as tests described in section 3.3.1.1.

For the Scanning Electron Microscopy observations first type of sample was freshly prepared and sterilized by means of electron beam (25 kGy) at the same day. Further, the sample was stretched and images were taken. Second type of sample was left to age for three days and next, sterilization with electron beam (25 kGy) was performed.

3.3.3.1 SEM

The combined effect of aging of sample and sterilization was verified by observation of physical features formed during stretching of the sample. The apparition and regularity of cracks, their size of aperture were observed and compared. In both cases cracks appear after 20% of elongation (see **Figure 3-11** 20% and **Figure 3-12** 20%). For both types of samples, between 40% and 80% of elongation, appeared cracks are regular and propagate along the fiber. There is no distinction for cracks to appear between different places on the fiber in the mesh structure (close to weave or along the fiber between two weaves).

Interestingly, comparing to the results from previous section, cracks appear with the same distance from one to another along the whole length of the fibers, (without differences between places closer to weave or in between two weaves on the fiber).

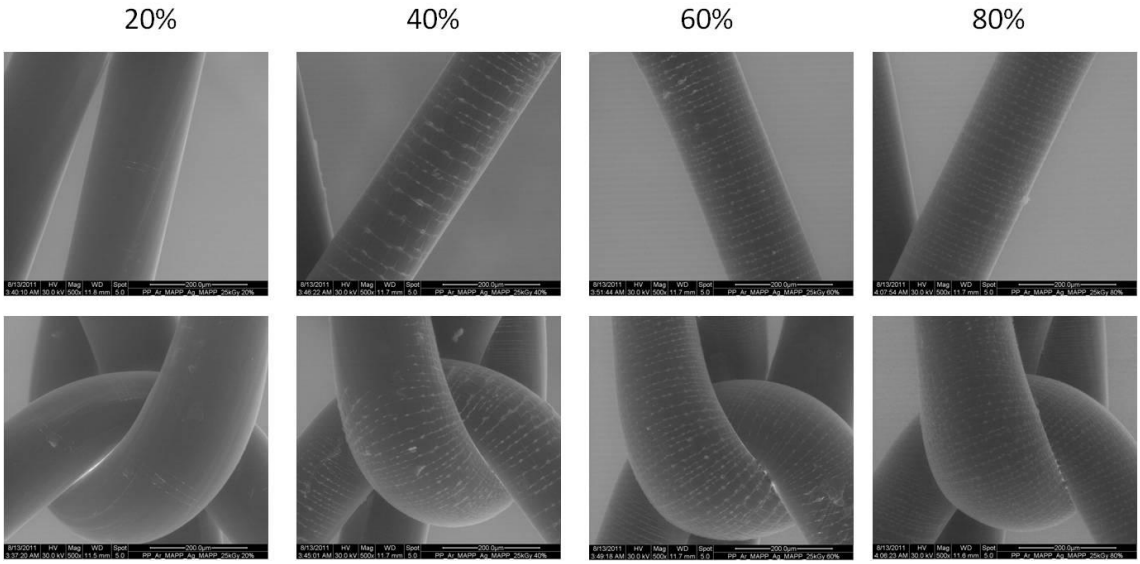

Figure 3-11: Plasma polymer multilayer system deposited on polypropylene mesh. Sample freshly prepared and sterilized by means of electron beam (25 kGy) the same day.

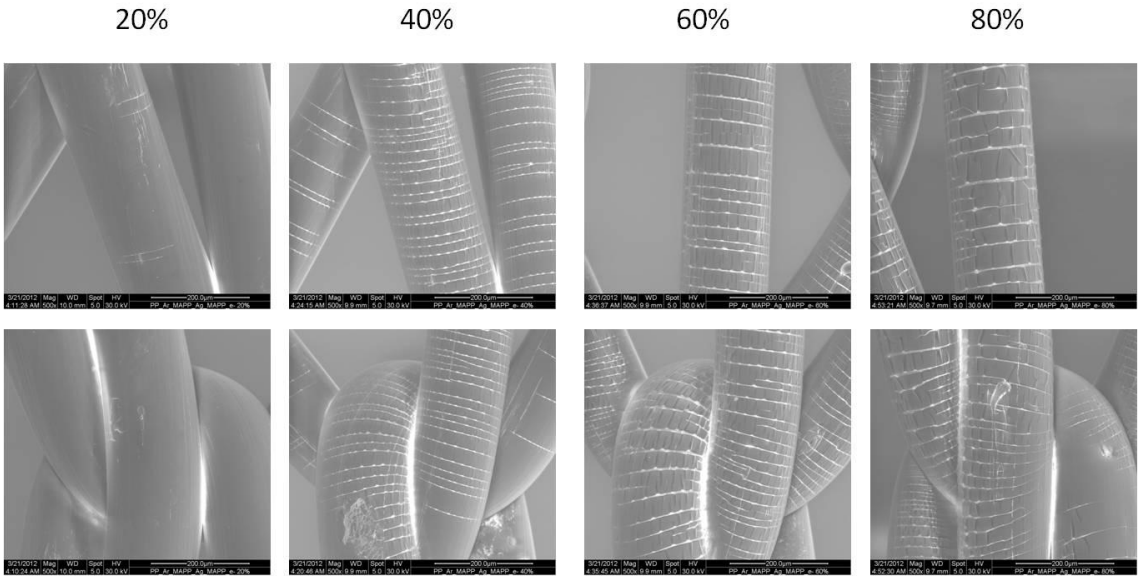

Figure 3-12: Plasma polymer multilayer system deposited on polypropylene mesh. Sample aged for three days and sterilized by means of electron beam (25 kGy).

In both cases no delamination occurred during the stretching even up to 80 % of elongation. This indicates that ageing combined with sterilization have a beneficial influence on plasma polymer multilayer system properties, which is related to changes in crosslink density after sterilization and absorption of water molecules which acts as plasticizer for plasma polymer. Ageing and sterilization allows to tailor the “crackability” of plasma polymer and thus it allows to achieve the desired properties of plasma polymer multilayer system.

3.4 Conclusions

Result of studies of the effects of sterilization and ageing on plasma polymer multilayer system suggests that during ageing some identifiable changes occur in the high resolution C(1s) envelope indicating hydrolysis of anhydride groups and migration of short chains of plasma polymer to the extreme surface

Preferable method of sterilization for these systems is electron beam irradiation. Autoclave treatment influence surface structure unfavorably. Also, tears-like shaped features, dark spots suggesting degradation and irregularities were observed on the surface of plasma deposited layers, after autoclave treatment in 121°C for 15 min. Electron beam irradiation with the dose 25 kGy did not induce surface physical or topographical changes. Autoclave sterilization did not significantly affect the main chemical character of coatings. However, electron beam sterilization induces changes in chemistry of the surface causing decrease in O/C elemental concentration ratio. Resistance against sterilization procedures of surface which is intended to undergo sterilization has to be carefully analyzed. Engineered surfaces designed for biomedical application which consist of silver nanoparticles have to be verified after undergoing the sterilization procedures. Humid environment and high temperature during autoclave sterilization have affected the size and distribution of silver nanoparticles in the multilayer system. Visually compared microphotographs

which show nanoparticles, prove that autoclave sterilization induces changes in nanoparticles size and distribution. However, electron beam irradiation chosen as a method of sterilization for plasma polymer multilayer system did not induce any aggregation or any other modification of silver nanoparticles. Additionally, plasma multilayer system after electron beam irradiation showed better antibacterial efficiency towards planktonic bacteria. This is related to preserved size and distribution of silver nanoparticles after electron beam sterilization procedure.

Observations of stretched samples after ageing and electron beam sterilization suggest that electron beam method of sterilization has beneficial effect on final properties of the material.

CHAPTER IV

4 Bacterial colonization and biofilm formation on plasma polymer modified surgical polypropylene mesh

4.1 Introduction

Synthetic surgical meshes are widely used for the tension free repair (does not put tension on muscles) of abdominal wall and gynecological defects. Use of this material has proven their effect in reduction of recurrence rate of abdominal hernia to less than 1.5 percent [418]. Structural design of yarn types of materials is nowadays used routinely for repair of abdominal wall defects in more than 50 percent of cases [77]. In case of gynecological procedures, for example management of stress urinary incontinence, synthetic meshes are now the gold standard [419]. However, the use of implant exposes the patient to a lifelong risk of infection. The infection caused by bacterial colonization may occur even up to 39 months [420, 421]. In case of gynecological procedures with such mesh, complications appear in 33-45% [419], including mesh exposure into the vagina or even the bladder or bowel, infection and pain syndrome [421]. This has impact on the recurrence of abdominal wall or gynecological defect by interfering with the recovery process after the operation and can cause the reoperation with increased patient morbidity, hospital costs and mortality rates [83, 419].

Among complications, mesh-related infections are difficult to treat and can induce morbidity recurrence [419]. Unfortunately, anti-infection strategies using antibiotics are often failing. This is due to microorganisms which adhere to the surface of implant, and start to form biofilm. In the biofilm, microorganisms develop higher resistance to environmental stresses, antibiotic treatments and they effectively protect themselves from host's immune system.

For this reason, it is important to understand the meshes-related bacterial colonization and biofilm formation. For example, it was shown by Burger *et al.* that the mesh characteristics have impact on infection rates [422, 423]. Study of Engelsman *et al.* [77] on the bacterial colonization on different meshes materials has revealed the existence of niches in the morphology of the meshes where the bacteria tend to grow. The niches were found between the filaments in case of multifilament meshes providing increased surface area and more contact points permitting the adhesion between microorganisms and implant. This has influenced the biofilm properties, resulting in massive production of slime and increased biofilm density on the multifilament meshes compared to monofilament ones [77]. Engelsman *et al.* [332] have shown that consequently, different rates of infection were associated to the different types of surgical meshes.

Polypropylene mesh, which is used in this study, was reported to be associated with an infection rate between 2.5% – 5.9% in case of abdominal wall implants [424-426], similarly to polyester meshes. It was shown that both gram-negative and gram-positive bacteria form biofilms on these types of materials [77, 427]. However, it is dependent on the surgical technique used (open or laparoscopic implantation) and patient characteristics. The material structure (PP or expanded Polytetrafluoroethylene (ePTFE), multifilament or monofilament mesh) influenced the infection rate. Changes in material composition and textile properties influenced bacterial adherence as well [77, 332, 427].

One of the strategies to reduce the rate of infection on mesh materials was introduced by Scheibach *et al*. [428]. Authors rendered the surface of mesh anti-adherent for bacteria. *S. epidermidis* and *S. aureus* adherence on titanium coating on polypropylene mesh surface was evaluated *in vitro*. Results showed the biocompatibility of modified polypropylene and the reduction of bacterial adhesion. Similar study on coatings for mesh material was performed by Saygun *et al.* [429]. Authors have used similar anti-adhesive coatings for bacteria using gold and gold/ palladium coatings. Their study revealed significant reduction of bacterial colonization on gold/ palladium coated meshes. Another strategy to reduce mesh related infection is proposed in commercially available surgical meshes such as the GORE® DUALMESH® PLUS. This strategy includes presence of biocide in the coating, which can be released to the environment. In this case, material is made of polytetrafluoroethylene (ePTFE) which contains silver carbonate and chlorhexidine diacetate. It is claimed to resist to initial biofilm formation on the device up to 14 days post-implantation.

Before studying the development of biofilms on mesh materials, some aspects of bacterial biofilm should be noted. Tolker-Nielsen and Molin [430] have noted that every microbial biofilm community is unique, however some structural attributes can be generally considered universal. In particular, biofilms are not always continuous monolayers. They can be very heterogeneous, containing microcolonies of bacterial cells organized in various ways. Heterogeneity of biofilms exists not only for mixed culture biofilms (these can be found in environmental biofilms) but also for pure culture biofilms common on medical devices and those associated with infectious diseases. Heterogeneity can be a result of chemical gradients, adaptation to local environmental conditions, e.g. nutrition, temperature.

Stoodley *et al*. [431] defined some criteria and characteristics that could be considered for biofilms in general. In particular, biofilms are thin flat film, ranging

from a monolayer of cells to a film consisting of several layers, which contain water channels. The microorganisms, which compose the biofilm also have an impact on the biofilm structure. For example, it was showed that biofilm thickness can be affected by the number of component organisms [432]. Pure cultures of *K. pneumoniaeor* and *P. aeruginosa* biofilms in a laboratory reactor were thinner than biofilm composed of both species (thickness *of* 15 µm for *K. pneumoniaeor,* 30 µm for *P. aeruginosa* and around 40 µm for mixed biofilm*)*.

Biofilm architecture is heterogeneous both in space and time, changing due to external and internal processes and conditions. Structure of biofilm depends also on the environmental conditions such as temperature of cultivation, growth media compositions and diluted or rich compositions of the same kind of growth medium [433-436]. Differences in bacterial biofilm architectures result in different susceptibility of bacteria towards antibacterial agents [390, 437]. It was determined by Teitzel *et al*. [366] that biofilms of *P. aeruginosa* were more resistant between 2 to 600 times to heavy metal stress than planktonic bacteria cells. Only bacteria at the border of the biofilm structure were killed after exposure to elevated concentrations of copper. Near the substratum, cells were still alive. EPS matrix was suggested to protect cells from heavy metal stress by binding the heavy metals and retarding their diffusion within the biofilm. Differences in the susceptibility of planktonic and biofilm cell populations of *P. aeruginosa* were also showed by Abdi-Ali *et al.* [437] for various antibiotics. It was suggested, that matrix prevents access of antibiotics to the bacterial cells embedded in the community. Sommerfeld *et al*. [390] have studied susceptibility of bacteria to ciprofloxacin hydrochloride, in two bacterial populations such as bacteria in connected biofilm structures (bacteria that grow in close proximity inside the biofilm) and planktonic bacteria, or unconnected bacteria (bacteria outside of biofilm). The study revealed that bacteria in unconnected population were more susceptible to antibiotics.

To visualize biofilms, Confocal Laser Scanning Microscopy (CLSM) technique is often used. This technique allows fluorescence imaging at different planes within the biofilm, which allows to generate 3D images with high resolution. For the quantification and further analysis of such biofilms micrographs, diverse softwares have been developed. In particular, detailed quantification of biofilm using parameters such as biomass, average thickness, and roughness coefficient, surface to biovolume ratio, maximum thickness, surface coverage is possible with COMSTAT software [70]. In the software function called Connected Volume Filtering (CVF) bacterial elements that are not part of a biofilm are removed from the stack of images, when quantifying the biofilm parameters. Then the removed part is not included in the further calculations [438]. For example, Sommerfeld *et. al* [390] used the function CVF of Comstat2 software to analyze the susceptibility of bacteria in connected biofilms and unconnected sections. Sanchez *et al.* [436] have used Comstat software for the quantification of the biomass, average thickness, roughness coefficient, surface to biovolume ratio, maximum thickness and surface coverage to follow the changes in biofilm architecture caused by different nutrition concentrations. However, in their opinion, the quantitative analysis using these parameters does not necessarily predict the differences in biofilm architecture. Apart from surface coverage parameter which differed significantly, other analyzed structural parameters did not show significant differences in biofilm architectures although visual observations from CLSM micrographs clearly showed morphological differences [436]. This is probably due to implemented CVF parameter which removed parts of biofilm from analysis. Heydorn *et al*. [70] analyzed biofilm structures of four *Pseudomonas* sp. strains which formed different patterns. The analysis of biofilm structures in terms of roughness coefficient, substratum coverage and surface to volume ratio by Comstat was able to show very weak differences. This allows to consider that the use of CLSM technique together with Comstat2 software gives an opportunity to analyze in details the architecture of biofilms.

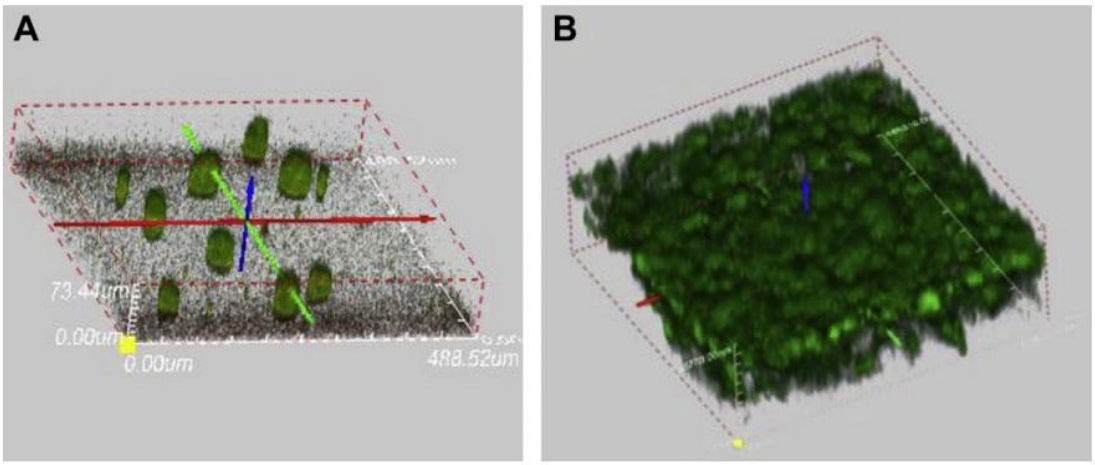

Figure 4-1: Three-dimensional reconstructions of GFP-labeled *P. aeruginosa* PAO1 biofilms show round, dispersed cellular aggregates when grown in LB medium (A), and flat-compact, sheet-like structures in 1/3-diluted LB medium (B) at 72 h. Each image consists in thin optical sections collected at 1-mm intervals in z-section. Image resolution: 512x512 pixel; size: 488.52mm x488.52mm. Images obtained from Sanchez *et al.* [436].

In this chapter, we present study of the bacterial colonization, biofilm development together with biofilm structure analysis on plasma polymer mechanoresponsive antibacterial coating deposited on PP mesh substrate. Additionally the study of the impact of Ag ions released from the coating on planktonic bacteria living in the surrounding of the developed material is presented. Moreover, the preliminary study of the biocompatibility of the developed plasma polymer multilayer coating deposited on PP mesh is evaluated using eukaryotic cells and can be found in the annex (section 6).

4.2 Materials and Methods

4.2.1 Bacterial strain

Experiments were conducted with the laboratory strain *Escherichia coli (E. coli)* SCC1. This bacteria strain is autofluorescent through a genetic insertion, expresses curli and produces exo-cellular polymeric substances (EPS). *E coli* was purchased by Prof. Miao [66] from the Technological Institute, Singapore. *E. coli* bacterial strain was long term stored either in liquid nitrogen at -180°C or in freezer at -80°C.

4.2.2 Cultivation

Bacteria were taken from frozen stock (-80°C) and were spread on an agar plate (Luria–Bertani medium) for an overninght culture.

One colony of bacteria was inoculated in 10 mL of Luria–Bertani (LB) (LB purchased from Sigma-Aldrich) medium and cultivated at 30°C, overnight. A second preculture was inoculated from the first preculture (10 vol-% of the first culture) in 10 mL of selective M63G-B1 medium [380] (see **Table 4-1**) and cultured overnight. A third preculture was inoculated from the second preculture in M63G-B1 (10 vol-% of the second preculture) and cultured for 4 h at 30°C. The final culture used to perform the experiments was inoculated from 4 h preculture (10 vol-%). The optical density at 600 nm (Abs_{600}) was adjusted to 0.01 (i.e. 10^6 bacterial/mL).

Table 4-1: M63G-B1 medium composition [380].

M63G-B1	
KH_2PO_4	0.1 M
$(NH_4)SO_4$	20 % wt
$FeSO_4$	0.1 % wt
$MgSO_4$	20 % wt
KOH	6 M
agar	1.5 % wt optional, adjust to pH 6,8
	Autoclave for 20 min at 120°C
Vitamine B1	0.05 % wt
glucose	10 % wt

4.2.3 Substrates

The substrates developed during this research and described in details in the chapter 1 have been used for bacterial adhesion (4 hours culture) and bacterial biofilm development (168 hours culture) experiments. Their toxicity towards bacterial cells has been evaluated. Untreated PP substrate and PP substrate with deposition of the only second layer of plasma polymer (PP/Ar/MAPP(2^{nd})) were used as controls. Substrate toxicity experiments were performed two times, each time in a double determination (i.e. two samples of each condition). Bacterial colonization and biofilm development experiments were performed three times, each time in a double determination.

Table 4-2: Samples identification and description.

Sample Identification	Description
PP	Polypropylene mesh

PP/Ar/MAPP(2nd)	Polypropylene mesh after argon plasma treatment and deposition of plasma polymer layer with the conditions used for 2nd plasma polymer layer (overlayer) in the multilayer plasma polymer system, described in details in section 2.3.3
PP/Ar/MAPP/Ag	Polypropylene mesh after argon plasma treatment and deposition of first plasma polymer layer with the synthesis of silver nanoparticles afterwards
PP/Ar/MAPP/Ag/MAPP	Complete plasma polymer multilayer system deposited on polypropylene mesh
PP/Ar/MAPP/Ag/MAPP-60%	Complete plasma polymer multilayer system deposited on polypropylene mesh, stretched with the 60% of elongation compared to initial length of the sample

4.2.4 Sterilization

Sterilization of the samples used for the experiments was performed in the Center of Irradiation Aérial (CRITT, Aérial, Illkirch). Samples were sterilized by electron beam with the electrostatic generator of Van Graff type with maximal voltage of 2.5 MV and maximal power 500W. Voltage can be varied between 0.5 and 2.5 MV and intensity of electric current between 0.01 à 200 µA. Dose of irradiation received by samples was set to 25 kGy. Sterilization of the samples was performed two days before each experiment. Silicon wafers and stainless steel wires used during experiments were sterilized in dry oven for 1 hour at 180°C.

4.2.5 Analysis of the effect on planktonic bacteria

In order to test the potential toxicity of the coating and/or Ag^+ ions releasing from the surface on bacteria, cell growth in planktonic state was measured. For

this purpose, substrates were placed into small Petri dishes (Ø 35 mm) on the previously placed and sterilized in oven (180°C for 1 h) silicon wafers. Stainless steel wire was used as a support for keeping the substrate immersed in solution. 4 mL of the bacterial culture (Abs $_{600}$= 0.01) was added to the substrates. Bacteria were grown for 4 h and 168 h at 30°C on the samples. After incubation, the samples were thoroughly and carefully rinsed with NaCl (9 g/L in distilled water), to eliminate non-adherent or loosely attached bacteria from the substrate surfaces and remove media from the Petri dish. For this purpose, 2 mL of supernatant i.e., bacterial suspension for the first rinsing and NaCl solution for further rinsing, were removed and replaced by fresh NaCl solution (9 g/L in water). The rinsing step was performed without direct flushing, with the stream directed to the walls of a Petri dish and with the attention to the force of rinsing fluid. The substrate surface remained immersed in liquid during the rinsing steps (i.e., adhered bacteria and biofilm were not dried by air-surface interface creation). The effect of the new coatings on bacterial growth in the planktonic state was tested by measuring the absorbance at 600 nm (A_{600}) of a culture in which the substrate was immersed.

4.2.6 Analysis of bacterial colonization and the biofilm formation

Substrates were placed into small Petri dishes (Ø 35 mm) on the previously placed and sterilized in oven (180°C for 1 h) silicon wafers. Stainless steel wire was used as a support for keeping the substrate immersed in solution.

4 mL of the bacterial culture (Abs $_{600}$= 0.01) was added to the substrates. Bacteria were grown for 4 h and 168 h at 30°C on the samples. After incubation, the samples were thoroughly and carefully rinsed with NaCl (9 g/L in distilled water), to eliminate non-adherent or loosely attached bacteria from the

substrate surfaces and remove media from the Petri dish. For this purpose, 2 mL of supernatant i.e., bacterial suspension for the first rinsing and NaCl solution for further rinsing were removed and replaced with fresh NaCl solution (9 g/L in water). The rinsing step was performed without direct flushing, with the stream directed to the walls of a Petri dish and with the attention to the force of rinsing fluid. The substrate surface remained immersed in liquid during the rinsing steps. The rinsing step was repeated six times for the inoculation time of 4 h and 16 times for the inoculation time of 168 h.

4.2.6.1 Adhered bacteria and biofilm observations and fluorescence staining

4.2.6.1.1 Fluorescence staining

In order to visualize cells and monitor their viability, bacteria were stained after last rinsing step with NaCl, with 1 µL/mL of Live/Dead® bacterial viability stain kit (Molecular Probes) for 15 minutes. The kit employs two nucleic acid stains – green-fluorescent Syto®9 and red-fluorescent propidium iodide stain [439]. Syto®9 stains cells with intact membranes and propidium iodide stains cells with compromised membranes [440, 441]. The green Syto®9 dye enters all cells, while the red propidium iodide enters only cells with damaged membranes. This approach was used to expand the information obtained from CLSM images for qualitative and quantitative analysis of bacteria in connected and non-connected biomasses.

4.2.6.1.2 Microscopy

Confocal microscopy 3D images with the constant interval in z-direction equal to 2 µm were taken. Experiments were conducted using an upright confocal

microscope (Carl Zeiss, LSM 700) with a 9.1 mm working distance focal objective (Zeiss LD EC “epiplan neofluar” 50X/0.55 DIC M27). Fluorescence with Syto®9 labeling was exploited for imaging with laser wavelength of 488 nm for excitation with pinhole size of 1 AU. The collection of emission fluorescence was performed in the range of 420 – 550 nm. In case of propidium iodide (PI), collection of emission fluorescence was collected in the range of 560 – 700 nm with the excitation wavelength of 555 nm. In addition, excitation at 405 nm and pinhole size 0.3 AU was used in reflection mode allowing to perform image of the surface of the substrate. Confocal 3D images were taken for 5 randomly chosen locations of each sample. CLSM were treated with the Zen2009 software provided by Carl Zeiss, Image J V1.46d software with LSM toolbox V4.0g plug-ins [69, 381] and Comstat2 [70, 438].

CLSM images of biofilms on mesh materials can be considered to be not always suitable for quantifying the number of adhered bacteria on the meshes, due to the observer’s bias toward “nice” images as it was pointed by Engelsman *et al.* [77]. In present study, the investigated area was chosen randomly, even if the bacteria or biofilm were not present on the mesh surface in particular place. Biofilms never cover 100% of the surface of a biomaterial, and biofilm-surface free area was not considered out of the scope of interests. Due to this approach the variation of number of bacteria or biomass in case of biofilm, may differ greatly on this type of material. However, variability represents the reality of the bacterial adhesion and biofilm development on mesh monofilament material.

4.2.6.1.3 Image analysis of bacterial colonization after 4h of incubation time

Number of adherent bacteria on each location observed on the surface was quantified in this experiment. For this purpose, the stacks of images were

treated with the Image Processing Software - ImageJ 1.46 [69] to perform the counting of bacteria on the three dimensional surface of a fiber. Firstly, separation of fluorescence images and reflection images was performed. Secondly, summing up of the slices corresponding to the fluorescence images was executed. Further, Particle Detector &Tracker plug-in was used to count the number of adherent bacteria [442].

4.2.6.1.4 Analysis of biofilm micrographs after 168 h of incubation time

For the quantification of biofilms after 168h of incubation time, a novel computer program Comstat 2 was used. This is a development from its original Comstat 1 version [70, 71] and was developed by Heydorn A, Nielsen AT, Hentzer M, Sternberg C, Givskov M, Ersbøll BK, Molin S. It was provided by Claus Sternberg. The software was analyzing the native confocal LSM Zeiss format images. Manual thresholding was performed and fixed threshold value was kept for all analyzed images The total biomass was measured.

Parameters that are extracted:

- The parameter named “Connected Volume Filtering” (CVF) is used to separate the CLSM image pixels of connected biofilms from unconnected bacteria, or to remove elements that are not part of the biofilm. The algorithm extracts the bacteria that are not part of a biofilm from an image stack [438]. In addition, “if an element in the image stack is not in some way connected to the substratum (first layer of the detected biofilm), it is not considered part of biofilm”. It can be piece of torn biomaterial but it might be also the part of biofilm connected to the substratum outside the scope of the image stack under observation [438]. The bacteria retained after using this function to calculate biomass are those in the connected biofilm. The bacteria which are eliminated are considered to be outside of the biofilm. Due to the geometrical shape of

the substrate, use of this function was explored to investigate the "connectivity" of observed biofilms, i.e. if biofilm is likely in forms of separated colonies and/or single bacteria or as a one "connected" (cohesive) compact structure. By using this parameter, our aim was to extract additional information about biofilm architecture, growth and viability. This feature of biofilm structure is crucial in the antibiotic or other biocides therapies due to the efficiency of penetration [443] and the protection of bacterial cells by structural organization of the biofilm [444].

- Biovolume is definied as the number of biomass pixels in all images of a stack multiplied by the voxel size and divided by the substratum area of the image stack. The resulting value is the biomass volume divided by substrate area unit. Biovolume represents the overall volume of the biofilm, and also provides an estimate of the biomass in the biofilm. In the present study, calculation of biomass was performed after using CVF function (biomass named "connected") and as well without activating this function (biomass named "total biomass"). Further, the "non-connected" part of biofilm was calculated by subtraction of "connected" biomass from "total biomass".
- Another parameter, which was calculated, was the surface to biovolume ratio, defined as surface area of biofilm divided by the biovolume. The surface to biovolume can be considered as reflecting what fraction of the biofilm is in fact exposed to the nutrient flow, and thus may indicate how the biofilm adapts to the environment. For instance, it could be speculated that in the environments of low nutrient concentration, the surface to biovolume ratio would increase in order to optimize access to the limited supply of nutrients [70]. In our study, it may reflect also the response of bacteria to low concentration of silver ions release from the substrate.
- The average diffusion distance has been also calculated. The diffusion distance is defined as the minimum distance from a given living cell to

the void (distance from all points in the image stack to the nearest void (background)). Since the void can potentially contain nutrients, oxygen etc, the diffusion distance plays a serious role in the development and understanding of biofilms. In the present study we have also calculated all above mentioned parameters for the PI stained bacteria (red) in biofilms.

Parameters that are further calculated on the basis of the previous four parameters are:

— Inhibition rate compared to reference sample

$$I_i(\%) = \frac{OD_{ref} - OD_i}{OD_{ref}} * 100$$

- *OD_{ref} - Optical density of reference sample*
- *OD_i Optical density of measured sample*

— Rate of connected biomass

$$BC_i = \frac{Biomass_{CVF(i)}}{Biomass_{Total(i)}} * 100$$

- *Biomass $_{CVF\ (i)}$ - Biomass calculated with CVF parameter*
- *Biomass $_{Total\ (i)}$ – Biomass calculated without CVF parameter*

— “Viability” (rate of cells with non-compromised membrane)

$$Viability_{(green)}(\%) = \frac{\overline{Nb}_{green}}{\overline{Nb}_{Total}} * 100$$

$$\Delta\, Viability_{green} = \left(\frac{\Delta_{green}}{\overline{Nb}_{green}} + \frac{\Delta_{Total}}{\overline{Nb}_{Total}}\right) * \overline{Nb}_{green} * \overline{Nb}_{Total}$$

- $\overline{Nb_{green}}$ - *Average number of bacteria with non-compromised membrane*
- $\overline{Nb_{Total}}$ *– Average Total number of bacteria*
- Δ_{green} *- Standard deviation of number of bacteria with non-compromised membrane*
- Δ_{Total} *- Standard deviation of number of total number of bacteria*

— Rate of bacteria with compromised membrane in connected biofilms

$$RBred_i = \frac{BiomassRed_{CVF(i)}}{BiomassTotal_{CVF(i)}} * 100$$

- *BiomassRed* $_{CVF\ (i)}$ *- Biomass of bacteria with compromised membrane calculated with CVF parameter*
- *BiomassTotal* $_{CVF(i)}$ *– Total Biomass calculated with CVF parameter*

— Green/Red (G/R) parameter

$$G/R_i = \frac{Surface\ to\ Biovolume\ ratio_{green(i)}}{Surface\ to\ Biovolume\ ratio_{red\ (i)}}$$

- $Surface\ to\ Biovolume\ ratio_{green(i)}$ *– surface to biovolume ratio of bacteria with non-compromised membrane*
- $Surface\ to\ Biovolume\ ratio_{red\ (i)}$ *- surface to biovolume ratio of bacteria with compromised membrane*

4.2.6.1.5 Quality control

The results are expressed in terms of mean values and standard deviations for two samples of each substrate including positive and negative controls. Significant differences between sample sets were determined using the classical parametric test for mean comparison, so-called Student test (t- test) (n-1 degree of freedom).

To test the reproducibility, bacterial colonization, biofilm formation and the effect on the planktonic bacteria experiments were repeated several times. The number of repetition for effect on planktonic bacteria experiment was 2 times. The number of reproduction for bacterial colonization after 4h of incubation and biofilm formation after 168 h of incubation was 3 times using Live/Dead dye. Additional two times repetition were performed for those studies using only Syto®9 dye. Graphs presented in following results are average of the experiment repetitions.

4.3 Results and discussion

The following section consists of the study of the anti-bacterial properties of the PP and PP modified mesh substrates. The effect of these materials on planktonic bacteria growth is described as first. Secondly, bacterial colonization and biofilm formation is discussed, together with the viability of bacterial cells. The biofilm architecture on the studied substrates is also analyzed.

4.3.1 Effect on planktonic bacteria tests

The effect of the new coatings on bacterial growth in the planktonic state was tested by measuring the absorbance at 600 nm (A_{600}) of a culture in which the substrate was immersed. Results are expressed in terms of “Inhibition rate” compared to bacterial colonization on PP reference sample for the set of PP/Ar/MAPP(2^{nd}), PP/Ar/MAPP/Ag and PP/Ar/MAPP/Ag/MAPP substrates. The effect of stretching on the Ag^{+} release and subsequent anti-bacterial property was expressed in terms of “Inhibition rate” of stretched PP/Ar/MAPP/Ag/MAPP-60% samples compared to not stretched PP/Ar/MAPP/Ag/MAPP samples.

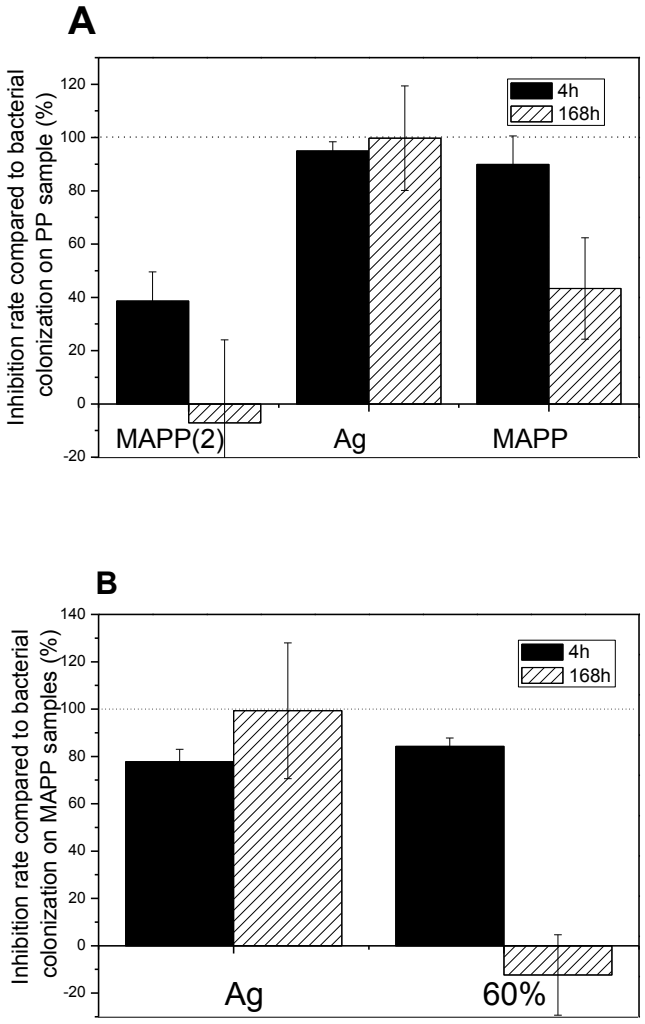

Figure 4-2: Effect of modified PP surfaces on planktonic bacteria expressed as A) Inhibition rate for PP/Ar/MAPP/MAPP(2nd), PP/Ar/MAPP/Ag and PP/Ar/MAPP/Ag/MAPP samples compared to PP sample, B) Inhibition rate for PP/Ar/MAPP/Ag and PP/Ar/MAPP/Ag/MAPP stretched -60% sample, compared to not stretched PP/Ar/MAPP/Ag/MAPP samples (only PP/Ar/MAPP/Ag/MAPP samples with sufficient barrier effect were taken into account for calculation in B. Abbreviations MAPP(2), Ag, MAPP, 60% on the graph represent PP/Ar/MAPP(2nd), PP/Ar/MAPP/Ag, PP/Ar/MAPP/Ag/MAPP, stretched PP/Ar/MAPP/Ag/MAPP samples respectively.

The potential growth inhibition of planktonic bacteria free-living in liquid medium surrounding immersed samples was evaluated. Results, that are expressed as referred to bacterial growth around uncoated PP samples showed that PP/Ar/MAPP(2^{nd}) substrates have influence on the bacterial proliferation in the planktonic state, reaching the inhibition rate equal 38% for incubation time 4 h, comparing to bacterial colonization on PP samples (**Figure 4-2 A**). This suggests that PP/Ar/MAPP(2^{nd}) surface may exert antibacterial properties on planktonic bacteria in the first 4 h of incubation time. This may be due to the elution of low molecular weight water soluble fractions of plasma polymer [386]. Nevertheless, there is no difference in planktonic bacteria proliferation between PP/Ar/MAPP(2^{nd}) and PP sample for 168 h of incubation time, suggesting that this low molecular fraction is in small amount and is easily extracted during the first time of immersion. Such effect of MAPP was never highlighted in previous studies so far. Importantly, the results also showed that the concentration of silver ions that is released in the liquid medium from PP/Ar/MAPP/Ag samples was high enough to significantly inhibit planktonic bacteria growth in case of 4 and 168 hours (**Figure 4-2 A**). Surprisingly, of PP/Ar/MAPP/Ag and PP/Ar/MAPP/Ag/MAPP samples for 4 h of incubation time lead to similar values of inhibition rates, in contrast to expected. This can be explained by the presence of silver nanoparticles close to the surface region in case of PP/Ar/MAPP/Ag/MAPP samples (which may provide a fast release of silver ions when in contact with liquid environment). As it is shown in the chapter 2, presence of silver ions in the supernatant solution was detected (see section 2.4.5) only after 24 hours of immersion in case of PP/Ar/MAPP/Ag/MAPP samples The concentration of Ag^{+} released from PP/Ar/MAPP/Ag/MAPP sample before this time was under the limit of detection with UV-Vis spectroscopy (i.e., 1.5 ppm (8,8 μM) - **Figure 4-3**). However, bacteria can be sensitive to concentration of silver under this level. As it is shown on **Figure 4-4**, bacterial growth of *Escherichia coli* is inhibited by presence of silver ions, even at concentration as low as 0.5 ppm. With the concentration lower than 0.5 ppm,

results suggest that effect of slowing down the growth may also exist after 4 hours although after longer time of incubation (in this case 24 hours), bacterial growth is not affected any more.

In contrast, inhibition rate of PP/Ar/MAPP/Ag/MAPP samples is significantly less than for PP/Ar/MAPP/Ag samples, for 168 hours of bacterial incubation. In case of PP/Ar/MAPP/Ag sample, the high level of inhibition rate is due to sufficient release of antibacterial agent in the adequate concentration/time rate, which blocks and/or inhibits the bacterial proliferation in planktonic state. In case of PP/Ar/MAPP/Ag/MAPP samples, the decrease in inhibition rate to 43% is observed, which implies the efficiency of the barrier effect for a part of the samples, blocking Ag^+ release from the nanoparticles which are enclosed in the plasma polymer overlayer. The release kinetics of the ionic form of silver from the plasma polymer containing silver nanoparticles is influenced by several factors, as discussed in the section 2.4.5 of this work. The difference in inhibition rate for PP/Ar/MAPP/Ag/MAPP samples in case of 4 and 168 h can be explained as followed: the "short" time (4h) antibacterial effect of PP/Ar/MAPP/Ag/MAPP samples without stretching is coming from the ion release from nanoparticles distributed in the near surface plasma polymer overlayer. The reservoir of Ag^+ constituted by these AgNPs at the extreme surface is probably too small to perform long-term release of Ag^+. In other words, this Ag^+ quantity is probably not high enough to efficiently block long-term bacteria proliferation. If the release of silver is relatively low, the susceptibility of bacterial organisms can give different outcomes of microbial behavior such as growth delay with later re-growth or complete inhibition of the growth [445]. The growth delay involves short-term cell killing, prolongs lag phase ([446]) and decreases specific growth rate in the log phase [447]. In addition, the microbial population size may be a limiting factor in the inhibition activity of the silver ions (e.g. the ratio of silver ions per cell plays a role in the inhibition of bacterial growth) [445].

Due to the presence of Ag nanoparticles in the depth of ~10 nm from the surface in different quantities from one sample to another (see **Figure 2-8**) and to the insufficient barrier effect of second plasma polymer overlayer, as discussed before in section 2.4.5, the Ag^+ ions releasing profile differed from one sample to another (see **Figure 4-3**). The example of sample with not sufficient barrier effect is presented in **Figure 4-3 a**, while in **Figure 4-3 b** UV-Vis spectrum represents the sample with very limited release of Ag^+ (probably due to lesser quantity of silver nanoparticles in the top layer). For this reason, in the experiment verifying the efficiency of stretching represented on **Figure 4-2 B**, the samples with no efficient barrier effect (see **Figure 4-3** a) were not used for the determination of "Inhibition rates" of planktonic state bacteria.

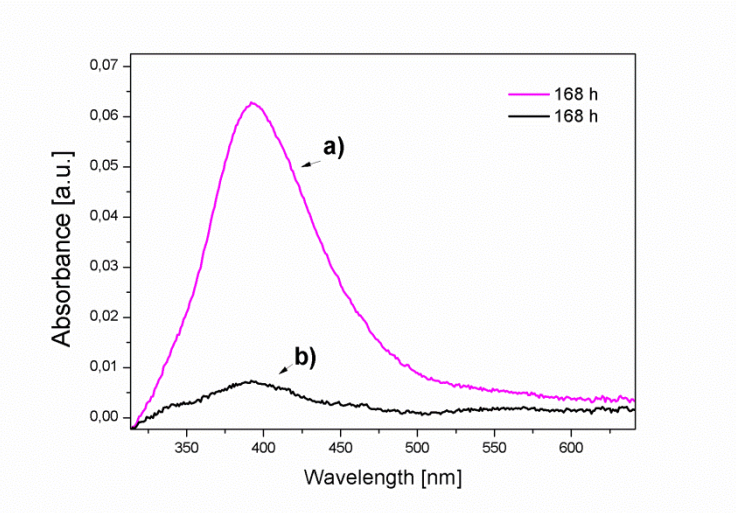

Figure 4-3: UV-Vis measurement of the supernatant solution after immersion of two PP/Ar/MAPP/Ag/MAPP materials without stretching during 168 h in distilled water. Measurements were performed after addition of reductant solution in order to reduce the silver ions to silver nanoparticles. **a)** 168h without barrier effect, **b)** 168h with barrier effect. After integration of a and b peak area, and on the basis of **Figure 2-18** (a and b), the concentration of silver ions was estimated to 6 ppm (35.3 µM) for the peak a and 1.5 ppm (8.8 µM) for the peak b.

By stretching samples, a similar inhibition rate to those obtained with PP/Ar/MAPP/Ag samples was obtained in the first 4 h after stretching and inoculation with bacteria. Nevertheless, inhibition of bacteria growth could not be achieved for long incubation time. This is probably the consequence of a too low quantity of silver ions that released from samples. The surface area covered by cracks compared to the total area of fibers in a sample was estimated at 1%, which may reduce concentrations of Ag^+ released in liquid surroundings of a factor around 10^{-2} for stretched PP/Ar/MAPP/Ag/MAPP samples compared to PP/Ar/MAPP/Ag ones. Concentrations in silver ions of the bacterial suspensions in contact with PP/Ar/MAPP/Ag and PP/Ar/MAPP/Ag/MAPP samples are therefore estimated at 10^{-6} M and 10^{-8} M respectively. Hence, concentration obtained with stretched PP/Ar/MAPP/Ag/MAPP referred as “60%” on the **Figure 4-2**, may not be high enough to lead to bacteria growth inhibition on the contrary to those obtained with PP/Ar/MAPP/Ag substrate. Nevertheless, as shown by **Figure 4-4**, even concentration of silver ion as low as 3.0 µM has weak impact on short term of bacterial growth.

On the **Figure 4-4**, it is shown, that bacterial growth is inhibited even after 24 hours of incubation, with the presence of Ag ions in the medium at the concentration as low as 0.5 ppm. Considering this data, there is clear evidence of silver ions release from the coatings at very low concentration, which inhibit bacterial growth at 4 hours of bacterial culture and it is less pronounced at 168 h of bacterial culture due to not sufficient release to kill all bacteria, which proliferate further.

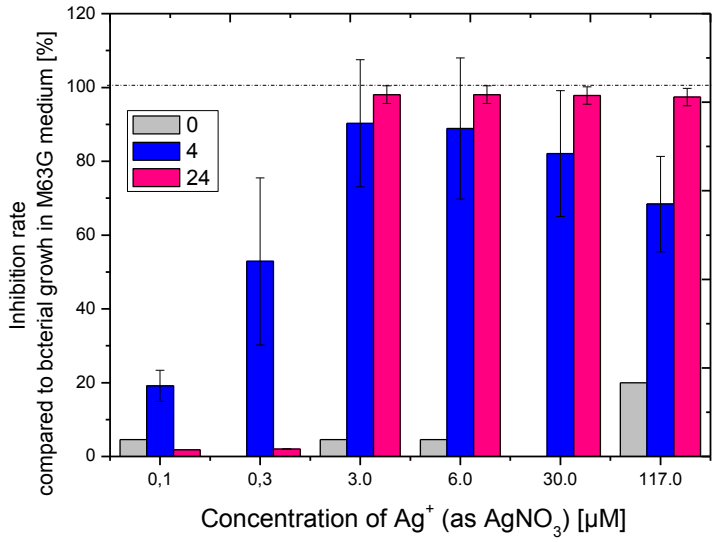

Figure 4-4: Inhibition rate of bacterial growth of *Escherichia coli* (PHL 628 [66]) in M63G-B1 medium with the presence of Ag ions (as $AgNO_3$). The legend shows the time of bacterial incubation in hours. Concentrations 0.1 µM, 0.3 µM, 3.0 µM, 6.0 µM, 30.0 µM, 117.0 µM are 0.02 ppm, 0.05 ppm, 0.5 ppm, 1 ppm, 5 ppm and 20 ppm respectively.

4.3.2 Effect on bacterial colonization of the substrates

We have quantified the number of adherent bacteria on the different surfaces in order to examine the bacterial adhesion, biofilm growth, biofilm structure and viability (i.e. permeability of the membrane) of the bacterial cells on PP, PP/Ar/MAPP(2^{nd}), PP/Ar/MAPP/Ag, PP/Ar/MAPP/Ag/MAPP and PP/Ar/MAPP/Ag/MAPP-60% substrates.

4.3.2.1 Bacterial colonization extent

4.3.2.1.1 Bacteria adhesion at 4h incubation time

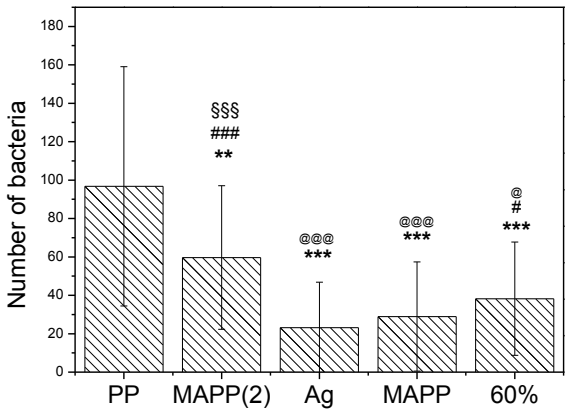

Figure 4-5: Number of bacteria on the surface of substrates recorded after 4 hours of incubation time. *, @, # and § symbols indicate significant differences to PP, PP/Ar/MAPP(2nd), PP/Ar/MAPP/Ag, PP/Ar/MAPP/Ag/MAPP respectively. Probability is noted with the number of symbols: 1 symbol for p>95.0%, 2 symbol for p>99.0%, 3 symbols for p>99.9%. Abbreviations MAPP(2), Ag, MAPP, 60% on the graph represent PP/Ar/MAPP(2nd), PP/Ar/MAPP/Ag, PP/Ar/MAPP/Ag/MAPP, 60% stretched PP/Ar/MAPP/Ag/MAPP samples respectively.

After 4 hours of bacterial incubation, in immersion and after neat rinsing, the bacterial adhesion was evaluated on PP and PP modified substrates (**Figure 4-5**). The most pronounced bacteria colonization was on PP samples (**Figure 4-5**). Less bacterial colonization on all the surfaces containing MAPP, especially the surface of PP/Ar/MAPP(2nd), compared to PP substrate can be explained by two types of features of this coating: first, the release of low molecular weight water soluble fractions of plasma polymer, which may influence the bacterial proliferation in planktonic state and, as well, of adhered bacteria, compared to PP samples (see **Figure 4-5**); second, by adhesion preventive properties of

plasma polymer layer which may due to hydrophilic character and charge of the coating surface. Hydrophilic/hydrophobic characters influence the structure of water in the region near to the surface. The structure is perturbed over distances of up to several tens of molecular layers. Near a hydrophobic surface such as the one of PP samples the water layer is less structured in terms of intermolecular hydrogen bonding between the water molecules, than near to hydrophilic surface. Then, bacterial adhesion is usually observed in higher extent on hydrophobic than on hydrophilic surfaces [448], even if opposite results are also observed [23, 134]. Surface charge was also shown to influence bacterial adhesion. Since bacteria in aqueous suspension are almost always negatively charged at physiological pH, negative charges on the surface can repel the bacteria, probably due to repulsive electrostatic interactions ([153, 449]), with strength depending on bacterial species, growth medium, pH and the ionic strength of the suspending buffer, bacterial age and bacterial surface structure [47, 450]. The high quantity of COO^- groups on PP/Ar/MAPP(2^{nd}) samples may therefore have resulted in the lower value of number of bacteria recorded on PP/Ar/MAPP(2^{nd}) samples, compared to PP sample. This is in agreement with previous studies conducted on maleic anhydride plasma polymer coatings with the same *E.coli* strain as used in the present study. Ploux *et al*. studied bacterial adhesion on micro/nanopatterned surfaces, prepared by pulsed plasma polymerization [148]. Bacteria were cultivated on polymers films and patterned polymer films. The result of their study showed that bacteria number increased with time on plasma polymerized films. However, after 14 h of incubation, bacteria number differed and was negatively correlated to surface coverage with negatively charged groups (carboxylic acid groups in this case).

In addition to the chemical modification of the surface induced by the coating, the smoothening of surface of polypropylene after deposition of plasma polymer one layer or multilayer system may also have influenced the bacterial adhesion from the topographical point of view. For example, bacteria well attach to

cavities, groove-like features, which correspond to their size, where they can be protected from shear forces [135]. This type of behavior was observed on the PP sample, where bacteria showed preference to adhere in groove-like features of the surface (see **Figure 4-6**). However, quantitative investigations of the modified surface roughness was not performed to support this hypothesis.

Numbers of bacteria on the substrates containing silver nanoparticles (PP/Ar/MAPP/Ag/MAPP, PP/Ar/MAPP/Ag/MAPP-60%) were found to be significantly lower (p>99.9%) than the number of bacteria on PP sample (see **Figure 4-5**). It was also found that bacteria number on all containing silver samples was significantly lower (p>99.9% in case of PP/Ar/MAPP/Ag and PP/Ar/MAPP/Ag/MAPP, p>99.0% in case of PP/Ar/MAPP/Ag/MAPP-60% sample p>95,5%) than on PP/Ar/MAPP(2^{nd}) sample (**Figure 4-5**). This is with agreement with the presence of silver nanoparticles as a reservoir for silver ion release from these samples, which have influenced the bacterial adhesion on silver containing samples after 4 hours of incubation time.

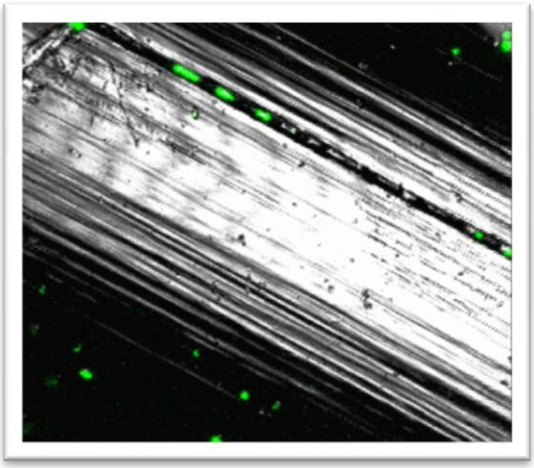

Figure 4-6: Bacteria adhesion on Polypropylene sample after 4 hours of incubation. The preferential places for bacterial (green) attachment are found in groove-like features on the surface sample and on the side of the fiber.

However, in contrast to expected due to the MAPP barrier effect, but in agreement with what was observed for planktonic bacteria, number of bacteria adhered on PP/Ar/MAPP/Ag and PP/Ar/MAPP/Ag/MAPP samples were not significantly different. As previously mentioned, the release of silver ions from the PP/Ar/MAPP/Ag/MAPP samples can vary (see **Figure 4-3**) from one to another sample due to incomplete barrier effect and/or presence of silver nanoparticles at the 2nd MAPP top layer. Here, PP/Ar/MAPP/Ag/MAPP samples with incomplete barrier effect and PP/Ar/MAPP/Ag/MAPP samples with efficient barrier effect were both taken into account, leading to an average of number of adhered bacteria at 4h similar to those observed on PP/Ar/MAPP/Ag samples.

Bacterial adhesion on samples that were subjected to stretching (**Figure 4-5**, 60%) was not significantly different from bacterial adhesion on unstretched plasma polymer multilayer system – PP/Ar/MAPP/Ag/MAPP. However, a trend can be observed, which reveals a slight increase in the number of attached bacteria on these substrates. Typical aperture of cracks formed under stretching in case of PP/Ar/MAPP/Ag/MAPP-60% is between 3 and 5 µm. Considering these topographical changes of the surface induced by stretching, bacterial adhesion may be considered to increase as well. As previously mentioned, the size and orientation of topographical features can influence the retention of cells on the surfaces [23, 134, 135]. The greatest bacterial cell retention is usually found to occur on the materials with size of features value close to the bacterial size [140, 143, 451, 452]. In our study, at 4h of incubation, some bacteria that adhered on PP/Ar/MAPP/Ag/MAPP-60% stretched samples are in this situation. Therefore, stretching at 60% rate of initial length of the coated PP may not provide the expected increase of bacterial colonization inhibition, compared to unstretched samples. Nevertheless, the number of bacteria on stretched samples remains lower than bacteria numbers on substrates without silver (PP and PP/Ar/MAPP substrates). As discussed in this section and in section 2.4.5, significant increase of the polymer overlayer crosslinking could allow to

enhance the contrast between the efficiencies of stretched and unstretched materials. On the other hand, the quantity of Ag^+ released from the coating could also be increased to reach better antibacterial efficiency of the stretched materials. For this purpose, the Ag reservoir formed by AgNPs enclosed in plasma polymer should be increased.

Results of bacterial adhesion study after 4h of culture time are in accordance with the planktonic bacteria proliferation study at 4h of incubation time (**Figure 4-2** and **Figure 4-5**). Inhibition of bacterial proliferation and decrease of bacterial adhesion on the surface was observed for PP/Ar/MAPP(2^{nd}) substrates compared to PP substrates. Significant decrease in adhesion of bacterial cells on surfaces containing silver also correlates with the inhibition rate of bacterial proliferation of planktonic bacteria for the same substrates. Antibacterial effect of those substrates toward planktonic and adhered bacteria comes from silver ion release. It can be caused by retard of the nutrient uptake of cells or nutrient utilization efficiency [453]. It was also recently showed that antimicrobial substrates can prevent the division of cells [453].

4.3.2.1.2 Biofilm development after 168 h of incubation

Biofilm development was observed after 168 hours of incubation on PP mesh and modified PP mesh substrates and further analyzed and quantified with Comstat 2 [70, 71]. Biofilm quantity is expressed as total biomass.

Some examples of biofilm development on polypropylene and polypropylene modified substrates visualized using confocal microscopy are shown on **Figure 4-7**. Total biomass values calculated from confocal images are shown in **Figure 4-8**. Total biomass measured for PP/Ar/MAPP(2^{nd}) sample was found to be significantly lower ($p>99.0\%$) than the total biomass measured on PP, in agreement with the results observed at 4h, which was hypothesized to result from low molecular fractions from the polymer and/or the chemical properties of

the coating. Inhibition of bacterial biofilm development was the most pronounced on PP/Ar/MAPP/Ag sample. This result is an evidence of the efficiency of the low quantity of silver ions release from the sample without the second polymer overlayer, on biofilm growth inhibition (**Figure 4-8**) as observed for the cultivation time of 4h (see **Figure 4-5**). The difference between PP/Ar/MAPP/Ag and PP/Ar/MAPP/Ag/MAPP samples after 168 h of incubation is found to be significantly different with p>99.9%. This result suggests that barrier effect of plasma polymer overlayer, which was not pronounced at 4h, is playing a role for longer incubation time. For bacteria in planktonic state also, the barrier effect of PP/Ar/MAPP/Ag/MAPP sample was found to have a significant efficiency at 168 h, while it was inefficient at 4h to block the antibacterial inhibition effect of Ag^+ released from the coating. A slightly significantly higher colonization was observed on PP/Ar/MAPP/Ag/MAPP than on PP/Ar/MAPP(2^{nd}), which may be attributed to the presence of silver in PP/Ar/MAPP/Ag/MAPP samples. Ag^+ released from the unstretched material resulted in a significant decrease of the colonization at 4h, due to the antibacterial effect of Ag^+. In contrast, this weak quantity of Ag^+ may have been too low to lead to antibacterial effect at 168h, but may have stimulate the growth of biofilm as a protection environment for bacteria [454, 455].

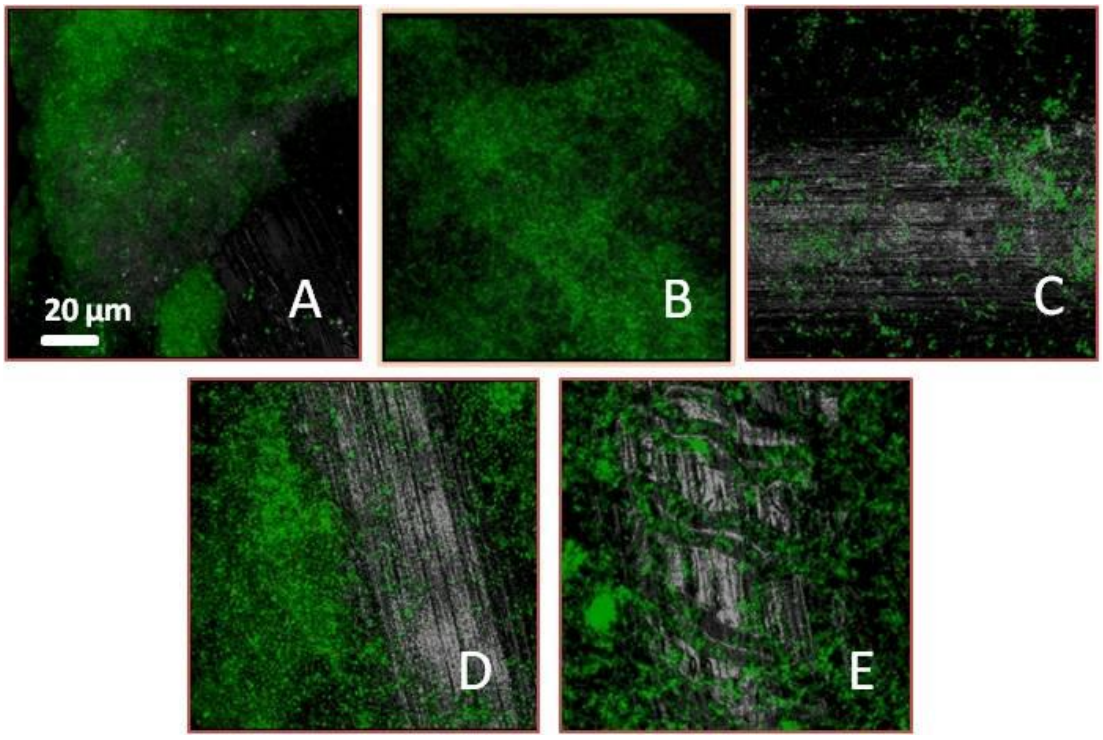

Figure 4-7: Confocal 3D images (50x magnification), transformed to 2D using ZEN software, representing biofilm development of *Escherichia coli* after 168 hours of incubation on **A)** polypropylene **B)** polypropylene with only second plasma polymer deposited layer, PP/Ar/MAPP(2^{nd}) **C)** polypropylene with plasma deposited layer with loaded silver nanoparticles, PP/Ar/MAPP/Ag **D)** plasma multilayer system deposited on polypropylene substrate, PP/Ar/MAPP/Ag/MAPP **E)** plasma multilayer system on PP mesh under stretching with elongation 60%, PP/Ar/MAPP/Ag/MAPP-60%.

In case of longer time of incubation (168 h) the difference of biomass values between PP/Ar/MAPP/Ag/MAPP and PP/Ar/MAPP/Ag/MAPP-60% was significant (p>99.0%) in contrast to 4 h incubation time. The increase in inhibition of biofilm development in PP/Ar/MAPP/Ag/MAPP-60% stretched materials is attributed to the presence of cracks, which facilitates the release of silver ions and leads therefore to increase the concentration of Ag^+ in contact with sessile bacteria. However, colonization on stretched samples remains in similar extend to on PP/Ar/MAPP(2^{nd}). This shows that the efficiency of the

plasma multilayer system under stretching is not sufficient to completely inhibit bacterial biofilm development (**Figure 4-8**). Even for samples in which silver nanoparticles are loaded in the first plasma polymer layer without any additional layer on the top, bacteria are able to adhere in moderate quantity and biofilm can develop. This suggests that the quantity of loaded silver nanoparticles which are the reservoir for released silver ions is not sufficient to inhibit biofilm development even on PP/Ar/MAPP/Ag sample for this time of incubation (**Figure 4-8**). Parameters that can be modified to increase the bacterial killing of this system is the quantity of AgNPs which serves as a reservoir, as well as the size distribution, which is an important issue to optimize surface to volume ratio of AgNPs and therefore available surface for oxidation for subsequent Ag^+ release. The quantity of silver in the plasma polymer layer can also be modified by changing the thickness of plasma polymer. In this way, the efficiency of the system could be modulated.

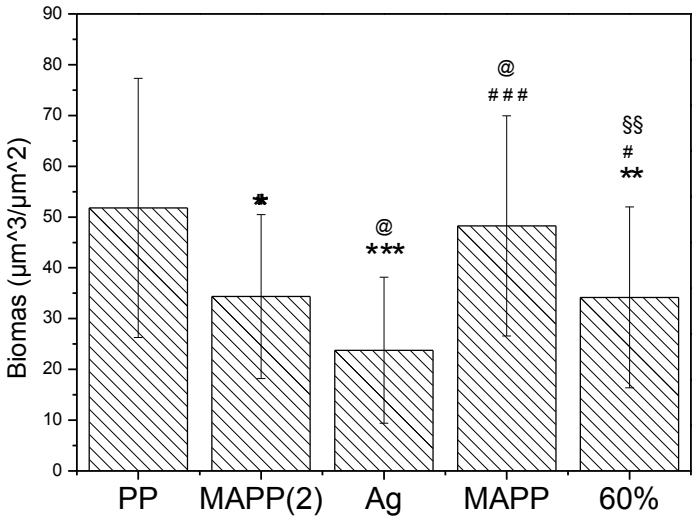

Figure 4-8: Total biomass value calculated from the CLSM images using Comstat 2 software. *, @, # and § symbols indicate significant differences to PP, PP/Ar/MAPP(2nd), PP/Ar/MAPP/Ag, PP/Ar/MAPP/Ag/MAPP respectively. Probability is noted with the number of symbols: 1 symbol for p>95.0%, 2 symbol for p>99,0%, 3 symbols for p>99,9%. Abbreviations MAPP(2), Ag, MAPP, 60% on the graph represent PP/Ar/MAPP(2nd), PP/Ar/MAPP/Ag, PP/Ar/MAPP/Ag/MAPP, stretched PP/Ar/MAPP/Ag/MAPP samples respectively.

4.3.2.2 Bacterial membrane integrity and biofilm structure

4.3.2.2.1 Viability of bacteria adhered after 4h of incubation

"Viability" of bacteria adhered after 4h of incubation was monitored as a function of the cell membrane integrity. Measurements of viability provide an indicator of the physiological state of individual bacteria in mono-culture or in consortia with low numbers of species. Cells with a compromised membrane, that are considered to be dead or with depleted "viability" are stained red, whereas cells with an intact (non-compromised) membrane are stain green

[439]. Further in the text, terms “compromised” and “non-compromised” membrane are used together with viability term, indicating the state of bacterial membrane.

Figure 4-9 shows the viability of bacteria adherent on the polypropylene and polypropylene modified substrates. In all of the cases, the viability of bacterial cells is above 50%. The viability on PP/Ar/MAPP/Ag/MAPP samples is considered “normal”. It was already shown in literature that ~80% of viability can be found for control samples. For example, in the work of Terada *et al.* [456], the bacterial viability on surfaces containing amino groups was found between 70-90%. In the work of Kostenko *et al*. [457] who studied silver-containing dressings on bacterial biofilm viability, the value of bacterial viability observed after 24h was found between 2.6% and 99.8%, depending on the type of bacteria and material used. In our study, viability on the silicon wafer placed during experiment at the bottom of the Petri dish, was also of about 80%. Thus, in this study, 80% viability is considered as a reference for further discussion.

The lowest viability was observed for the bacteria adhered on PP surface. However, the highest number of bacteria was observed for the same surface. This suggests that here, bacterial membrane changes may not be an indication of viability but rather the result of a more advanced step for the formation of biofilm. Adherent bacteria adapt to the biofilm phenotype. They change their sensitivity to the environment and their activity (integrity of membrane for better uptake of nutrient and oxygen) by adjusting the gene expression pattern when they are included in a biofilm [458]. In particular, it was already shown that a part of the bacteria of a biofilm have membranes allowing bacterial staining by propidium iodide, the molecule used for indicating compromised membranes [390, 439, 459]. Therefore, the highest bacterial adhesion but highest permeability of the bacterial membrane on PP surfaces compared to MAPP-covered surfaces may suggest that biofilm formation is in a more advanced stage.

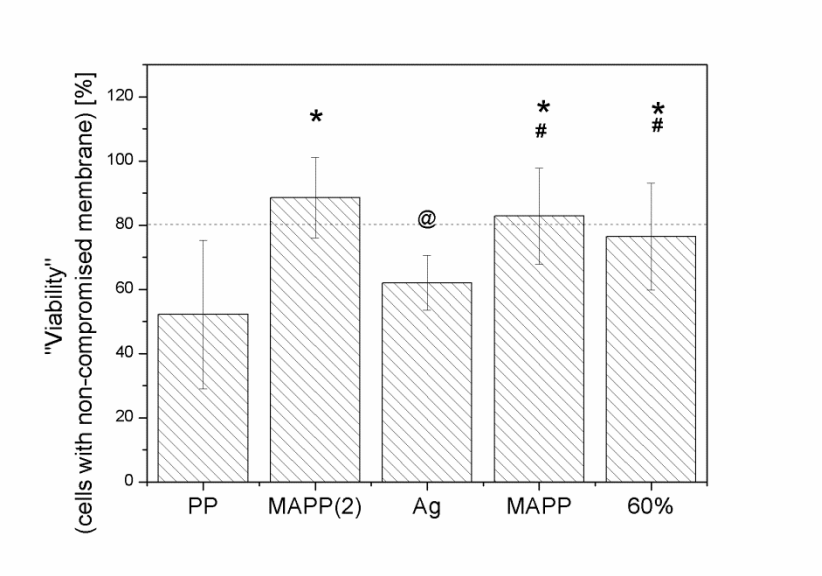

Figure 4-9: "Viability" of bacteria on the surface of substrates after 4 hours of incubation time. *,@,# and § symbols indicate significant differences (probability p> minimum 95,0%) to PP, PP/Ar/MAPP(2nd), PP/Ar/MAPP/Ag, PP/Ar/MAPP/Ag/MAPP respectively. Abbreviations MAPP(2), Ag, MAPP, 60% on the graph represent PP/Ar/MAPP(2nd), PP/Ar/MAPP/Ag, PP/Ar/MAPP/Ag/MAPP, stretched PP/Ar/MAPP/Ag/MAPP samples respectively.

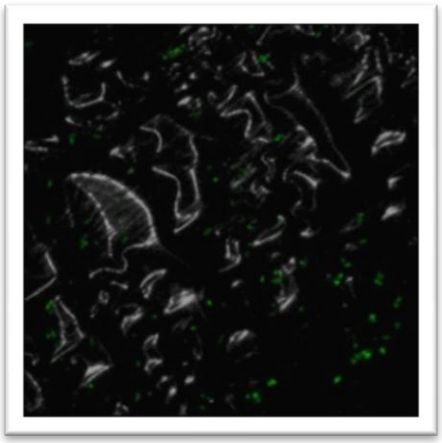

Figure 4-10: Bacterial adhesion on PP/Ar/MAPP(2nd) substrate after 4h of incubation. Surface irregularities are the results of swelling properties of plasma polymer.

A lower viability was observed on PP/Ar/MAPP/Ag compared to PP/Ar/MAPP(2^{nd}) (**Figure 4-9**). This trend is due to the release of a sufficient amount of Ag^+ to damage the bacterial membranes (increase their permeability) [237]. Higher apparent "viability" on PP/Ar/MAPP/Ag/MAPP-60%, stretched materials is probably due to the insufficient quantity of released Ag^+ associated to a greater rigidity of the membrane in response to the contact with toxic compounds. Such decrease of the membrane fluidity has already been reported as the result of a toxic environment [460].

4.3.2.2.2 Biofilm structure and membrane integrity of the bacteria in biofilms

Connected-biomass was measured using Comstat 2 and the "Connected Volume Filtering" parameter coupled to the biomass calculations, providing indications about the structure of the biofilm. Additionally, the biomass stained by Syto®9 and Propidium Iodide of Live/Dead® staining, revealed two significantly different physiological states in the biofilm.

4.3.2.2.2.1 General structure of biofilms

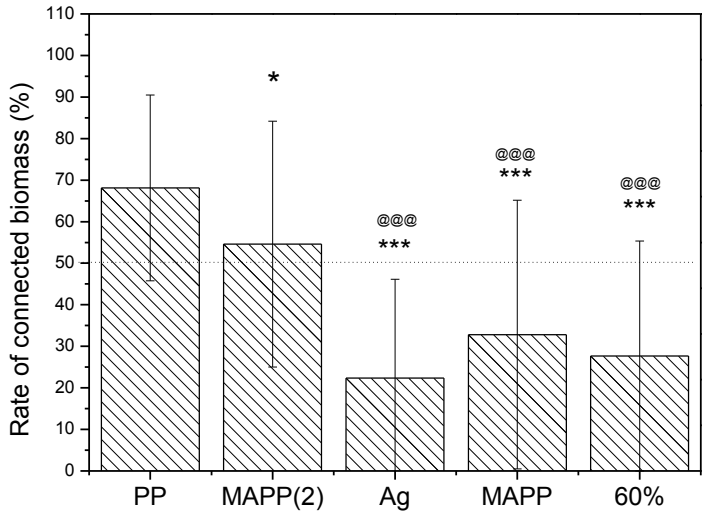

Figure 4-11: Rate of connected biomass calculated using Comstat2 software. *,@,# and § symbols indicate significant differences to PP, PP/Ar/MAPP(2nd), PP/Ar/MAPP/Ag, PP/Ar/MAPP/Ag/MAPP respectively. Probability is noted with the number of symbols: 1 symbol for p>95,0%, 2 symbol for p>99,0%, 3 symbols for p>99,9%. Abbreviations MAPP(2), Ag, MAPP, 60% on the graph represent PP/Ar/MAPP(2nd), PP/Ar/MAPP/Ag, PP/Ar/MAPP/Ag/MAPP, stretched PP/Ar/MAPP/Ag/MAPP samples respectively.

The rate of connected biomass for polypropylene and polypropylene modified substrates, corresponding to the ratio between connected and total biomass, is shown on **Figure 4-11**. Using this approach, it is possible to distinguish if biofilm is in the form of one connected biofilm or in form of colonies or bacteria not connected one to another (**Figure 4-12**).

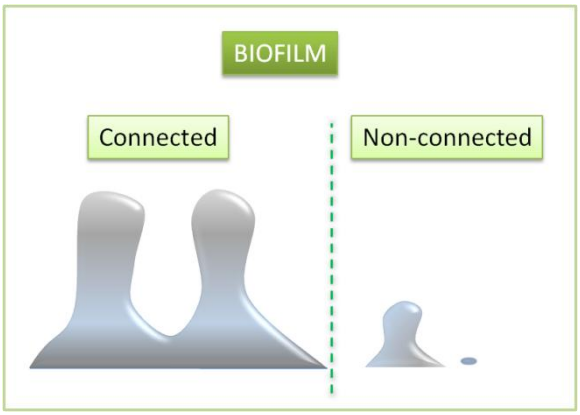

Figure 4-12: Schematic representation of "connected" biofilm and “non-connected” bacteria or colonies. Green and red colors represent alive bacteria and bacteria with compromised membrane respectively.

Results of the study on connected and non-connected bacterial population can be divided into two groups. In the first group, the rate of connected biomass value is above 50% (**Figure 4-11**). PP and PP/Ar/MAPP(2nd) substrates are in this group. Second group includes PP/Ar/MAPP/Ag, PP/Ar/MAPP/Ag/MAPP and PP/Ar/MAPP/Ag/MAPP-60% substrates and the rate of connected biomass value in this group is between 20% and 40%. These results show that the silver ions released from the substrates have significantly influenced the biofilm structure.

More specifically, biofilm in form of “connected” colonies was mainly found on PP substrates. On the average, only ~30% of biomass was considered not-connected. In case of biofilms developed on PP/Ar/MAPP(2nd) substrates, this value increased to 46%. The difference between biofilm structures observed on both substrates confirms that biofilms are more developed on PP than on PP/Ar/MAPP(2nd), in agreement with the hypothesis of a more advanced biofilm formation on PP than on the other substrates. In the case of the samples containing silver nanoparticles, rate of connected biomass was significantly lower than values measured for PP and PP/Ar/MAPP(2nd) substrates. These

results indicate that even low concentration (1.5-6.0 ppm - 8,8- 35,3 µM) of released silver ions can influence the biofilm development. This shows in addition that the bacterial susceptibility to slightly toxic conditions can be highlighted when biofilm structure is investigated (**Figure 4-11**). This specific impact of low quantity of silver ions on the biofilm structure is here demonstrated for the first time. Consequences for treating biofilms may be important since “unconnected” parts of biofilm may be more accessible to antibiotics or other biocides administrated by the classical systemic way. Sommerfeld *et al*. [390] observed that unconnected bacteria populations were more susceptible to antibiotics. Since they are less encased within the biofilm, but they may be mobile and may be therefore able to recolonize elsewhere. Susceptibility of bacteria in smaller population was also showed by Moronez-Ramirez *et al.* [237]. They showed that bacteria in the form of smaller populations, can be more susceptible to additional antibacterial treatment. Their study revealed that silver enhances antibiotic activity against gram negative bacteria. They have used lethal (10 ppm; 60 µM) and sublethal (5 ppm; 30µM) concentrations of Ag^+ to demonstrate that Ag^+ can potentiate the activity of broad range of antibiotics against gram-negative bacteria in distinct metabolic states. The synergistic effect between Ag^+ and the different antibiotics was achieved by adding 2.5 ppm (15 µM) and 5 ppm (30 µM) of Ag^+ (as $AgNO_3$) for cells metabolically active and dormant cells, respectively [237]. Our results suggest that the synergistic effect is principally due to the “structuration” of the biofilm resulting from the Ag^+ treatment.

4.3.2.2.2.1 Membrane of the bacteria in biofilms

For 168 hours of bacterial culture, the state of bacterial membrane was investigated for both bacteria populations in connected biofilms and in non-connected populations.

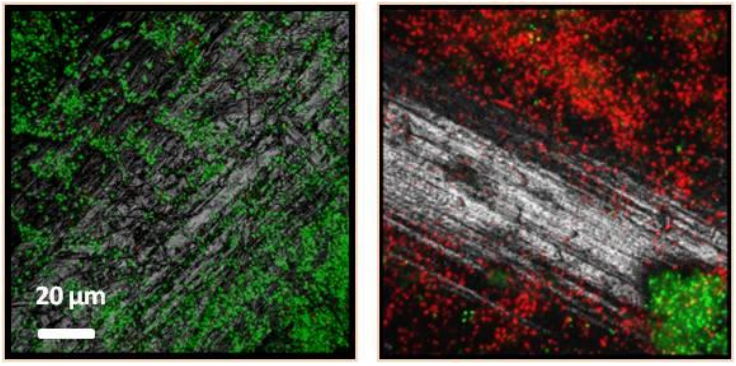

Figure 4-13: Two examples of confocal 3D images (50x magnification), transformed to 2D using ZEN software, representing biofilm development of *Escherichia coli* after 168 hours of incubation on polypropylene (PP) sample. Left and right images show respectively that there are places where majority of bacteria are alive (green color) or have compromised membrane.

An example which shows the variety of situations on one sample (majority of bacteria with non-compromised or, in contrast, compromised membrane state- left and right respectively) is shown on **Figure 4-13**. Using Comstat 2 software, biomass values corresponding to “green” and “red” bacteria in respective populations (connected biofilm, non connected populations) was calculated. Results are shown as a “rate of bacteria with compromised membrane” in a connected biofilm and non-connected populations (**Figure 4-14**).

In general, state of bacteria with compromised membranes are similar on all the substrates (between ~50% and 65% for non-connected biofilms and between ~30% and ~40% for connected biofilms) except on the PP/Ar/MAPP/Ag substrate (~50% for both connected and non-connected biofilms).

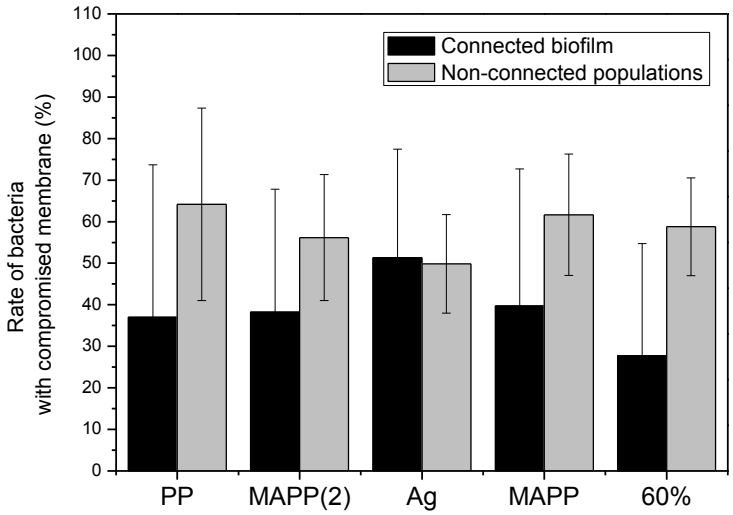

Figure 4-14: Rate of bacteria with compromised membrane in connected biofilm and non-connected colonies after 168 h of incubation. Abbreviations MAPP(2), Ag, MAPP, 60% on the graph represent PP/Ar/MAPP(2^{nd}), PP/Ar/MAPP/Ag, PP/Ar/MAPP/Ag/MAPP, stretched PP/Ar/MAPP/Ag/MAPP samples respectively.

To understand these results, it must be considered that, in the case of biofilms, red staining of bacteria with Live/Dead® mixture is the result of increase of membrane permeability due to the balance of different effects: 1) the fluidity of the membrane, which allows permeability, decreases to prevent entrance of toxic agent i.e., here Ag^+, and then to protect bacteria from biocide effect. This protection may be further enhanced by the specific biofilm-related conditions of life. Especially starvation, due to nutrient limitation in micro-environments of the biofilm, has been shown to increase antibiotic tolerance [51]; 2) the membrane is compromised by the incorporation of Ag^+ ions, leading to increase in the membrane permeability [237]; 3) the specific physiology of the bacteria in biofilms can modify the membrane fluidity.

It was shown that in the depths of a biofilm, bacteria showed similarities to stationary-phase planktonic cells [51]. Both are affected by nutrient limitation and high cell densities, which result in an accumulation of metabolic waste products and/or extracellular signaling molecules [51]. Therefore, bacteria in high-density biofilms are differentiated from low-density cultures which results for example in different antibiotic tolerance. Population density is a factor which determines bacterial physiology. For example, in *rhizobium*, more cells survived stationary phase if starved at high density [461]. In *E.coli*, high-density ($6x10^8$ bacteria/ml) cultures expressed stationary-phase characteristics and reduced outer membrane permeability while going through the exponential phase of growth [459].

In the present study, therefore, differences in biomass (**Figure 4-8**) measured for each type of the samples indicate that cell densities are different allowing to expect associated differences in the bacterial membrane permeability. However, the other factors may counter-balance this effect due to the opposite influences on membrane permeability. Therefore, the reasons of weak differences between biofilms formed on the different substrates cannot be elucidated. Hence, the bacterial susceptibility may vary, which results also in differences in the permeability of the bacterial membrane.

Only, the rates of bacteria with compromised membrane in connected and non-connected biofilms for samples with silver nanoparticles without second plasma polymer overlayer (PP/Ar/MAPP/Ag) follow a significantly different trend as on the other substrates. In this case, the rate of bacteria with compromised membrane in connected biofilm has very similar value to the one in non-connected colonies (**Figure 4-14**). This is in agreement with the faster release of silver ions (already after 30 min of sample immersion Ag^+ is detected; section 2.4.5; **Figure 2-10** compared with the other silver containing coatings). The bacterial metabolism is then similarly influenced if bacteria are in biofilms as if they are in smaller colonies. This is probably the result from the size of the

bacterial colonies composing the connected part of the biofilm, since, in the presence of silver ions, bacteria have difficulty to form biofilm structures. As discussed previously, this is due to the growth delay which probably involves both short-term cell killing [445] and inhibition of the biofilm development.

4.3.2.2.2.2 Relation between biofilm structure and bacterial membrane integrity in biofilms

To better understand the differences in biofilm structure on the various modified substrates, two additional parameters were calculated for bacteria with non-compromised and compromised membrane living in the connected biofilms: (i) the “surface to biovolume ratio” (S/V). It reflects the fraction of the biofilm which is exposed to the surrounding (potentially nutrient, toxic, etc.) medium. It gives indications about the shape of the biofilm outer surface and may also indicate how the biofilm adapts to the environment (e.g., in environments of low nutrient concentration, the surface to volume ratio may increase in order to optimize access to the limited supply of nutrients [438]); (ii) the “average diffusion distance”. It is the distance from living cell to the “void”, that potentially contains nutrients, oxygen etc. The average diffusion distance gives therefore indications about compactness of the biofilm structure. In this study, “red” and “green” bacteria and or biofilm parts have been distinguished. The average diffusion distance of red part (ADD_R) is therefore the distance to void or green parts, while the average diffusion distance of green part (ADD_G) is the distance to void or red parts.

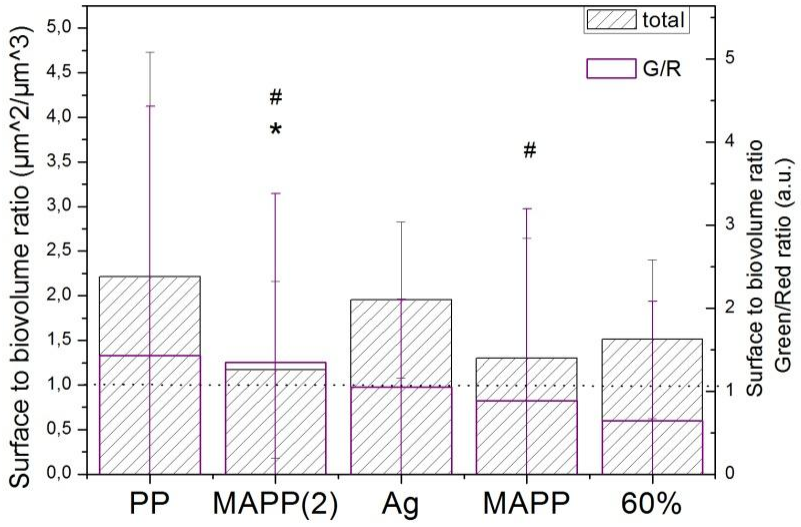

Figure 4-15: Surface to biovolume ratio for total and green to red ratio in biofilm. G/R represents ratio of bacteria with non-compromised membrane to bacteria with compromised membrane. Abbreviations MAPP(2), Ag, MAPP, 60% on the graph represent PP/Ar/MAPP(2nd), PP/Ar/MAPP/Ag, PP/Ar/MAPP/Ag/MAPP, stretched PP/Ar/MAPP/Ag/MAPP samples respectively. *, # symbols indicate significant differences (probability p> 95,0%) to PP, Ag respectively.

The highest surface to biovolume ratio was found for biofilms developed on PP and PP/Ar/MAPP/Ag substrates. For PP, this indicates a highly rough outer surface of the thick biofilm, while it corresponds to the apparent roughness of the destructed (i.e., non-connected) biofilm for PP/Ar/MAPP/Ag. For the three other substrates, the surface to volume ratio around 1 indicates almost smooth outer surface of the biofilms. However, the slightly rougher surface for PP/Ar/MAPP/Ag/MAPP-60% is probably due to more non-connected structure of the biofilm (**Figure 4-15**).

The so-called G/R ratio was also calculated. It represents the surface to biovolume ratio of bacteria with non-compromised membrane and compared to

those of bacteria with compromised membrane. This G/R ratio gives indication about the distribution of both types of bacteria (i.e., with non-compromised and compromised membrane) inside the biofilms. If G/R parameter is close to 1, then surface to biovolume ratio (in other words “specific surface”) of bacteria with compromised and non-compromised membrane are similar. If G/R is below 1, the “specific surface” of the bacteria with compromised membrane is higher than for the one with non-compromised membrane. For example, bacteria with compromised membrane may be inside a smooth biofilm as small clusters or as separate cells in the biofilm matrix, increasing in this way the specific surface of the red part of the biofilm. For PP and PP/Ar/MAPP(2^{nd}), the value was superior to 1 probably due to a rough outer surface of the biofilm (less rough for PP/Ar/MAPP(2^{nd}) than for PP) with a smoother outer surface of the red biofilm part. For the samples containing AgNPs, the G/R value is equal 1 in case of PP/Ar/MAPP/Ag sample and below 1 in case of PP/Ar/MAPP/Ag/MAPP and PP/Ar/MAPP/Ag/MAPP-60%. For PP/Ar/MAPP/Ag sample, this indicates that parts of biomass with compromised membrane and non-compromised membrane respectively have similar “specific surfaces”, This suggests that “red” biomass is distributed uniformly, intimately mixed with the “green” bacteria. All together, they form small clusters of bacteria. In case of biofilms developed on PP/Ar/MAPP/Ag/MAPP and PP/Ar/MAPP/Ag/MAPP-60%, “red” biomass has higher “specific surface” than “green” biomass, suggesting multiple clusters of “red” biomass distributed uniformly in a “green” biofilm matrix.

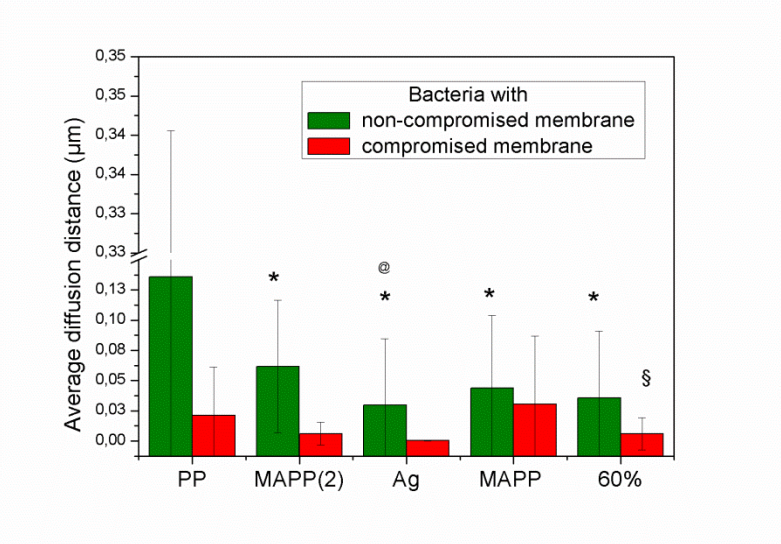

Figure 4-16: Average diffusion distance calculated for bacteria with non-compromised membrane (green on the graph) and for bacteria with compromised cell membrane (red on the graph). Values are calculated for the biofilms after 168 hours of incubation. Abbreviations MAPP(2), Ag, MAPP, 60% on the graph represent PP/Ar/MAPP(2^{nd}), PP/Ar/MAPP/Ag, PP/Ar/MAPP/Ag/MAPP, stretched PP/Ar/MAPP/Ag/MAPP-60% samples respectively. *, @, § symbols indicate significant differences (probability p> 95.0%) to PP, MAPP(2) and MAPP respectively.

Average diffusion distance of "green" biomass (ADD_G) is the average of diffusion distances among biomass pixels. The highest value of this parameter is observed for biofilm developed on PP substrates. Average diffusion distance of "green" biomass in this case is significantly different from the same parameter calculated for all other samples. ADD_G for PP/Ar/MAPP/Ag sample has the lowest value and is significantly different from PP and PP/Ar/MAPP(2^{nd}). ADD_G parameter calculated for other substrates shows slight tendency following the order from the higher value: PP/Ar/MAPP(2^{nd})>PP/Ar/MAPP/Ag/MAPP> PP/Ar/MAPP/Ag/MAPP-60%.

In case of ADD_G calculated for PP substrates, results show that biofilm developed on this substrate is the thickest, which is in agreement with the

highest biomass. For PP/Ar/MAPP/Ag, biofilm is the least thick, which agrees with the least biomass and the antibacterial action of Ag^+ released from the substrate in an efficient concentration. Tendency observed for ADD_G parameter which follow the order (from the highest to the lowest): PP/Ar/MAPP(2^{nd})> PP/Ar/MAPP/Ag/MAPP > PP/Ar/MAPP/Ag/MAPP-60% are also in agreement with the measured biomasses and it suggests that variations in the thicknesses of biofilms follow variations in Ag^+ releasing.

Average diffusion distance of "red" bacteria (ADD_R) parameter calculated for biofilms shows the following tendency (from the highest to the lowest): PP/Ar/MAPP/Ag/MAPP > PP > PP/Ar/MAPP(2^{nd}) > PP/Ar/MAPP/Ag/MAPP-60% > PP/Ar/MAPP/Ag. Significant difference between ADD_R calculated for PP/Ar/MAPP/Ag/MAPP and PP/Ar/MAPP/Ag/MAPP-60% is observed. These results are in agreement with "red" biomass in form of big clusters for PP/Ar/MAPP/Ag/MAPP and PP samples. On PP/Ar/MAPP(2^{nd}), PP/Ar/MAPP/Ag and PP/Ar/MAPP/Ag/MAPP-60% substrates, red biomass have lower thickness compared to PP and PP/Ar/MAPP/Ag/MAPP suggesting flat or small clusters of "red" biomasses or even single bacteria.

Finally, results of ADD_G show that, in the presence of Ag^+, bacteria have difficulties to build thick complex structures. At the same time, the release of Ag^+ from PP/Ar/MAPP/Ag and PP/Ar/MAPP/Ag/MAPP-60% samples leads to the smallest "red" bacteria clusters and/or even single cells, present in large number in the biofilms developed on these substrates.

4.3.2.2.2.3Summary

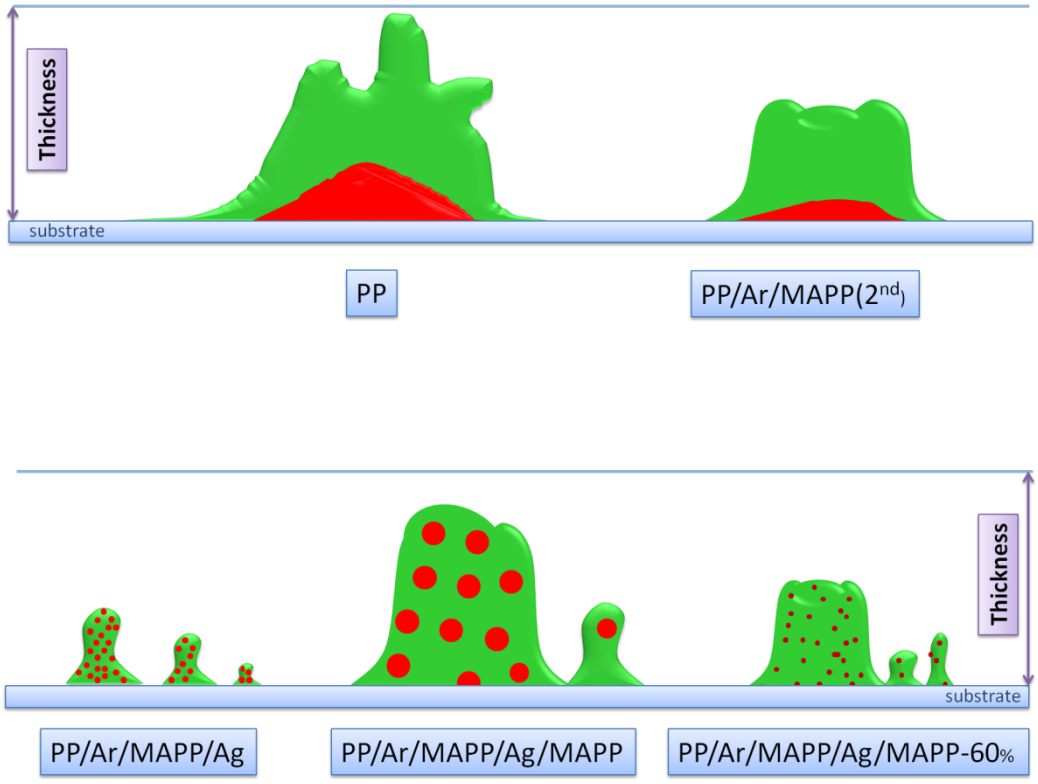

Figure 4-17: Schematic representation of the biofilm structure on PP and PP/Ar/MAPP/Ag samples. Green color represents bacteria with non-compromised membrane. Red color represents bacteria with compromised membrane. Connected and non-connected biomasses are also represented as separated from the biofilm colonies.

On the **Figure 4-17** simplified representations of bacterial biofilm structures are presented in regards to results obtained for biomass (**Figure 4-8**), rate of connected biomass (**Figure 4-11**), surface to biovolume ratio (**Figure 4-15**), rate of bacteria with compromised membrane (**Figure 4-15**) and average diffusion distance value (**Figure 4-16**).

Characteristics of the biofilms on the basis of four calculated parameters such as “connected” biomass, thickness of biofilm, surface to biovolume ratio, which

gives the indication about roughness of outer surface of biofilm, G/R and ADD is sum up below in **Table 4-3**. The thickness of biofilm is deducted from total biomass (shown in **Figure 4-8**) which is expressed in $\frac{\mu m^3}{\mu m^2}$. Between the brackets, values of the parameter which confirm the given hypothesis are written.

	Biofilm characteristics			
	"Connected" Biomass [%]	Thickness	Outer surface of the biofilm	"Red biomass"
PP	>50%	~ 50 µm and the high value of ADDG parameter	Rough (*high value of S/V total ~ 2*)	High value of "red" parts of biofilm due to biofilm maturity. "Red" biomass in close proximity, as cohesive clusters *(G/R > 1)*
PP/Ar/MAPP(2^{nd})	>50%	~30 - 35 µm and ADD_R ~ ½ ADD_R of PP)	Smooth (*S/V total ~ 1*)	High value of "red" parts of biofilm due to biofilm maturity *(~ 40%)*. "Red" biomass in close proximity (*G/R >1*), as homogenous, thick and connected part form *(ADD_R ~ 0)*
PP/Ar/MAPP/Ag	~ 20 - 25%	~20 µm and ADD_G = ¼ ADD_G of PP	Rough (*S/V > 1*)	High value of "red" biomass (~ 50 - 55%), due to sufficient concentration of Ag^+. Red biomass in the form of small clusters or single bacteria, uniformly distributed together with "green" parts *(ADD_R ~ 0)*
PP/Ar/MAPP/Ag/MAPP	~30%	~ 50 µm	Smooth *(S/V total ~1)*	"Red" biomass present in the form of big clusters (S/V red ≥ S/V green, G/R ~ 1; ADDR ~ ADDG)
PP/Ar/MAPP/Ag/MAPP-60%	~25%	~30 µm	Higher roughness of the outer surface than in case PP/Ar/MAPP/Ag/MAPP (*S/V ~1.5*)	"Red" biomass in the form of small clusters or single bacteria in the biofilm *(S/V red > S/V green, G/R > 1; ADD_R ~ 0)*.

Table 4-3: Characteristics of the biofilms

4.4 Conclusions

For short time of bacterial culture (4h), plasma modified substrates (PP/Ar/MAPP/Ag/MAPP and PP/Ar/MAPP/Ag) showed antibacterial properties, inhibiting between 90% and 100% of bacterial growth. Small antibacterial effect was also observed for substrate with only second plasma polymer (PP/Ar/MAPP(2^{nd})). For long time of bacterial culture (168 h), high antibacterial effect was preserved in case of PP/Ar/MAPP/Ag substrate. For complete plasma polymer modified system, antibacterial effect decreased to ~40% due to barrier effect of the plasma polymer second layer. The antibacterial efficiency of the PP/Ar/MAPP/Ag/MAPP-60% against planktonic bacteria could be only demonstrated for 4h of bacterial culture.

Bacterial adhesion tested after 4h of bacterial culture showed antibacterial effect of PP/Ar/MAPP/Ag and PP/Ar/MAPP/Ag/MAPP substrates. Comparing to PP surface, lower number of bacteria was also observed for PP/Ar/MAPP(2^{nd}) substrates due to different chemistry of the surface for this substrate. Study of bacterial membrane integrity after 4h of bacterial culture also showed lower “viability” of bacteria which adhered on the substrates containing silver nanoparticles (PP/Ar/MAPP/Ag and PP/Ar/MAPP/Ag/MAPP) comparing to the ones adhered on the substrate without AgNPs (PP/Ar/MAPP(2^{nd})).

At longer culture time (168h), total biomass measurements revealed significantly lower bacterial retention on PP/Ar/MAPP/Ag compared to PP substrates, due to released silver ions which inhibit bacterial growth. Similarly to the antibacterial effect on planktonic bacteria, in case of PP/Ar/MAPP/Ag/MAPP sample, bacterial growth was only slightly inhibited due to the barrier effect of the plasma polymer second layer.

More detailed study of the biofilm structure revealed differences in biofilms developed on PP, PP/Ar/MAPP(2^{nd}), PP/Ar/MAPP/Ag and

PP/Ar/MAPP/Ag/MAPP substrates. On the substrates containing AgNPs, biofilms have less cohesive structures probably due to the presence of silver ions. Quantity of bacteria with compromised membrane in the biofilm is the highest in case of sample PP/Ar/MAPP/Ag sample, which is related to the fast release of silver ions that disturb bacteria to build complex biofilm matrix. Calculations of surface to biovolume ratio, G/R parameter and average diffusion distance revealed the distribution of “green” and “red” biomass inside the biofilm matrix for the biofilms on each type of substrates. Due to presence of Ag+, contribution and distribution of bacteria with compromised membrane changes. “Red” bacteria form small clusters inside the biofilm.

Finally, antibacterial efficiency of the system under stretching (PP/Ar/MAPP/Ag/MAPP-60%) is also superior to the efficiency of PP/Ar/MAPP/Ag/MAPP after 168h of culture time. Biomass value for stretched samples after 168 h of culture is significantly lower than biomass measured for PP/Ar/MAPP/Ag/MAPP samples. Study of the biofilm structure on PP/Ar/MAPP/Ag/MAPP-60% compared to PP/Ar/MAPP/Ag/MAPP also indicates that:

- Biofilm presents a non-well-cohesive structure i.e., small clusters of bacteria (lower value of “connected biomass” with higher value of S/V total parameter) at 168 h of culture
- Bacteria with compromised membrane are in the form of small clusters or single cells (ADD_R), spread between bacteria with “non-compromised” membrane (G/R) at 168 h of culture

5 General conclusion and Perspectives

The objective of this work was to develop a new antibacterial mechanoresponsive coating for textile material. The need of implants with controlled antibacterial properties is increasing due to the risk of infections which follows the implantation of biomaterials.

In the first part of experimental section of this work, detailed description of development and characterization of mechanically sensitive materials made of plasma polymer multilayers and silver nanoparticles was given. It has been demonstrated that tailoring of the release of an active agent can be achieved by mechanical stimulation of the designed material. Silver ions as a biocide are stored as AgNPs in the plasma polymer multilayer system and released in the material surroundings. Taking advantage of different mechanical properties between the different layers, a system of cracks in the plasma polymer overlayer allowed control of the diffusion of silver ions. Antibacterial properties of the developed system have been confirmed by disk diffusion method.

Due to the fact that biomaterial device has to be sterile before the implantation in the body, the sterilization step was studied as the last step of the material modification during elaboration. Influence of ageing and two types of sterilization procedures (autoclave and electron beam irradiation) on the material surface chemistry and morphology was analyzed. Results showed that autoclave treatment influences surface structure unfavorably, causing degradation of the material without significantly changing the surface chemistry. Electron beam sterilization did not influence surface physical or topographical changes. However, it induced changes in chemistry of the surface causing decrease in O/C elemental concentration ratio. It was also shown that autoclave

sterilization should be carefully considered for biomedical devices containing silver nanoparticles due to changes that it induces in nanoparticles size and distribution. In contrast, electron beam sterilization did not affect particles size or distribution.

Further investigations were focused on the antibacterial properties. In this study, the effects of PP and PP-modified mesh substrates on planktonic bacteria, bacterial adhesion and biofilm formation were studied. The antibacterial efficiency of the mechanoresponsive coating was verified under stretching conditions.

Plasma polymer itself have shown to influence bacteria proliferation in planktonic state for short time of incubation (4h) suggesting that elution of low molecular weight water soluble fractions of plasma polymer takes place. Nevertheless, there is no difference in planktonic bacteria proliferation between PP/Ar/MAPP(2^{nd}) and PP sample for 168 h of incubation time, suggesting that this low molecular fraction is in small amount and is easily extracted during the first time of immersion. In contrast, no similar effect was observed with eukaryotic cells (results are shown in Annex). Substrates without plasma polymer overlayer (PP/Ar/MAPP/Ag) have shown to inhibit bacterial proliferation in planktonic state after 4 and 168 h. Plasma polymer multilayer system and the same system under stretching conditions have exhibited antibacterial properties for short time of incubation (4h), inhibiting the bacterial proliferation in planktonic state, despite of the presence of the second polymer layer in the case of PP/Ar/MAP/Ag/MAPP. This was proposed to be due to presence of silver nanoparticles close to the surface region which may provide a fast release of silver ions when in contact with liquid environment and due to the insufficient barrier effect of second plasma polymer overlayer. For longer time of incubation, the barrier effect of plasma polymer overlayer was playing a role, showing only a weak inhibition rate.

Quantitative and qualitative evaluations of bacterial adhesion after 4 hours of incubation and biofilm formation after 168 hours of incubation for Polypropylene and plasma polymer modified polypropylene substrates have been done using of Confocal Laser Scanning Microscopy. Such comprehensive study of biofilm characteristics on coatings with loaded silver nanoparticles, especially on mesh materials, have not been performed before. In the case of surfaces which were releasing silver ions, bacteria adhered after 4h in lower quantity than on polypropylene and polypropylene modified with plasma polymer layer without silver nanoparticles. Bacterial behaviors have shown similar trends when incubation time increased to 168 h: Biomasses calculated for polypropylene (PP) and plasma multilayer system (PP/Ar/MAPP/Ag/MAPP) have shown similar values. For substrates with higher and/or faster release of silver ions (PP/Ar/MAPP/Ag and PP/Ar/MAPP/Ag/MAPP-60%), the biomass value have significantly decreased. More detailed study based on rate of connected biomass, surface to biovolume ratio, average diffusion distance and bacterial rates with compromised membrane have shown structural differences of biofilms developed on the different substrates: coatings releasing silver ions favored the formation of a weakly connected biofilm, composed of frequent bacterial clusters of small size. The biofilm was in mushroom-like structures with low biomass value and with important amount of colonies which were not part of a biofilm. This is in agreement with a recent study that showed that even sublethal concentration of silver ions can remarkably increase the efficiency of antibiotics against gram-negative bacteria. Our study suggest that this may be due to the less cohesive structure (therefore less protective for bacteria) resulting from the action of Ag^{+}.

These results give therefore new argument to use silver as antibacterial agent in implant materials. Even in low quantity, it may reduce the infection on site, and, additionally, in case of higher risk of infection, may enhance the efficiency of an antibiotic therapy.

Results from this work, give a strong base for the future of intelligent silver containing materials that controls the release at the site of infection. For PP mesh materials, this way of preventing infection is very promising due to the low quantity of silver release sufficient to act on site against the infection. Additionally, in case of higher risk of infection, the antibiotic therapy together with silver containing implant material may prevent the infection development and biofilm formation on implanted biomaterial.

The investigations included in this thesis give a strong base for the further development of antimicrobial polymer mesh-like materials and biomaterials surfaces that will eventually be used as implants. The new concept proposed in this thesis has been proved.

Further investigations should include the optimization of the developed system. Plasma polymer second layer barrier properties should be improved by changing the crosslink density of plasma polymer, to provide efficient barrier effect for Ag^+ release. The quantity of silver nanoparticles which serves as an Ag^+ reservoir should be increased to prolong the antibacterial effect. This can be performed by changing the thickness of the first plasma polymer layer, which serves as a matrix for embedded nanoparticles. Control over size of nanoparticles should be improved, since this affects releasing properties of the coating. Better control over size of nanoparticles embedded in the plasma polymer could be achieved by changing the method of synthesis of silver nanoparticles to an *in situ* photochemically assisted synthesis. Further, the effects of ethylene oxygen sterilization method on the developed system could be studied, since this method of sterilization is also often used in the health care facilities and may only weakly affect the initial properties of the material.

Antibacterial efficiency of the system should be further investigated under flow culture conditions by real time observation. This will allow to study bacterial attachment and detachment involved during bacterial adhesion and biofilm

growth on these substrates. Additional studies could involve antibacterial properties study conducted in a modular bioreactor where it is possible to apply series of stretching and retraction cycles to the material ("similarly" to [462]). Further fundamental investigations of influence of Ag^+ release on biofilm structure are also possible using developed system and Comstat 2 software. Parameters such as "thickness distribution", "area occupied in layers", "substratum coverage", "microcolonies at substratum", "volume of microcolonies at substratum", "fractal dimension" or "dimensionless roughness coefficient" can serve to provide profound study on the influence of low concentration of Ag^+ release on biofilm development and structure. For example, "volume of microcolonies at substratum" parameter can serve to investigate how micro-colony volumes vary under different Ag^+ release kinetics, or to establish whether there exists an "optimal micro-colony volume" depending on the quantity of Ag^+ released from the material, so that micro-colony growth ceases when a certain micro-colony size is reached.

Further investigations using clinically relevant cell lines such as fibroblasts and better simulation of the in vivo conditions should be the next step towards confirmation of the absence of cytotoxicity of developed system.

6 ANNEX

6.1 Cytotoxicity of plasma polymer modified mesh substrates

6.1.1 Introduction

Abdominal surgery is associated with significant risk of incisional hernia (10-20%) (see **Figure 6-1**) and gynecological defects operation [421, 463, 464]. The best and often used method to repair hernia is use of synthetic mesh that bridges the abdominal wall defect in a tension-free way [418] (see **Figure 6-2**). Mesh implants are also used in vaginal prolapse repair of the anterior vaginal wall. One of the complications after mesh implantation is infection. This is described in details in the previous section – 4.1. Although for the gynecological operations the cellular adhesion on meshes is not a problem, in case of abdominal wall defect operation adhesions between the visceral side of the mesh and adjacent organs can take place [465-467] and become a serious complication [428, 467]. Such adhesions between the implanted material and organs can lead to chronic pain, recurrence of the hernia, intestinal obstruction or enterocutaneous fistulas. The ideal mesh for vaginal prolapse repair should prevent infection but favor cell adhesion. For abdominal wall defect operation, ideal mesh should also show integration with the tissue of the abdominal wall (primarily to prevent mesh migration and hernia recurrence), but no adhesions on the visceral side.

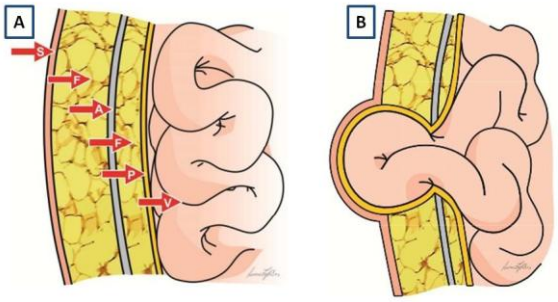

Figure 6-1: (**A**) Schematic drawing of a normal abdominal wall and its layers: Skin (S); Fat Tissue (F); Aponeurosis (A); Pre-peritoneal Fat Tissue (F); Peritoneum (P); and the abdominal viscera (V). (**B)** Schematic drawing of a hernia. Illustration adopted from Zogbi *et al*.[83].

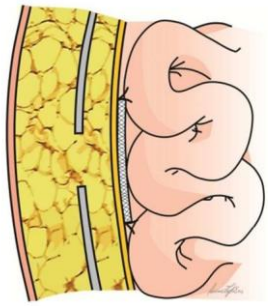

Figure 6-2: Possible way of mesh implantation. Illustration adopted from Zogbi *et al*. [83]

This approach was explored by Van't Riet *et al.* [465] to develop non adhesive coatings. They performed an in vivo study, in which they implanted meshes that were coated with collagen on their visceral side. There was a clear positive effect of the collagen coating, with less visceral adhesions. Other studies have shown less successful results with different coatings from a biological origin such as sodium hyaluronate /carboxymethylcellulose [465, 468] or an absorbable layer of oxidized regenerated cellulose [465, 469, 470]. However the long term prevention should be also provided by this type of coatings. Indeed, considering that biological coatings are susceptible to hydrolytic or enzymatic degradation, it can be expected that these coatings will not provide long-term non-adhesiveness [471]. In the study of Emans *et al.* [471], a synthetic and

biocompatible hydrophilic coating on the PP mesh was tested. The coating was based on N-vinylpyrrolidinone (NVP) and N-butylmethacrylate (BMA) as hydrophilic and hydrophobic building blocks, respectively. The coated mesh was compared in a series of in vivo experiments (using a rat model) with the uncoated PP meshes. The histological evaluation after 30 days follow-up, have shown that in case of PP-coated meshes no adhesions were observed and in case of PP-uncoated meshes adhesion and tissue granulations were present. At 30 days follow-up the implanted material is expected to not form any new adhesions. Thus, the results of this study showed that stable hydrophilic polymer coating has a beneficial effect on adhesion formation after implantation of a mesh.

The authors suggested also that “A hydrophilic coating (degradable or stable) may be exploited in another manner such as a reservoir for controlled release of an antibiotic agent. A hydrophilic surface *per se* may play a role in the prevention of bacterial adhesion [332], while controlled swelling of the coating after implantation may provide a mean to engineer and control the release kinetics”.

Bringman *et al* [472] in an article which sum up over 50 years of advances in hernia repair techniques, concluded that ideal mesh prostheses would be a monofilament mesh that would prevent adhesions, yet still enable growth of the adjacent tissue for optimal augmentation.

As it was showed in the section 4.3.2.1.2, the presence of plasma polymer coating and presence of plasma polymer multilayer system deposited on PP mesh has a beneficial influence for preventing the bacterial colonization on the mesh material. In the following section the preliminary study of the biocompatibility of the developed plasma polymer multilayer coating deposited on PP mesh is evaluated.

6.1.2 Material and Methods

6.1.2.1 Cell line

STRO1A+ cells were provided by Dr P. Marie (Inserm U606, Lariboisiere Hospital, Paris, France) [473]. They are immortalized human osteoblast progenitor cells derived from fetal bone marrow.

6.1.2.2 Substrates

Substrates developed during this research and described in details in the section 2.3.3 have been used for cytotoxicity assay. Substrates identification and description is seen in **Table 6-1**.

Sample Identification	Description
PP	Polypropylene mesh
PP/Ar/MAPP(^{2nd})	Polypropylene mesh after argon plasma treatment and deposition of plasma polymer layer with the conditions used for 2nd plasma polymer layer (overlayer) in the multilayer plasma polymer system, described in details in section **2.3.3**
PP/Ar/MAPP/Ag	Polypropylene mesh after argon plasma treatment and deposition of first plasma polymer layer with the synthesis of silver nanoparticles afterwards
PP/Ar/MAPP/Ag/MAPP	Complete plasma polymer multilayer system deposited on polypropylene mesh

Table 6-1: Identification of substrates used in the cytotoxicity study.

6.1.2.3 Sterilization

Sterilization of the samples used for the experiments was performed in the Aérial Center of Irradiation (CRITT Aérial, Illkirch). Samples were sterilized by means of electron beam with the electrostatic generator of Van Graff type. Dose of irradiation received by samples was set to 25 kGy.

6.1.2.4 *In-vitro* cytotoxicity test by direct and indirect (extracts) contact

Firstly, the eventual cytotoxicity of products that could be released from substrates was evaluated. Extracts were prepared in accordance with International Standard ISO 10993-12 (1996). Substrates were totally immersed in cell culture DMEM medium (Sigma-Aldrich, D5546) containing penicillin-streptomycin (Sigma-Aldrich, P0781) and L-glutamine (Sigma-Aldrich, G7513) and incubated at 37°C for 24h under static condition. Two conditions were tested: extraction in culture medium with or without addition of foetal bovine serum (VWR, BWSTS1830). Control groups included Phenol (dilution at 25% of a solution at 6.4 gL^{-1} in culture medium) as a positive cytotoxicity control and Thermanox® coverslips extraction medium as negative cytotoxicity controls. In parallel, cells were seeded in 24-well culture plates (80000 cells/ml of medium) and incubated for 24h to allow attachment. Then, the culture medium was replaced with 500 µl of test extract or control extract. Cytotoxicity was assessed after a further 24h of incubation. After this time, viability was evaluated using MTT test (Sigma-Aldrich, M5655). Three samples were used for each experiment. For each sample, measurements of the optical density using 570nm and 620nm for reference were obtained on three aliquots.

Secondly, the cytotoxicity of substrates directly in contact with cells was evaluated. Four types of substrates were used: PP, P/Ar/MAPP(2^{nd}), PP/Ae/MAPP/Ag/MAPP, PP/Ae/MAPP/Ag (see **Table 6-1**). Substrates were immersed overnight in complete DMEM medium (Sigma-Aldrich, D5546) containing penicillin-streptomycine (Sigma-Aldrich, P0781) and L-glutamine (Sigma-Aldrich, Sigma G7513). Further, cells were seeded at 80000 cells on each sample and 35000 cells on control Thermanox® coverslips in a 24-well polystyrene plate coated with a layer of 2% agar in the bottom of each well to avoid adhesion and proliferation of cells on polystyrene around or below the substrates. Cells were incubated for 24 hours in 37°C and 5% of CO_2 containing

atmosphere. After this time, viability using PrestoBlue (Lifetechnologies, A-13261) was evaluated.

Cell adhesion on substrates was also observed by confocal microscopy. For that, cells were fixed with a solution of 2% (v/v) paraformaldehyde in NaK2P buffer for 30 min and permeabilized with 0.1% (v/v) of Triton X-100 for 15 min. Actin filaments were labeled during 1 hour using phalloidin-FITC at a concentration of 0.4 µg/ml^{-1}.

6.1.3 Results

The extraction test with culture medium without serum demonstrated that all test specimens were non-toxic compared with the negative control (see **Figure 6-3**). Indeed the viability of all tested samples was higher than 75% of the negative control (Thermanox®) that is considered as the threshold of cytotoxicity. The PP/Ar/MAPP(2nd) sample was shown to elicit significantly higher cell viability compared to negative control. Additionally, PP/Ar/MAPP/Ag substrate has shown significantly higher ($p>95.0\%$) toxicity compared to PP sample. The least cell viability was logically found for the positive control ($p<0.001$).

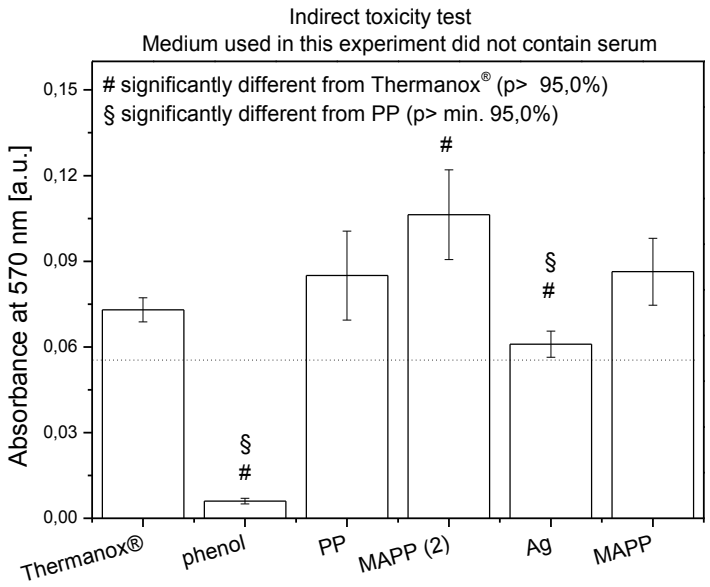

Figure 6-3: Cytotoxicity of plasma polymerized coatings deposited on PP mesh evaluated using the extraction test method. Medium used in this experiment did not contain serum. Abbreviations MAPP(2), Ag, MAPP on the graph represent PP/Ar/MAPP(2^{nd}), PP/Ar/MAPP/Ag, PP/Ar/MAPP/Ag/MAPP samples respectively.

The extraction test performed in the same manner but with medium containing serum demonstrated that all test specimens were non-toxic compared with the negative control (see **Figure 6-4**). The PP sample was shown to elicit significantly higher cell viability compared to negative control. Additionally, PP/Ar/MAPP/MAPP(2), PP/Ar/MAPP/Ag and PP/Ar/MAPP/Ag/MAPP substrates have shown significantly higher (p>95,0%) toxicity compared to PP sample. Positive control contributed to the highest level of cell death (p<0.001) among all variables.

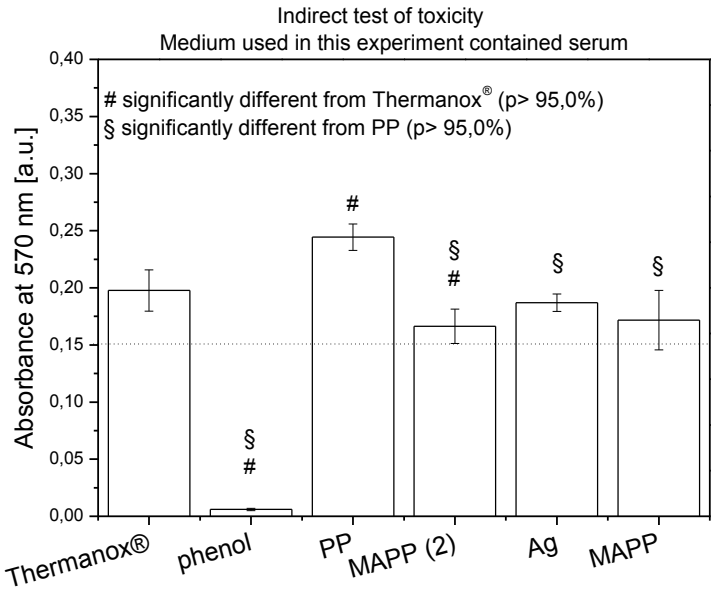

Figure 6-4: Cytotoxicity of plasma polymerized coatings deposited on PP mesh evaluated using the extraction test method. Medium used in this experiment contained serum. Abbreviations MAPP(2), Ag, MAPP, on the graph represent PP/Ar/MAPP(2^{nd}), PP/Ar/MAPP/Ag, PP/Ar/MAPP/Ag/MAPP samples respectively.

Figure 6-5 illustrates the influence of the serum addition in the extraction medium on the indirect contact test. The results are presented as a rate of cell viability on PP and PP modified substrates, compared to cell viability on Thermanox® negative control. No significant influence of serum was observed except for PP/Ar/MAPP(2^{nd}) samples for which the cytotoxicity of the extraction medium increased in presence of serum.

The response of STRO1A+ cells in direct contact with the tested materials was studied. However, it appears that the absorbance measured by UV-Vis spectroscopy for PP samples and PP modified samples was extremely low representing less than 500 cells per sample. Therefore, the cell adhesion on above mentioned substrates was observed by confocal microscopy (**Figure 6-6**). From these images, the conclusions can be drawn that cells are effectively not able to adhere on the tested substrates. Very few adhering cells were visible

on each mesh fiber and they were less spread than on Thermanox® negative control. An auto-fluorescence due to PP/Ar/MAPP/Ag/MAPP coating was observed.

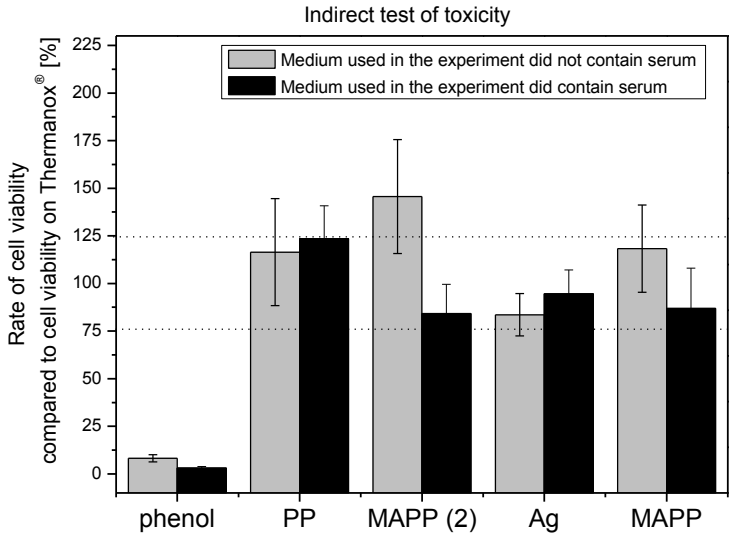

Figure 6-5: Influence on the indirect toxicity test of serum addition in the extraction medium. The results are presented as a rate of cell viability on PP and PP modified substrates compared to cell viability on Thermanox® negative control. Dashed line represents 75 % of Thermanox® control which represents the threshold of cytotoxicity. Abbreviations MAPP(2), Ag, MAPP on the graph represent PP/Ar/MAPP(2nd), PP/Ar/MAPP/Ag, PP/Ar/MAPP/Ag/MAPP samples respectively.

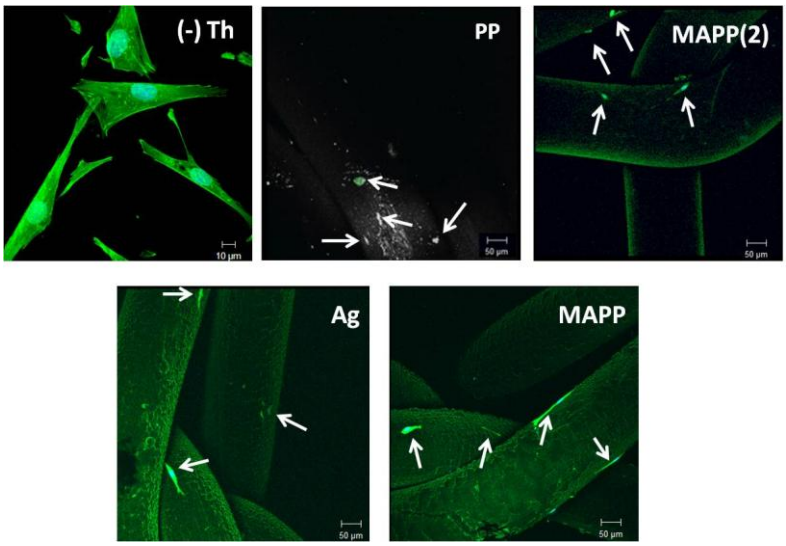

Figure 6-6: Confocal images representing cell adhesion on PP and PP modified substrates after 24 hours of incubation. (-) Th represents Thermanox® negative control. Arrows: Cells adhering on mesh fibers. MAPP(2), Ag, MAPP on the images represent PP/Ar/MAPP(2nd), PP/Ar/MAPP/Ag, PP/Ar/MAPP/Ag/MAPP samples respectively.

6.1.4 Discussion

Differences in sensitivities were observed from the results of the three tests performed, despite the fact that factors such as type of cells used and endpoint viability assay were standardized. The ranking order of substrates in the extract tests performed with and without serum was found to be slightly different. In the test with medium without serum, PP/Ar/MAPP/Ag substrate was found to be significantly different compared to negative control while it was not the case in the test with medium containing serum. In this last case, the leaching of components (silver ions) from PP/Ar/MAPP/Ag substrate may be insufficient to give a similar response as in test where serum was not used. This can be explained by the presence of adsorbed proteins on the surface lowering down the diffusion of silver ions. It has been effectively reported that the composition and the solution parameters of the solvent used for extraction influence the kinetics and mechanism of the elution process [474]. Similarly,

PP/Ar/MAPP(2^{nd}) substrates have given an opposite response in presence or in absence of serum comparing to negative control. A slight increase in viability was obtained without serum while a slight decrease in viability was observed with serum containing medium. Leaching of low molecular weight water soluble fractions of plasma polymer takes place [386] and it can differ according to the medium content. How the presence of serum could increase the leaching of cytotoxic molecules or decrease the leaching of favorable ones is unclear. Moreover, although using extracts in a culture medium at 37°C for 24 h is a common procedure according ISO guidelines, the importance of the duration of extraction may play a role and need to be optimized to ensure complete elution of the leached components. Dilution of extracts must be also used to definitively conclude for PP/Ar/MAPP(2^{nd}) and PP/Ar/MAPP/Ag indirect cytotoxicity. However, as the testing method using medium containing serum is closer to the *in vivo* conditions, we can already conclude that silver release from samples should not have any cytotoxic effect on cells of the surrounding tissues.

The direct observations using confocal microscopy of cell adherence on PP and PP modified substrates revealed a very low affinity of the cells for these substrates (see **Figure 6-6**). This can be explained either by an unfavorable surface chemistry or surface morphology. Concerning the surface chemistry, PP is known to be unfavorable to cell adhesion due to its hydrophobic surface. Efforts are made to tailor polypropylene surface more favorable to cell attachment, often using plasma discharge surface treatments [475-478]. Increase of surface energy, roughness and incorporation of various functional groups on PP surface often results in improved cell adhesion [479] even after only one day [476]. In spite that polypropylene surface is not favorable for cell attachment, in vivo study of polypropylene lightweight meshes revealed adverse effects of this material, resulting in high risk of adhesions [465, 471]. Additionally in case of gynecological surgeries such as in pelvic reconstructive surgery the use of mesh is based on substitution or replacement of lacking supportive tissue, reinforcement of weak or defective supportive tissues or

induction of new supportive tissue by mesh material [419]. Thus, as for the meshes used in the pelvic reconstructive surgery the adhesion of cells is required, in case of meshes for abdominal wall surgeries efforts are made to render surface of mesh anti-adhesive, yet still favorable for growth of the adjacent tissue. For this reason the developed PP/Ar/MAPP/Ag/MAPP substrate might be a promising way to achieve this property of meshes materials. This hypothesis is supported by work of Ploux *et al* [148]. In their study, cell behavior on maleic anhydride plasma polymer deposited thin films with chemical and topographical patterns was verified. Results showed that adherent human osteoprogenitor cells (HOP) presented normal morphology at different times of incubation. The differences in number of cells between the substrates were correlated with the differences in surface charge. It appeared that the negatively charged surfaces favored the formation of conditioning layer on the surface and consequently cell adhesion. Negative surface charge of these surfaces was related to presence of -C(=O)-O^- groups. Similar chemistry of the surface was observed for the PP modified meshes, including the presence of –C(=O)-O^- groups. However it is important to note that differences in substrate, condition of deposition and sterilization procedures may play a role and more detailed study have to be performed to prove the biocompatibility of developed PP modified materials.

Nevertheless, as the cell adhesion was low on mesh fibers whatever their chemistry, it can be concluded that it may be more probably the topography of the fibers that is unfavorable for cell adhesion than surface chemistry. Indeed, Bigerelle *et al*. [480] who studied the adhesion of mesenchymal stem cells on electro-eroded titanium surfaces presenting peaks and valleys morphology, showed that when the distance between surface features (peaks or valleys) was equal to 110 µm, the number of adherent cells drop drastically to 50 %. With this level of roughness, the peaks and valleys were slightly wider than the cell size but not enough that the cells will see a flat surface. The surface curvatures at this level are detected by the cells and may constrain the cell body impeding

cell adhesion. Similarly, Park *et al.* [481] used surface features on PMMA substrates with dimensions very similar with the mesh fiber diameter used in our study. Cell culture on concave and convex hemispheric microstructures measuring 200 μm in diameter and 50 μm in depth/height have shown greater adhesion of fibroblasts and hMSC cells on convex structures compared with concave structures. The researchers concluded that the concave micro-wells provided unfavorable conditions for cell attachment, cell growth and that it stimulated cell mobility and migration of cells to a more favorable location. Hence, from both of the studies [480, 481] it can be concluded that in case of PP mesh and PP modified mesh substrates, cell adhesion may be impeded because of the curvature of fibers. Additionally since the adhesion on fiber was not favorable, the manipulation during preparation of samples before examination under confocal microscopy (move of the plate when removing from incubator) could strongly influence the number of cells adhered on the surface of the fiber and must be better controlled.

6.1.5 Conclusions

In summary, plasma polymer coatings deposited on polypropylene mesh substrate have not shown cytotoxic effects compared to controls. The effects of silver ions release from samples are minor in conditions close to the in vivo ones i.e. in presence of serum. The adhesion of cells on meshes is limited probably because of the morphology of fibers. Considering chemistry of the surface, the application of a modified mesh material should serve well in gynecological defects operations. Also, the objective to produce meshes able to prevent cell adhesion for abdominal wall operations but without leaching cytotoxic molecules, is also possible to be reached.

However, the cytotoxicity tests performed herein using an established cell line would serve only as a general and preliminary study. Selection of appropriate testing method, as well as the use of more clinically relevant cell lines should be

the next step towards confirmation of the absence of cytotoxicity of plasma polymer modified multilayer systems. Use of flat surfaces to facilitate this study must be performed. Moreover, further research should concentrate on better simulation of the in vivo conditions within cell cultures.

Bibliography

1. Gristina, A., P. Naylor, and Q. Myrvik, *Biomaterial-Centered Infections: Microbial Adhesion versus Tissue Integration*, in *Pathogenesis of Wound and Biomaterial-Associated Infections*, T. Wadström, et al., Editors. 1990, Springer London. p. 193-216.
2. Kost, J. and R. Langer, *Responsive polymeric delivery systems.* Advanced Drug Delivery Reviews, 2001. 46(1–3): p. 125-148.
3. Katz, J.S. and J.A. Burdick, *Light-Responsive Biomaterials: Development and Applications.* Macromolecular Bioscience, 2010. 10(4): p. 339-348.
4. Nicoletta, F.P., et al., *Light Responsive Polymer Membranes: A Review.* Membranes, 2012. 2(1): p. 134-197.
5. Thevenot, J., et al., *Magnetic responsive polymer composite materials.* Chemical Society Reviews, 2013.
6. Filipcsei, G., et al., *Magnetic Field-Responsive Smart Polymer Composites*, in *Oligomers - Polymer Composites - Molecular Imprinting*2007, Springer Berlin Heidelberg. p. 137-189.
7. Lentacker, I., et al., *Ultrasound-Responsive Polymer-Coated Microbubbles That Bind and Protect DNA.* Langmuir, 2006. 22(17): p. 7273-7278.
8. Yamato, M., et al., *Release of adsorbed fibronectin from temperature-responsive culture surfaces requires cellular activity.* Biomaterials, 2000. 21(10): p. 981-986.
9. Chilkoti, A., et al., *Targeted drug delivery by thermally responsive polymers.* Advanced Drug Delivery Reviews, 2002. 54(5): p. 613-630.
10. Yoshizako, K., et al., *Regulation of protein binding toward a ligand on chromatographic matrixes by masking and forced-releasing effects using thermoresponsive polymer.* Anal Chem, 2002. 74(16): p. 4160-6.
11. Moroder, P., et al., *Material properties and electrical stimulation regimens of polycaprolactone fumarate–polypyrrole scaffolds as potential conductive nerve conduits.* Acta Biomaterialia, 2011. 7(3): p. 944-953.
12. Gillies, E.R. and J.M.J. Fréchet, *pH-Responsive Copolymer Assemblies for Controlled Release of Doxorubicin.* Bioconjugate Chemistry, 2005. 16(2): p. 361-368.
13. Saito, G., J.A. Swanson, and K.-D. Lee, *Drug delivery strategy utilizing conjugation via reversible disulfide linkages: role and site of cellular reducing activities.* Advanced Drug Delivery Reviews, 2003. 55(2): p. 199-215.
14. Miyata, T., T. Uragami, and K. Nakamae, *Biomolecule-sensitive hydrogels.* Advanced Drug Delivery Reviews, 2002. 54(1): p. 79-98.
15. del Rio, A., et al., *Stretching single talin rod molecules activates vinculin binding.* Science, 2009. 323(5914): p. 638-41.
16. Zhong, C., et al., *Rho-mediated contractility exposes a cryptic site in fibronectin and induces fibronectin matrix assembly.* J Cell Biol, 1998. 141(2): p. 539-51.
17. Arm, D.M. and A.F. Tencer, *Effects of cyclical mechanical stress on the controlled release of proteins from a biodegradable polymer implant.* Journal of Biomedical Materials Research, 1997. 35(4): p. 433-441.
18. Hemmerlé, J., et al., *Mechanically Responsive Films of Variable Hydrophobicity Made of Polyelectrolyte Multilayers.* Langmuir, 2005. 21(23): p. 10328-10331.
19. Mertz, D., et al., *Mechanically Responding Nanovalves Based on Polyelectrolyte Multilayers.* Nano Letters, 2007. 7(3): p. 657-662.
20. Mertz, D., et al., *Mechanotransductive surfaces for reversible biocatalysis activation.* Nat Mater, 2009. 8(9): p. 731-735.
21. Bacharouche, J., et al., *Biomimetic Cryptic Site Surfaces for Reversible Chemo and Cyto-Mechanoresponsive Substrates.* ACS Nano, 2013.

22. **Park, M.V.D.Z., et al., *The effect of particle size on the cytotoxicity, inflammation, developmental toxicity and genotoxicity of silver nanoparticles.* Biomaterials, 2011. 32(36): p. 9810-9817.**
23. **Ploux, L., A. Ponche, and K. Anselme, *Bacteria/Material Interfaces: Role of the Material and Cell Wall Properties.* Journal of Adhesion Science and Technology, 2010. 24(13-14): p. 2165-2201.**
24. **Percival, S.L., J.T. Walker, and P.R. Hunter, *Microbiological Aspects of Biofilms and Drinking Water*2010: Taylor & Francis.**
25. **Hall-Stoodley, L., J.W. Costerton, and P. Stoodley, *Bacterial biofilms: from the Natural environment to infectious diseases.* Nat Rev Micro, 2004. 2(2): p. 95-108.**
26. **Schmidt, I., et al., *New concepts of microbial treatment processes for the nitrogen removal in wastewater.* FEMS Microbiology Reviews, 2003. 27(4): p. 481-492.**
27. **Nicolella, C., M.C.M. van Loosdrecht, and J.J. Heijnen, *Wastewater treatment with particulate biofilm reactors.* Journal of Biotechnology, 2000. 80(1): p. 1-33.**
28. **Alami, Y., et al., *Rhizosphere soil aggregation and plant growth promotion of sunflowers by an exopolysaccharide-producing Rhizobium sp. strain isolated from sunflower roots.* Appl Environ Microbiol, 2000. 66(8): p. 3393-8.**
29. **Ashraf, M., et al., *Inoculating wheat seedlings with exopolysaccharide-producing bacteria restricts sodium uptake and stimulates plant growth under salt stress.* Biology and Fertility of Soils, 2004. 40(3): p. 157-162.**
30. **Keevil, C.W. and R.S.o. Chemistry, *Biofilms in the aquatic environment*1999: Royal Society of Chemistry.**
31. **Marsh, P.D. and D.J. Bradshaw, *Dental plaque as a biofilm.* Journal of Industrial Microbiology, 1995. 15(3): p. 169-175.**
32. **Macfarlane, S., B. Bahrami, and G.T. Macfarlane, *Mucosal biofilm communities in the human intestinal tract.* Adv Appl Microbiol, 2011. 75: p. 111-43.**
33. **Tenke, P., et al., *Update on biofilm infections in the urinary tract.* World Journal of Urology, 2012. 30(1): p. 51-57.**
34. **Goller, C.C. and T. Romeo, *Environmental influences on biofilm development.* Curr Top Microbiol Immunol, 2008. 322: p. 37-66.**
35. **Teughels, W., et al., *Effect of material characteristics and/or surface topography on biofilm development.* Clinical Oral Implants Research, 2006. 17(S2): p. 68-81.**
36. **Bos, R., H.C. van der Mei, and H.J. Busscher, *Physico-chemistry of initial microbial adhesive interactions – its mechanisms and methods for study.* FEMS Microbiology Reviews, 1999. 23(2): p. 179-230.**
37. **Melo, L.F. and N.A.T.O.S.A. Division, *Biofilms--science and Technology*1992: Kluwer Academic Publishers.**
38. **Percival, S.L., D.C. Knottenbelt, and C.A. Cochrane, *Biofilms and Veterinary Medicine*2011: Springer.**
39. **Rijnaarts, H.H.M., et al., *DLVO and steric contributions to bacterial deposition in media of different ionic strengths.* Colloids and Surfaces B: Biointerfaces, 1999. 14(1–4): p. 179-195.**
40. **Bayoudh, S., et al., *Assessing bacterial adhesion using DLVO and XDLVO theories and the jet impingement technique.* Colloids and Surfaces B: Biointerfaces, 2009. 73(1): p. 1-9.**
41. **Boks, N.P., et al., *Forces involved in bacterial adhesion to hydrophilic and hydrophobic surfaces.* Microbiology, 2008. 154(Pt 10): p. 3122-33.**
42. **Hermansson, M., *The DLVO theory in microbial adhesion.* Colloids and Surfaces B: Biointerfaces, 1999. 14(1–4): p. 105-119.**
43. **Wang, Q., et al., *Sensing wetness: a new role for the bacterial flagellum.* EMBO J, 2005. 24(11): p. 2034-42.**
44. **Ponsonnet, L., et al., *Local pH variation as an initial step in bacterial surface-sensing and biofilm formation.* Materials Science and Engineering: C, 2008. 28(5–6): p. 896-900.**
45. **Booth, I.R., et al., *Mechanosensitive channels in bacteria: signs of closure?* Nat Rev Microbiol, 2007. 5(6): p. 431-40.**

46. Costerton, J.W., P.S. Stewart, and E.P. Greenberg, *Bacterial Biofilms: A Common Cause of Persistent Infections.* Science, 1999. 284(5418): p. 1318-1322.
47. Katsikogianni, a., *CONCISE REVIEW OF MECHANISMS OF BACTERIAL ADHESION TO BIOMATERIALS AND OF TECHNIQUES USED IN ESTIMATING BACTERIAMATERIAL INTERACTIONS.* M. Katsikogianni and Y.F. European Cells and Mater iMaliss, 2004. 8: p. 37-57.
48. Prigent-Combaret, C., et al., *Developmental pathway for biofilm formation in curli-producing Escherichia coli strains: role of flagella, curli and colanic acid.* Environmental Microbiology, 2000. 2(4): p. 450-464.
49. Flemming, H.-C., *Relevance of biofilms for the biodeterioration of surfaces of polymeric materials*, in *Polymer Degradation and Stability*1998.
50. Flemming, H.-C., T. Neu, and D. Wozniak, *The {EPS} Matrix: The {"House of Biofilm Cells"}.* Journal of Bacteriology, 2007. 189(22).
51. Fux, C.A., et al., *Survival strategies of infectious biofilms.* Trends in microbiology, 2005. 13(1): p. 34-40.
52. Kolenbrander, P.E., et al., *Bacterial interactions and successions during plaque development.* Periodontology 2000, 2006. 42(1): p. 47-79.
53. Rickard, A.H., et al., *Phylogenetic relationships and coaggregation ability of freshwater biofilm bacteria.* Appl Environ Microbiol, 2002. 68(7): p. 3644-50.
54. Drinka, P.J., *Complications of chronic indwelling urinary catheters.* J Am Med Dir Assoc, 2006. 7(6): p. 388-392.
55. Kaplan, J.B., et al., *Enzymatic detachment of Staphylococcus epidermidis biofilms.* Antimicrob Agents Chemother, 2004. 48(7): p. 2633-6.
56. Molin, S. and T. Tolker-Nielsen, *Gene transfer occurs with enhanced efficiency in biofilms and induces enhanced stabilisation of the biofilm structure.* Current Opinion in Biotechnology, 2003. 14(3): p. 255-261.
57. Percival, S., et al., *Introduction to Biofilms*, in *Biofilms and Veterinary Medicine*, S. Percival, D. Knottenbelt, and C. Cochrane, Editors. 2011, Springer Berlin Heidelberg. p. 41-68.
58. Sauer, K., et al., *Pseudomonas aeruginosa displays multiple phenotypes during development as a biofilm.* J Bacteriol, 2002. 184(4): p. 1140-54.
59. Brözel, V.S., G.M. Strydom, and T.E. Cloete, *A method for the study of de novo protein synthesis in pseudomonas aeruginosa after attachment.* Biofouling, 1995. 8(3): p. 195-201.
60. Marsh, P.D., *Dental plaque: biological significance of a biofilm and community life-style.* Journal of Clinical Periodontology, 2005. 32: p. 7-15.
61. Miller, M.B. and B.L. Bassler, *Quorum sensing in bacteria.* Annu Rev Microbiol, 2001. 55: p. 165-99.
62. Donlan, R.M., *Biofilms: microbial life on surfaces.* Emerg Infect Dis, 2002. 8(9): p. 881-90.
63. Sutherland, I., *Biofilm Exopolysaccharides*, in *Microbial Extracellular Polymeric Substances*, J. Wingender, T. Neu, and H.-C. Flemming, Editors. 1999, Springer Berlin Heidelberg. p. 73-92.
64. Lawrence, J.R. and T.R. Neu, *[9] Confocal laser scanning microscopy for analysis of microbial biofilms*, in *Methods in Enzymology*, J.D. Ron, Editor 1999, Academic Press. p. 131-144.
65. Burton, E.A., et al., *Molecular Gradients of Bioinertness Reveal a Mechanistic Difference between Mammalian Cell Adhesion and Bacterial Biofilm Formation.* Langmuir, 2009. 25(3): p. 1547-1553.
66. Miao, H., et al., *Dual fluorescence system for flow cytometric analysis of Escherichia coli transcriptional response in multi-species context.* Journal of Microbiological Methods, 2009. 76(2): p. 109-119.
67. Bateman, B.T., et al., *Evaluation of a tetracycline-inducible promoter in Staphylococcus aureus in vitro and in vivo and its application in demonstrating the role of sigB in microcolony formation.* Infect Immun, 2001. 69(12): p. 7851-7.

68. Selinummi, J., et al., *Software for quantification of labeled bacteria from digital microscope images by automated image analysis.* Biotechniques, 2005. 39(6): p. 859-63.
69. Schneider, C.A., W.S. Rasband, and K.W. Eliceiri, *NIH Image to ImageJ: 25 years of image analysis.* Nat Meth, 2012. 9(7): p. 671-675.
70. Heydorn, A., et al., *Quantification of biofilm structures by the novel computer program COMSTAT.* Microbiology, 2000. 146 (Pt 10): p. 2395-407.
71. Heydorn, A., et al., *Experimental reproducibility in flow-chamber biofilms.* Microbiology, 2000. 146 (Pt 10): p. 2409-15.
72. Chavez de Paz, L.E., *Image analysis software based on color segmentation for characterization of viability and physiological activity of biofilms.* Appl Environ Microbiol, 2009. 75(6): p. 1734-9.
73. Ziebuhr, W., et al., *Detection of the intercellular adhesion gene cluster (ica) and phase variation in Staphylococcus epidermidis blood culture strains and mucosal isolates.* Infect Immun, 1997. 65(3): p. 890-6.
74. Pratt, L.A. and R. Kolter, *Genetic analyses of bacterial biofilm formation.* Current Opinion in Microbiology, 1999. 2(6): p. 598-603.
75. Katsikogianni, M.G. and Y.F. Missirlis, *Interactions of bacteria with specific biomaterial surface chemistries under flow conditions.* Acta Biomaterialia, 2010. 6(3): p. 1107-1118.
76. Olofsson, A.C., M. Hermansson, and H. Elwing, *N-acetyl-L-cysteine affects growth, extracellular polysaccharide production, and bacterial biofilm formation on solid surfaces.* Appl Environ Microbiol, 2003. 69(8): p. 4814-22.
77. Engelsman, A.F., et al., *Morphological aspects of surgical meshes as a risk factor for bacterial colonization.* British Journal of Surgery, 2008. 95(8): p. 1051-1059.
78. Thomas, B., *Fossilized Biomaterials Must Be Young.* Acts & Facts, 2009. 38 (6): p. 17.
79. Ramakrishna, S., et al., *Biomedical applications of polymer-composite materials: a review.* Composites Science and Technology, 2001. 61(9): p. 1189-1224.
80. Donaruma, L.G., *Definitions in biomaterials, D. F. Williams, Ed., Elsevier, Amsterdam, 1987, 72 pp.* Journal of Polymer Science Part C: Polymer Letters, 1988. 26(9): p. 414-414.
81. Williams, D.F., *On the nature of biomaterials.* Biomaterials, 2009. 30(30): p. 5897-5909.
82. Ramsden, J.J., et al., *The Design and Manufacture of Biomedical Surfaces.* CIRP Annals - Manufacturing Technology, 2007. 56(2): p. 687-711.
83. Zogbi, L., *The Use of Biomaterials to Treat Abdominal Hernias*, 2011, Prof. Rosario Pignatello (Ed.) InTech: Biomaterials Applications for Nanomedicine, .
84. Arciola, C.R., et al., *Biofilm formation in Staphylococcus implant infections. A review of molecular mechanisms and implications for biofilm-resistant materials.* Biomaterials, 2012. 33(26): p. 5967-5982.
85. Lorenz, U., et al., *In Vivo Detection of Staphylococcus aureus in Biofilm on Vascular Prostheses Using Non-invasive Biophotonic Imaging.* European Journal of Vascular and Endovascular Surgery, 2011. 41(1): p. 68-75.
86. Rohde, H., et al., *Polysaccharide intercellular adhesin or protein factors in biofilm accumulation of Staphylococcus epidermidis and Staphylococcus aureus isolated from prosthetic hip and knee joint infections.* Biomaterials, 2007. 28(9): p. 1711-1720.
87. Donlan, R.M., *Biofilms and device-associated infections.* Emerg Infect Dis, 2001. 7(2): p. 277-81.
88. Arciola, C.R., et al., *Antibiotic resistance in exopolysaccharide-forming Staphylococcus epidermidis clinical isolates from orthopaedic implant infections.* Biomaterials, 2005. 26(33): p. 6530-6535.
89. Vuong, C. and M. Otto, *Staphylococcus epidermidis infections.* Microbes and Infection, 2002. 4(4): p. 481-489.
90. Bagnall, N.M., S. Vig, and P. Trivedi, *Surgical-site infection.* Surgery (Oxford), 2009. 27(10): p. 426-430.

91. McCann, M.T., B.F. Gilmore, and S.P. Gorman, *Staphylococcus epidermidis device-related infections: pathogenesis and clinical management.* J Pharm Pharmacol, 2008. 60(12): p. 1551-71.
92. Weigelt, J.A., et al., *Surgical site infections: Causative pathogens and associated outcomes.* American Journal of Infection Control, 2010. 38(2): p. 112-120.
93. Wargo, M.J. and D.A. Hogan, *Fungal—bacterial interactions: a mixed bag of mingling microbes.* Current Opinion in Microbiology, 2006. 9(4): p. 359-364.
94. Peter Kaali, E.S.a.S.K., *Prevention of Biofilm Associated Infections and Degradation of Polymeric Materials Used in Biomedical Applications, Biomedical Engineering, Trends in Materials Science, ,* Mr Anthony Laskovski (Ed.), Editor 2011, .
95. Gu, J.-D., *Microbiological deterioration and degradation of synthetic polymeric materials: recent research advances.* International Biodeterioration & Biodegradation, 2003. 52(2): p. 69-91.
96. de Boer, A.S., et al., *Risk assessment for surgical-site infections in orthopedic patients.* Infection control and hospital epidemiology : the official journal of the Society of Hospital Epidemiologists of America, 1999. 20(6): p. 402-407.
97. Sheng, W.H., et al., *Comparative impact of hospital-acquired infections on medical costs, length of hospital stay and outcome between community hospitals and medical centres.* Journal of Hospital Infection, 2005. 59(3): p. 205-214.
98. Darouiche, R.O., *Treatment of Infections Associated with Surgical Implants.* New England Journal of Medicine, 2004. 350(14): p. 1422-1429.
99. Simões, M., L.C. Simões, and M.J. Vieira, *A review of current and emergent biofilm control strategies.* LWT - Food Science and Technology, 2010. 43(4): p. 573-583.
100. Srinivasan, R., et al., *Biofilm parameters influencing biocide efficacy.* Biotechnology and Bioengineering, 1995. 46(6): p. 553-560.
101. William A. Rutala, D.J.W., Healthcare Infection Control Practices Advisory Committee (HICPAC) *Guideline for Disinfection and Sterilization in Healthcare Facilities*. 2008.
102. Simoes, L.C., et al., *Persister cells in a biofilm treated with a biocide.* Biofouling, 2011. 27(4): p. 403-11.
103. Frostling, H., et al., *Analytical, occupational and toxicologic aspects of the degradation products of polypropylene plastics.* Scand J Work Environ Health, 1984. 10(3): p. 163-9.
104. O'Kane, W.J., R.J. Young, and A.J. Ryan, *The effect of annealing on the structure and properties of isotactic polypropylene films.* Journal of Macromolecular Science, Part B, 1995. 34(4): p. 427-458.
105. Weir, N.A., et al., *Processing, annealing and sterilisation of poly-l-lactide.* Biomaterials, 2004. 25(18): p. 3939-3949.
106. Matthews, I.P., C. Gibson, and A.H. Samuel, *Sterilisation of implantable devices.* Clinical Materials, 1994. 15(3): p. 191-215.
107. An, Y.H., et al., *Effects of sterilization on implant mechanical property and biocompatibility.* Int J Artif Organs, 2005. 28(11): p. 1126-37.
108. Kubyshkina, B.Z., M. Štukelj, D. Grošelj, L. Marion and I. Emri,, *The Influence of Different Sterilization Techniques on the Time-Dependent Behavior of Polyamides.* Journal of Biomaterials and Nanobiotechnology, 2011. 2 No. 4: p. 361-368.
109. Lucas, A.D., et al., *Residual ethylene oxide in medical devices and device material.* Journal of Biomedical Materials Research Part B: Applied Biomaterials, 2003. 66B(2): p. 548-552.
110. Benson, R.S., *Use of radiation in biomaterials science.* Nuclear Instruments and Methods in Physics Research Section B: Beam Interactions with Materials and Atoms, 2002. 191(1–4): p. 752-757.
111. Ley, F., *The effect of irradiation on packaging materials.* J. Soc. Cosmet. Chem, 1976. 27(482-489): p. 483-489.
112. E-BEAM Services, I.r. *Relative Radiation Stability of Medical Polymers*. 2012; Available from: http://www.ebeamservices.com/pdf/relative-radiation-stability-medical-polymers.pdf.

113. **Bargmann, L.S., et al., *Current sterilization and packaging methods for polyethylene.* Clin Orthop Relat Res, 1999(369): p. 49-58.**
114. **Williams, I.R., M.B. Mayor, and J.P. Collier, *The impact of sterilization method on wear in knee arthroplasty.* Clin Orthop Relat Res, 1998(356): p. 170-80.**
115. **Oral, E. and O.K. Muratoglu, *Radiation cross-linking in ultra-high molecular weight polyethylene for orthopaedic applications.* Nucl Instrum Methods Phys Res B, 2007. 265(1): p. 18-22.**
116. **Guignot, C., et al., *Degradation of segmented poly(etherurethane) Tecoflex® induced by electron beam irradiation: Characterization and evaluation.* Nuclear Instruments and Methods in Physics Research Section B: Beam Interactions with Materials and Atoms, 2001. 185(1–4): p. 100-107.**
117. **Chye Joachim Loo, S., C. Ping Ooi, and Y. Chiang Freddy Boey, *Influence of electron-beam radiation on the hydrolytic degradation behaviour of poly(lactide-co-glycolide) (PLGA).* Biomaterials, 2005. 26(18): p. 3809-3817.**
118. **Darouiche, R.O., *Preventing infection in surgical implants.* US Surgery, 2007: p. 40-45.**
119. **Jensen, L.J., M.T. Aagaard, and S. Schifter, *Prophylactic vancomycin versus placebo in arterial prosthetic reconstructions.* Thorac Cardiovasc Surg, 1985. 33(5): p. 300-3.**
120. **Singh, R., et al., *Penetration of antibiotics through Staphylococcus aureus and Staphylococcus epidermidis biofilms.* Journal of Antimicrobial Chemotherapy, 2010. 65(9): p. 1955-1958.**
121. **Dirschl, D.R. and F.C. Wilson, *Topical antibiotic irrigation in the prophylaxis of operative wound infections in orthopedic surgery.* Orthop Clin North Am, 1991. 22(3): p. 419-26.**
122. **Braithwaite, B.D., et al., *Early results of a randomized trial of rifampicin-bonded Dacron grafts for extra-anatomic vascular reconstruction. Joint Vascular Research Group.* Br J Surg, 1998. 85(10): p. 1378-81.**
123. **Mashaqi, B., et al., *Antibiotic pretreatment of heart valve prostheses to prevent early prosthetic valve endocarditis.* J Heart Valve Dis, 2011. 20(5): p. 582-6.**
124. **Darouiche, R.O., *Antimicrobial Approaches for Preventing Infections Associated with Surgical Implants.* Clinical Infectious Diseases, 2003. 36(10): p. 1284-1289.**
125. **Lynch, A.R., GT ed. *Bacterial and fungal biofilm infections*. ANNUAL REVIEW OF MEDICINE Vol. 59. 2008. 415-428.**
126. **Tiller, J.C., et al., *Designing surfaces that kill bacteria on contact.* Proceedings of the National Academy of Sciences, 2001. 98(11): p. 5981-5985.**
127. **Cheng, G., et al., *A Switchable Biocompatible Polymer Surface with Self-Sterilizing and Nonfouling Capabilities.* Angewandte Chemie International Edition, 2008. 47(46): p. 8831-8834.**
128. **Advincula, R., *Polymer Brushes by Anionic and Cationic Surface-Initiated Polymerization (SIP)*, in *Surface-Initiated Polymerization I*, R. Jordan, Editor 2006, Springer Berlin Heidelberg. p. 107-136.**
129. **Edmondson, S., V.L. Osborne, and W.T.S. Huck, *Polymer brushes via surface-initiated polymerizations.* Chemical Society Reviews, 2004. 33(1): p. 14-22.**
130. **Hammond, P.T., *Engineering materials layer-by-layer: Challenges and opportunities in multilayer assembly.* AIChE Journal, 2011. 57(11): p. 2928-2940.**
131. **Lyklema, J. and L. Deschênes, *The first step in layer-by-layer deposition: Electrostatics and/or non-electrostatics?* Advances in Colloid and Interface Science, 2011. 168(1–2): p. 135-148.**
132. **Friedrich, J., *Mechanisms of Plasma Polymerization – Reviewed from a Chemical Point of View.* Plasma Processes and Polymers, 2011. 8(9): p. 783-802.**
133. **Bazaka, K., et al., *Plasma-assisted surface modification of organic biopolymers to prevent bacterial attachment.* Acta Biomaterialia, 2011. 7(5): p. 2015-2028.**
134. **Anselme, K., et al., *The interaction of cells and bacteria with surfaces structured at the nanometre scale.* Acta Biomaterialia, 2010. 6(10): p. 3824-3846.**
135. **Hochbaum, A.I. and J. Aizenberg, *Bacteria Pattern Spontaneously on Periodic Nanostructure Arrays.* Nano Letters, 2010. 10(9): p. 3717-3721.**

136. **Jeyachandran, Y.L., et al., *Bacterial adhesion studies on titanium, titanium nitride and modified hydroxyapatite thin films.* Materials Science and Engineering: C, 2007. 27(1): p. 35-41.**
137. **Jeyachandran, Y.L., et al., *A study on bacterial attachment on titanium and hydroxyapatite based films.* Surface and Coatings Technology, 2006. 201(6): p. 3462-3474.**
138. **Harris, L.G. and R.G. Richards, *Staphylococcus aureus adhesion to different treated titanium surfaces.* Journal of Materials Science: Materials in Medicine, 2004. 15(4): p. 311-314.**
139. **Characklis, W.G. and I.b. James D. Bryers, *Bioengineering report: Fouling biofilm development: A process analysis.* Biotechnology and Bioengineering, 2009. 102(2): p. 309-347.**
140. **Whitehead, K.A. and J. Verran, *The Effect of Surface Topography on the Retention of Microorganisms.* Food and Bioproducts Processing, 2006. 84(4): p. 253-259.**
141. **Whitehead, K.A., J. Colligon, and J. Verran, *Retention of microbial cells in substratum surface features of micrometer and sub-micrometer dimensions.* Colloids and Surfaces B: Biointerfaces, 2005. 41(2–3): p. 129-138.**
142. **Medilanski, E., et al., *Influence of the Surface Topography of Stainless Steel on Bacterial Adhesion.* Biofouling, 2002. 18(3): p. 193-203.**
143. **Edwards, K.J. and A.D. Rutenberg, *Microbial response to surface microtopography: the role of metabolism in localized mineral dissolution.* Chemical Geology, 2001. 180(1–4): p. 19-32.**
144. **Friedlander, R.S., et al., *Bacterial flagella explore microscale hummocks and hollows to increase adhesion.* Proceedings of the National Academy of Sciences, 2013. 110(14): p. 5624-5629.**
145. **Bruinsma, G.M., et al., *Influence of wear and overwear on surface properties of etafilcon A contact lenses and adhesion of Pseudomonas aeruginosa.* Invest Ophthalmol Vis Sci, 2002. 43(12): p. 3646-53.**
146. **Bakker, D.P., et al., *Multiple linear regression analysis of bacterial deposition to polyurethane coatings after conditioning film formation in the marine environment.* Microbiology, 2004. 150(Pt 6): p. 1779-84.**
147. **Mitik-Dineva, N., et al., *Differences in colonisation of five marine bacteria on two types of glass surfaces.* Biofouling, 2009. 25(7): p. 621-31.**
148. **Ploux, L., et al., *Opposite Responses of Cells and Bacteria to Micro/Nanopatterned Surfaces Prepared by Pulsed Plasma Polymerization and UV-Irradiation.* Langmuir, 2009. 25(14): p. 8161-8169.**
149. **Tegoulia, V.A. and S.L. Cooper, *Staphylococcus aureus adhesion to self-assembled monolayers: effect of surface chemistry and fibrinogen presence.* Colloids and Surfaces B: Biointerfaces, 2002. 24(3–4): p. 217-228.**
150. **Park, K.D., et al., *Bacterial adhesion on PEG modified polyurethane surfaces.* Biomaterials, 1998. 19(7–9): p. 851-859.**
151. **Shi, L., et al., *Mucin coating on polymeric material surfaces to suppress bacterial adhesion.* Colloids and Surfaces B: Biointerfaces, 2000. 17(4): p. 229-239.**
152. **Kiremitçi-Gümüşderelioğlu, M. and A. Peşmen, *Microbial adhesion to ionogenic PHEMA, PU and PP implants.* Biomaterials, 1996. 17(4): p. 443-449.**
153. **Gottenbos, B., et al., *Antimicrobial effects of positively charged surfaces on adhering Gram-positive and Gram-negative bacteria.* J Antimicrob Chemother, 2001. 48(1): p. 7-13.**
154. **Harkes, G., et al., *Physicochemical characterization ofEscherichia coli.* Cell Biochemistry and Biophysics, 1992. 20(1): p. 17-32.**
155. **Terada, A., et al., *The effect of surface charge property on Escherichia coli initial adhesion and subsequent biofilm formation.* Biotechnology and Bioengineering, 2012. 109(7): p. 1745-1754.**
156. **Terada, A., et al., *Bacterial adhesion to and viability on positively charged polymer surfaces.* Microbiology, 2006. 152(Pt 12): p. 3575-83.**

157. **Dague, E., et al., *Probing surface structures of Shewanella spp. by microelectrophoresis.* Biophys J, 2006. 90(7): p. 2612-21.**
158. **Li, B. and B.E. Logan, *Bacterial adhesion to glass and metal-oxide surfaces.* Colloids and Surfaces B: Biointerfaces, 2004. 36(2): p. 81-90.**
159. **Ploux, L., et al., *Quantitative and morphological analysis of biofilm formation on self-assembled monolayers.* Colloids and Surfaces B: Biointerfaces, 2007. 57(2): p. 174-181.**
160. **Bakker, D.P., et al., *Bacterial deposition to fluoridated and non-fluoridated polyurethane coatings with different elastic modulus and surface tension in a parallel plate and a stagnation point flow chamber.* Colloids and Surfaces B: Biointerfaces, 2003. 32(3): p. 179-190.**
161. **Lichter, J.A., et al., *Substrata Mechanical Stiffness Can Regulate Adhesion of Viable Bacteria.* Biomacromolecules, 2008. 9(6): p. 1571-1578.**
162. **N.Cottenye, *Antimicrobial surfaces based on self-assembled nanoreactors: from block copolymer synthesis to bacterial adhesion study*, 2010, Université de Haute Alsace , Universität Basel Basel**
163. **Saha, N., et al., *Influence of Polyelectrolyte Film Stiffness on Bacterial Growth.* Biomacromolecules, 2013. 14(2): p. 520-528.**
164. **Nathan, A., et al., *Copolymers of lysine and polyethylene glycol: a new family of functionalized drug carriers.* Bioconjugate Chemistry, 1993. 4(1): p. 54-62.**
165. **Benjawan Boonkaew, M.K., Roy Kimble, Pitt Supaphol, Leila Cuttle *Antimicrobial efficacy of a novel silver hydrogel dressing compared to two common silver burn wound dressings: Acticoat™ and PolyMem Silver.* Burns - 24 June 2013 2013.**
166. **Yurkov, G.Y., et al., *Copper Nanoparticles in a Polyethylene Matrix.* Inorganic Materials, 2001. 37(10): p. 997-1001.**
167. **Schwartz, V.B., et al., *Antibacterial Surface Coatings from Zinc Oxide Nanoparticles Embedded in Poly(N-isopropylacrylamide) Hydrogel Surface Layers.* Advanced Functional Materials, 2012. 22(11): p. 2376-2386.**
168. **Sun, G., W.B. Wheatley, and S.D. Worley, *A new cyclic N-halamine biocidal polymer.* Industrial & Engineering Chemistry Research, 1994. 33(1): p. 168-170.**
169. **Schnieders, J., et al., *Controlled release of gentamicin from calcium phosphate—poly(lactic acid-co-glycolic acid) composite bone cement.* Biomaterials, 2006. 27(23): p. 4239-4249.**
170. **Alt, V., et al., *The effects of combined gentamicin–hydroxyapatite coating for cementless joint prostheses on the reduction of infection rates in a rabbit infection prophylaxis model.* Biomaterials, 2006. 27(26): p. 4627-4634.**
171. **Nablo, B.J., A.R. Rothrock, and M.H. Schoenfisch, *Nitric oxide-releasing sol–gels as antibacterial coatings for orthopedic implants.* Biomaterials, 2005. 26(8): p. 917-924.**
172. **Jones, S.A., et al., *Controlling wound bioburden with a novel silver-containing Hydrofiber® dressing.* Wound Repair and Regeneration, 2004. 12(3): p. 288-294.**
173. **Kumar, R. and H. Münstedt, *Silver ion release from antimicrobial polyamide/silver composites.* Biomaterials, 2005. 26(14): p. 2081-2088.**
174. **Kenawy, E.-R., S.D. Worley, and R. Broughton, *The Chemistry and Applications of Antimicrobial Polymers: A State-of-the-Art Review.* Biomacromolecules, 2007. 8(5): p. 1359-1384.**
175. **Lagaron, J.M., M.J. Ocio, and A. Lopez-Rubio, *Antimicrobial Polymers*2011: John Wiley & Sons.**
176. **Lin, J., et al., *Bactericidal Properties of Flat Surfaces and Nanoparticles Derivatized with Alkylated Polyethylenimines.* Biotechnology Progress, 2002. 18(5): p. 1082-1086.**
177. **Lee, S.B., et al., *Permanent, Nonleaching Antibacterial Surfaces. 1. Synthesis by Atom Transfer Radical Polymerization.* Biomacromolecules, 2004. 5(3): p. 877-882.**
178. **Jampala, S.N., et al., *Plasma-Enhanced Synthesis of Bactericidal Quaternary Ammonium Thin Layers on Stainless Steel and Cellulose Surfaces.* Langmuir, 2008. 24(16): p. 8583-8591.**

179. **Vasilev, K., S.S. Griesser, and H.J. Griesser, *Antibacterial Surfaces and Coatings Produced by Plasma Techniques.* Plasma Processes and Polymers, 2011. 8(11): p. 1010-1023.**
180. **Thierry, B., et al., *Reactive Epoxy-Functionalized Thin Films by a Pulsed Plasma Polymerization Process.* Langmuir, 2008. 24(18): p. 10187-10195.**
181. **Vreuls, C., et al., *Prevention of bacterial biofilms by covalent immobilization of peptides onto plasma polymer functionalized substrates.* Journal of Materials Chemistry, 2010. 20(37): p. 8092-8098.**
182. **Conte, A., et al., *Antimicrobial activity of immobilized lysozyme on plasma-treated polyethylene films.* J Food Prot, 2008. 71(1): p. 119-25.**
183. **Dizman, B., M.O. Elasri, and L.J. Mathias, *Synthesis, Characterization, and Antibacterial Activities of Novel Methacrylate Polymers Containing Norfloxacin.* Biomacromolecules, 2004. 6(1): p. 514-520.**
184. **Lawson, M.C., et al., *Polymerizable Vancomycin Derivatives for Bactericidal Biomaterial Surface Modification: Structure–Function Evaluation.* Biomacromolecules, 2009. 10(8): p. 2221-2234.**
185. **Turos, E., et al., *Antibiotic-conjugated polyacrylate nanoparticles: new opportunities for development of anti-MRSA agents.* Bioorg Med Chem Lett, 2007. 17(1): p. 53-6.**
186. **Kenawy, E.-R., et al., *Biocidal polymers: Synthesis, antimicrobial activity, and possible toxicity of poly (hydroxystyrene-co-methylmethacrylate) derivatives.* Journal of Applied Polymer Science, 2011. 120(5): p. 2734-2742.**
187. **Discher, D.E. and A. Eisenberg, *Polymer Vesicles.* Science, 2002. 297(5583): p. 967-973.**
188. **Pack, D.W., et al., *Design and development of polymers for gene delivery.* Nat Rev Drug Discov, 2005. 4(7): p. 581-93.**
189. **Liang, J., et al., *Improved Antimicrobial Siloxane.* Industrial & Engineering Chemistry Research, 2007. 46(7): p. 1861-1866.**
190. **Page, K., et al., *Titania and silver-titania composite films on glass-potent antimicrobial coatings.* Journal of Materials Chemistry, 2007. 17(1): p. 95-104.**
191. **Liu, Y., S. He, and K. Huang, *Self-assembled structures of colloidal silver nanoparticles on solid substrates.* Journal of Wuhan University of Technology-Mater. Sci. Ed., 2011. 26(5): p. 883-887.**
192. **Guyomard, A., et al., *Incorporation of a Hydrophobic Antibacterial Peptide into Amphiphilic Polyelectrolyte Multilayers: A Bioinspired Approach to Prepare Biocidal Thin Coatings.* Advanced Functional Materials, 2008. 18(5): p. 758-765.**
193. **Follmann, H.D.M., et al., *Antiadhesive and Antibacterial Multilayer Films via Layer-by-Layer Assembly of TMC/Heparin Complexes.* Biomacromolecules, 2012. 13(11): p. 3711-3722.**
194. **Airoudj, A., et al., *Mechanically Switchable Biocide Plasma-Polymer Coatings for Biomaterials.* Advanced Engineering Materials, 2011. 13(10): p. B360-B368.**
195. **Webb, J.C.J. and R.F. Spencer, *The role of polymethylmethacrylate bone cement in modern orthopaedic surgery.* Journal of Bone & Joint Surgery, British Volume, 2007. 89-B(7): p. 851-857.**
196. **Aumsuwan, N., S. Heinhorst, and M.W. Urban, *The Effectiveness of Antibiotic Activity of Penicillin Attached to Expanded Poly(tetrafluoroethylene) (ePTFE) Surfaces: A Quantitative Assessment.* Biomacromolecules, 2007. 8(11): p. 3525-3530.**
197. **Aumsuwan, N., et al., *Attachment of Ampicillin to Expanded Poly(tetrafluoroethylene): Surface Reactions Leading to Inhibition of Microbial Growth.* Biomacromolecules, 2008. 9(7): p. 1712-1718.**
198. **Nablo, B.J., T.-Y. Chen, and M.H. Schoenfisch, *Sol–Gel Derived Nitric-Oxide Releasing Materials that Reduce Bacterial Adhesion.* Journal of the American Chemical Society, 2001. 123(39): p. 9712-9713.**
199. **Nablo, B.J. and M.H. Schoenfisch, *Antibacterial properties of nitric oxide–releasing sol-gels.* Journal of Biomedical Materials Research Part A, 2003. 67A(4): p. 1276-1283.**
200. **Mancinelli, R.L. and C.P. McKAY, *Effects of nitric oxide and nitrogen dioxide on bacterial growth.* Appl Environ Microbiol, 1983. 46(1): p. 198-202.**

201. **Wink, D.A. and J.B. Mitchell, *Chemical biology of nitric oxide: insights into regulatory, cytotoxic, and cytoprotective mechanisms of nitric oxide.* Free Radical Biology and Medicine, 1998. 25(4–5): p. 434-456.**
202. **Garthwaite, J., *Glutamate, nitric oxide and cell-cell signalling in the nervous system.* Trends in Neurosciences, 1991. 14(2): p. 60-67.**
203. **Garthwaite, J., S.L. Charles, and R. Chess-Williams, *Endothelium-derived relaxing factor release on activation of NMDA receptors suggests role as intercellular messenger in the brain.* Nature, 1988. 336(6197): p. 385-388.**
204. **Bergmann, L., et al., *Cytotoxic action of IL-1β against pancreatic islets is mediated via nitric oxide formation and is inhibited by NG-monomethyl-l-arginine.* FEBS Letters, 1992. 299(1): p. 103-106.**
205. **Yu, D.-G., *Formation of colloidal silver nanoparticles stabilized by Na+–poly(γ-glutamic acid)–silver nitrate complex via chemical reduction process.* Colloids and Surfaces B: Biointerfaces, 2007. 59(2): p. 171-178.**
206. **Durán, N., et al., *Antibacterial Effect of Silver Nanoparticles Produced by Fungal Process on Textile Fabrics and Their Effluent Treatment.* Journal of Biomedical Nanotechnology, 2007. 3(2): p. 203-208.**
207. **Diggins, F.W., *The true history of the discovery of penicillin, with refutation of the misinformation in the literature.* Br J Biomed Sci, 1999. 56(2): p. 83-93.**
208. **Sampedro, M.F. and R. Patel, *Infections Associated with Long-Term Prosthetic Devices.* Infectious Disease Clinics of North America, 2007. 21(3): p. 785-819.**
209. **Mombelli, A., et al., *Treatment of peri-implantitis by local delivery of tetracycline.* Clinical Oral Implants Research, 2001. 12(4): p. 287-294.**
210. **Zhao, L., et al., *Antibacterial coatings on titanium implants.* Journal of Biomedical Materials Research Part B: Applied Biomaterials, 2009. 91B(1): p. 470-480.**
211. **Kälicke, T., et al., *Effect on infection resistance of a local antiseptic and antibiotic coating on osteosynthesis implants: An in vitro and in vivo study.* Journal of Orthopaedic Research, 2006. 24(8): p. 1622-1640.**
212. **Harris, L.G., et al., *Bacteria and cell cytocompatibility studies on coated medical grade titanium surfaces.* Journal of Biomedical Materials Research Part A, 2006. 78A(1): p. 50-58.**
213. **Darouiche, R.O., et al., *In vivo efficacy of antimicrobial-coated devices.* J Bone Joint Surg Am, 2007. 89(4): p. 792-7.**
214. **Darouiche, R.O., et al., *A Comparison of Two Antimicrobial-Impregnated Central Venous Catheters.* New England Journal of Medicine, 1999. 340(1): p. 1-8.**
215. **Falagas, M.E., et al., *Rifampicin-impregnated central venous catheters: a meta-analysis of randomized controlled trials.* J Antimicrob Chemother, 2007. 59(3): p. 359-69.**
216. **Walder, B., D. Pittet, and M.R. Tramer, *Prevention of bloodstream infections with central venous catheters treated with anti-infective agents depends on catheter type and insertion time: evidence from a meta-analysis.* Infect Control Hosp Epidemiol, 2002. 23(12): p. 748-56.**
217. ***Needed, new paradigms in antibiotic development.* Expert Opinion on Pharmacotherapy, 2010. 11(8): p. 1233-1237.**
218. **Stewart, P.S. and J. William Costerton, *Antibiotic resistance of bacteria in biofilms.* The Lancet, 2001. 358(9276): p. 135-138.**
219. **Broxton, P., P.M. Woodcock, and P. Gilbert, *A study of the antibacterial activity of some polyhexamethylene biguanides towards Escherichia coli ATCC 8739.* Journal of Applied Bacteriology, 1983. 54(3): p. 345-353.**
220. **Cornell, R.J. and L.G. Donaruma, *2-METHACRYLOXYTROPONES. INTERMEDIATES FOR THE SYNTHESIS OF BIOLOGICALLY ACTIVE POLYMERS.* J Med Chem, 1965. 8: p. 388-390.**
221. **WORLEY, et al., *Biocidal polymers*. Vol. 4. 1996, Cambridge, ROYAUME-UNI: Elsevier.**
222. **Tashiro, T., *Antibacterial and Bacterium Adsorbing Macromolecules.* Macromolecular Materials and Engineering, 2001. 286(2): p. 63-87.**

223. **Timofeeva, L. and N. Kleshcheva, *Antimicrobial polymers: mechanism of action, factors of activity, and applications.* Applied Microbiology and Biotechnology, 2011. 89(3): p. 475-492.**
224. **Tew, G.N., et al., *De Novo Design of Antimicrobial Polymers, Foldamers, and Small Molecules: From Discovery to Practical Applications.* Accounts of Chemical Research, 2009. 43(1): p. 30-39.**
225. **Franklin, T.J. and G.A. Snow, *Antiseptics, antibiotics and the cell membrane*, in *Biochemistry and Molecular Biology of Antimicrobial Drug Action*2000, Springer Netherlands. p. 43-59.**
226. **Gabriel, G.J., et al., *Infectious disease: Connecting innate immunity to biocidal polymers.* Materials Science and Engineering: R: Reports, 2007. 57(1–6): p. 28-64.**
227. **Feng, Q.L., et al., *A mechanistic study of the antibacterial effect of silver ions on Escherichia coli and Staphylococcus aureus.* Journal of Biomedical Materials Research, 2000. 52(4): p. 662-668.**
228. **Lansdown, A.B.G., *A Pharmacological and Toxicological Profile of Silver as an Antimicrobial Agent in Medical Devices.* Advances in Pharmacological Sciences, 2010. 2010.**
229. **Liu, J. and R.H. Hurt, *Ion Release Kinetics and Particle Persistence in Aqueous Nano-Silver Colloids.* Environmental Science & Technology, 2010. 44(6): p. 2169-2175.**
230. **Liu, J., et al., *Controlled Release of Biologically Active Silver from Nanosilver Surfaces.* ACS Nano, 2010. 4(11): p. 6903-6913.**
231. **Jain, P. and T. Pradeep, *Potential of silver nanoparticle-coated polyurethane foam as an antibacterial water filter.* Biotechnology and Bioengineering, 2005. 90(1): p. 59-63.**
232. **Radzig, M.A., et al., *Antibacterial effects of silver nanoparticles on Gram-negative bacteria: Influence on the growth and biofilms formation, mechanisms of action.* Colloids and Surfaces B: Biointerfaces, (0).**
233. **Ruth Hall Sedlaka, M.H., Carolynn Groshc, Hanson Fongb, Francois Baneyxc, Dan Schwartzc, Mehmet Sarikayab, Candan Tamerlerb, Beth Traxlera, *Engineered Escherichia coli Silver-Binding Periplasmic Protein That Promotes Silver Tolerance.* Appl. Environ. Microbiol., 2012. 78 (7): p. 2289-2296**
234. **Gogoi, S.K., et al., *Green Fluorescent Protein-Expressing Escherichia coli as a Model System for Investigating the Antimicrobial Activities of Silver Nanoparticles.* Langmuir, 2006. 22(22): p. 9322-9328.**
235. **Carlson, C., et al., *Unique Cellular Interaction of Silver Nanoparticles: Size-Dependent Generation of Reactive Oxygen Species.* The Journal of Physical Chemistry B, 2008. 112(43): p. 13608-13619.**
236. **Park, H.-J., et al., *Silver-ion-mediated reactive oxygen species generation affecting bactericidal activity.* Water Research, 2009. 43(4): p. 1027-1032.**
237. **Morones-Ramirez, J.R., et al., *Silver Enhances Antibiotic Activity Against Gram-Negative Bacteria.* Science Translational Medicine, 2013. 5(190): p. 190ra81.**
238. **Lin, Y.-s.E., et al., *Inactivation of Mycobacterium avium by copper and silver ions.* Water Research, 1998. 32(7): p. 1997-2000.**
239. **Sharma, V.K., R.A. Yngard, and Y. Lin, *Silver nanoparticles: Green synthesis and their antimicrobial activities.* Advances in Colloid and Interface Science, 2009. 145(1–2): p. 83-96.**
240. **Schrand, A.M., et al., *Can silver nanoparticles be useful as potential biological labels?* Nanotechnology, 2008. 19(23): p. 235104.**
241. **Trop, M., *Silver-coated dressing acticoat caused raised liver enzymes and argyria-like symptoms in burn patient.* J Trauma, 2006. 61(4): p. 1024.**
242. **Hardes, J., et al., *Lack of toxicological side-effects in silver-coated megaprostheses in humans.* Biomaterials, 2007. 28(18): p. 2869-75.**
243. **Furno, F., et al., *Silver nanoparticles and polymeric medical devices: a new approach to prevention of infection?* J Antimicrob Chemother, 2004. 54(6): p. 1019-24.**

244. **Rai, M., A. Yadav, and N. Cioffi, *Silver Nanoparticles as Nano-Antimicrobials: Bioactivity, Benefits and Bottlenecks*, in *Nano-Antimicrobials*, N. Cioffi and M. Rai, Editors. 2012, Springer Berlin Heidelberg. p. 211-224.**
245. **Pal, S., Y. Tak, and J. Song, *Does the Antibacterial Activity of Silver Nanoparticles Depend on the Shape of the Nanoparticle? A Study of the Gram-Negative Bacterium Escherichia coli.* Appl. Environ. Microbiol., 2007. 73(6): p. 1712-1720.**
246. **De Gusseme, B., et al., *Biogenic silver for disinfection of water contaminated with viruses.* Appl Environ Microbiol, 2010. 76(4): p. 1082-7.**
247. **Lara, H.H., et al., *Mode of antiviral action of silver nanoparticles against HIV-1.* J Nanobiotechnology, 2010. 8: p. 1.**
248. **Endo, T., et al., *Stimuli-responsive hydrogel–silver nanoparticles composite for development of localized surface plasmon resonance-based optical biosensor.* Analytica Chimica Acta, 2008. 611(2): p. 205-211.**
249. **Hsu, S.-h., H.-J. Tseng, and Y.-C. Lin, *The biocompatibility and antibacterial properties of waterborne polyurethane-silver nanocomposites.* Biomaterials, 2010. 31(26): p. 6796-6808.**
250. **Shah, M.S.A.S., et al., *Silver on PEG-PU-TiO2 Polymer Nanocomposite Films: An Excellent System for Antibacterial Applications.* Chemistry of Materials, 2008. 20(7): p. 2455-2460.**
251. **Guggenbichler, J.P., et al., *A new technology of microdispersed silver in polyurethane induces antimicrobial activity in central venous catheters.* Infection, 1999. 27(1): p. S16-S23.**
252. **Kong, H. and J. Jang, *Antibacterial Properties of Novel Poly(methyl methacrylate) Nanofiber Containing Silver Nanoparticles.* Langmuir, 2008. 24(5): p. 2051-2056.**
253. **Lee, E., et al., *Multihollow structured poly(methyl methacrylate)/silver nanocomposite microspheres prepared by suspension polymerization in the presence of dual dispersion agents.* Colloid and Polymer Science, 2008. 286(12): p. 1379-1385.**
254. **Vimala, K., et al., *Controlled silver nanoparticles synthesis in semi-hydrogel networks of poly(acrylamide) and carbohydrates: A rational methodology for antibacterial application.* Carbohydrate Polymers, 2009. 75(3): p. 463-471.**
255. **Pinto, R.J.B., et al., *Antibacterial activity of nanocomposites of silver and bacterial or vegetable cellulosic fibers.* Acta Biomaterialia, 2009. 5(6): p. 2279-2289.**
256. **Nadagouda, M.N. and R.S. Varma, *Synthesis of Thermally Stable Carboxymethyl Cellulose/Metal Biodegradable Nanocomposites for Potential Biological Applications.* Biomacromolecules, 2007. 8(9): p. 2762-2767.**
257. **Pandey, S., G.K. Goswami, and K.K. Nanda, *Green synthesis of biopolymer–silver nanoparticle nanocomposite: An optical sensor for ammonia detection.* International Journal of Biological Macromolecules, 2012. 51(4): p. 583-589.**
258. **Sankar, M.U., et al., *Biopolymer-reinforced synthetic granular nanocomposites for affordable point-of-use water purification.* Proceedings of the National Academy of Sciences, 2013.**
259. **Cowan, M., et al., *Antimicrobial efficacy of a silver-zeolite matrix coating on stainless steel.* Journal of Industrial Microbiology and Biotechnology, 2003. 30(2): p. 102-106.**
260. **Inoue, Y., et al., *Bactericidal activity of Ag–zeolite mediated by reactive oxygen species under aerated conditions.* Journal of Inorganic Biochemistry, 2002. 92(1): p. 37-42.**
261. **Balogh, L., et al., *Dendrimer–Silver Complexes and Nanocomposites as Antimicrobial Agents.* Nano Letters, 2000. 1(1): p. 18-21.**
262. **Lesniak, W., et al., *Silver/Dendrimer Nanocomposites as Biomarkers: Fabrication, Characterization, in Vitro Toxicity, and Intracellular Detection.* Nano Letters, 2005. 5(11): p. 2123-2130.**
263. **Zhang, Y., et al., *Facile preparation and characterization of highly antimicrobial colloid Ag or Au nanoparticles.* Journal of Colloid and Interface Science, 2008. 325(2): p. 371-376.**
264. **Loher, S., et al., *Micro-organism-Triggered Release of Silver Nanoparticles from Biodegradable Oxide Carriers Allows Preparation of Self-Sterilizing Polymer Surfaces.* Small, 2008. 4(6): p. 824-832.**

265. **Schneider, O.D., et al., *Flexible, silver containing nanocomposites for the repair of bone defects: antimicrobial effect against E. coli infection and comparison to tetracycline containing scaffolds.* Journal of Materials Chemistry, 2008. 18(23): p. 2679-2684.**
266. **Brohede, U., et al., *Multifunctional implant coatings providing possibilities for fast antibiotics loading with subsequent slow release.* Journal of Materials Science: Materials in Medicine, 2009. 20(9): p. 1859-1867.**
267. **Shimazaki, T., et al., *In vivo antibacterial and silver-releasing properties of novel thermal sprayed silver-containing hydroxyapatite coating.* Journal of Biomedical Materials Research Part B: Applied Biomaterials, 2010. 92B(2): p. 386-389.**
268. **Eksik, O., A.T. Erciyes, and Y. Yagci, *In situ Synthesis of Oil Based Polymer Composites Containing Silver Nanoparticles.* Journal of Macromolecular Science, Part A, 2008. 45(9): p. 698-704.**
269. **Thomas, V., et al., *A versatile strategy to fabricate hydrogel–silver nanocomposites and investigation of their antimicrobial activity.* Journal of Colloid and Interface Science, 2007. 315(1): p. 389-395.**
270. **Vachon, D.J. and D.R. Yager, *Novel sulfonated hydrogel composite with the ability to inhibit proteases and bacterial growth.* Journal of Biomedical Materials Research Part A, 2006. 76A(1): p. 35-43.**
271. **Varaprasad, K., et al., *Synthesis and characterization of hydrogel-silver nanoparticle-curcumin composites for wound dressing and antibacterial application.* Journal of Applied Polymer Science, 2011. 121(2): p. 784-796.**
272. **Zaporojtchenko, V., et al., *Physico-chemical and antimicrobial properties of co-sputtered Ag–Au/PTFE nanocomposite coatings.* Nanotechnology, 2006. 17(19): p. 4904.**
273. **Lee, H., et al., *Substrate-Independent Layer-by-Layer Assembly by Using Mussel-Adhesive-Inspired Polymers.* Advanced Materials, 2008. 20(9): p. 1619-1623.**
274. **Furno, F., et al., *Silver nanoparticles and polymeric medical devices: a new approach to prevention of infection?* Journal of Antimicrobial Chemotherapy, 2004. 54(6): p. 1019-1024.**
275. **Yu, H., et al., *Preparation and antibacterial effects of PVA-PVP hydrogels containing silver nanoparticles.* Journal of Applied Polymer Science, 2007. 103(1): p. 125-133.**
276. **Jones, D.S., et al., *Characterization of the physicochemical, antimicrobial, and drug release properties of thermoresponsive hydrogel copolymers designed for medical device applications.* Journal of Biomedical Materials Research Part B: Applied Biomaterials, 2008. 85B(2): p. 417-426.**
277. **de Santa Maria, L.C., et al., *Synthesis, characterization, and bactericidal properties of composites based on crosslinked resins containing silver.* Journal of Applied Polymer Science, 2008. 107(3): p. 1879-1886.**
278. **Dai, J. and M.L. Bruening, *Catalytic Nanoparticles Formed by Reduction of Metal Ions in Multilayered Polyelectrolyte Films.* Nano Letters, 2002. 2(5): p. 497-501.**
279. **Lee, D., R.E. Cohen, and M.F. Rubner, *Antibacterial Properties of Ag Nanoparticle Loaded Multilayers and Formation of Magnetically Directed Antibacterial Microparticles.* Langmuir, 2005. 21(21): p. 9651-9659.**
280. **Li, Z., et al., *Two-Level Antibacterial Coating with Both Release-Killing and Contact-Killing Capabilities.* Langmuir, 2006. 22(24): p. 9820-9823.**
281. **Lee, D., M.F. Rubner, and R.E. Cohen, *Formation of Nanoparticle-Loaded Microcapsules Based on Hydrogen-Bonded Multilayers.* Chemistry of Materials, 2005. 17(5): p. 1099-1105.**
282. **Fu, J., et al., *Construction of antibacterial multilayer films containing nanosilver via layer-by-layer assembly of heparin and chitosan-silver ions complex.* Journal of Biomedical Materials Research Part A, 2006. 79A(3): p. 665-674.**
283. **Malcher, M., et al., *Embedded Silver Ions-Containing Liposomes in Polyelectrolyte Multilayers: Cargos Films for Antibacterial Agents.* Langmuir, 2008. 24(18): p. 10209-10215.**
284. **Decher, G., *Fuzzy Nanoassemblies: Toward Layered Polymeric Multicomposites.* Science, 1997. 277(5330): p. 1232-1237.**

285. **Boudou, T., et al.,** ***Multiple Functionalities of Polyelectrolyte Multilayer Films: New Biomedical Applications.*** **Advanced Materials, 2010. 22(4): p. 441-467.**
286. **Poulter, N., et al.,** ***An organo-silver compound that shows antimicrobial activity against Pseudomonas aeruginosa as a monomer and plasma deposited film.*** **Chemical Communications, 2009. 0(47): p. 7312-7314.**
287. **Vasilev, K., et al.,** ***Tunable Antibacterial Coatings That Support Mammalian Cell Growth.*** **Nano Letters, 2009. 10(1): p. 202-207.**
288. **Körner, E., et al.,** ***Formation and Distribution of Silver Nanoparticles in a Functional Plasma Polymer Matrix and Related Ag+ Release Properties.*** **Plasma Processes and Polymers, 2010. 7(7): p. 619-625.**
289. **Conrads, H. and M. Schmidt,** ***Plasma generation and plasma sources.*** **Plasma Sources Science and Technology, 2000. 9(4): p. 441.**
290. **Chu, P.K., et al.,** ***Plasma-surface modification of biomaterials.*** **Materials Science and Engineering: R: Reports, 2002. 36(5–6): p. 143-206.**
291. **Desmet, T., et al.,** ***Nonthermal Plasma Technology as a Versatile Strategy for Polymeric Biomaterials Surface Modification: A Review.*** **Biomacromolecules, 2009. 10(9): p. 2351-2378.**
292. **Sreenivasan, R., et al.,** ***Ultra-thin, gas permeable free-standing and composite membranes for microfluidic lung assist devices.*** **Biomaterials, 2011. 32(16): p. 3883-3889.**
293. **Siow, K.S., et al.,** ***Plasma Methods for the Generation of Chemically Reactive Surfaces for Biomolecule Immobilization and Cell Colonization - A Review.*** **Plasma Processes and Polymers, 2006. 3(6-7): p. 392-418.**
294. **Yasuda, H. and T. Hsu,** ***Some aspects of plasma polymerization investigated by pulsed R.F. discharge.*** **Journal of Polymer Science: Polymer Chemistry Edition, 1977. 15(1): p. 81-97.**
295. **Yasuda, H.,** ***Glow discharge polymerization.*** **Journal of Polymer Science: Macromolecular Reviews, 1981. 16(1): p. 199-293.**
296. **Tibbitt, J.M., et al.,** ***A Model for the Kinetics of Plasma Polymerization.*** **Macromolecules, 1977. 10(3): p. 647-653.**
297. **Stille, J.K., R.L. Sung, and J.V. Kooi,** ***The Reaction of Benzene in a Radiofrequency Glow Discharge1.*** **The Journal of Organic Chemistry, 1965. 30(9): p. 3116-3119.**
298. **J. Beck, A., et al.,** ***Ion flux and deposition rate measurements in the RF continuous wave plasma polymerisation of acrylic acid.*** **Chemical Communications, 1998. 0(11): p. 1221-1222.**
299. **Fraser, S., et al.,** ***A Multi-Technique Investigation of the Pulsed Plasma and Plasma Polymers of Acrylic Acid: Millisecond Pulse Regime.*** **The Journal of Physical Chemistry B, 2002. 106(22): p. 5596-5603.**
300. **Wavhal, D.S., et al.,** ***Investigation of Gas Phase Species and Deposition of SiO2 Films from HMDSO/O2 Plasmas.*** **Plasma Processes and Polymers, 2006. 3(3): p. 276-287.**
301. **Massines, F., et al.,** ***Atmospheric pressure plasma deposition of thin films by Townsend dielectric barrier discharge.*** **Surface and Coatings Technology, 2005. 200(5–6): p. 1855-1861.**
302. **Biederman, H., S.M. Ojha, and L. Holland,** ***The properties of fluorocarbon films prepared by r.f. sputtering and plasma polymerization in inert and active gas.*** **Thin Solid Films, 1977. 41(3): p. 329-339.**
303. **Dilks, A. and E. Kay,** ***Plasma polymerization of ethylene and the series of fluoroethylenes: plasma effluent mass spectrometry and ESCA studies.*** **Macromolecules, 1981. 14(3): p. 855-862.**
304. **Asandulesa, M., et al.,** ***Influence of operational parameters on plasma polymerization process at atmospheric pressure.*** **Journal of Applied Physics, 2010. 108(9): p. 093310-093310-6.**
305. **Yasuda, H. and T. Hirotsu,** ***Distribution of polymer deposition in plasma polymerization. III. Effect of discharge power.*** **Journal of Polymer Science: Polymer Chemistry Edition, 1978. 16(10): p. 2587-2592.**

306. Yasuda, H., et al., *Plasma polymerization of some organic compounds and properties of the polymers.* Journal of Polymer Science: Polymer Chemistry Edition, 1976. 14(1): p. 195-224.
307. Yasuda, H. and T. Hirotsu, *Critical evaluation of conditions of plasma polymerization.* Journal of Polymer Science: Polymer Chemistry Edition, 1978. 16(4): p. 743-759.
308. R. Alexander, M. and T. M. Duc, *The chemistry of deposits formed from acrylic acid plasmas.* Journal of Materials Chemistry, 1998. 8(4): p. 937-943.
309. Ward, A.J. and R.D. Short, *A time-of-flight secondary ion mass spectrometry and X-ray photoelectron spectroscopy investigation of the structure of plasma polymers prepared from the methacrylate series of monomers.* Polymer, 1993. 34(20): p. 4179-4185.
310. Truica-Marasescu, F. and M.R. Wertheimer, *Nitrogen-Rich Plasma-Polymer Films for Biomedical Applications.* Plasma Processes and Polymers, 2008. 5(1): p. 44-57.
311. Gilliam, M.A., Q. Yu, and H. Yasuda, *Plasma Polymerization Behavior of Fluorocarbon Monomers in Low-Pressure AF and RF Discharges.* Plasma Processes and Polymers, 2007. 4(2): p. 165-172.
312. Roualdes, S., J. Durand, and R.W. Field, *Comparative performance of various plasma polysiloxane films for the pervaporative recovery of organics from aqueous streams.* Journal of Membrane Science, 2003. 211(1): p. 113-126.
313. Alexander, M.R., F.R. Jones, and R.D. Short, *Radio-Frequency Hexamethyldisiloxane Plasma Deposition: A Comparison of Plasma- and Deposit-Chemistry.* Plasmas and Polymers, 1997. 2(4): p. 277-300.
314. Retzko, I., et al., *Chemical analysis of plasma-polymerized films: The application of X-ray photoelectron spectroscopy (XPS), X-ray absorption spectroscopy (NEXAFS) and fourier transform infrared spectroscopy (FTIR).* Journal of Electron Spectroscopy and Related Phenomena, 2001. 121(1): p. 111-129.
315. Ryan, M.E., A.M. Hynes, and J.P.S. Badyal, *Pulsed Plasma Polymerization of Maleic Anhydride.* Chemistry of Materials, 1996. 8(1): p. 37-42.
316. Rinsch, C.L., et al., *Pulsed Radio Frequency Plasma Polymerization of Allyl Alcohol: Controlled Deposition of Surface Hydroxyl Groups.* Langmuir, 1996. 12(12): p. 2995-3002.
317. Flemming, R., et al., *Effects of synthetic micro-and nano-structured surfaces on cell behavior.* Biomaterials, 1999. 20(6): p. 573-588.
318. Eves, P.C., et al., *A chemically defined surface for the co-culture of melanocytes and keratinocytes.* Biomaterials, 2005. 26(34): p. 7068-7081.
319. Gancarz, I., et al., *Plasma modified polymers as a support for enzyme immobilization 1.: Allyl alcohol plasma.* European Polymer Journal, 2003. 39(8): p. 1615-1622.
320. Zhang, S., et al., *Biological surface engineering: a simple system for cell pattern formation.* Biomaterials, 1999. 20(13): p. 1213-1220.
321. A. D. Jenkins, P.K., R. F. T. Stepto and U. W. Suter, *Glossary of basic terms in polymer science (IUPAC Recommendations 1996).* Pure Appl. Chem, 1996. 68(12): p. 2287-2311.
322. Tessmar, J., A. Mikos, and A. Göpferich, *The use of poly(ethylene glycol)-block-poly(lactic acid) derived copolymers for the rapid creation of biomimetic surfaces.* Biomaterials, 2003. 24(24): p. 4475-4486.
323. Yameen, B., et al., *Surface initiated polymerization on pulsed plasma deposited polyallylamine: a polymer substrate-independent strategy to soft surfaces with polymer brushes.* Macromol Rapid Commun, 2011. 32(21): p. 1735-40.
324. Friedrich, J., *The Plasma Chemistry of Polymer Surfaces*2012: Wiley.
325. Yameen, B., et al., *Surface Initiated Polymerization on Pulsed Plasma Deposited Polyallylamine: A Polymer Substrate-Independent Strategy to Soft Surfaces with Polymer Brushes.* Macromolecular Rapid Communications, 2011. 32(21): p. 1735-1740.
326. Siffer, F., et al., *A chemometric investigation of the effect of the process parameters during maleic anhydride pulsed plasma polymerization.* Analytica Chimica Acta, 2005. 539(1–2): p. 289-299.

327. **Meichsner, J., et al., *Nonthermal Plasma Chemistry and Physics*2012: Taylor & Francis Group.**
328. **H. Yasuda, *Plasma Polymerization,* 1985., London, : Academic Press.**
329. **Tatoulian, M., et al., *Deposition of Poly(acrylic acid) Films by Electrohydrodynamic Atomization in Postdischarge at Atmospheric Pressure in Air.* Chemistry of Materials, 2006. 18(25): p. 5860-5863.**
330. **Rossi, F. and P. Colpo, *Applications and challenges of plasma processes in nanobiotechnology.* Journal of Physics D: Applied Physics, 2011. 44(17): p. 174017.**
331. **Ward, L.J., et al., *Atmospheric Pressure Plasma Deposition of Structurally Well-Defined Polyacrylic Acid Films.* Chemistry of Materials, 2003. 15(7): p. 1466-1469.**
332. **Engelsman, A.F., et al., *The phenomenon of infection with abdominal wall reconstruction.* Biomaterials, 2007. 28(14): p. 2314-2327.**
333. **Bako, A. and R. Dhar, *Review of synthetic mesh-related complications in pelvic floor reconstructive surgery.* Int Urogynecol J, 2009. 20(1): p. 103-111.**
334. **Amrute, K.V., et al., *Analysis of outcomes of single polypropylene mesh in total pelvic floor reconstruction.* Neurourology and urodynamics, 2007. 26(1): p. 53-58.**
335. **Nilsson, C.G., et al., *Long-term results of the tension-free vaginal tape (TVT) procedure for surgical treatment of female stress urinary incontinence.* Int Urogynecol J, 2001. 12(2): p. S5-S8.**
336. **Afonso, J.S., et al., *Structural and thermal properties of polypropylene mesh used in treatment of stress urinary incontinence.* technology, 2009. 7: p. 10.**
337. **Earle, D.B. and L.A. Mark, *Prosthetic Material in Inguinal Hernia Repair: How Do I Choose?* Surgical Clinics of North America, 2008. 88(1): p. 179-201.**
338. **G. Ducel, J.F., L. Nicolle,, *Prevention of hospital-acquired infections, a practical guide, 2nd edition*, 2002, Canada World Health Organization, : Geneva, Switzerland**
339. **Richards, M.J., et al., *Nosocomial infections in combined medical-surgical intensive care units in the United States.* Infect Control Hosp Epidemiol, 2000. 21(8): p. 510-5.**
340. **Bagshaw, S.M. and K.B. Laupland, *Epidemiology of intensive care unit-acquired urinary tract infections.* Current Opinion in Infectious Diseases, 2006. 19(1): p. 67-71.**
341. **Samore M.H., E.R.S., Lassen A., Gould P., Lloyd J., Gardner R.M., Abouzelof R., Taylor C., Woodbury D.A., Willy M., Bright R.A. , *Using a Clinical Data Repository to Estimate the Frequency and Costs of Adverse Drug Events.* JAMA 2004. 291 p. 325-34.**
342. **Hendricks, S.K., et al., *Plasma-deposited membranes for controlled release of antibiotic to prevent bacterial adhesion and biofilm formation.* Journal of Biomedical Materials Research, 2000. 50(2): p. 160-170.**
343. **Fu, J., et al., *Construction of anti-adhesive and antibacterial multilayer films via layer-by-layer assembly of heparin and chitosan.* Biomaterials, 2005. 26(33): p. 6684-6692.**
344. **Chua, P.-H., et al., *Surface functionalization of titanium with hyaluronic acid/chitosan polyelectrolyte multilayers and RGD for promoting osteoblast functions and inhibiting bacterial adhesion.* Biomaterials, 2008. 29(10): p. 1412-1421.**
345. **Bazaka, K., et al., *Efficient surface modification of biomaterial to prevent biofilm formation and the attachment of microorganisms.* Applied Microbiology and Biotechnology, 2012. 95(2): p. 299-311.**
346. **Glinel, K., et al., *Antibacterial surfaces developed from bio-inspired approaches.* Acta Biomaterialia, 2012. 8(5): p. 1670-1684.**
347. **Eichler, M., et al., *The impact of dendrimer-grafted modifications to model silicon surfaces on protein adsorption and bacterial adhesion.* Biomaterials, 2011. 32(35): p. 9168-9179.**
348. **Zimmermann, A.K., et al., *Effect of biopassive and bioactive surface-coatings on the hemocompatibility of membrane oxygenators.* Journal of Biomedical Materials Research Part B: Applied Biomaterials, 2007. 80B(2): p. 433-439.**
349. **Chung, C.-J., et al., *An antimicrobial TiO2 coating for reducing hospital-acquired infection.* Journal of Biomedical Materials Research Part B: Applied Biomaterials, 2008. 85B(1): p. 220-224.**

350. **Page, K., M. Wilson, and I.P. Parkin, *Antimicrobial surfaces and their potential in reducing the role of the inanimate environment in the incidence of hospital-acquired infections.* Journal of Materials Chemistry, 2009. 19(23): p. 3819-3831.**
351. **Taha, M., et al., *Validating the poly-cyclodextrins based local drug delivery system on plasma-sprayed hydroxyapatite coated orthopedic implant with toluidine blue O.* Mater Sci Eng C Mater Biol Appl, 2013. 33(5): p. 2639-47.**
352. **Lan, S.-F., et al., *Controlled release of metronidazole from composite poly-ε-caprolactone/alginate (PCL/alginate) rings for dental implants.* Dental materials : official publication of the Academy of Dental Materials, 2013. 29(6): p. 656-665.**
353. **van den Bogaard, A.E. and E.E. Stobberingh, *Epidemiology of resistance to antibiotics: Links between animals and humans.* Int J Antimicrob Agents, 2000. 14(4): p. 327-335.**
354. **Chopra, I. and M. Roberts, *Tetracycline antibiotics: mode of action, applications, molecular biology, and epidemiology of bacterial resistance.* Microbiol Mol Biol Rev, 2001. 65(2): p. 232-60 ; second page, table of contents.**
355. **Palmer, A.C. and R. Kishony, *Understanding, predicting and manipulating the genotypic evolution of antibiotic resistance.* Nat Rev Genet, 2013. 14(4): p. 243-248.**
356. **Beceiro, A., M. Tomas, and G. Bou, *Antimicrobial resistance and virulence: a successful or deleterious association in the bacterial world?* Clin Microbiol Rev, 2013. 26(2): p. 185-230.**
357. **Hardes, J., et al., *Reduction of periprosthetic infection with silver-coated megaprostheses in patients with bone sarcoma.* Journal of Surgical Oncology, 2010. 101(5): p. 389-395.**
358. **Paladini, F., et al., *Silver-doped self-assembling di-phenylalanine hydrogels as wound dressing biomaterials.* Journal of Materials Science: Materials in Medicine, 2013: p. 1-12.**
359. **Contreras RG, S.H., Nakajima H, Shimada J, *Type of cell death induced by various metal cations in cultured human gingival fibroblasts.* In Vivo, 2010. 24(4): p. 513-7.**
360. **Hardes, J., et al., *Lack of toxicological side-effects in silver-coated megaprostheses in humans.* Biomaterials, 2007. 28(18): p. 2869-2875.**
361. **Morones, J.R., et al., *The bactericidal effect of silver nanoparticles.* Nanotechnology, 2005. 16(10): p. 2346-53.**
362. **Upendra Kumar Parashar, P.S.S., Anchal Srivastava, *ROLE OF NANOMATERIALS IN BIOTECHNOLOGY* Digest Journal of Nanomaterials and Biostructures, 2008. 3(2): p. 81-87.**
363. **Jradi, S., et al., *Spatially controlled synthesis of silver nanoparticles and nanowires by photosensitized reduction.* Nanotechnology, 2010. 21(9): p. 095605.**
364. **Nies, D.H., *Microbial heavy-metal resistance.* Applied Microbiology and Biotechnology, 1999. 51(6): p. 730-50.**
365. **Bruins, M.R., S. Kapil, and F.W. Oehme, *Microbial Resistance to Metals in the Environment.* Ecotoxicology and Environmental Safety, 2000. 45(3): p. 198-207.**
366. **Teitzel, G.M. and M.R. Parsek, *Heavy metal resistance of biofilm and planktonic Pseudomonas aeruginosa.* Appl Environ Microbiol, 2003. 69(4): p. 2313-2320.**
367. **Percival, S.L., P.G. Bowler, and D. Russell, *Bacterial resistance to silver in wound care.* The Journal of hospital infection, 2005. 60(1): p. 1-7.**
368. **Chopra, I., *The increasing use of silver-based products as antimicrobial agents: a useful development or a cause for concern?* Journal of Antimicrobial Chemotherapy, 2007. 59(4): p. 587-590.**
369. **Boening, H.V., *Fundamental of plasma chemistry and technology*1988: Technomic Publishing Company, Inc.**
370. **Roucoules, V., et al., *Strengthening the Junction Between EPDM and Aluminium Substrate via Plasma Polymerisation.* The Journal of Adhesion, 2007. 83(10): p. 875-895.**
371. **Geissler, A., et al., *Chemical Force Titration of Plasma Polymer-Modified PDMS Substrates by Using Plasma Polymer-Modified AFM Tips.* Langmuir, 2008. 24(9): p. 4874-4880.**

372. Roucoules, V., et al., *Changes in Silicon Elastomeric Surface Properties under Stretching Induced by Three Surface Treatments.* Langmuir, 2007. 23(26): p. 13136-13145.
373. Øye, G., et al., *Plasmachemical Amine Functionalization of Porous Polystyrene Spheres: The Importance of Particle Size.* The Journal of Physical Chemistry B, 2003. 107(15): p. 3496-3499.
374. Geissler, A., et al., *Multifunctional Stretchable Plasma Polymer Modified PDMS Interface for Mechanically Responsive Materials.* Plasma Processes and Polymers, 2010. 7(1): p. 64-77.
375. Woodward, I.S., et al., *Micropatterning of Plasma Fluorinated Super-hydrophobic Surfaces.* Plasma Chemistry and Plasma Processing, 2006. 26(5): p. 507-516.
376. Boldyryeva, H., et al., *Composite Ag/C:H films prepared by DC planar magnetron deposition.* Thin Solid Films, 2003. 442(1–2): p. 86-92.
377. Hlídek, P., et al., *Composite Ag/C:H:N films prepared by planar magnetron deposition.* Thin Solid Films, 2008. 516(14): p. 4581-4586.
378. Zanna, S., et al., *Ageing of plasma-mediated coatings with embedded silver nanoparticles on stainless steel: An XPS and ToF-SIMS investigation.* Applied Surface Science, 2010. 256(22): p. 6499-6505.
379. Beier, O., et al., *Low Temperature Deposition of Antibacterially Active Silicon Oxide Layers Containing Silver Nanoparticles, Prepared by Atmospheric Pressure Plasma Chemical Vapor Deposition.* Plasma Processes and Polymers, 2013. 10(1): p. 77-87.
380. Vidal, O., et al., *Isolation of an Escherichia coli K-12 mutant strain able to form biofilms on inert surfaces: involvement of a new ompR allele that increases curli expression.* J Bacteriol, 1998. 180(9): p. 2442-9.
381. WS, R., *ImageJ*, 1997—2012, U.S. National Institutes of Health, Bethesda, Maryland, USA.
382. Dietz, H.P., et al., *Mechanical properties of urogynecologic implant materials.* Int Urogynecol J Pelvic Floor Dysfunct, 2003. 14(4): p. 239-43; discussion 243.
383. Nurul Huda, M., et al., *A study of the crystallinity index of polypropylene fibres.* Colloid and Polymer Science, 1985. 263(9): p. 730-737.
384. France, R.M. and R.D. Short, *Plasma Treatment of Polymers: The Effects of Energy Transfer from an Argon Plasma on the Surface Chemistry of Polystyrene, and Polypropylene. A High-Energy Resolution X-ray Photoelectron Spectroscopy Study.* Langmuir, 1998. 14(17): p. 4827-4835.
385. Dirani, A., et al., *Nanopatterning of Plasma Polymer Thin Films by ArF Photolithography: Impact of Polymer Structure on Patterning Properties.* Plasma Processes and Polymers, 2010. 7(7): p. 571-581.
386. Vasilev, K., et al., *Solvent-Induced Porosity in Ultrathin Amine Plasma Polymer Coatings.* The Journal of Physical Chemistry B, 2008. 112(35): p. 10915-10921.
387. Mishra, G. and S.L. McArthur, *Plasma Polymerization of Maleic Anhydride: Just What Are the Right Deposition Conditions?* Langmuir, 2010. 26(12): p. 9645-9658.
388. Hegemann, D., et al., *Macroscopic Description of Plasma Polymerization.* Plasma Processes and Polymers, 2007. 4(3): p. 229-238.
389. Callegari, A., D. Tonti, and M. Chergui, *Photochemically Grown Silver Nanoparticles with Wavelength-Controlled Size and Shape.* Nano Letters, 2003. 3(11): p. 1565-1568.
390. Sommerfeld Ross, S., J.M. Reinhardt, and J. Fiegel, *Enhanced analysis of bacteria susceptibility in connected biofilms.* Journal of Microbiological Methods, 2012. 90(1): p. 9-14.
391. Gengenbach, T.R., R.C. Chatelier, and H.J. Griesser, *Characterization of the Ageing of Plasma-deposited Polymer Films: Global Analysis of X-ray Photoelectron Spectroscopy Data.* Surface and Interface Analysis, 1996. 24(4): p. 271-281.
392. Gahleitner, M.W., J.; Fiebig, J.; Dobianer, K.; Hametner, C, *Sterilisation Effects on Polypropylene: Technology and Polymer Type Effects*, in *Proc. 9th European PLACE Conferance* 2003: Rome, 3/12
393. Serbetci, K., et al., *Effects of resterilization on mechanical properties of polypropylene meshes.* American journal of surgery, 2007. 194(3): p. 375-379.

394. Martakis, N., M. Niaounakis, and D. Pissimissis, *Gamma-sterilization effects and influence of the molecular weight distribution on the postirradiation resistance of polypropylene for medical devices.* Journal of Applied Polymer Science, 1994. 51(2): p. 313-328.
395. Ding, Z., et al., *Effects of annealing on structure and deformation mechanism of isotactic polypropylene film with row-nucleated lamellar structure.* Journal of Applied Polymer Science, 2013. 130(3): p. 1659-1666.
396. O'Leary, R.K. and W.L. Guess, *Toxicological studies on certain medical grade plastics sterilized by ethylene oxide.* Journal of Pharmaceutical Sciences, 1968. 57(1): p. 12-17.
397. Mendes, G.C.C., T.R.S. Brandão, and C.L.M. Silva, *Ethylene oxide sterilization of medical devices: A review.* American Journal of Infection Control, 2007. 35(9): p. 574-581.
398. Haddow, D.B., et al., *Plasma-polymerized surfaces for culture of human keratinocytes and transfer of cells to an in vitro wound-bed model.* Journal of Biomedical Materials Research Part A, 2003. 64A(1): p. 80-87.
399. Calderon, J.G., et al., *Stability of plasma-polymerized allylamine films with sterilization by autoclaving.* Journal of Biomedical Materials Research, 1998. 42(4): p. 597-603.
400. Brétagnol, F., et al., *The effect of sterilization processes on the bioadhesive properties and surface chemistry of a plasma-polymerized polyethylene glycol film: XPS characterization and L929 cell proliferation tests.* Acta Biomaterialia, 2008. 4(6): p. 1745-1751.
401. Ademovic, Z., et al., *Surface Modification of PET Films Using Pulsed AC Plasma Polymerisation Aimed at Preventing Protein Adsorption.* Plasma Processes and Polymers, 2005. 2(1): p. 53-63.
402. Förch, R., Z. Zhang, and W. Knoll, *Soft Plasma Treated Surfaces: Tailoring of Structure and Properties for Biomaterial Applications.* Plasma Processes and Polymers, 2005. 2(5): p. 351-372.
403. Thomas, M., et al., *Generation of Stable Coatings with Carboxylic Groups by Copolymerization of MAA and VTMS using DBD at Atmospheric Pressure.* Plasma Processes and Polymers, 2007. 4(S1): p. S475-S481.
404. Nitschke, M., et al., *Surface modification of cell culture carriers: Routes to anhydride functionalization of polystyrene.* Colloids and Surfaces B: Biointerfaces, 2012. 90(0): p. 41-47.
405. Hearle, J.W.S., et al., *Atlas of Fibre Fracture and Damage to Textiles*1998: CRC Press.
406. K. Schneider, L.H.a.S.V.R., *Tailoring of Morphology and Mechanical Properties of Isotactic Polypropylene by Processing,* , in *Polypropylene*, I.-.-.-.-.-. Dr. Fatih Dogan (Ed.), Editor 2012 InTech, .
407. Matthias Friedrich, S.M., Thilo Wedel, Frank Fischer, Uwe J. Roblick, Jens Habermann, Hans-Peter Bruch and Stefan Farke, *Effects of Resterilization on the Surface-Structure of Lightweight Polypropylene Hernia Meshes-An in vitro Study.* Research Journal of Medical Sciences, 2010. 4: p. 330-333.
408. Serbetci, K., et al., *Effects of resterilization on mechanical properties of polypropylene meshes.* The American Journal of Surgery, 2007. 194(3): p. 375-379.
409. Charlesby, A. and N.H. Hancock, *The Effect of Cross-Linking on the Elastic Modulus of Polythene.* Proceedings of the Royal Society of London. Series A. Mathematical and Physical Sciences, 1953. 218(1133): p. 245-255.
410. Acar, N., *Radiation synthesis of poly(2-vinylpyridine) gels and their swelling characteristics.* Radiation Physics and Chemistry, 2002. 63(2): p. 185-191.
411. Assumpção, T.A.A., et al., *Influence of the heat treatment on the nucleation of silver nanoparticles in Tm3+ doped PbO-GeO2 glasses.* Applied Physics B, 2011. 103(1): p. 165-169.
412. Brito-Silva, A.M., et al., *Silver nanoparticles formation within unsaturated polyester/styrene resins induced by UV irradiation and thermal treatment.* Polymer Engineering & Science, 2010. 50(12): p. 2350-2355.
413. Jiang, X., et al., *Role of Temperature in the Growth of Silver Nanoparticles Through a Synergetic Reduction Approach.* Nanoscale Res Lett, 2011. 6(1): p. 32.

414. Yamamoto, M., Y. Kashiwagi, and M. Nakamoto, *Size-Controlled Synthesis of Monodispersed Silver Nanoparticles Capped by Long-Chain Alkyl Carboxylates from Silver Carboxylate and Tertiary Amine.* Langmuir, 2006. 22(20): p. 8581-8586.
415. Iravani, H.K.a.S. *Silver Nanoparticles, The Delivery of Nanoparticles,* . Silver Nanoparticles, (2012). . DOI: DOI: 10.5772/34157. .
416. Kittler, S., et al., *Toxicity of Silver Nanoparticles Increases during Storage Because of Slow Dissolution under Release of Silver Ions.* Chemistry of Materials, 2010. 22(16): p. 4548-4554.
417. Alissawi, N., et al., *Tuning of the ion release properties of silver nanoparticles buried under a hydrophobic polymer barrier.* Journal of Nanoparticle Research, 2012. 14(7): p. 1-12.
418. Grant, A., *Mesh compared with non-mesh methods of open groin hernia repair: systematic review of randomized controlled trials.* British Journal of Surgery, 2000. 87(7): p. 854-859.
419. Bako, A. and R. Dhar, *Review of synthetic mesh-related complications in pelvic floor reconstructive surgery.* Int Urogynecol J Pelvic Floor Dysfunct, 2009. 20(1): p. 103-11.
420. Taylor, S.G. and P.J. O'Dwyer, *Chronic groin sepsis following tension-free inguinal hernioplasty.* British Journal of Surgery, 1999. 86(4): p. 562-565.
421. Tijdink, M.M., et al., *Surgical management of mesh-related complications after prior pelvic floor reconstructive surgery with mesh.* Int Urogynecol J, 2011. 22(11): p. 1395-404.
422. Burger, J.W., et al., *Long-term follow-up of a randomized controlled trial of suture versus mesh repair of incisional hernia.* Ann Surg, 2004. 240(4): p. 578-83; discussion 583-5.
423. Hesselink, V.J., et al., *An evaluation of risk factors in incisional hernia recurrence.* Surg Gynecol Obstet, 1993. 176(3): p. 228-34.
424. Petersen, S., et al., *Deep prosthesis infection in incisional hernia repair: predictive factors and clinical outcome.* Eur J Surg, 2001. 167(6): p. 453-7.
425. Luijendijk, R.W., et al., *A comparison of suture repair with mesh repair for incisional hernia.* N Engl J Med, 2000. 343(6): p. 392-8.
426. Leber, G.E., et al., *Long-term complications associated with prosthetic repair of incisional hernias.* Arch Surg, 1998. 133(4): p. 378-82.
427. Aydinuraz, K., et al., *In Vitro S. epidermidis and S. aureus Adherence to Composite and Lightweight Polypropylene Grafts1.* The Journal of surgical research, 2009. 157(1): p. e79-e86.
428. Scheidbach, H., et al., *Influence of titanium coating on the biocompatibility of a heavyweight polypropylene mesh. An animal experimental model.* Eur Surg Res, 2004. 36(5): p. 313-7.
429. Saygun, O., et al., *Gold and gold-palladium coated polypropylene grafts in a S. epidermidis wound infection model.* J Surg Res, 2006. 131(1): p. 73-9.
430. Tolker-Nielsen, T. and S. Molin, *Spatial Organization of Microbial Biofilm Communities.* Microbial Ecology, 2000. 40(2): p. 75-84.
431. Stoodley , P., Boyle, John D., Dodds, Ian and Lappin-Scott, Hilary M, *Consensus model of biofilm structure.* Biofilms: Community Interactions and Control: 3rd meeting of the Biofilm Club., 1997: p. 1-9.
432. James, G.A., L. Beaudette, and J.W. Costerton, *Interspecies bacterial interactions in biofilms.* Journal of Industrial Microbiology, 1995. 15(4): p. 257-262.
433. Chang, W.-S., et al., *Alginate Production by Pseudomonas putida Creates a Hydrated Microenvironment and Contributes to Biofilm Architecture and Stress Tolerance under Water-Limiting Conditions.* J. Bacteriol., 2007. 189(22): p. 8290-8299.
434. Lawrence, J.R., et al., *Optical sectioning of microbial biofilms.* J Bacteriol, 1991. 173(20): p. 6558-67.
435. Jayaraman, A., A.K. Sun, and T.K. Wood, *Characterization of axenic Pseudomonas fragi and Escherichia coli biofilms that inhibit corrosion of SAE 1018 steel.* Journal of Applied Microbiology, 1998. 84(4): p. 485-492.

436. **Sanchez, Z., et al., *Assessment of change in biofilm architecture by nutrient concentration using a multichannel microdevice flow system.* Journal of Bioscience and Bioengineering, 2013. 115(3): p. 326-331.**
437. **Abdi-Ali, A., M. Mohammadi-Mehr, and Y. Agha Alaei, *Bactericidal activity of various antibiotics against biofilm-producing Pseudomonas aeruginosa.* Int J Antimicrob Agents, 2006. 27(3): p. 196-200.**
438. **Martin Vorregaard, A.H., Janus Haagensen, Liang Yang, Alex Toftgaard Nielsen, Morten Hentzer, Michael Givskov, Matt Parsek *Stepbystep guide to using Comstat2*. 2010.**
439. **Haugland, R.P., *LIVE/DEAD BacLight bacterial viability kits.* 2002. ninth edition: p. 626-628.**
440. **Lin, S.M., et al., *Effects of hydrogen peroxide on dental unit biofilms and treatment water contamination.* Eur J Dent, 2011. 5(1): p. 47-59.**
441. **Shen, Y., et al., *The Synergistic Antimicrobial Effect by Mechanical Agitation and Two Chlorhexidine Preparations on Biofilm Bacteria.* Journal of endodontics, 2010. 36(1): p. 100-104.**
442. **Sbalzarini, I.F. and P. Koumoutsakos, *Feature point tracking and trajectory analysis for video imaging in cell biology.* Journal of Structural Biology, 2005. 151(2): p. 182-195.**
443. **Davies, D., *Understanding biofilm resistance to antibacterial agents.* Nat Rev Drug Discov, 2003. 2(2): p. 114-122.**
444. **Folkesson, A., et al., *Biofilm Induced Tolerance towards Antimicrobial Peptides.* PLoS ONE, 2008. 3(4): p. e1891.**
445. **Zhao, G. and S.E. Stevens, Jr., *Multiple parameters for the comprehensive evaluation of the susceptibility of Escherichia coli to the silver ion.* Biometals, 1998. 11(1): p. 27-32.**
446. **Matthew D. Rolfea, C.J.R., Sacha Lucchinia, Carmen Pina, Arthur Thompsona, Andrew D. S. Camerone, Mark Alstona, Michael F. Stringerb, Roy P. Bettsb, József Baranyia, Michael W. Pecka and Jay C. D. Hintona,e, *Lag Phase Is a Distinct Growth Phase That Prepares Bacteria for Exponential Growth and Involves Transient Metal Accumulation.* J. Bacteriol., 2012. 194(3): p. 686-701**
447. **Sezonov, G., D. Joseleau-Petit, and R. D'Ari, *Escherichia coli Physiology in Luria-Bertani Broth.* Journal of Bacteriology, 2007. 189(23): p. 8746-8749.**
448. **Boks, N.P., et al., *Mobile and immobile adhesion of staphylococcal strains to hydrophilic and hydrophobic surfaces.* Journal of Colloid and Interface Science, 2009. 331(1): p. 60-64.**
449. **Gottenbos, B., H.C. van der Mei, and H.J. Busscher, *Initial adhesion and surface growth of Staphylococcus epidermidis and Pseudomonas aeruginosa on biomedical polymers.* Journal of Biomedical Materials Research, 2000. 50(2): p. 208-214.**
450. **An, Y.H. and R.J. Friedman, *Concise review of mechanisms of bacterial adhesion to biomaterial surfaces.* Journal of Biomedical Materials Research, 1998. 43(3): p. 338-348.**
451. **Scheuerman, T.R., A.K. Camper, and M.A. Hamilton, *Effects of Substratum Topography on Bacterial Adhesion.* Journal of Colloid and Interface Science, 1998. 208(1): p. 23-33.**
452. **Flint, S.H., J.D. Brooks, and P.J. Bremer, *Properties of the stainless steel substrate, influencing the adhesion of thermo-resistant streptococci.* Journal of Food Engineering, 2000. 43(4): p. 235-242.**
453. **Yamada, H., et al., *Direct observation and analysis of bacterial growth on an antimicrobial surface.* Appl Environ Microbiol, 2010. 76(16): p. 5409-5414.**
454. **Lappin-Scott, H.M., *Microbial biofilms*2003, Cambridge [u.a.: Cambridge Univ. Press.**
455. **Mah, T.-F.C. and G.A. O'Toole, *Mechanisms of biofilm resistance to antimicrobial agents.* Trends in microbiology, 2001. 9(1): p. 34-39.**
456. **Terada, A., et al., *Bacterial adhesion to and viability on positively charged polymer surfaces.* Microbiology, 2006. 152(12): p. 3575-3583.**

457. **Kostenko, V., et al.,** ***Impact of silver-containing wound dressings on bacterial biofilm viability and susceptibility to antibiotics during prolonged treatment.*** **Antimicrob Agents Chemother, 2010. 54(12): p. 5120-31.**
458. **Costerton, J.W.,** ***The Biofilm Primer*****2007: Springer.**
459. **Liu, X., C. Ng, and T. Ferenci,** ***Global adaptations resulting from high population densities in Escherichia coli cultures.*** **J Bacteriol, 2000. 182(15): p. 4158-64.**
460. **Sikkema, J., J.A. de Bont, and B. Poolman,** ***Mechanisms of membrane toxicity of hydrocarbons.*** **Microbiol Rev, 1995. 59(2): p. 201-22.**
461. **Thorne, S.H. and H.D. Williams,** ***Cell density-dependent starvation survival of Rhizobium leguminosarum bv. phaseoli: identification of the role of an N-acyl homoserine lactone in adaptation to stationary-phase survival.*** **J Bacteriol, 1999. 181(3): p. 981-90.**
462. **Dermenoudis, S. and Y. Missirlis,** ***Design of a novel rotating wall bioreactor for the in vitro simulation of the mechanical environment of the endothelial function.*** **Journal of biomechanics, 2010. 43(7): p. 1426-1431.**
463. **Kingsnorth, A.,** ***The management of incisional hernia.*** **Ann R Coll Surg Engl, 2006. 88(3): p. 252-60.**
464. **Mudge, M. and L.E. Hughes,** ***Incisional hernia: a 10 year prospective study of incidence and attitudes.*** **Br J Surg, 1985. 72(1): p. 70-1.**
465. **van 't Riet, M., et al.,** ***Prevention of adhesion to prosthetic mesh: comparison of different barriers using an incisional hernia model.*** **Ann Surg, 2003. 237(1): p. 123-8.**
466. **Altinli, E., et al.,** ***Prevention of adhesion to prosthetic mesh: comparison of oxidized generated cellulose, polyethylene glycol and hylan G-F 20.*** **Ulus Travma Acil Cerrahi Derg, 2011. 17(5): p. 377-82.**
467. **Scheidbach, H., et al.,** ***In vivo studies comparing the biocompatibility of various polypropylene meshes and their handling properties during endoscopic total extraperitoneal (TEP) patchplasty: an experimental study in pigs.*** **Surgical Endoscopy And Other Interventional Techniques, 2004. 18(2): p. 211-220.**
468. **Greenawalt, K.E., et al.,** ***Evaluation of Sepramesh Biosurgical Composite in a Rabbit Hernia Repair Model.*** **The Journal of surgical research, 2000. 94(2): p. 92-98.**
469. **Judge, T.W., D.M. Parker, and R.C. Dinsmore,** ***Abdominal Wall Hernia Repair: A Comparison of Sepramesh and Parietex Composite Mesh in a Rabbit Hernia Model.*** **Journal of the American College of Surgeons, 2007. 204(2): p. 276-281.**
470. ***Comparison of Adhesive Properties of Five Different Prosthetic Materials Used in Hernioplasty.*** **Journal of Investigative Surgery, 2005. 18(2): p. 89-95.**
471. **Emans, P., et al.,** ***Polypropylene Meshes to Prevent Abdominal Herniation. Can Stable Coatings Prevent Adhesions in the Long Term?*** **Annals of Biomedical Engineering, 2009. 37(2): p. 410-418.**
472. **Bringman, S., et al.,** ***Hernia repair: the search for ideal meshes.*** **Hernia, 2010. 14(1): p. 81-7.**
473. **Oyajobi, B.O., et al.,** ***Isolation and Characterization of Human Clonogenic Osteoblast Progenitors Immunoselected from Fetal Bone Marrow Stroma Using STRO-1 Monoclonal Antibody.*** **Journal of Bone and Mineral Research, 1999. 14(3): p. 351-361.**
474. **Geurtsen, W., et al.,** ***Cytotoxicity of 35 dental resin composite monomers/additives in permanent 3T3 and three human primary fibroblast cultures.*** **Journal of Biomedical Materials Research, 1998. 41(3): p. 474-480.**
475. **Cui, N.-Y. and N.M.D. Brown,** ***Modification of the surface properties of a polypropylene (PP) film using an air dielectric barrier discharge plasma.*** **Applied Surface Science, 2002. 189(1–2): p. 31-38.**
476. **Takagi, M., et al.,** ***Enhanced adhesion of endothelial cells onto a polypropylene hollow-fiber membrane by plasma discharge treatment and high inoculum cell density.*** **Journal of Artificial Organs, 2001. 4(3): p. 220-225.**
477. **Li, D.J. and L.F. Niu,** ***Cell attachment of polypropylene surface-modified by COOH+ ion implantation.*** **Nuclear Instruments and Methods in Physics Research Section B: Beam Interactions with Materials and Atoms, 2002. 192(4): p. 393-401.**

478. **N.Gomathi, D.M., Tapas Kumar Maiti, Sudarsan Neogi,** ***Surface Modification of Polypropylene using Argon Plasma for Biomedical Applications*** **in** ***International Symposium on Plasma Chemistry ISPC 20, conferrence paper*****2011: Philadelphia, US.**

479. **N. Gomathi, S.N.,** ***Development of Bio/Blood Compatible Polypropylene by Radio-Frequency Plasma Treatment*** **in** ***International Symposium on Plasma Chemistry ISPC 20, conferrence paper*****2011: Philadelphia, US.**

480. **Bigerelle, M., S. Giljean, and K. Anselme,** ***Existence of a typical threshold in the response of human mesenchymal stem cells to a peak and valley topography.*** **Acta Biomaterialia, 2011. 7(9): p. 3302-3311.**

481. **Park, J.Y., et al.,** ***Study of cellular behaviors on concave and convex microstructures fabricated from elastic PDMS membranes.*** **Lab Chip, 2009. 9(14): p. 2043-9.**